

# **BREACH EROSION PROCESS OF HOMOGENEOUS EARTHFILL DAMS AND FUSE PLUGS DUE TO OVERTOPPING FLOW**

*A Thesis Submitted  
In Partial Fulfilment of the Requirements  
for the Degree of  
DOCTOR OF PHILOSOPHY*

*by*

**PRADIP KUMAR DAS**

*to the*

**DEPARTMENT OF CIVIL ENGINEERING  
INDIAN INSTITUTE OF TECHNOLOGY KANPUR  
DECEMBER, 1997**

21 JUN 1997  
**CENTRAL LIBRARY**  
I. I. T. KANPUR

**Acc. No. A 128596**

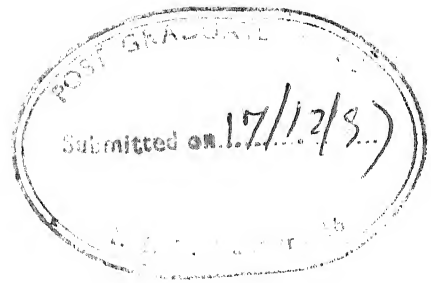
TH  
CE/1997/P  
D26b



A128596



# CERTIFICATE



It is certified that the work contained in the thesis entitled "**BREACH EROSION PROCESS OF HOMOGENEOUS EARTHFILL DAMS AND FUSE PLUGS DUE TO OVERTOPPING FLOW**", by **Pradip Kumar Das** (Roll No. 9410366), has been carried out under my supervision and that this work has not been submitted elsewhere for a degree.

(T Gangadharaiyah)

Professor

Department of Civil Engineering

Indian Institute of Technology

Kanpur, India

7 December, 1997

## SYNOPSIS

Dams play an important role in surface water management. The importance of a dam is greater in a country like India where precipitation is not uniform in time and space. However, when a dam fails, it results in a sudden release of large quantity of stored water causing havoc in the downstream region. The damages in terms of life and property associated with a dam failure can be catastrophic. So the failure of a dam in any form is not desirable. Among the dams, earthen dams are more vulnerable to failure. The main causes of the failure of an earthen dam are due to overtopping and piping. In this 'International Decade for Natural Disaster Reduction', (1990 - 2000 A. D.), a natural disaster like the dam breach problem, has its relevance to study.

The present study is dealing with the process involved in the dam breach and the washout characteristics of fuse plug due to overtopping flow. The results of the present study on dam breach have a direct bearing on the field, particularly for flood warning and evacuation planning measure as remedial efforts towards the probable disaster mitigation. In more technical terms, knowing the initial conditions at the dam site, the routing of water and sediment discharge on the downstream can be carried out more effectively. Fuse plug works as a safety valve of an earthen dam. The height of fuse plug is equal to the difference between full reservoir level(FRL) and maximum reservoir level(MRL). This is provided intentionally to be washed-out during high flood and to be reconstructed after the passage of flood. The objective of providing fuse plug in the design of earthen dam is to make the spillway much smaller in height to handle floods of lower return period compared to the maximum probable flood at substantial savings to the project cost. In an eventuality of failure of crest gates to operate in time it also serves as an emergency outlet.

project cost. In an eventuality of failure of crest gates to operate in time it also serves as an emergency outlet.

The causes of overtopping of flood over the embankment may be due to improper design criteria of determination of probable maximum flood (PMF) for the reservoir, sedimentation of reservoir, adopting the erroneous seasonal reservoir operational rules, or due to any unexpected flash flood.

Embankment breach process is three dimensional in nature where erosion occurs freely in vertical, lateral and longitudinal directions of flow. As such, understanding of the dam breach process i.e. breach hydraulics and breach morphology and breach erosion is of paramount importance to predict outflow hydrograph and sediment discharge. During the last 25 years, though substantial numerical models on dam breach problem have been developed, yet relatively much less attention has been given to study the mechanism of dam breach with experimental observation support. In an experimental set up the measurement of variation of one or more controlling breach variables with time and space can be made to study their effects on dam breach problem. The dam breach process is also related to sediment transport under highly accelerated flow conditions. The aspect of accelerated flow has not been addressed in almost all the numerical models. On the contrary, these numerical models rely on sediment transport formulae meant to be used in streams with uniform flow.

There is not much literature on the wash out of a fuse-plug. Dam breach process and fuse-plug wash out look outwardly to be same. Washout process in a fuse-plug is of two dimensional erosion where erosion occurs in vertical and longitudinal direction freely, erosion is restricted in lateral direction. This causes the flow characteristics to change.

The washout process involved in fuse plug may be taken as a preliminary study towards the understanding of dam breach process behaviour.

The present work, essentially a laboratory investigation, has been conducted in two parts, I and II.

Part I presents the mechanism associated with breach erosion process of homogeneous earthen embankment dam caused due to overtopping flow. From the results of the present investigation, a methodology has been suggested to analyse dam breach process behaviour.

Part II comprises of the experimental investigations of wash out process of fuse-plug in a dam body. A procedure has been suggested from the analysis of present experimental results to estimate the major parameters in the washout process.

The common variables involved in the part I and II studies can be grouped as:

i. *predictor variables* and ii. *criterion variables*. The predictor variables controlling the dam breach problem are the dam geometry, capacity of the reservoir and the inflow discharge to the reservoir. The criterion variables are the variables for which a predicted value is necessary in design. In the present problem criterion variables can be listed as the breach discharge, sediment discharge, duration of breach, time of occurrence of peak sediment, and water discharges and the terminal breach morphological variables like final breach width, final depth of erosion, final breach cross section. To relate the measured criterion variables to predictor variables in functional relations, the empirical constants are involved. These constants are called either *parameters* or *coefficients*. In the present problem of dam breach, the parameters / coefficients comes out of the properties of the dam fill material. These are cohesion ( $c$ ), angle of friction ( $\phi$ ), bulk density ( $\gamma_b$ ) and average grain size ( $d_{50}$ ) of the dam fill material.

With this in view experiments were carried out in Hydraulics laboratory of the Civil engineering Department of Indian Institute of Technology, Kanpur for both dam breach process and fuse plug wash out study. A 20m long tilting flume, 0.60m wide and of 0.50m height was used to conduct these experiments for both part I and part II studies.

In dam breach study, 17 number of experiments were carried out with varying model geometry and inflow to the reservoir. Out of these 17 number of experiments, 12 sets of models were constructed with fine *cohesionless* soil (type-A soil) and 5 sets of models were prepared with *cohesive* soil (type-B soil). The dam height were varied from 14.5 cm to 35cm keeping the upstream and downstream slope constant as 1V:2.5H for all the 17sets of models. The width of dam crest was varied from 15cm to 156 cm for the dam models with cohesionless soil, whereas it was kept constant as 15cm for all the five dam models with type-B soil. The angle of friction ( $\phi$ ), cohesion ( $c$ ), average bulk density of the soil ( $\bar{\gamma}_b$ ) for the soil fill embankment dam model of before overtopping of flow and the average grain size diameter( $d_{50}$ ) for these soils are given in the Table 0.1.

TABLE 0.1

**DESCRIPTION OF THE PROPERTIES OF SOIL USED IN DAM  
BREACH STUDIES AND FUSE PLUG WASHOUT**

Types of soil	$d_{50}$ (mm)	$\phi$ (degree)	C (KPA)	$\gamma_b$ gm/cc	w %	Remark
A	0.16	32.1	0.00	1.58	12	Cohesionless fine sand collected from River Ganga near Kanpur, India
B	0.28	33.1	1.60	1.98	14	Cohesive soil collected from I.I.T, Kanpur campus
C	0.18	29.2	0.85	2.03	15	Mix of Type-A and Type-B soil in the proportion 3:2
D	0.60	36.6	0.00	1.62	12	Coarse sand from River Yamuna at Kalpi 100km south of Kanpur
E	0.37	35.2	0.00	1.65	12	Mix of Type-A and Type-D soil in the proportion 1:1

$\gamma_b$  = bulk density of soil (used in dam or fuse plug) before overtopping

w = water content of soil in percentage

The range of constant incoming flow( $Q_{in}$ ) to the reservoir for dam model with *type-A* soil and *type-B* soil was  $169.7 - 1616 \times 10^{-6} \text{ m}^3/\text{sec}$  and  $940-6088.6 \times 10^{-6} \text{ m}^3/\text{sec}$  respectively. For all these 17 sets of dam models, the upstream edge of the top dam crest was kept at 8m from the inlet section of the flume. The measurement of the water level, sediment bed level and breach width along the dam cross section with time were carried out at six and eight selected stations, respectively for dam model with cohesionless and cohesive soils. These measurements were carried out by different persons using point gauges with common reference of time shown on an electronic digital clock.

In part II study, on fuse plug wash out, a model of earthen dam was made in wood with a rectangular breach section at the centre. The dam section had the dimensions as top width( $B_t$ ) 0.15m, bottom width ( $B_b$ ) 0.90m and height ( $H_D$ ) 0.145m with upstream and down stream slope as 1vertical to 2.5horizontal. The central rectangular breach section was 20cm width. In the present study the filled portion in the breach section of this model with compacted soil is called as fuse plug. Rajpal (1995) conducted *sixteen number* of experiments on the same fuse plug model with type-A ,type-B and type-C soil. These data are also included in the present

analysis. Here type-C soil is the mix of type-A and type-B in ratio of 3:2. In this part II experimental study two phases of experiments were conducted namely, phase-A and phase-B. The purpose of experiments of phase-B are discussed subsequently. The upstream edge of the dam was kept for all the experiments in phase-A and phase-B at 15m from the inlet section of the flume. The inflow variation was of the range of  $560.85-1267.8 \times 10^{-6} \text{ m}^3/\text{sec}$  and  $247.2-10838.3 \times 10^{-6} \text{ m}^3/\text{sec}$  for phase-A and phase-B studies respectively. In phase-B study coarse cohesionless sand (Type-D) and mix of type-A and type-D soil in 1:1 ratio (type-E), are used. In experiments on fuse plug the water levels were measured at 4 selected stations. The sediment bed profiles were marked on the two non-erodible sides of the fuse-plug at different intervals of time. This marking was carried out using coloured pencil. At an instant five persons made the observations at various locations.

## **Part I : Mechanism of Breach Process of Homogeneous Earthfill Dam due to Overtopping Flow**

The mechanism associated with dam breach process can broadly be categorised into three viz. a) Breach morphology b) Breach hydraulics and c) Breach erosion. These three aspects of dam breach are implicitly related to each other.

The breach morphology is analysed from the measured sediment level and the corresponding breach width at different selected sections. Depletion of the reservoir level during the breach process is continuously measured. From the measured longitudinal sediment bed profile and the eroded breach section, the volume of eroded sediment is computed. All criterion variables relating to breach flow and sediment discharge are computed from the three measured basic variables viz. water level, sediment bed level, and width of breach at different breach sections. Using some of the computed variables, along with known predictor variables like properties of dam fill and embankment geometry, various non-dimensional breach parameters are developed like  $V_{SRN}$ ,  $Q_{PN}$ ,  $Q_{APN}$ ,  $Q_{PSN}$ ,  $CAP_N$ ,  $\tau_{*c}$  which are very often used in the analysis. The flow over the erodible sediment crest is considered to be broad crested weir type of flow. The coefficient of discharge for the flow over the crest is analysed in terms of ratio of head acting over the spillway to the crest height. The breach

geometry, breach out flow hydrograph and breach sediment discharge graphs are analysed using measured flow information.

The analyses of data are carried out in four phases:

- a. for the model data of cohesionless soil,
- b. for the model data of cohesive soil,
- c. for the combined data of cohesive and cohesionless dam models, and
- d. for the field and lab data analysis.

The results of these analyses are compared with the observed values of two historical dam breach cases namely:

- i. Teton Dam, Idaho, U. S. A
- ii. Huaccoto Dam, Peru

The validated results include the following:

1. Breach peak outflow discharge( $Q_{wp}$ ).
2. Time of occurrence of peak outflow discharge( $t_{wp}$ ).
3. Final breach width, depth of erosion, slope of the final breach cross section at crest,  $\left((B_{cr})_f, D_{er} \text{ and } z\right)$  respectively.
4. Duration of breach( $t_{gs}$ ).
5. Breach outflow discharge hydrograph ( $t \sim Q_w$ ).

The simulated results of above breach variables for Teton dam and Huaccoto dam failure obtained from numerical model, BEED (Breach Erosion of Earthfill Dams) developed by V. P. Singh and P. D. Scarlatos for U. S. army Corps of Engineers (1989) are also compared with the present estimated results.

As there is no observed information on breach sediment discharge either for Teton Dam or Huaccoto dam, the simulated result of BEED model is taken for comparison with the present estimated values. This has been done only for Teton Dam case. These validated results are:

1. peak sediment discharge ( $Q_{sp}$ ),
2. time of occurrence of peak sediment discharge ( $t_{sp}$ ) and
3. sediment discharge during at any time of breach( $Q_s$ ).

Finally a methodology has been suggested to study the dam breach process for any given situation.

### Observations on Dam Breach Process

From the experimental study on dam breach the following critical observations are made.

- a. Planform of breach channel has contraction, throat and diverging sections. The position of throat moves upstream as the breach process continues. The cross section of breach during erosion will be almost trapezoidal in shape in the contraction section and rectangular at the throat and again trapezoidal in diverging section.
- b. The discharge over the breach crest can be simulated with the weir of erodible crest or spillway type of flow. The coefficient of discharge in the use of weir type formula is found to vary with ratio of head acting over the weir to the crest height of sediment bed profile. The magnitude of discharge coefficient found to decrease initially and later on remains constant.
- c. The rate of lateral and vertical erosion are high during initial phase of breach process and decrease as final state of breach occurs. The rate of lateral erosion is higher than the rate of vertical erosion in cohesive soil embankment and is reverse in the case of cohesionless soil embankment breach.
- d. The depth of erosion, width of erosion and lateral slope of bank at the crest vary with drop in water level between the upstream and downstream of the embankment during breach process. The final breach width varies with magnitude of peak flow discharge. The final depth of erosion varies mainly with height of the dam.
- e. The mean velocity of flow in a breach is a function of average hydraulic radius  $\bar{R}_h$  and average energy slope ( $\bar{S}_f$ ) and varies as:  $\bar{R}_h^{-0.28} \bar{S}_f^{0.34}$ . The flow velocity at downstream top edge of the embankment varies with critical velocity of flow and water surface slope.
- f. Sediment discharge intensity  $q_s$  is found to vary with water discharge intensity with a power as  $q_s^{1.43}$  and sediment load per unit width varies as the square of average bed shear stress for dam model with cohesionless soil. But in a generalised analysis for any type of



soil fill it varies in a quadratic form with the square of average shear velocity along with  $Q_{PSN}$  and  $V_{SRN}$  numbers.

- g. Relative energy loss in the breach is found to vary with average water surface slope, square root of  $Q_{PSN}$  number along with average shear velocity.
- h. The final breach geometry like breach width( $B_{cr}$ )<sub>f</sub>, depth of erosion( $D_{er}$ ) and flow parameters like peak water discharge( $Q_{WP}$ ) and sediment peak discharge( $Q_{SP}$ ) and their time of occurrence  $t_{wp}$  and  $t_{sp}$  respectively and time of breach  $t_{95}$  are analysed using lab data and field data. The functional relations are developed based on the geometry, soil properties of embankment, reservoir capacity and inflow characteristics into the reservoir. Two field dam breach failure data are included in the analysis.
- i. The variation of outflow hydrograph and sediment discharge graph based on the shape of hydrograph is presented. The validation of these functional relations are strengthened by including two field breach data of Teton dam and Huaccoto dam in the analysis.
- j. A method in the form of algorithm and a flow chart is presented for computation of variation of breach geometry, flow discharge, sediment discharge during the breach process and at the final stage of breach.

The details of breach process evolved from the experimental study will be of helpful in getting a good insight into the mechanism of breaching and in the development of a better numerical model for dam breach.

## **Part II : Study on Washout Process of Fuse Plug**

The experiments were conducted in two phases for Fuse-plug washout study.

**Phase-A** This phase of the study refers to the experiments which were conducted to know the mechanism of wash out of the fuse-plug. The major objectives of this part of study were to obtain the following viz. a) water level variations in the reservoir, b) water level variation over the fuse-plug model and c) sediment bed variation with respect to time. With these three basic information, the involved mechanism in soil-water interaction under highly dynamic condition like washout process of fuse-plug are analysed. In this phase, *six number* of experiments (with cohesionless fuse-plug fill) were carried out. In the analysis, Rajpal

(1995)'s data obtained from *sixteen numbers* of experiment on this fuse-plug model with cohesive and cohesionless soil fill are used. The inflow discharge were varied keeping the fuse-plug geometry constant.

**Phase-B** The second phase of experiments were carried out on *rigid bed profile analogous* to the instant erodible bed profile of fuse-plug wash out. For this purpose six erodible profiles of run number 1404 were chosen and experiments were carried out with different  $h_u/h_{cm}$  condition by varying inflow discharge to the reservoir. Here,  $h_u$  is head acting over the crest and  $h_{cm}$  is crest height of washout profile. In this category altogether 35 experiments were carried out. The main objective of these experiments were:

- a. to verify outflow discharge relation for a erodible bed of constant width
- b. energy loss characteristics during wash out of the fuse-plug.

In an effort to know the effect of particle size on energy loss characteristics in wash out process, four number of experiments were conducted with coarse( $d_{50}=0.6\text{mm}$ ) cohesionless soil.

### Analysis of Fuse Plug Washout Process

From the rate of depletion of reservoir water level, two scales viz. *reservoir time scale* and *reservoir drop scale* were obtained. These two scales and other non-dimensional parameters like  $X_{22}$ ,  $Q_{PN2}$  are extensively used in the analysis to know the rate of sediment crest erosion and sediment discharge characteristics. Finally, a procedure is suggested for the prediction of wash put process of fuse-plug. The sediment discharge ( $Q_s$ ) and water discharge ( $Q_w$ ) can be computed at any time using the suggested methodology in addition to other erosional features of the fuse plug washout.

### Observations on Fuse Plug Washout

1. The flow hydraulics over the crest of erodible bed profile does not follow weir formula, rather the outflow discharge depends on head of water( $h_u$ ) over the crest and its height( $h_{cm}$ ).
2. Reservoir drop scale ( $H_*$ ) and time scale ( $T_*$ ) are two most important parameters controlling the washout behaviour of the fuse plug.
3. Rate of crest height erosion ( $dh_{cm}/dt$ ) with time depends on incoming flow velocity  $\sqrt{2gh_u}$  and its maximum value  $(dh_{cm}/dt)_{\max}$  varies with  $q_{wp}^3$ , where  $q_{wp}$  is peak outflow discharge intensity.

4. Sediment concentration ( $C=q_s/q_w$ ) is almost independent of average bed shear velocity  $\bar{V}$ . However, it is found to be a function of drop in water level between upstream and downstream of dam  $\Delta H$ .
5. Sediment concentration during the washout of fuse plug and the ratio of energy in the downstream ( $E_2$ ) to upstream ( $E_1$ ) of fuse plug, ( $E_2/E_1$ ) are functions of  $h_u/h_{cm}$ .
6. From the experiment in phase-B the discharge relation for flow over nonerrodible fuse-plug crest follows the weir type relation with discharge varying with head acting over the crest  $h_u$  as  $h_u^{3/2}$ . This observation confirms the variable nature of discharge coefficient  $c_d$  in washout process is due to the crest erosion.
7. Explicitly energy loss due to erosion and transport of sediment is related with sediment concentration( $C$ ) for type-A soil.
8. The duration of washout( $t_{gs}$ ) is found to be varying between 1 to 2.5 times of  $T_*$  depending on inflow discharge, soil resisting velocity and height of the fuse plug.
9. The ratio of time of occurrence of sediment peak discharge ( $t_{sp}$ ) to time of occurrence of peak water discharge ( $t_{wp}$ ) vary inversely to the square root of peak water discharge intensity.
10. Peak water discharge intensity ( $q_{wp}$ ) is proportional to nearly square root of inflow discharge intensity( $\bar{q}_{in}$ )

The results of the present study have a direct bearing on field applications. An insight into the basic process involved in the dam breach and washout of fuse plug has helped in suggesting the methodology to predict the breach geometry, water discharge and sediment discharge during breach erosion. It is hoped that the insight knowledge obtained through this experimental study will help in better understanding of the flow mechanism involved in the breach process. The evolved functional relations among the breach variables will enable one to formulate the numerical model on dam breach and fuse plug wash out in better scientific and more logical way.

dedicated  
to my late father

*Choudhury Pratap Chandra Das*

# ACKNOWLEDGMENTS

On completion of the thesis, I take this opportunity, with pleasure, to place on record my profound sense of gratitude and indebtedness to Prof. T. Gangadharaiah, my teacher and thesis supervisor for his unfailing support and constant encouragement that he has bestowed on me and also for his tremendous patience with which he has attended to my work. I admit, he has been a hard task master which to my advantage helped to gain confidence to work independently. My association with him has been extremely remarkable and fruitful not only from academic point of view but also to imbibe the qualities he possesses as a person. After all, to me, he has been like a father figure.

The stimulating and informal atmosphere of the Hydraulics and Water Resources Engineering section, Civil Engineering Department has been a great help to me. It has been a great pleasure to learn and study in association with Prof. S. Ramaseshan, Prof. K. Subramanya, Prof. S. Surya Rao, and Prof. Bithin Datta.

I would also like to thank Prof. B. S. Murty, Prof. P. K. Basudhar and Prof. A. K. Gupta for giving me useful suggestions and taking interest in my work.

I am also thankful to Prof. Vijay P. Singh, Louisiana State University, U.S.A and Prof. Erich J. Plate, Karlsruhe University, Germany for their encouragement through letters.

Thanks are due to the staff of Hydraulics lab in particular to Shri Kalyan Das, Shri Ram Shanker, Shri Sitaram and Sandeep. The help and cooperation extended by the staff of Geotech Engineering lab is gratefully acknowledged.

I am thankful to Mr. Nirmal Roberts for photographing the details of the phenomenon under study with much care and patience. With regards, I convey my special thanks to Shri Suresh Kumar for his help in reading the proofs which gave me enough confidence.

I am grateful to my parent university, OUAT, Bhubaneswar for having deputed me to this institute for my Ph.D. I express my gratitude to Dr. S. C. Mishra, Dean, College of Engineering and Technology, who has always been a source of inspiration for me, encouraged me at all stages of the work. I am also thankful to my colleagues at CET, Bhubaneswar: Captain P. K. Sahoo, Prof. H. N. Dash, Prof. K. C. Patra, Umesh Mishra, Falgunee, Ranjeet, Pravat K. Parhi, Hemanta, and Sarat, to mention some of them.

I express my sincere feelings to Mrs Gangadharaiah for her kind support and keen interest she showed to my family. We will cherish all your care for time to come.

I am thankful to Chitta and his family for the hospitality during the stay at SBRA.

I consider myself extremely fortunate to have friends like Himanshu Shee, Debasish Nanda(Badal) at Bhubaneswar, my childhood friend Ananda, friends at IITK: Ashok Nayak, Kamalakanta Mohapatra, S. Dandapat, Pranab, Vivekananda Singh, Siby, and P. S. Mahar . I must acknowledge the courtesy and interest with which they responded to me.

I should like to express my acknowledgment of the help I received from my friends in the lab, mainly Rajpal S. Verma, Ravi Bhushan, Waheed and Prasad Rao. I am also thankful to Mrs Nazima, research associate for all possible helps from her.

The help from R. Seshagiri Rao needs a special mention. Thank you very much Giri !

It was my great pleasure to share and discuss the views and ideas with Baldev Setia.

Words and space are not real tribute to the blessings and countless sacrifices of my parents. Whatever I am today, it is their encouragement and unseen prayer of silence at God for me. My father-in-law Shri Ullash chandra Samantaray and mother-in-law have willingly taken up tasks to make me feel comfortable. Their inspiring presence has been instrumental in uplifting my confidence. My brothers Jyotish, Nagen, *bhai* Kishore and sister Rupashree Ragini, my brother-in-laws Alok and Arun also stood by me throughout my work.

The immense patience and understanding of my wife Sasmita has been a source of strength for me. Finally, my feelings to my son *Prayas* who made his presence felt at the fag end of this thesis work.

**Pradip Kumar Das**

# CONTENTS

	Page
CERTIFICATE	ii
SYNOPSIS	iii
ACKNOWLEDGMENTS	xiv
CONTENTS	xvi
LIST OF FIGURES	xxiii
LIST OF TABLES	xxxiii
LIST OF SYMBOLS	xxxv
DEFINITIONS	xl
 CHAPTER I	
INTRODUCTION	1
1.1. An Overview of Dam Breach	1
1.2. Concept of Fuse Plug	3
1.3. Types of Dam Failures	3
1.4. Causes of Overtopping of Flood	3
1.5. Necessity for Dam Breach Study	5
1.6. Variables and Parameters Involved in the Problem	6
1.7. Present Status of Knowledge on the Dam Breach	7
a. Erodibility	7
b. Mechanics of Breach Formation	7
c. Hydraulics of Breach Flow	8
d. Breach Morphology	8
e. Erosion of Sediment and its Transport	9
f. Stability of Breach Slope	9
1.8. Aims of the Present Study	9
1.9. Organisation of Thesis	10

<b>CHAPTER II</b>	<b>REVIEW OF LITERATURE</b>	<b>11</b>
	2.1. Introduction	11
	2.2. Experimental Observations	12
	2.3. Field Observations	14
	2.4. Empirical Model	14
	2.5. Mathematical Modelling	17
	a. Reservoir Hydraulics.	18
	b. Breach Hydraulics	18
	c. Breach Geometry	19
	d. Sediment Transport	20
	e. Breach Slope Collapsing	20
	f. Downstream Flood Routing	21
	2.6. Ancillary Literature Relating to Dam Breach	22
	2.7. Fuse Plug	24
	2.8. Scope for the Present Study	26
<b>PART I</b>	<b>BREACH EROSION OF HOMOGENEOUS EARTHFILL DAMS DUE TO OVERTOPPING FLOW</b>	<b>27</b>
<b>CHAPTER III</b>	<b>SCHEME OF EXPERIMENTATION ON DAM BREACH</b>	
	3.1. Scheme of Experiments	29
	a. Details of Flume	29
	b. Model Details	31
	i. Embankment Dam Models with Cohesionless Soil	31
	ii. Embankment Dam Model with Cohesive Soil	32
	c. Properties of Soil used in Embankment Model	33
	d. Preparation of Embankment Dam Model	33
	3.2. Some Observations of the Breach Process	35
	a. Observation on Erosion process due to Overtopping Flow in Cohesionless Soil Embankment Dam.	35
	b. Erosion Process due to Overtopping of Flow on the Cohesive Soil Embankment	46
	3.3. Data Collection	46
	a. Measurement of Breach Data During Breach Process	46
	b. Final Measurements After the Attainment of Complete Breach Process	48
	c. Basic Data Presentation for the Embankment dam Model of Cohesionless Soil	50



d. Basic Data Presentation for the Embankment dam of Cohesive Soil	50
3.4. Computation of Parameters Controlling Breach Process	50
a. Flow Parameters	50
b. Sediment Parameters	57
3.5. Frequency Analysis of Deviations of Data From the Mean Value.	58
3.6. Concluding Remarks	58

## CHAPTER IV

<b>MECHANISM OF DAM BREACH PROCESS</b>	62
4.1. General	62
4.2. Parametric Formulation	63
a. Breach Hydraulics	63
b. Breach Morphology	63
c. Time Components of Breach	64
d. Energy Loss Parameters	64
e. Sediment Transport Parameters	64
4.3. Analysis of Breach Process in Cohesionless Soil Embankment	65
a. Breach Morphology	66
i. Morphological Variations of Breach	66
ii. Breach Cross-sectional Variation with Time	67
b. Breach Hydraulics	71
i. Discharge Characteristics	71
ii. Computation of Head of Water Acting Over the crest of Weir	73
iii. Breach Average Velocity	76
iv. Flow Velocity at the downstream top edge of the Embankment	79
v. Breach Hydrograph	82
vi. Energy Loss During the Breach Process	85
c. Breach Erosion	88
i. Variation of Sediment Bed Profile with Time.	88
ii. Variation of Crest Height ( $h_{cm}$ )	88
iii. Rate of Crest Height Variation	96
iv. Variation of Sediment Bed at the Downstream top Edge of the Embankment	98
v. Lateral Erosion at the Crest	98
vi. Rate of Lateral Erosion of Crest	103
vii. Variation of Width of downstream top Edge of the Embankment	106
viii. Variation of Sediment Volume	109
ix. Variation of Sediment Discharge Intensity	109
x. Variation of Sediment Concentration	111

xi. Sediment Load Computation	113
4.4. Analysis of Cohesive Soil Embankment	115
a. Breach Morphology	115
i. Breach Planform Variation	115
ii. Variations of Bed and Flow Profiles Along the Flow in the Breach	117
iii. Breach Cross-Sectional Variations	117
b. Breach Hydraulics	119
c. Breach Erosion	122
i. Rate of Crest Variation	122
ii. Variation of Crest Width	124
iii. Rate of Width Erosion of Cohesive Soil Embankment Model	126
iv. Rate of Variation of Cross-Sectional Area at Crest ( $A_{cr}$ )	127
d. Comparative Study Between Cohesionless and Cohesive Soil Embankment Breach Observations.	127
4.5. Analysis of Breach Process for Cohesive and Cohesionless Soil Embankments	132
a. Variation of Water Surface in the Reservoir	132
b. Variation of Reservoir Water Level in Relation to Downstream Water Level	134
c. Variation of Crest Height	138
d. Rate of Crest Height Erosion	141
e. Variation of Head of Water Over the crest	145
f. Variation of Energy Loss During the Breach Process.	150
g. Sediment Load Variation	150
h. Variation of Sediment Concentration.	152
4.6. Analysis of Laboratory Data along with Field Data.	155
a. Peak Outflow Discharge	155
b. Depth of Erosion	155
c. Top Width of Erosion	157
d. Relation Between Breach Froude Number and Breach Shape Factor	158
4.7. Discussion of the Results	159
a. Breach Morphology	159
b. Breach Hydraulics	160
c. Breach Erosion	161
4.8. Concluding Remarks	161

<b>CHAPTER V</b>	<b>COMPARISON OF DAM BREACH RESULTS WITH TETON AND HUACCOTO DAMS</b>	<b>163</b>
	5.1. Introduction	163
	a. Teton Dam	164
	b. Huaccoto Dam	166
	c. BEED Model	167
	d. Breach Variables to be Compared	168
	5.2. Comparison of Estimated Breach Variables	172
	a. Duration of Breach	172
	b. Peak Breach Outflow Discharge	173
	c. Time of Occurrence of peak outflow Discharge	175
	d. Width of Breach	175
	e. Depth of Breach	178
	f. Side Slope of the Final Breach Cross-Section	178
	g. Peak Sediment Discharge Intensity	179
	h. Time of Occurrence of Sediment Peak Discharge	182
	5.3. Influence of Average Inflow Discharge, Capacity of Reservoir, and Cross-Sectional Area of embankment on Final Breach Morphological Parameters	184
	5.4. Breach Hydrograph	187
	5.5. Breach Sediment Discharge with Time.	196
	5.6. Suggested Procedure to Compute the Dam Breach Process	199
	a. Methodology for Computation of Parameters Governing the Breach Process.	199
	b. Method to Compute Breach Hydrograph and Breach Sediment Discharge Graph.	202
	c. Comparison of Overall Estimated Breach Parameters.	202
	d. Flow Chart for Computation of Breach Process.	203
	5.7. Discussion of Results and Method of Computation	208
	a. Discussion of Results	208
	b. Comments on the Procedure to compute Dam Breach Process.	208
	c. Limitations of the Present Approach	209
	5.8. Concluding Remarks	210
<b>PART II</b>	<b>WASHOUT PROCESS OF FUSE PLUG</b>	<b>211</b>

## CHAPTER VI

### SCHEME OF EXPERIMENTS ON FUSE PLUG WASHOUT

6.1. Details of Flume and Fuse-Plug Model	214
a. Fuse-Plug Model Preparation	214
b. Source of Soil Used for the Preparation of Fuse-Plug	217
c. Preparation of Fuse-Plug Model	219
6.2. Experimental Procedure	219
a. Aim of the Study	219
b. Basic Data Collected	220
i. Water Surface Variation	220
ii. Sediment Bed Profiles	220
6.3. Method of Computation of Basic Variables	222
a. Breach Water Discharge ( $Q_w$ )	222
b. Sediment Discharge ( $Q_s$ )	222
6.4. Details on the Number of Experimental Conducted.	225

## CHAPTER VII

### ANALYSIS AND RESULTS OF WASHOUT PROCESS OF FUSE PLUG

7.1. Reservoir Time Scale and Length Scale	228
7.2. Outflow Discharge Relation	233
7.3. Erosional Characteristics of Sediment Crest and Bed Profiles	235
a. Crest Location	235
b. Sediment Bed Profile Downstream of Crest	235
c. Crest Level Variation with Time.	239
d. Rate of Crest Erosion	239
7.4. Erosion Velocity	243
7.5. Sediment Discharge Characteristics	246
a. Sediment Concentration	246
7.6. Analogous rigid Bed Profile study	251
a. Discharge Characteristics	251
b. Energy Loss Characteristics	253
7.7. Hydrograph and Sediment Discharge Graphs	256
a. Variation of Water Discharge Intensity with Time	256
b. Sediment Discharge Intensity with Time.	261
c. Time of Erosion	264
7.8. Methodology to Predict Washout Process of Fuse-Plug	265
a. Procedure to Predict Washout Variables	265
b. Prediction of Water and Sediment Discharge During Washout Process	266
c. Flow Chart	266

7.9. Conclusions and Limitations	268
----------------------------------	-----

## CHAPTER VIII

<b>CONCLUSIONS AND RECOMMENDATIONS</b>	270
8.1. General	270
8.2. Dam Breach Process	271
a. Morphological Characteristics	271
b. Discharge Characteristics of Flow	272
c. Erosional Characteristics of Breach	272
d. Flow Characteristics	273
e. Sediment Transport Characteristics	274
f. Energy Loss Characteristics	275
g. Final Breach Dimensions Based on Laboratory Data and Field Data	275
h. Major Criterion Variables Controlling the Breach Process	276
i. Methodology to Predict Breach Process.	277
8.3. Washout Process in Fuse Plug	278
a. Outflow Discharge Relation	279
b. Washout Profile Characteristics	279
c. Sediment Transport Characteristics	280
d. Energy Loss Characteristics	281
e. Hydrograph and Sediment Discharge	281
f. Outflow Hydrograph Characteristics.	281
8.4. Suggestion for Further Work	282

REFERENCES	283
APPENDIX	288

# LIST OF FIGURES

Figure	Title	Page
1.1	Simulation of dam breach phenomena due to overtopping flow in laboratory	2
1.2	Schematic diagram for possible location of fuse plug	4
3.1	(a). Plan view of tilting flume with dam model	30
	(b). Sectional elevation of tilting flume with dam model	30
	(c). Particle size distribution of soil types- A and B	34
3.2	(a). Flow of reservoir water on the dam crest after overtopping, just eroding downstream top edge of the embankment.	36
	(b). Flow of water on the downstream slope of the dam just after the overtopping	36
	(c). Initiation of erosion near toe of the dam	37
	(d). Lateral enlargement of erosion at toe of the dam and formation of gully on downstream slope of the embankment.	37
	(e). Receding of toe erosion in upstream direction	38
	(f). Deep vertical cut in the downstream face of the dam along with receding of toe erosion in upstream direction.	38
	(g). Widening of the path of erosion on downstream slope of the dam with steeper vertical fall and bank collapse	40
	(h). Under scouring on the downstream slope of the dam with breach channel having contraction section upstream and diverging section downstream with a throat are visible	40
	(i). Widening of the breach channel by bank collapse spillway type crest formation are visible	41
	(j). Washout of bank collapsed soil contracted throat, spillway type of crest flow at upstream are visible	41
	(k). Widening of flow path of water contracted throat, spillway type of crest flow are visible	42
	(l). Spillway type flow over the erodible crest with large width at	42

	upstream edge, contraction at the centre and enlargement of breach width at downstream and are visible	
	(m). Flow over the crest behaves like flow over erodible spillway	43
	(n). Pool-formation at downstream of erodible crest and flow associated hydraulic jump	43
	(o). Widening of breach with pool formation at downstream of the crest, and hydraulic jump formation at toe erodible spillway at the upstream.	44
	(p). Curved crest spillway type flow, hydraulic jump form at the toe of the spillway flow more lateral erosion on side bank are visible	44
	(q). Reduction in reservoir level lateral erosion touching one side of the flume, flow concentration on one side are visible	45
	(r). State of breach channel process nearing to the final state of erosion is observed	45
3.3	(a). Longitudinal cross section showing location of selected measuring sections for cohesionless soil embankment models	47
	(b). Longitudinal cross-section showing location of selected measuring sections for cohesive soil embankment models	49
3.4	(a). Variation of water level in the reservoir, at section-1 along with crest variation at section-2 with time	52
	(b). Variation of water level and sediment bed level at section-2 with time	52
	(c). Variation of water level and sediment bed level at section-5 with time.	52
	(d). Variation of water level at section-6 with time	52
	(e). Variation of sediment bed level at section-3 with time	52
	(f). Variation of sediment bed level at section-4 with time	52
	(g). Variation of breach width at section-2 with time	53
	(h). Variation of breach width at section-3 with time.	53
	(i). Variation of breach width at section-4 with time	53
	(j). Variation of breach width at section-5 with time	53
3.5	(a). Variation of reservoir water levels with time at sections-1 and 2	54
	(b). Variation of water surface levels with time at section-3	54
	(c). Variation of water surface and sediment bed levels at section-4 with time	54
	(d). Variation of water surface and sediment bed levels at section-5 with time	54
	(e). Variation of water surface and sediment bed levels with time at section-6	54
	(f). Variation of water surface and sediment bed levels with time at section-7	54
	(g). Variation of water surface and sediment bed levels with time at section-8	55
	(h). Variation of breach width at section-4 with time	55
	(i). Variation of breach width at section-5 with time	55
	(j). Variation of breach width at section-6 with time	55
	(k). Variation of breach width at section-7 with time	55
	(l). Variation of breach width at section-8 with time	55

3.6	Definition sketch for the terms used in dam breach analysis	56
3.7	(a). Recorded water levels at section - 6 with time (Sample data)	59
	(b). Frequency analysis for deviations of water level ( $h_w$ ) measurement from the mean curve during the breach process (for Fig. 3.18(a))	59
3.8	(a). Recorded sediment bed levels at section - 4 with time (Sample data)	60
	(b). Frequency analysis for deviations of sediment bed level ( $h_c$ ) measurement from the mean curve during the breach process (for Fig. 3.8(a))	60
3.9	(a). Recorded breach width at section - 2 with time (sample data)	61
	(b). Frequency analysis for deviations of measurement of breach width from mean curve during the breach process (for Fig. 3.9(a))	61
4.1	A typical breach hydrograph for run no. 0405	66
4.2	(a), (b), (c), (d) The variation of water surface levels, sediment bed levels and breach width along the longitudinal direction of the dam model of cohesionless soil, Run no 0405: before, at and after breach peak discharge	68
4.3	Variation of breach cross-sectional area before, at and after peak discharge ( $Q_{WP}$ )	69
4.4	Variation of eroded area with time at upstream edge of the embankment	70
4.5	Variation of cumulative eroded sediment volume with time for run no. 0405	70
4.6	Different phases of flow defined during the breach process	72
4.7	(a). Relation between head of water over the erodible crest, ( $h_u$ ) and breach outflow discharge intensity, $q_w$ for dam models of cohesionless soil	74
	(b). Relation between discharge coefficient ( $c_d$ ) and the ratio of head of water over erodible crest to the crest height at any time of breach.	74
4.8	(a). Frequency of deviation of discharge coefficient from weir formula (Cohesionless soil)	75
4.9	A typical variation of head of water ( $h_u$ ) over erodible crest with time for run no. 1005, dam model with cohesionless soil	77
4.10	(a). Variation of normalised head of water ( $h_u/h_{up}$ ) with normalised time	77
	(b). Nondimensional variation of maximum water level over the erodible crest, ( $h_{up}$ ) with average inflow discharge to the reservoir, height of dam ( $H_D$ ), and dam cross-sectional area ( $A_D$ )	77
	(c). Functional relation of $t_{hup}$ with $t_{95}$ , $h_{up}$ and $H_D$	77
4.11	(a). Variation of average breach flow velocity ( $V_w$ ) <sub>av</sub> with average breach hydraulic radius ( $R_h$ ) <sub>av</sub>	78
	(b). Variation of average breach flow velocity ( $V_w$ ) <sub>av</sub> with average breach energy gradient ( $S_f$ ) <sub>av</sub>	78
	(c). Variation of nondimensional average breach flow velocity with nondimensional drop of water at crest	80
	(d). Comparison of Manning's equation in breach flow	80
4.12	(a). Variation of nondimensional breach flow velocity at downstream edge of the dam to the critical flow velocity at that section with average water surface gradient ( $S_w$ ) <sub>av</sub> .	81
	(b). Variation of the ratio of downstream edge breach velocity to the	83



	downstream shear velocity with average water surface gradient ( $S_w$ ) <sub>av</sub>	
4.13	(a). A typical breach outflow hydrograph for run no. 1005	84
	(b). Nondimensional breach outflow with nondimensional time	84
4.14	(a). Variation of nondimensional breach energy loss with drop in water level between upstream and downstream of the dam, $\Delta H$	86
	(b). Variation of nondimensional drop in water level between upstream and downstream ( $\Delta H$ ) with nondimensional time	87
4.15	(a). A typical variation of sediment bed profile for run no. 1005, ( $H_D=35\text{cm}$ ), dam model with cohesionless soil	89
	(b). A typical variation of sediment bed profile for run no. 3004, ( $H_D=14.5\text{cm}$ ), dam model with cohesionless soil	89
4.16	(a). Nondimensional variation of sediment bed height ( $h_c$ ) at any location of breach with its nondimensional distance, $X$ from heel of the dam (for dams of height=19.5cm, 30cm and 35cm)	90
	(b). Nondimensional variation of sediment bed height ( $h_c$ ) at any location of breach with its nondimensional distance, $X$ from heel of the dam (for dams of height=14.5cm)	90
4.17	(a). Nondimensional variation of crest of erodible sediment bed, $h_{cm}$ at any time of breach with its nondimensional time of occurrence	91
	(b). Variation of time scale $t_{50}$ in nondimensional form with $Q_{APN}$ number	93
	(c). Variation of final depth of erosion at crest, ( $D_{cr}$ ) in nondimensional form with peak breach discharge ( $Q_{WP}$ ) and height of the dam ( $H_D$ )	93
	(d). Variation of final depth of erosion at crest, ( $D_{cr}$ ) in nondimensional form with average inflow discharge to the reservoir, height ( $H_D$ ) and cross-sectional area, ( $A_D$ ) of the dam	94
	(e). Variation of nondimensional depth of erosion at any time, ( $H_D-h_{cm}$ ) with nondimensional drop of water level at the crest	95
4.18	(a). Variation of rate of crest height, ( $dh_{cm}/dt$ ) with drop flow velocity, $(2gh_d)^{0.5}$	97
	(b). Variation of rate of crest height, ( $dh_{cm}/dt$ ) with crest flow velocity, ( $V_{WC}$ )	97
	(c). Variation of rate of nondimensional rate of crest height, ( $dh_{cm}/dt$ ) with nondimensional drop of water at that section	99
	(d). Variation of sediment bed height at downstream edge of the dam with drop of water level at that section in a nondimensional form	99
4.19	(a). Comparison of rate of crest height erosion to its lateral erosion with time in a nondimensional form	101
	(b). Variation of nondimensional breach crest width at any time of breach, ( $B_{cr}$ ) with nondimensional drop of water at crest	101
	(c). Variation of nondimensional final breach crest width, ( $B_{cr}$ ) <sub>f</sub> with $Q_{PN}$ number	102
4.20	Variation of nondimensional breach crest width at any time of breach with drop in water level between crest and toe of the dam, $\Delta H_c$ and $Q_{PN}$	102
4.21	(a). Variation of rate of lateral erosion with time	104
	(b). Variation of rate of lateral erosion with nondimensional time	104

	(c). Variation of nondimensional crest width erosion with its nondimensional crest flow velocity	105
4.22	(a). Variation of nondimensional breach width erosion at the downstream top edge of the dam with nondimensional water drop between upstream and downstream of the dam, $\Delta H$	107
	(b). Variation of rate of breach width at downstream top edge of the dam with the flow velocity at that section	107
	(c). Comparison of variation of width of erosion at crest and the downstream top edge of the dam with nondimensional time	108
4.23	(a). Variation of nondimensional cumulative eroded sediment volume by cumulative flow of water in breach section with nondimensional time	110
	(b). Variation of sediment discharge intensity, ( $q_s$ ) with breach water discharge intensity, ( $q_w$ )	110
	(c). Variation of sediment discharge intensity, ( $q_s$ ) with square of the average shear velocity ( $V_*^2$ ).	112
	(d). Variation of sediment concentration with drop in water level $\Delta H$ .	112
4.24	Variation of sediment with nondimensional shear velocity	114
4.25	a, b, c, d. Variation of water levels, sediment bed levels and breach width along the longitudinal direction of dam breach at different time for cohesive soil embankment model	116
4.26	Variation of eroded cross sectional area of measuring sections - 5, 6, and 7 before, at and after breach peak discharge for dam made of cohesive soil, Run no. 0405	118
4.27	(a). Relationship between head of water ( $h_u$ ) over crest of erodible sediment bed with breach outflow discharge ( $Q_w$ )	120
	(b). Variation of discharge co-efficient ( $c_d$ ) with the ratio of erodible crest to its height at any time of breach	120
	(c). Frequency analysis for computed discharge coefficient $C_d$ for the data in Figure 4.27(b) in bar chart form	121
4.28	(a). Variation of rate of crest height with time in a nondimensional form	123
	(b). Variation of crest height with drop in water level between upstream and downstream of the dam, $\Delta H$ , in a nondimensional form	123
4.29	(a). Variation of the ratio of crest width to height of the dam with nondimensional drop of water at crest	125
	(b). Relative variation of breach crest width to breach width at section - 7 with time in nondimensional form	125
4.30	(a). Variation of rate of width erosion at crest for cohesive soil model with time	126
	(b). Variation of nondimensional rate of breach width with nondimensional time for cohesive soil embankment dam	128
4.31	Variation of nondimensional eroded crest area ( $A_{cr}$ ) with nondimensional drop in water level between upstream and downstream of the dam, $\Delta H/H_D$	128
4.32	(a). Comparison of the variation of crest level of erodible sediment bed for the breach model of cohesionless and cohesive soil embankment dams.	129
	(b). Comparison of the variation of head of water level over the crest of erodible sediment bed for breach model of cohesionless and cohesive	129

	soil embankment dams	
	(c). Comparison of the variation of crest width of erodible sediment bed for the dam breach model of cohesionless and cohesive soil embankment dams	129
4.33	(a). Comparison of the rate of variation of crest height of erodible sediment bed for the dam breach model of cohesionless (type A) and cohesive soil (type B)	131
	(b). Comparison of the rate of variations of crest width of erodible sediment bed for the dam breach model of cohesionless (type A) and cohesive soil (type B)	131
4.34	(a). Variation of normalised reservoir water level ( $h_{wr}$ ) by its maximum value with normalised time	133
	(b). Variation of $\beta$ , the X-intercept at $y=0.7$ in Figure 4.34 (a) for different runs of experiments on dam breach model of cohesive and cohesionless soil with $\lambda$ , as a function of peak outflow discharge, soil resisting velocity and the height of dam.	135
	(c). Variation of reservoir time scale ( $t_*$ ) with peak breach outflow discharge, height of the dam and its cross sectional area	135
	(d). Variation of reservoir water level ( $h_{wr}$ ) with time in a nondimensional form along with $V_{SRN}$ and $Q_{PSN}$ number	135
4.35	(a). Variation of normalised water level difference ( $\Delta H$ ) between upstream and downstream of the dam model with time in nondimensional form.	137
	(b). Variation of $\Omega$ , X - intercept at $y=0.7$ in Figure 4.35 (a), with parameter K	139
	(c). Variation of reservoir drop time scale ( $t_{**}$ ) with peak breach outflow discharge, height of the dam and its cross sectional area	139
	(d). Variation of water level difference ( $\Delta H$ ) between upstream and downstream of the dam with time in a nondimensional form	140
4.36	Variation of nondimensional crest height of erodible sediment bed at any time, ( $h_{cm}$ ), with $\chi$ , a function of nondimensional drop in water level, $\Delta H$ and soil resisting number, $V_{SRN}$	142
4.37	(a). Variation of exponent $n_{22}$ with soil resisting velocity number, $V_{SRN}$	143
	(b). Variation of $k_{22}$ , sediment erosion coefficient, with soil resisting velocity number $V_{SRN}$	143
	(c). Variation of nondimensional rate of erosion of crest height, $h_{cm}$ , with $\Delta H$ and $V_{SRN}$	144
4.38	(a). Variation of normalised head of water over erodible crest of sediment bed with corresponding normalised time	146
	(b). Variation of normalised head of water over erodible crest of sediment bed with normalised reservoir water level	148
	(c). Variation of exponent, $\eta$ of the equation 4.20 (a) with soil resisting velocity number, $V_{SRN}$	148
	(d). Variation of scale $RL_*$ with soil resisting number $V_{SRN}$	149
	(e). Variation of ratio of crest height ( $h_{cm*}$ ) to reservoir level, ( $h_{wr}$ ) at value of $h_{up}$ , with soil resisting velocity number, $V_{SRN}$	149
4.39	Variation of nondimensional energy loss, $\Delta E$ with nondimensional $\Delta H$	151

4.40	Variation of nondimensional sediment load, $g_s^*$ , with nondimensional bed shear stress	153
4.41	Variation of nondimensional sediment concentration ( $C_s$ ) with $h_u$ , $\Delta H$ , $L_{DB}$ , $V_*^2$ and $Q_{PSN}$	154
4.42	Variation of peak breach water discharge ( $Q_{WP}$ ) with capacity of the reservoir and height of the dam ( $H_D$ ) for both lab and field data	156
4.43	(a). Variation of final depth of erosion with height of the dam	156
	(b). Relation between nondimensional $D_{cr}$ with nondimensional reservoir capacity	156
4.44	Final breach width variation with peak discharge, height dam and capacity of reservoir	157
4.45	The relation between breach Froude number ( $F_b$ ) with breach shape factor ( $S_f$ )	158
5.1	(a). Cross-sectional details of Teton dam	165
	(b). Cross-sectional view of Huaccoto dam natural dam built by landslide material	165
5.2	Variation of nondimensional duration of breach ( $t_{95}$ ) with soil resisting velocity number ( $V_{SRN}$ )	174
5.3	Variation of nondimensional breach peak discharge ( $Q_{WP}$ ) with Shield's entrainment number ( $\tau_{*c}$ ) and reservoir capacity number ( $CAP_N$ )	174
5.4	Variation of nondimensional time of occurrence of breach peak outflow discharge ( $t_{wp}$ ) with Shield's entrainment number, $\tau_{*c}$ and $Q_{PN}$ , soil resisting number, $V_{SRN}$	177
5.5	Variation of nondimensional final top breach crest width, $(B_{cr})_f$ with Shield's entrainment number, $\tau_{*c}$ and $Q_{PN}$	177
5.6	Variation of final breach width to depth ratio with $Q_{PSN}$ and $V_{SRN}$ numbers	180
5.7	Variation of side slope ( $Z$ ) of breach depth of erosion and width of erosion	180
5.8	(a). Variation of nondimensional sediment peak discharge intensity ( $q_{sp}$ ) with soil resisting number, $V_{SRN}$	183
	(b). Variation of time of occurrence of sediment peak discharge intensity, ( $t_{sp}$ ) in a nondimensional form with $Q_{PSN}$ number	183
5.9	(a). Variation of nondimensional final breach crest width by average inflow discharge with soil resisting velocity number, ( $V_{SRN}$ )	185
	(b). Variation of nondimensional final depth of erosion at crest, ( $D_{er}$ ) by average inflow discharge with soil resisting velocity number, ( $V_{SRN}$ )	185
	(c). Variation of nondimensional final eroded crest area, $A_{er}$ by average inflow discharge with soil resisting velocity number, ( $V_{SRN}$ )	186
	(d). Variation of reservoir capacity number with $Q_{PSN}$ number	186
5.10	Definition sketch showing how $m_{wr}$ and $m_{wf}$ are computed	188
5.11	(a). An aid to compute $m_{wr}$ for a known $Q_w/Q_{WP}$ and its corresponding $t/t_{wp}$	189
	(b). An aid to compute $m_{wf}$ for a known $Q_w/Q_{WP}$ and its corresponding $t/t_{wp}$	189
5.12	(a). Variation of exponent ( $m_{wr}$ ) for rising limb of normalised hydrograph as per equation 5.12 with soil resisting velocity number	191
	(b). Variation of exponent ( $m_{wf}$ ) for falling limb of normalised hydrograph	191

	as per equation 5.12 with Shield's entrainment number and soil resisting velocity number	
5.13	(a). Comparison of normalised hydrograph of observed with estimated for run no 2204, dam model with cohesive soil	192
	(b). Comparison of normalised hydrograph of observed with estimated for run no. 1005, dam model with cohesionless soil	192
5.14	(a). Observed breach hydrograph for Teton dam breach	193
	(b). Observed breach hydrograph for Huaccoto dam.	193
5.15	(a). Comparison of estimated normalised hydrograph with observed and simulated BEED model's result for Teton dam breach by overtopping flow	194
	(b). Comparison of estimated normalised hydrograph with observed and simulated BEED model result for Huaccoto dam breach by overtopping flow	195
5.16	(a). Variation of exponent, $m_{sf}$ in equation 5.12 for falling limb of normalised sediment discharge graph with Shield's entrainment number, reservoir capacity number and $Q_{APN}$	197
	(b). Simulated sediment discharge with time for Teton dam failure by BEED model	197
	(c). Comparison of present estimated normalised sediment discharge graph with simulated result of BEED model for Teton dam.	198
5.17	(a). Comparison of estimated flow variables for Teton dam with observed and simulated value of BEED model	204
	(b). Comparison of estimated final breach dimensions for Teton dam with observed and simulated value of BEED model	205
	(c). Comparison of estimated final breach dimensions for Huaccoto dam with observed and simulated value of BEED model	206
5.18	Flow chart for computation of criterion variables during breach process	207
6.1	(a). Fuse plug model in plan and sectional view	215
	(b). Photographs of fuse plug model	216
6.2	Particle size distribution for soil type-A, B, and C	218
6.3	Typical variation of water surface profiles at four different sections, a, b, c and d for run no. 1404	221
6.4	Typical variation of sediment bed level with time for run no. 1404.	221
6.5	Typical variation of crest of erodible bed profile for run 1404	223
6.6	A typical washout hydrograph for run no. 1404 during washout of fuse plug	223
6.7	A typical variation of cumulative volume of eroded volume of sediment from fuse plug body with time for run no. 1404	224
6.8	Variation of eroded sediment discharge with time for run no. 1404	224
7.1	(a). A typical variation of reservoir water level indicating reservoir time scale ( $T_*$ ) and reservoir length scale ( $H_*$ )	230
	(b). Variation of rate of reservoir water level with time indicating time scale ( $T_*$ )	230
	(c). Variation of nondimensional reservoir length scale with average inflow discharge intensity, soil resisting velocity and height of the dam	231
	(d). Variation of nondimensional reservoir time scale with average inflow	231

	discharge intensity soil resisting velocity and height of the dam	
7.2	(a). Relation between head of water over erodible sediment crest ( $h_u$ ) with outflow discharge $Q_w$	234
	(b). Variation of coefficient of discharge ( $c_d$ ) with ratio of head of water over erodible sediment crest to the height of the erodible crest	234
7.3	(a). Variation of receding length of the erodible sediment crest ( $X_m$ ) with the drop in water level	236
	(b). Variation of nondimensional receding length of sediment crest with nondimensional drop of water level at the crest	236
	(c). Variation of nondimensional erodible sediment bed profile	237
	(d). Definition sketch for $X_m$ , $X_{50}$ , $L_{DB}$ and $h_{cm}$	237
	(e). Variation of nondimensional sediment bed profile length scale ( $X_{50}$ ) with nondimensional time ( $t$ )	238
	(f). Variation of nondimensional crest height ( $h_{cm}/H_D$ ) with nondimensional time ( $t/t_{50}$ )	240
	(g). Variation of nondimensional time scale of erodible sediment bed profile, ( $t_{50}/T_*$ ) with reservoir length scale ( $H_*$ ) and height of fuse plug	240
	(h). Rate of erosion of crest height of erodible sediment bed with incoming flow velocity ( $V_u$ )	241
	(i). Variation of nondimensional rate of erodible sediment crest with its nondimensional time	241
	(j). Variation of maximum rate of erodible sediment crest in a nondimensional form with its nondimensional maximum outflow discharge intensity ( $q_{wp}$ ), reservoir length scale and soil resisting velocity	242
7.4	(a). Variation of average sediment erosion velocity ( $V_{sv}$ ) at any time of washout of fuse plug with in coming flow velocity ( $V_u$ )	243
	(b). Variation of nondimensional average sediment erosion velocity ( $V_{sv}$ ) at any time of washout of fuse plug with nondimensional incoming flow velocity ( $V_u$ )	244
	(c). Variation of nondimensional scale of sediment erosion velocity ( $V_{svM}$ ) with maximum outflow discharge intensity, reservoir length scale ( $H_*$ ) and $V_{SR}$	245
7.5	(a). a typical variation of sediment discharge ( $Q_s$ ) with time	247
	(b). Nondimensional sediment discharge graph	247
	(c). Receding limb of nondimensional sediment discharge graph	248
	(d). Variation of sediment concentration with the ratio of head of water over crest of erodible bed to the crest height ( $h_{cm}$ )	248
	(e). variation of the ratio of head of water over the crest ( $h_u$ ) over the sediment bed to its height ( $h_{cm}$ ) to the nondimensional drop of water $\Delta H$	249
	(f). Variation of sediment concentration ( $C$ ) with average shear velocity ( $V_*$ ) and soil resisting velocity ( $V_{SR}$ )	250
	(g). Variation of sediment concentration ( $C$ ) with average shear velocity ( $V_*$ ) and soil resisting velocity ( $V_{SR}$ ) and $\Delta H$ .	250
7.6	(a). The relation of head of water over analogous rigid sediment bed crest	252

	with its corresponding outflow discharge intensity ( $q_w$ ) without considering contraction length of weir	
	(b). The relation of head of water over analogous rigid sediment bed crest with its corresponding outflow discharge intensity ( $q_w$ ) by considering the contraction length of weir	252
	(c). Variation of energy ratio, between downstream and upstream of the dam to the ratio of head of water over the rigid crest of analogous erodible sediment bed to its crest height	254
	(d). Energy loss characteristics in mobile and analogous rigid sediment bed profile models with different $h_u/h_{cm}$	254
	(e). Variation of nondimensional magnitude of the difference in energy loss between mobile and its analogous rigid sediment bed profile with the concentration of sediment (C)	255
7.7	(a). A typical variation of water discharge intensity ( $q_w$ ) with time for run no. 1804	257
	(b). Nondimensional hydrograph for washout of fuse plug with type-A soil fill	257
	(c). Variation of nondimensional outflow discharge intensity ( $q_w$ ) with normalised time ( $t/t_{wp}$ ) for fuse plug with type-B soil fill	258
	(d). Variation of normalised outflow discharge intensity ( $q_w$ ) with normalised time ( $t/t_{wp}$ ) for fuse plug with type-C soil fill	258
	(e). variation of nondimensional outflow discharge scale ( $q_{wp}$ ) with average inflow discharge intensity and soil resisting velocity, $V_{SR}$	260
	(f). Variation of nondimensional time with nondimensionalised maximum outflow discharge intensity	260
	(g). A typical variation of the sediment discharge intensity for run no. 1804 with time	262
	(h). Variation of nondimensional sediment discharge intensity with its normalised time ( $t/t_{sp}$ )	262
	(i). variation of sediment discharge intensity scale ( $q_{sp}$ ) for type-A soil with peak outflow discharge ( $q_{wp}$ ) and $V_{SR}$	263
	(j). Lag in the time of occurrence of peak sediment discharge with respect to peak outflow discharge	263
	(k). Variation of nondimensional duration of washout process with average inflow discharge intensity $V_{SR}$ and height of fuse plug	264
	(l). Flow chart to compute the variables controlling fuse plug washout process	267
A.1	Variation of nondimensional bed shear stress with particle size(mm) of soil obtained from Shield's diagram	291

# LIST OF TABLES

Table	Title	Page
2.1	a. Components of various mathematical models for dam breach erosion.	21
2.1	b. Treatment of components of various mathematical models for dam breach erosion.	22
3.1	a. Dimensions of dam model with cohesionless soil.	31
3.1	b. Dimensions of dam model with cohesive soil.	32
3.2	Soil properties of cohesionless and cohesive soil used in model preparation.	33
3.3	a. Variables measured during dam breach at different sections of dam model with cohesionless soil.	48
3.3	b. Variables measured at different sections of dam models with cohesive soil.	48
5.1	Characteristics of dam geometry, and soil fill properties of Teton dam and Huaccoto dam.	166
5.2	a. Various nondimensional number for the experiments conducted on dam models with cohesionless soil.	170
5.2	b. Various nondimensional number for the experiments conducted on dam models with cohesive soil.	170
5.2	c. Various nondimensional number for Teton and Huaccoto dams.	171
5.3	Comparison of estimated duration of Breach ( $t_{95}$ ) with observed dam data.	172
5.4	Comparison of the present estimated value of ( $Q_{WP}$ ) for Teton dam breach with observed and computed value by BEED model.	173



5.5	Comparison of estimated time of occurrence of peak outflow discharge ( $t_{wp}$ ) for Teton Dam and Huaccoto dam with observed and simulated value by BEED model.	175
5.6	Comparison of estimated final top breach width ( $B_{cr}$ ) <sub>f</sub> for Teton dam and Huaccoto dam with observed and simulated value by BEED model	176
5.7	Comparison of final breach depth ( $D_{cr}$ ) for Teton and Huaccoto dam breach.	178
5.8	Comparison of estimated side slope of breach cross-section for Teton dam and Huaccoto dam failure.	179
5.9	Comparison of estimated and simulated BEED result sediment peak discharge for Teton dam.	181
5.10	Comparison of estimated time of occurrence of sediment peak discharge for Teton dam	182
5.11	Comparison of estimated variables of final breach geometry for Teton dam breach.	184
5.12	Functional relations for final breach geometry with different regression scenario.	187
5.13	Comparison of estimated results for Teton and Huaccoto dam breach.	203
6.1	Types of soil used for the fill of fuse plug.	217
6.2	Number of experiments conducted on fuse plug washout studies in different phases.	225
6.3	a. Experiments conducted on washout of fuse plug with type - A soil fill.	225
6.3	b. Experiments conducted by Rajpal (1995) on washout of fuse plug with three different soil fills: A, B and C.	226
6.4	Experiments conducted in phase - B.	226
6.5	Details of experiments on rigid sediment bed profiles (in phase - B) analogous to mobile bed profiles of run No. 1404.	227
7.1	Variables used in fuse plug analysis present study (Type - A Soil)	232
8.1	Comparison of estimated results for Teton and Huaccoto dams.	278

# LIST OF SYMBOLS

$A_D$	Cross-sectional area of dam
$A_{er}$	Final eroded cross-sectional area at crest
$B'_{cr}$	Breach width at downstream top edge of the dam at any time (t)
$B_{CL}$	Crest length of dam model
$B_{cr}$	Breach top width of crest at any time (t) during the breach process.
$B_f$	Width of fuse plug
$B_{fb}$	Bottom width of fuse plug
$B_{ft}$	Top width of fuse-plug
$c$	Cohesive stress of soil
$C$	Sediment concentration ( $Q_s/Q_w$ )
$CAP_N$	Reservoir capacity number
$c_d$	Discharge coefficient
$d_{50}$	Median particle size of the soil
$dB_{cr}$	Change of breach crest width at any time difference dt
$D_{er}$	Final depth of erosion of crest
$dh_{cm}$	Change in $h_{cm}$ corresponding dt
$E_1$	Upstream energy head $\cong h_{wr}$ (at any time, during breach)
$E_2$	Energy level at the downstream end of the dam (near toe of the dam)
$F_b$	Breach Froude number
$g$	Acceleration due to gravity

$g_s^*$	Non-dimensional eroded sediment load
$h''_w$	Down stream (near toe) water level from the flume bed
$h'_c$	Sediment bed level at downstream edge of the dam.
$h'_w$	Water level over the sediment bed profile at downstream edge of the dam
$H_*$	Reservoir length scale used in fuse-plug analysis
$h_c$	Sediment bed height at any location 'x' from the origin chosen
$h_{cm}$	Crest height of erodible sediment profile.
$h_d$	Drop of water at crest ( $H_D - h_{wc} - h_{cm}$ )
$H_D$	height of Dam/Fuse-plug
$h_u$	Water head over the crest of the sediment bed.
$h_{up}$	Maximum value of $h_u$
$h_{wc}$	Water level over the crest of the sediment profile.
$h_{wrm}$	Maximum water level in the reservoir
$K_{11}$	The ratio of height of sediment crest to reservoir water level
$K_{22}$	constant of proportionality in Equation (4.19b)
$L$	Crest width of the weir
$L_{DB}$	Bottom width of dam
$L_{eff}$	Effective crest width of the weir
$L_{is}$	Length of inclined sediment bed.
$L_{TD}$	Top width of Dam
$m_{sf}$	An exponent used in Equation 5.12 for falling limb of normalised sediment discharge graph
$m_{sr}$	An exponent used in Equation 5.12 for falling limb of normalised sediment discharge graph
$m_{wf}$	An exponent used in Equation 5.12 for falling limb of normalised hydrograph
$m_{wr}$	An exponent used in Equation 5.12 for rising limb of normalised hydrograph.
$n$	Exponent used in Equation 7.11a
$p_r$	Exponent used in Equation (4.2a)
$Q_{APN}$	Q - peak - cross-sectional number
$Q_{in}$	Inflow discharge to the reservoir
$Q_{INN}$	Inflow discharge number

$Q_{PN}$	Q - peak number
$Q_{PN2}$	A non-dimensional number, (described where it is used)
$Q_{PSN}$	Q - peak - sediment number
$Q_S$	Sediment discharge at any time 't'
$q_s$	Sediment discharge intensity
$Q_w$	Breach water discharge
$q_w$	Outflow breach discharge intensity
$Q_{wp}$	Peak breach water discharge
R	Regression coefficient
$S_f$	Breach Shape factor
t	Time (in Seconds, minutes and hours)
$T_*$	Reservoir time scale used in fuse-plug
$t_{50}$	Time at which 50% maximum crest (hcm) erosion has taken place
$t_{95}$	Time at which 95% of the sediment erosion occurs
$t_{hup}$	Time of occurrence of $h_{up}$
$t_{sp}$	Time of occurrence of peak sediment discharge
$t_{sp/2}$	Time in the receding limb of discharge hydrograph, when $Q_S = 0.5Q_{Sp}$
$t_{wp}$	Time of occurrence of breach peak discharge
$V'_*$	Shear velocity at the downstream edge of the dam
$V'_w$	Water flow velocity at downstream edge of the dam
$V_{SR}$	Soil resisting velocity
$V_{SRN}$	Sediment resisting velocity number
$V_{SV}$	Erosion velocity, (explained where it is used)
$V_{SVM}$	Maximum erosion velocity
$V_{wc}$	Velocity of water at crest of the sediment bed profile.
X	Distance along the flow, from the origin of the embankment.
$X_{22}$	A non-dimensional number, explained whenever it is used.
$X_{50}$	The distance at which $h_c = 0.5h_{cm}$
$X_m$	Value of X at $h_c = h_{cm}$
$y'_c$	Critical flow depth at downstream edge of the dam
Z	Datum energy head

$z$	Indicating the side slope of the final breach cross-section at crest i.e., V:H= 1:z
$\bar{V}$	Average bed shear velocity
$\bar{S}_f$	Average energy gradient in the breach channel
$\bar{A}_f$	Average flow area in the breach channel
$\Delta \bar{h}_c$	Average height of erosion between successive sediment profile of fuse plug
$\bar{R}_h$	Average hydraulic radius of the breach channel
$\bar{S}_w$	Average water surface slope in breach channel
$\phi$	Angle of friction of the soil
$\eta$	Exponent used in Equation (4.20a)
$\beta$	Intercept on X-axis for $h_{wt}/h_{wt*} = 0.7$ in Figure 4.36(a)
$\delta$	Non-dimensional form of $\Delta H$ used in Equation (4.21)
$\xi$	Nondimensional $h_u$ used in Equations (4.23a, b, c and d)
$\chi$	Normalised $\Delta H$ with $V_{SRN}$
$\psi$	Normalised bed shear stress with $Q_{PSN}$ and $V_{SRN}$ numbers
$\varepsilon$	Normalised reservoir drop time scale , $(t_{**})$ with $Q_{PSN}$ and $V_{SRN}$ numbers
$\alpha$	Normalised reservoir time scale $(t_*)$ with $Q_{PSN}$ and $V_{SRN}$
$\sigma$	Standard deviation of a variable
$\zeta$	Term containing $\Delta H$ , $L_{DB}$ and $V_{SRN}$ number
$\lambda$	Term containing $Q_{PSN}$ and $V_{SRN}$
$\mu$	The mean value of variable
$\sum \nabla_s$	Cumulative volume of eroded sediment
$\sum \nabla_w$	Cumulative volume of water
$\tau_{*c}$	Shield's entrainment number
$\tau_0$	Bed shear stress
$\xi_{11}$	Non-dimensional $\Delta H$ used in Equation (4.14c)
$\xi_{22}$	Non-dimensional eroded crest area at any time for dam model with cohesive soil with $Q_{PSN}$ number used in Equation (4.16) for cohesive soil
$\gamma_b$	Bulk density of soil fill in dams / fuse plugs.
$(B_{cr})_f$	Final breach top width at crest

$(dE)_{RM}$	Energy difference at toe of the dam for analogous rigid and mobile bed profile.
$(E_2)_{mobile}$	Energy level at toe of the dam for mobile sediment bed at any time of breach in fuse plug washout study.
$(E_2)_{rigid}$	Energy level at toe of the dam for rigid sediment bed at any time of breach in fuse plug washout study
$\sigma_g$	Geometric standard deviation
$\Delta H$	Difference in water level between upstream and downstream of the dam
$\Delta H_C$	Difference of water level between downstream end of the dam and the crest of sediment bed profile.
$(L_{er})_{av}$	Average length of the erosion between two successive sediment profile of fuse plug.
$\rho_s$	Density of sediment particle
$\rho_w$	Density of water

# DEFINITIONS

1. *Crest* : It refers to the position where erodible sediment bed profile height is maximum in breach section
2. *Upstream and downstream top edge* : It refers to the upstream and downstream end of the dam top length
3. *Variables* : Without any prefix, it refers to the controlling input and output variables in general involved in the process.

*Basic Variables* : In the present study three basic measured variables refer to variation of water level, sediment bed level and width along the breach.

*Computed Variables* : It refers to the computed from the measured basic variables like water and sediment discharge, average shear stress etc.

*Predictor Variables* : Predictor variables are variables for which values are measurable

*Criterion Variables* : It is the variables for which a predicted value is necessary for its estimation.

4. *Parameter* : A numerical measure of a property or characteristic that is constant for a system under specified conditions.
5. *Coefficient* : A variable or constant appearing in a mathematical relation, each value of which defines the specific form of the functional relation.
6. *Scales* : It refers to some critical value of a particular variable, which are used to in the analysis like  $x_{50}$ ,  $t_{50}$ ,  $t_{wp}$ ,  $t_{sp}$  etc. used in the present analysis.

7. *Erosion Coefficient* : In the present method it is defined as the ratio of rate of crest height variation to incoming velocity.
8. *Erosion Velocity* : It refers to the average velocity of eroded soil from the fuse plug body.
9. *Drop* : It refers to the drop in water level either at crest or between reservoir level and downstream of dam ( $\Delta H$ )
10. *Analogous Rigid Bed*: It refers to the rigid bed profile modelled in replica to the instantaneous mobile sediment bed during the washout process of fuse plug.
11. *Soil resisting Velocity*: This indirectly account for the resistance to erosion
12. *Embankment Dam* : The homogeneous dam constructed without filter or core inside the dam body.
13. *Erosion Process* : It refers to the internal mechanism between flow parameter, breach morphology and soil properties of the dam fill materials.
14. *Washout* : Breaching process in connection to the fuse plug (through its width uniformly) this word is used as the fuse plug is meant to be washed away during high flood.
15. *Normalised* : It refers to the nondimensional form of variables by its corresponding maximum value.



# **CHAPTER I**

## **INTRODUCTION**

### **1.1 An Overview of Dam Breach**

Among the natural resources, water is vital to life and economic growth. Dams play a major role in harnessing the surface water component of this precious resource by storing and distributing it in a proper planning and management for various economical use. Earthen dams are the most common among various types of dams constructed. It constitutes a vast majority of dams compared to other categories. Failure of a dam in any form is not desirable. When a dam fails, it results in the sudden release of stored water, which becomes a disaster in the downstream region. Among the dams, the earthen dams are more vulnerable to failure. The major causes of failure of earthen dams are overtopping and piping. Overtopping of flood on an earthen dam causes a breach in the body of the dam. The breaching phenomenon is a short time event due to which all parameters controlling the breach erosion are not possible to measure in field. However, under laboratory conditions, the phenomenon can be simulated to a good extent, which gives a better insight into the mechanism involved in breach process as shown in Figure 1.1. A better knowledge will help to develop more realistic numerical model for an earthen dam breach.



Fig. 1.1: Simulation of dam breach phenomena due to overtopping flow in laboratory

## 1.2 Concept of a Fuse Plug

Almost all dams should have spillway to permit excess flood discharge downstream to prevent the dam to be damaged. Gates on spillways permit the controlled operation of flood discharge. In the design of a dam, it is found that a weak granular embankment, which may or may not have a clay cover, is built at a suitable location of topography as indicated in Figure 1.2 as a possible location of fuse plug to act as automatic excess flood releasing device. During high floods these auxiliary outlets which augment the service spillway by passing the larger flood flows are called fuse plugs.

## 1.3 Types of Dam Failures

The most common causes and modes of failure of earthen dams can be attributed to:

- a. Overtopping caused by extreme floods.
- b. Structural failure due to internal erosion (piping).
- c. Structural failure due to shear slide.
- d. Structural failure due to foundation problem.
- e. Failure due to natural or induced seismicity.

It is found that more than 60 percent of earthen dam failures are caused by overtopping or piping (USCOLD, 1975; Middlebrooks, 1953).

## 1.4 Causes of Overtopping of Flood

The overtopping of flood over the embankment may be due to following reasons:

- a. Design criteria of probable maximum flood (PMF) for the reservoir
  - i. Ignoring the future catchment yield due to hydro-geological changes.
  - ii. Reduction of live storage capacity of reservoir due to sedimentation.
- b. Reservoir operational rules
  - i. Spillway and sluice gate operation during flood.
  - ii. Seasonal reservoir operational policy.

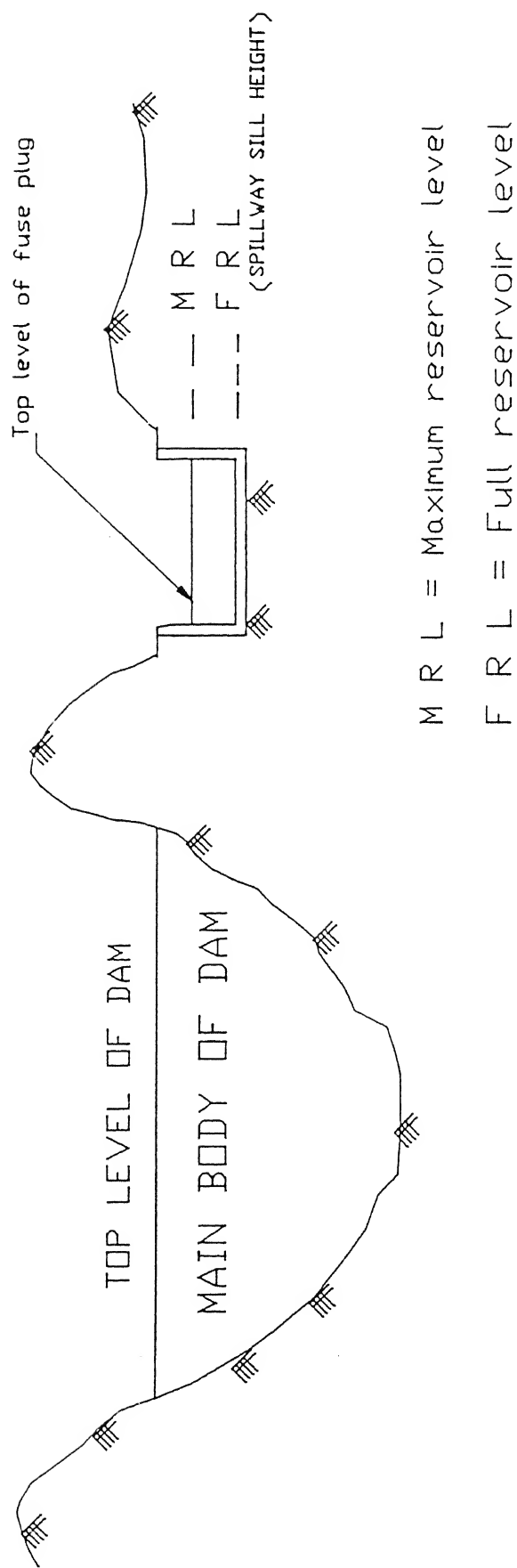


FIG: 1.2 SCHEMATIC DIAGRAM FOR POSSIBLE LOCATION OF FUSE PLUG

## 1.5 Necessity for Dam Breach Study

According to Gruner (1967a, b), the total number of dams that impose risk of serious damage in case of failure may well exceed 150,000. Jansen (1980) has noted that there have been approximately 2,000 dam failures around the world since the thirteenth century. Out of these, about 10 percent have occurred in 20th century itself. Berga (1992) has pointed out that 41 percent of historic dam failures were caused by the design flood having been exceeded. Loukola et. al. (1993) noted that 80% of nearly 87,000 dams in China are embankment dams and more than 90% are small dams. The dam failures in China associated with earthen dams are of the order of 93% and 96% with small earthen dams or small reservoirs. The main cause of failure was overtopping due to heavy rainfall and ensuing floods low design criteria for small dams and operational problem in appurtenant works. In India there are enough examples of earthen dam breach in recent past. A few of them can be cited, namely Machhu II (Irrigation scheme) dam (Gujarat), Panshet dam, Khadakwasla dam (Poona) Maharashtra, and Kodaganar dam (Tamilnadu) which breached either due to inadequate spillway capacity or due to inadequate provision of the outlet facility during emergency.

It is easy to infer from the statistical figures of the probable dam failures, that it is essential to have contingency planning for evacuation during the dam breach with the help of reliable flood forecasting in the downstream flood plain. In some of the dam-break numerical modelling, the routing of flood and sediment downstream are mostly carried out by assuming the failure of the dam as an instantaneous phenomenon. But from historical earthen dam failure records it is evident that the duration of failure varies from about half an hour to 12 hours depending upon the situations. That clearly indicates dam failure is a time-dependent and not a instantaneous process as assumed. Therefore, in order to accurately predict water and sediment discharge from the breach section of the dam, it is necessary to know as to how the breach process evolves with time. These quantities are controlled by the breach cross section or the morphology of the breach with time. The dam breach flood and its associated sediment discharge can be routed in downstream channel in a more accurate way to predict the stage and discharge at any reach, provided the breach formation in the dam can be predicted with time for a given condition.

## 1.6 Variables and Parameters Involved in the Problem

In the dam breach study the two types of variables involved are:

- a. Predictor variables
- b. Criterion variables

The predictor variables controlling the present problem are:

- i. Dam geometry
- ii. Capacity of the reservoir
  - Capacity and elevation relation,
  - Variation of discharge characteristics of spillway, sluice gate and other outlets, with head of water
- iii. Inflow discharge to the reservoir.

The criterion variable is the variable for which a predicted value is necessary in design. In the present problem criterion variables can be listed as:

- a. Peak breach outflow discharge.
- b. Peak outflow sediment discharge.
- c. Times to peak water and sediment discharges and duration of breach.
- d. Terminal breach morphology.
  - i. final breach width,
  - ii. final depth of erosion,
  - iii. final side slope of the breach cross-section.

Some parameters or coefficients are needed to relate various criterion variables to predictor variables in a functional relation. Parameter, a numerical measure of property or characteristics that is constant for a system under specified conditions. In the present problem the parameters / coefficients are obtained from the properties of dam fill material, namely, cohesion ( $c$ ), angle of friction ( $\phi$ ), bulk density of the dam fill material ( $\gamma_b$ ) and average grain size ( $d_{50}$ ).

## 1.7 Present Status of Knowledge on the Dam Breach

Conceptually, the dam breach hydraulics and the breach morphology due to overtopping flood comprises the dam breach process in a broader sense. Enlargement of the breach affects the rate of discharge, which subsequently controls the rate of erosion. This process continues till the reservoir water is depleted or till the dam resists further erosion.

Briefly the present state of the knowledge relevant to the dam breach problem may be described under the following subheads.

- a. Erodibility
- b. Mechanics of breach
- c. Hydraulics of breach flow
- d. Erosion of sediment and its transport

### a. Erodibility

Hydraulic erosion entails a soil-water interaction. Erosion occurs when shearing stresses induced by fluid flow on soil surface are high enough to overcome the force holding the particles together and to cause the dislodgment of particles from the surface. A cohesive soil erodes in a quite different way as compared to a cohesionless soil. In a cohesionless soil, erodibility primarily depends on grain size distribution, density and shape of the grain while the main resistance to erosion is offered by the submerged weight of the sediment. In a cohesive soil, the amount and type of clay percentage, chemical composition of the pore fluid, degree of saturation, presence of organic material and other cementing agents play a significant role in its erodibility.

### b. Mechanics of Breach Formation

The basic mechanism of breaching of earth fill dams is rooted in the erosion of the embankment material. Excessive shear stress on the surface induced by the flow of water over weak section of dam body initiates the process of erosion. The breach in the initial stages is predominantly 'V' shaped, three to four times as wider than its depth. As the erosion of surface progresses laterally the breach section grows. The extent of this lateral erosion depends upon the size of the reservoir and volume of water stored in it.

### c. Hydraulics of Breach Flow

Most of the earlier experimental and numerical studies assumed:

- i. Flow over the crest of the breach is analogous to the flow over the broad crested weir.
- ii. The unsteady flow is approximated by quasi-steady situation.
- iii. The tail water effect is considered suitably by reducing the discharge coefficient in some of the numerical models.
- iv. Manning's or Chezy's resistance equation used for flow depth calculation in the breach channel.

Pugh and Gray (1984) professed that the flow over the entire top section of the breach can be assumed to be critical i.e. initially an  $S_2$  water surface profile and supercritical flow thereafter along the breach. The governing equations for the flow over a dam are as:

- a. The continuity equation.
- b. Broad-crested weir formula.
- c. Breach shape geometry relation.
- d. The equation of resistance to motion.
- e. The equation of motion.

### d. Breach Morphology

Initial cross-section of the breach is of a narrow valley of V-shape. As the erosion progresses, the shape modifies to trapezoidal cross-section. In the numerical models on dam breach, the shape of breach section has been assumed to be of various shapes like rectangular, triangular, trapezoidal, parabolic and semicircular as reported in earlier works on dam breaching. But from the experimental observation it is found, that the terminal cross-section of the breach may be taken to be trapezoidal. There are two cross-sectional shapes derived on theoretical considerations based on:

- i. the concept of stable section of greater efficiency as a simple cosine curve, and
- ii. the minimum cross-sectional area maintaining stability for a given discharge, Lane (1985).



#### **e. Erosion of Sediment and its Transport**

Due to lack of experimental evidence and not having a complete understanding of sediment transport relations under highly dynamic conditions like a dam breach, most of the studies reported so far have been forced to resort to sediment transport formulae applicable to alluvial streams, like Du-Boys formula(1879), Schoklitsch formula(1935), Meyer-Peter-Muller formula (1948) and Einstein-Brown formula (1950). These formulae are based on the tractive force theory i.e., sediment bed load is a function of average shear stress, and are applicable to homogeneous bed load in alluvial streams.

The governing equations in breach erosion and sediment transport are:

- a. Continuity equation of sediment.
- b. Equation of motion of sediment.
- c. Shear stress relation with bed load.

#### **f. Stability of Breach Slope**

The side slope of the breach section becomes unstable during breaching when the gravity and hydrodynamic forces due to seepage become greater than the soil friction and cohesion and collapses, causing enlargement of breach section. Greater the breach flow, greater will be the breach erosion.

### **1.8 Aims of the Present Study**

- a. The present state of knowledge on earthen dam failures due to overtopping flood is postulated, mostly by assuming the principles of sediment transport in the rivers and hydraulics of flow over a weir. An insight into the mechanism involved in the breach erosion process is very essential for the better understanding of this type of earthen dam failures. With this aim, experiments are planned to study the breach process on homogeneous embankment dam models. Knowledge, thus obtained, is validated using field information.
- b. Fuse plug is a safety-valve for the dams. Little information is available on the washout process of the fuse-plug due to overtopping of flood. Therefore systematic experiments are planned to get a know-how on the washout mechanism involved in the erosion process of a fuse plug.

## 1.9 Organisation of Thesis

Experimental work has been carried out in two phases and the thesis is being presented in two parts I and II

Chapter I	:	Introduction
Chapter II	:	Review of Literature
Part - I	:	Breach Erosion of Homogeneous Earthfill Dams Due to Overtopping Flow
Chapter III	:	Scheme of Experimentation on Dam Breach
Chapter IV	:	Mechanism of Dam Breach Process
Chapter V	:	Comparison of Dam Breach Results with Teton and Huaccoto Dams
Part-II	:	Washout Process of Fuse Plug
Chapter VI	:	Scheme of Experiments on Fuse Plug Washout
Chapter VII	:	Analysis and Results of Washout Process of Fuse Plug
Chapter VIII	:	Conclusions and Recommendations

This is followed in succession by References and an Appendix.

## **CHAPTER II**

# **REVIEW OF LITERATURE**

### **2.1 Introduction**

A considerable body of literature has been accumulated over a span of last 150 years on the movement of flood wave resulting from instantaneous dam failure which in academic circle is coined as 'Dam Break' problem. But the historical earthen dam failure record derived from studies by Middlebrooks(1953), Gruner(1969), Babb and Mermel(1968), American society of Civil Engineers(1975), Singh and Scarlatos(1989), Singh and Snorrason(1982), Ponce(1981), Central Water Commission, Govt. of India(1989), and Jansen(1988) clearly have shown one striking common denominator: the failure is anything but sudden. So the gradual failure of an earth dam is of particular interest to disaster relief planners, because the rate of growth of the breach strongly influences the peak and shape of the ensuing flood waves. As a result the significant interest on dam safety among public has come in the last two decades or so. The research on different facets of earth dam breach has been augmented through different empirical and numerical modelling without much experimental data support. Going through the relevant literature on dam breach it seems to be appropriate to present the different concepts and methodologies of prediction of breach characteristics in the following subheads:

- a. Experimental Observations.
- b. Empirical Modelling.
- c. Mathematical Modelling.
- d. Ancillary literature relating to dam breach.

## 2.2 Experimental Observations

Powledge *et al* (1989a, b) carried out model and prototype research studies which have been conducted in the United State and Great Britain to evaluate how embankments for dams, levees, roadways perform when subjected to overtopping flows from probable maximum flood (PMF) or near PMF events. From their experimental observations, they concluded flow over an embankment passes through three zones, sub-critical flow over dam crest, supercritical flow over dam crest and supercritical flow on dam downstream slope. They have identified a potential negative pressure zone on the downstream slope immediately below the crest. The potential negative pressures can be quantified by superimposing the Nappe equation (theoretical ogee shape) on the embankment crest and slope profile from which sub-hydrostatic zone can be located.

Powledge *et al* disclaim about the applicability of the tractive stress approach for erosion rate analysis during the breaching process. The initiation of breach starts near the slope discontinuity, such as the toe or base of the dam. They have observed that the overflow discharge may be computed by using weir flow equation for both granular and cohesive embankments. In granular embankment, once the overtopping occurs, the seepage on the downstream slope accelerates slope erosion. The erosion phenomenon starts at or near the toe, where seepage is exiting and the turbulence of the impinging flow is greatest. Then quickly the erosion process propagate rapidly up the slope and cause the lowering of the crest, allowing increase in flow rates which accelerate the erosion process. For cohesive embankment, generally there is more resistant to erosion than granular fill due to existence of low seepage on the slopes because of low permeability. Factors which influence the erosion process are:

- i. Embankment configuration
- ii. Maximum velocity attained by flow
- iii. Discontinuities: such as berms, outlets, creates, local changes in momentum producing turbulence and erosion
- iv. Presence of tail water

Their main aim of the experimental study was to evaluate performance potential of different protective measures to prevent breach erosion. Focus on the mechanism of breach process was not given.

In August'1995 the sea defense at a MAFF / English Natural Experimental site at Tollesbury in Essex was deliberately breached. This prototype breaching was a part of a series of experiments into an approach to flood defence known as 'managed set-back'. The breaching operation, carried out as part of the MAFF flood and Coastal Defence Division strategic research program was carefully controlled and monitored by HR Wallingford to study the behaviour of clay embankments under simulated flood conditions. Information's about breach details are not available to the author.

The report from *Streamline (December'1995)* can be cited here in connection to the dam breaching:

[There are number of coastal lagoons in urban zones in New South Wales, Australia. These are usually blocked by a sand barrier built up by wave activity and reach 2-3m above sea level. Heavy rainfall causes water level in the closed lagoons to rise rapidly putting urban area at risk of flooding unless an entrance to the ocean is scoured through the barrier. This process can be initiated naturally by overtopping, or digging a small "starter channel" across the berm.]

HR Wallingford has studied above problem at the Wamberal Lagoon in New South Wales. Following are observed from the prototype non-cohesive embankment breach model test.

- i. initial vertical cutback across the breach
- ii. formation of a curved weir upstream in the sand plug behind the beach berm
- iii. rapid widening and deepening of the gap in the berm and final sub-critical phase

These two experimental studies gave only qualitative information on embankment breach.

## 2.3 Field Observations

From the 52 historical dam failure cases Singh and Scarlatos (1988) studied inter-relationship among terminal depth of erosion, top and bottom width of the breach section and side slope of breach section shown below:

Sl. No	Relation	Qualitative values
1	$B/b$	$\cong 1.06 \sim 1.74$ , with mean value of 1.29 and standard deviation 0.180
2	$B/d$	$\cong 0.84 - 10.93$ , with mean value of 4.18 and standard deviation of 2.62
3	$\tan \theta$	$\cong 1.0$
4	$t_f$	1/2 hr to 12 hr

Where  $B$  = final top breach width,

$b$  = final bottom breach width,

$d$  = final depth of erosion,

$\theta$  = angle of side slope of the breach section with vertical, and

$t_f$  = failure time.

The qualitative relations bring an insight into the problem of dam breach.

## 2.4 Empirical Model

The models express formalized concepts of real-life problem. They consists of two elements : input variables and empirical constants. Again the input variables can be categorised into two, namely:

- a. Criterion variable
- b. Predictor variables

The criterion variable is the variable for which a predicted variable is necessary in design. Predictor variables are used to make estimates of the criterion variable. Like in the present topic of interest, capacity of the reservoir, inflow hydrograph are examples of predictor variables, whereas the peak breach discharge, final breach width, time to peak discharge, duration of breach, final depth of erosion are examples of criterion variables. The empirical constants are derived by fitting the model with measured values of the criterion and predictor variables. These constants are either called coefficients or parameters. So parameter can be

defined as a numerical measure of a property or characteristic that is constant for a system under specified conditions, whereas coefficients is a variable or constant appearing in a model, each value of which defines the specific form of the model.

Major contributions to the modelling of breach process of an earthen embankment dam is from Singh and his associates. They looked in to the breach processes in depth and developed both empirical and mathematical models. Their contribution can be considered as a milestone in the modelling of embankment breach process. Singh and Scarlatos (1988) have developed an empirical model by relating two basic governing equations in dam breach problem i.e., reservoir water balance equation and rate of erosion. The water balance equation is:

$$A_s(H) \frac{dH}{dt} = I - Q_b - Q \quad (2.1)$$

Where  $A_s(H)$  = water surface area within the reservoir,  $I$  = inflow to the reservoir,  $Q$  = flow due to crest overtopping,  $Q_b$  = breach flow,  $(dH/dt)$  = rate of change of water level in the reservoir. They have brought down the equation 2.1 to a simple form by equating rate of change of volume in the reservoir to mean breach flow velocity ( $u$ ) times the wetted breach area ( $A_b$ ) assuming inflow to the reservoir ( $I$ ) and dam crest overtopping flow ( $Q$ ) to be negligible. The average breach flow velocity ( $u$ ) is calculated by adopting hydraulics of broad crested weir flow (Chow 1959, Pugh and Gray 1984) as:

$$u = \alpha_1 (H - Z)^{\beta_1} \quad (2.2)$$

Where  $Z$  = the bottom elevation from reference datum, and  $H$  = the water level surface from a reference datum. For critical flow conditions, the empirical coefficients:

$$\alpha_1 = \left[ \left( \frac{2}{3} \right)^3 g \right]^{\frac{1}{2}},$$

$$\beta_1 = 0.5.$$

so 
$$u = 1.7 \sqrt{(H - Z)} \text{ m/s}.$$

With the assumption erosion is directly proportional to shear and subsequently proportional to the water velocity. Then equation (2.1) reduces to:

$$\frac{dZ}{dt} = -\alpha_2 u(H, Z)^{\beta_2} \quad (2.3)$$

Value of  $\beta_2$  is related with the concept of Laursen, the rate of sediment transport is a power function of mean velocity. The values of  $\beta_2$  vary in the range 4 to 6. If the value of  $\beta_2$  is an integer, the solution to equation (2.3) becomes a closed form one.

They adopted three different breach shapes namely, rectangular breach cross-section with constant width, which enlarges in vertical direction, triangular breach with constant side slope and enlarges similar to rectangular breach, trapezoidal breach cross-section with constant bottom width and constant side slopes. With known initial conditions,  $H=H_0$ , and  $Z=Z_0$  at  $t=t_0$  and stated assumptions, closed form solutions are developed for each breach cross-section. Depending on the value obtained for  $\beta_2$ , two different cases, i.e., linear erosion ( $\beta_2 = 1.0$ ) and non-linear erosion ( $\beta_2 \neq 1.0$ ) are studied. In all these cases it has been tried to determine reservoir water level and breach bottom elevation with time i.e.,  $H(t)$  and  $Z(t)$ . The erosivity coefficient  $\alpha_2$  was estimated through calibration, based on maximum outflow discharge and the failure time. For 16 historical dam failure case  $\alpha_2$  is computed and is reported, it varies within a range 0.0008 ~ 0.008 for linear case and 0.00015 ~ 0.0021 for non-linear situation. It is found that the overall performance of the linear rate of erosion is better than the non-linear erosion rate. However the nonlinear erosion models gave better results for the rising limb of the breach hydrograph, while the linear models simulated better the recession limb. Calibration of erosivity coefficient in their model can be considered as major drawback for the application of their model. This could be overcome only when experimental data is available for prediction of erosivity coefficient. Validation of erosion coefficient with experimental data is needed for the application of their model to the field problems.

Macchione(1989) derived an analytical solution to the work of Singh and Quiroga(1988). He expressed the reservoir storage volume as a function of the depth of water ( $H$ ) in the reservoir. He proposed the exponent to  $H$ , to vary from 1 to 4. Regarding breach geometry he stressed that the final breach shape would be trapezoidal. Initially a triangular breach is formed, when it reaches the natural ground, the breach expands laterally. He stressed that the breach flow can be taken as critical, without undue loss-of accuracy. He has used du Boy's



equation for movement of sediment. His analytical procedures describe the evolution of breach hydrograph at the beginning for triangular breach and then for trapezoidal breach. He has defined explicitly the expression for the reservoir water level variation with time for both the breach sections triangular and trapezoidal shape. There is no mention to differentiate triangular breach from trapezoidal breach with respect to time. His visualisation of breach formation from triangular to trapezoidal shape keeping the angles of sides of breach constant does not satisfy the laboratory observation on the dam breach.

A close form dimensionless analytical solution to Equations 2.1 and 2.3 is tried by Singh and Quiroga(1988) for rectangular breach section. In this approach they have tried to relate the water surface elevation( $Z$ ) in a non-dimensional form to non-dimensionalised  $H$ , they have used dam bottom elevation ( $H_b$ ) and  $H_0$ , the reservoir water level at the starting of the breach,  $t = 0$ . Similarly the breach bottom elevation  $Z$  is non-dimensionalised with  $H_D$  and  $Z_0$ , where at  $t = 0$ ,  $Z(0) = Z_0$ . From the given dam geometry  $Z_0$  and  $H_b$  can be found out. Then they have related  $H$  and  $Z$  with respect to time. The time ( $t$ ) is also non-dimensionalised with breach formation time ( $t_f$ ). From this solution they have come out with following view:

“...For a breach to develop completely, the rate of erosion at the breach must be larger than the rate of depletion of the reservoir. This means that peak discharge occur when the difference between non-dimensional reservoir level elevation and breach bottom elevation is maximum. This normally happens at time is equal to the breach formation time”

With this approach, only the rising part of the breach hydrograph can be obtained, not the complete picture of hydrograph. A single overall erodibility factor is used for the rate of sediment erosion.

## 2.5 Mathematical Modelling

A good number of mathematical models for simulation of earth dam failure have been developed in the past twenty five years or so, though the models vary considerably in their physical content.

These models are: a) Cristofano model (1965), b) Harris-Wagner model (1967), c) BRDAM model (1977, 1981), d) Ponce-Tsivoglou model (1981), e) Lou model (1981) .

f) DAMBRK model (1984a and 1984b), g) SMPDBK model (1984), h) Breach model (1984b) and i) BEED model (1986a, 1987a, 1987b, 1988a).

The various components of these models are

- i. Reservoir hydraulics
- ii. Hydraulics of flow over dams (breach hydraulics)
- iii. Breach morphology
- iv. Flow routing

From these four angles these models can be reviewed, giving special importance to the breach hydraulics and breach morphology, as these two aspects are addressed in the present study.

#### **a. Reservoir Hydraulics**

The inflow routing and reservoir water elevation study comes under the component of dam breach modelling. Each of these models route the inflow using storage routing method and computes changes in the reservoir water level by volume balance. Outflows through spillways, outlet works and power plants during the breach constitute a part of the storage routing.

#### **b. Breach Hydraulics**

Except PT(1981), Lou(1981) and Nogueira(1984) models, all other models use the broad-crested weir formula. For a rectangular broad-crested weir with  $b$  defining the width of the breach channel and  $h_u$  the head acting over the crest, the discharge of flow over the weir  $Q$  is given by

$$Q = b\sqrt{g}\left(\frac{2}{3}H^{\frac{3}{2}}\right) = 1.7bH^{\frac{3}{2}} \quad (2.4)$$

where  $b$  is the width of breach,  $H$  the flow depth and  $Q$  the discharge.

The PT model employs a relation between breach top width and flow rate. This relation was applied from inception to peak flow, after which the breach width was kept constant and equal to the peak flow width. Lou and Nogueira models utilize respectively St. Venants equation and critical flow equation.

A majority of the models do not separately consider the flow through the breach channel. The PT, Lou and Nogueira models use the St. Venant equations for modelling this channel flow, whereas the BREACH and BEED models use a steady uniform formula like Manning's equation. The majority of the models never treat the flow through the crest and breach channel, separately rather combinedly as hydraulics of flow.

### c. Breach Geometry

Each model characterizes the breach morphology differently. Except the analytical expressions given in Lou and PT model for breach geometry, other models assume a breach shape. The DAMBRK, SMPDAM and BEED models use a trapezoidal shape but the program has the facilities to use rectangular and triangular shapes also. The Cristofano model uses trapezoidal breach assuming a constant bottom width. The same assumption was also made by the PT model. The HW model uses a parabolic shape, whereas the BRDAM model represents the breach by a triangular shape with  $45^\circ$  side slopes and parabolic bottom. The BREACH model expresses breach width as a function of the depth of flow in the breach. Lou model considered that the breach formation due to overtopping grows in space and time until an equilibrium section is attained. Based on this mechanism and hydraulic considerations, a most efficient stable section is derived for describing breach shape as:

$$y = D \cos\left(\frac{\pi}{B}x\right) \quad (2.5)$$

where  $y$  = depth at a distance  $x$ ,  $D$  = maximum depth at the center,  $x$  = distance from the center, and  $B$  = top width. This shape results in the smallest width having greatest hydraulic radius in order to keep channel stable. Similarly, Nogueira model(1984), following the work of Lane(1955) and effective shear stress analysis, an equation was derived to represent the breach profile as :

$$y = y_0 \cos\left(\frac{x \tan \phi}{y_0}\right) \quad (2.6)$$

where,  $y$  = depth at a distance  $x$ ,  $y_0$  = maximum depth at the center,  $x$  = distance from the center, and  $\phi$  = angle of repose of the bed material. The profile is a cosine curve and has a minimum cross-sectional area for a given discharge while keeping the stability.

#### d. Sediment Transport

The sediment transport equations that have been used are Schoklitsch formula, the Meyer-Peter and Muller equation, the DuBoys equation, and the Einstein-Brown equations. Three models namely PT, Lou and Nogueira, coupled the transport equation with Exner sediment continuity equation;

$$\frac{\partial Q_s}{\partial t} + (1-p)\gamma_s B \frac{\partial Z}{\partial t} = 0 \quad (2.7)$$

Where  $Q_s$  = Sediment transport rate by weight;  $p$  = porosity of the material forming the bed;  $B$  = average channel width;  $Z$  = bed elevation,  $\gamma_s$  = density of bed material. The change in bed elevation can thus be computed as a function of sediment transport rate and bed material properties. The Cristofano model derives its own erosion equation by equating the rate of

change of vertical and lateral erosion within the notch. He assumed to the rate of change of water flowing through the notch for a unit area as:

$$\frac{Q_s}{Q_b} = K_e \exp \left[ -\frac{l \tan \phi}{h} \right] \quad (2.8)$$

where  $Q_s$  = Volume of sediment discharge;  $Q_b$  = Volume of water discharge through the breach,  $K_e$  = Constant of proportionality,  $l$  = the base length of the flow at any time, and  $h$  = the hydraulic head at any given time. The Lou model has provision whereby sediment transport is expressed as a function of the duration of failure, erodibility index, and velocity of

water as:

$$E = \frac{C_e}{12} t_d u_w^4 \quad (2.9)$$

where  $C_e$  = constant,  $t_d$  = duration of failure,  $u_w$  = velocity of water and  $E$  = mass of soil lost.

#### e. Breach Slope Collapsing

Among the mathematical models discussed only three models, Nogueira, BREACH and BEED model, account for side slope instability and collapsing in a explicit way. The Nogueira model considers six cases to analyse lateral erosion by sliding, based on the

assumption that the sliding will occur into the breach along a line with the slope equal to the tangent of the angle of internal friction of the material. The BEED model uses the contour method to analyse the slope collapsing assuming saturated soil conditions. With similar line, BREACH model analyses the forces to compute collapsing of the breach side assuming dry soil conditions.

#### f. Downstream Flood Routing

The flood routing facility in the downstream channel and flood plain is in-built in the BEED and DAMBRK models. Whereas BEED model used Muskingum method, the DAMBRK model employs the dynamic flood routing based on the St. Venant equations. The BRDAM and SMPDAM models route the flow only in downstream channel. The former uses dynamic wave routing, and the latter uses dimensionless curves produced by the DAMBRK model. Other models have not incorporated flow routing in their model.

In the Table 2.1a and 2.1b, the different aspects like the components in various mathematical models and their treatment are summarised. The information about the different mathematical models listed in table 2.1(a), and 2.1(b) are collected from the book on 'Dam Breach Modeling Technology' by Singh(1996) and are presented in two broad headings viz. breach hydraulics and breach morphology.

**TABLE 2.1a**  
**COMPONENTS OF VARIOUS MATHEMATICAL**  
**MODELS FOR DAM BREACH EROSION**

Model	Author (year)	Breach Hydraulics			Breach Morphology		
		Flow over the Crest	Flow through the Breach	Flow through the Breach on the Downstream face	Sediment Transport	Breach Shape	Side Slopes Collapsing
Cristofano Model	Cristofano (1965)	No	Yes	No	Yes	Yes	No
HW Model	Harris and Wagner (1967)	No	Yes	No	Yes	Yes	No
BRDAM Model	Brown and Rogers (1977)	No	Yes	No	Yes	Yes	No
PT Model	Ponce and Tsivoglu (1981)	No	Yes	Yes	Yes	Yes	No
Lou Model	Lou (1981)	No	Yes	Yes	Yes	Yes	No
Nogueira Model	Nogueira (1984)	No	Yes	Yes	Yes	Yes	Yes
DAMBRK Model	Fread (1984a)	Yes	Yes	No	No	Yes	No
SMPDBK Model	Wetmore and Fread (1984)	Yes	Yes	No	No	Yes	No
BREACH Model	Fread (1984b)	Yes	Yes	Yes	Yes	Yes	Yes
BEED Model	Singh and Scarlatos (1989)	Yes	Yes	Yes	Yes	Yes	Yes

In Table 2.1(b) the various aspects pertaining to breach hydraulics and breach morphology adopted in different mathematical models on dam breach are presented.

**TABLE 2.1b**  
**TREATMENT OF COMPONENTS OF VARIOUS MATHEMATICAL**  
**MODELS FOR DAM BREACH EROSION**

Model	Breach Hydraulics			Breach Morphology		
	Flow over the Crest	Flow through the Breach	Flow through the Breach on the Downstream face	Sediment Transport	Breach Shape	Side Slopes Collapsing
Cristofano Model	N A	Broad Crested weir formula	N A	Empirical	Trapezoidal	N A
HW Model	N A	Broad Crested weir formula	N A	Modified Schoklitsch	Parabolic shape with 45° side slopes	N A
BRDAM Model	N A	Broad Crested weir formula	N A	Schoklitsch bed load formula	Parabolic shape with 45° side slopes	N A
PT Model	N A	Relation between top width and flow rate	Manning's equation	Mayer-Peter and Muller equation + Exner equation	Constant Width	N A
Lou Model	N A	Dynamic wave modelling	Dynamic wave modelling	DuBoys' bed load + Einstein's suspended load formula	Cosine Shape	N A
Nogueira Model	N A	Dynamic wave modelling	Dynamic wave modelling	Mayer-Peter and Muller equation + Exner continuity equation	Cosine Shape	Morphological mechanics
DAMBRK Model	Broad Crested weir formula	Broad Crested weir formula	N A	N A	Rectangular trapezoidal or triangular	N A
SMPDBK Model	Broad Crested weir formula	Broad Crested weir formula	N A	N A	Rectangular shape	N A
BREACH Model	Broad Crested weir formula	Manning's equation	Manning's equation	Mayer-Peter and Muller equation	Rectangular Trapezoidal shape	Balance of forces
BEED Model	Broad Crested weir formula	Broad Crested weir formula	Quasi-steady state approximation	Einstein Brown formula	Rectangular, triangular or trapezoidal shape	Contour method

## 2.6 Ancillary Literature Relating to Dam Breach

The following literature are not having direct bearing on Dam breaching as such. But the information helps to understand some of the aspects of dam breaching.

Annandale (1995) has enlightened the idea of erodibility with a rational approach for earth materials, ranging on a continuum from cohesionless granular soil through massive hard rock. His graphic relationship between the erodibility index of earth material and the rate of energy dissipation for the complete data set of 150 field observations and other published data on initiation of sediment motion exhibits an erodibility threshold that applies continuously across a broad range of materials. The erodibility index is used to characterize the ability of

earth material to resist erosion. The rate of energy dissipation is used to characterize the relative magnitude of the erosive power of water. The erodibility index is dimensionless. The erodibility index is used to characterize several geological parameters. The rate of energy dissipation is calculated for a variety of flow conditions that can lead to erosion.

Graf and Song(1995) have studied the behavior of bed shear stress in non-uniform and unsteady open channel flows. They have concluded the friction velocity  $V_*$ , increases in longitudinal direction of flow in accelerating, but decreases in decelerating flow. In unsteady flow it reaches its maximum in the rising branch of the hydrograph. They also mention friction factor is essentially constant in a non-uniform flow, but needs further investigation. In an unsteady flow the friction factor reaches its maximum in the rising branch, even before  $V_*$ , of the hydrograph and subsequently decreases.

Aragon(1996), have developed hydraulic shear stress model for a uniform, steady flow on a slope of a maximum of water and granular material at high concentration draws attention, as the concept is new and the approach is elegant. His model includes stresses generated by particle-particle interactions along with these generated by fluid-bed interaction. Bagnold's model of dispersive stress is modified by introducing Kinetic theory for granular flow. According to him an interesting finding from his experiment is: there is not a continuous increase in velocity with depth of flow as stated by Manning's formula for whole range of concentrations. His hydraulic shear-stress model gives an insight about the mechanical behaviour of the flow along with velocity-flow depth relation.

Lai and Shen(1996), in their research paper on 'Flushing Sediment Through Reservoir' have come out with some findings which it is felt is useful for the present study of dam breaching in particular to the morphological aspect of breach. From both laboratory and field data, they have found that the outflow sediment discharge in the flushing operation of sediment in the reservoir, can be well related to a hydraulic parameter which is a function of outlet discharge, water-surface gradient and flushing channel width. The equilibrium width of flushing channel is found to be proportional to  $Q_d^{0.5}$ , where  $Q_d$  is the dominant outflow discharge.

## 2.7 Fuse Plug

Tiney and Hsu(1962) conducted model study on fuse-plug in the laboratory adopting 1:20 and 1:40 scale. From their experimental analysis of the lab study data on fuse-plug washout, they found:

- a. The washout is a function of grain size of the materials the larger the size, the slower the rate of washout
- b. The washout rate for a fuse plug is between 1.05 and 1.2 times faster than the corresponding half-scale model.
- c. Increasing the volume of rockfill decreases the washout rate slightly. From this experimental observation and theoretical analysis, they have brought out these conclusions:
  - The mechanics of washout can be explained on the basis of the laws of sediment transport.
  - The rate of recession of the eroding face varies approximately with the  $1/3$  power of the scale ratio of fuse plug constructed with identical materials (non-cohesive).

In addition to the above laboratory model test, they carried out large scale field model tests to verify the design assumptions like depth of water required to effect a successful breach, mechanism of the breaching action at the pilot channel, completion of breach before lateral erosion and washout process for lateral erosion. They also observed the effect of core on rate of washout, completeness of washout. Based on direct observations and the motion picture record, the rate of washout results are summarized as follows:

- i. Completion of breach: 1 min and 27sec.
- ii. Rate of washout (uniform material): 5.6ft/min or 0.0284m/sec.
- iii. Rate of washout (well graded material): 1.4 ft/min or 0.0071m/sec.
- iv. Hold-up time of the core was insignificant.
- v. Fuse-plug was completely washed out to the concrete foundation.

Chee (1988) conducted a series of experiments in the laboratory to study the scale effects associated with modelling the erosion of granules embankments. In his investigation he carried out experiments with the smallest one measuring 150mm wide  $\times$  120 mm high to give a range with upstream slope 2:18 to 6:1 downstream slope 2:1 to 3:1 of model scales of up to 1:12. A wide range of material sizes and embankment shapes were utilized in the test. The



model dams were breached by overtopping and washed away at constant discharges. In the washout of the dams, special care was taken to ensure that the bed material was not subjected to backwater effect. Photographs were continuously taken during the scour process to capture all the significant phases of erosion phase through the Plexiglas walls of the flume. The washout rate was computed from this pictorial time record by enlarging the photographs. In studying the washout time of the dams, he has used two separate methods namely, one from experimental dimensionless equation with numerical values of the coefficient obtained from the laboratory data by statistical analysis and secondly from well known sediment bed load equations. The time averaged values of the measured variables are used to formulate non-dimensional equation of the wash out rate. He has related  $C = q_s/q_w$  sediment concentration with height of dam ( $H_D$ ) critical flow depth for  $q_w$ , mean grain size ( $d_{50}$ ), specific gravity of grain ( $S_s$ ), angle of repose of material in radians ( $\theta$ ) and acceleration due to gravity ( $g$ ), and mean width of dam has come out with a relation

$$\frac{q_s}{q_w} = C \left( \frac{gH_D^3}{2} \right)^{0.1} \left( \frac{y_c}{d_{50}} \right)^{0.125} \left( \frac{1}{S_s - 1} \right)^2 \left( \frac{1}{\theta} \right)^{0.125} \left( \frac{H}{B} \right)^{0.25} \left( \frac{E}{H_D} \right)^{0.375} \quad (2.10)$$

where  $E$  = initial distance between flume bed and dam crest, different to  $H_D$  as dam is placed on a deck

It has been shown, the experimental time scale for washout using Equation (2.10) depends on  $\theta_p/\theta_m = \theta_r$ , model scale ( $L_p/L_m$ ),  $d_r = d_p/d_m$  and  $S_r = ((S_s - 1)/(S_s - 1)_m)$  as:

$$T_r = \left( \frac{L_p}{L_m} \right)^{\frac{1}{8}} S_r^2 d_r^{\frac{1}{8}} \theta_r^{\frac{1}{8}} \quad (2.11)$$

Conclusions from his analysis of Experimental data are:

Washout time scale using Einstein bed load transport formula is independent of the model scale and depends on the properties of the granular material. Regarding the study of scale effects, he has also drawn the conclusion: for grain diameter scale, the model sediment grain, specific gravity decreases as the model material size increases and as the model sediment size decreases, the scale effect is reduced.

## 2.8 Scope for the Present Study

From the present review of the literature it is found that the following aspects of dam breach problem should be addressed for the better understanding of the mechanism associated with its process.

Dam breach problem due to overtopping flood lacks necessary experimental data support, particularly in the process behaviour. In the earlier experimental observations both lateral and vertical erosion process with time and space are not considered in the analysis. Reservoir capacity, inflow discharge to the reservoir and dam geometry and dam fill properties are not taken together for analysis in experimental data.

Regarding numerical modelling on dam breach, quite a good number of models are available. Some of the models have predicted well the historical dam failure cases pertaining to breach outflow hydrograph. But the dam breach problem essentially associated with the erosion of sediment and its movement under highly accelerated flow condition. So the bed shear stress and sediment discharge relation needs a special attention to have a functional relation among them along with other breach parameters. In the literature the investigators have mentioned their reservations about the use of sediment transport formulae in the dynamic situations like dam breach which is meant to be used for alluvial stream for uniform flow situation.

With these shortcomings in the present state of knowledge on dam breach due to overtopping of flood, the basic model studies are planned in the laboratory environment to study the dam breach process and to verify the obtained result with some field data on historical dam breach.

In fuse plug washout study there is not much reported literature either on experimental study or numerical modelling except a very few to name. Although both the dam breach and fuse-plug washout problems more or less come under the same category of study, the former is three dimensional and latter is two dimensional. In case of fuse plug there is restriction of lateral erosion. Keeping this state of knowledge on fuse plug in view, basic model study (for the better understanding of the washout process in the fuse plug) is planned in the laboratory.

**PART I**  
**BREACH EROSION OF HOMOGENEOUS**  
**EARTHFILL DAMS DUE TO OVERTOPPING**  
**FLOW**

## **PART I**

# **BREACH EROSION OF HOMOGENEOUS EARTHFILL DAMS DUE TO OVERTOPPING FLOW**

Part I deals with the erosion aspects of breach caused by overtopping flow on homogeneous earthfill dams. The details of experimentation carried out on the breach formation in homogeneous cohesionless earthen embankment and cohesive earthen embankment models are presented in Chapter III.

The mechanism of dam breach process includes the morphological aspects, flow hydraulics and erosion characteristics. These are studied, first for cohesionless soil embankment and for cohesive soil embankment separately and later on the combined study has been made. Analysis of the laboratory data combined with field data is carried out for final breach geometry and flow parameters. These aspects are presented in Chapter IV.

Chapter V includes further analysis of the lab data including two field data namely Teton dam breach and Huaccoto dam breach to predict the breach hydrograph, sediment discharge graph along with final breach geometry and flow parameters. A methodology is suggested for the computation of breach process based on the analysis presented in Chapters IV and V.

## **CHAPTER III**

# **SCHEME OF EXPERIMENTATION ON DAM BREACH**

### **3.1 Scheme of Experiments**

The breaching of an earthen embankment dam due to overtopping of flow is simulated by modelling earthen embankments with two different soils and varying embankment geometry in the Hydraulics laboratory of Indian Institute of Technology, Kanpur. The major objective of this experimental study was to understand the dam breach process due to overtopping flow.

In the present chapter, details of flume, dam model, soil used for model preparation, measurement of criteria variables, the procedure to compute other criteria variables involved in the problem have been presented. Besides these the photographs taken during the breach for a dam model with cohesionless soil are presented to familiarise oneself with the different phases of breach process. Statistical analysis of the measured data is carried out to assess the magnitude of the deviations from the mean values.

#### **a. Details of Flume**

The flume used for these experiments is a tilting flume 20m long, 0.60m wide and 0.50m in height. The details of flume dimensions, position of embankment model in the flume and dimensional details of embankment are shown in Figures 3.1(a) and (b). The water was supplied to the flume from a constant overhead tank which got its supply from an underground sump, through a pump. Flow straightener was kept at the entry point of reservoir (storage area between the dam model and the water inlet section) to check the unsteady wave formation in the reservoir during the time of experiments .

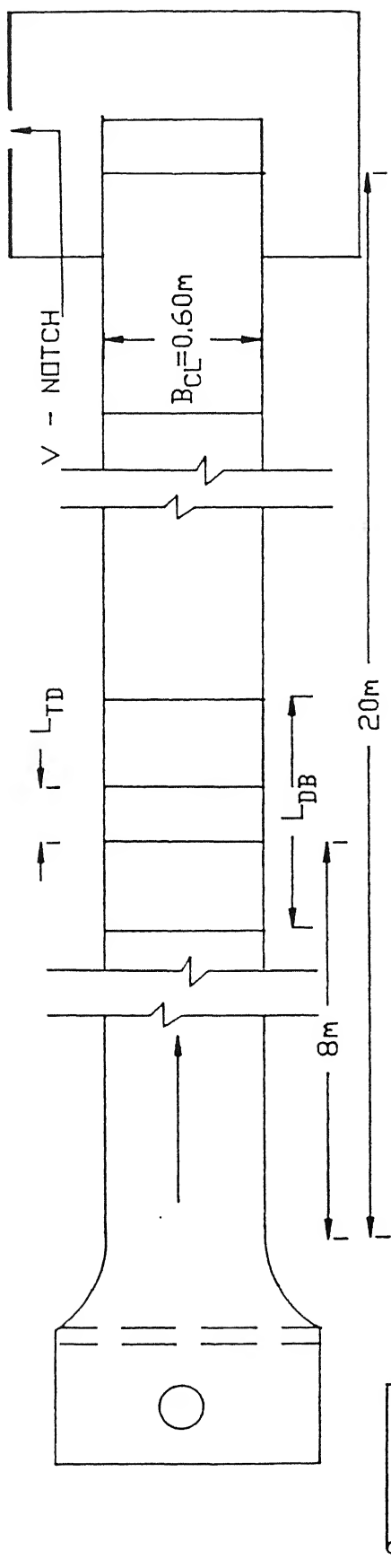


Fig 3.1a: PLAN VIEW OF TILTING FLUME WITH DAM MODEL

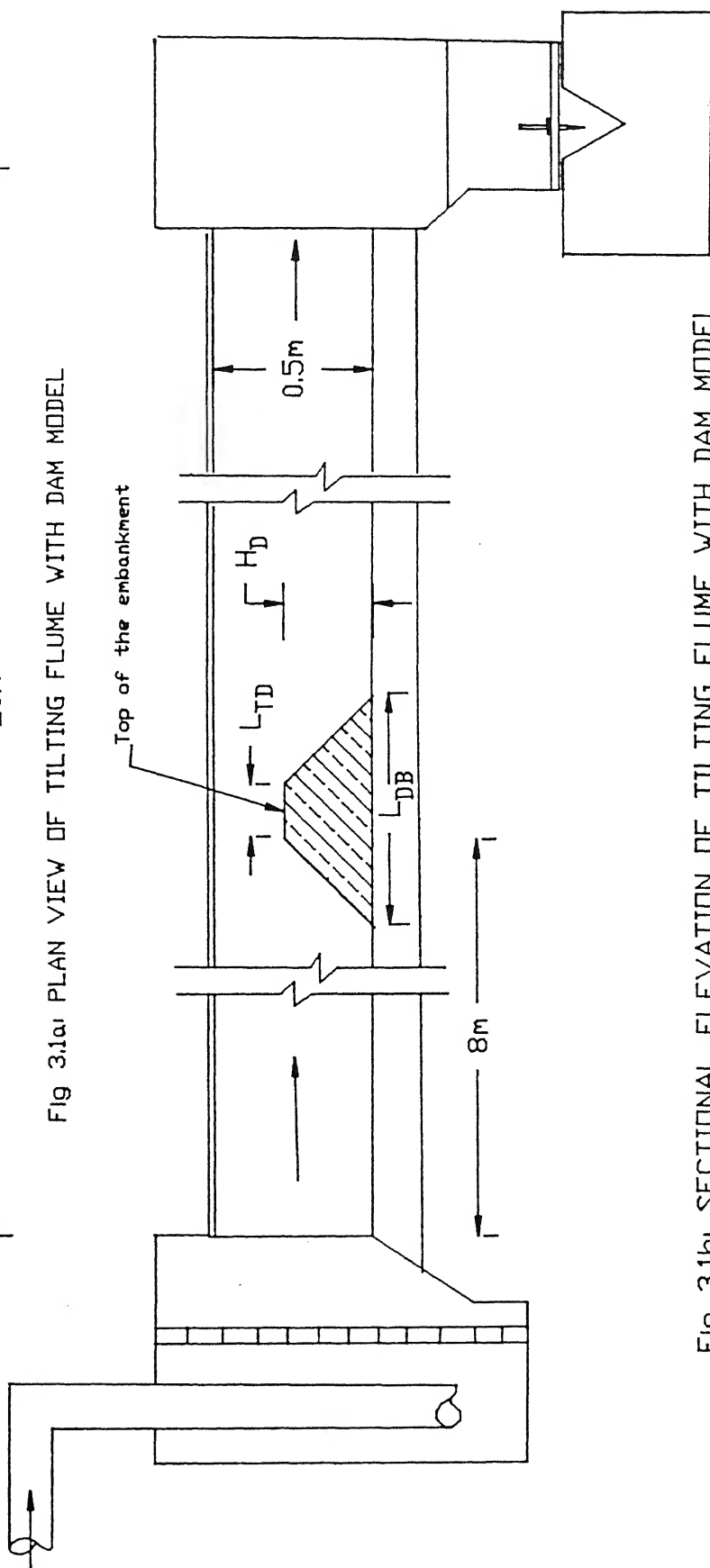


Fig 3.1b: SECTIONAL ELEVATION OF TILTING FLUME WITH DAM MODEL

Water supply into the reservoir was regulated by operating a valve in the inlet pipe. The test section for all the experiments was maintained at 8m from the inlet. A calibrated V-notch was used for measuring discharge passing through the flume after the breach flow comes to steady state.

## b. Model Details

Two types of soils are used in the preparation of the embankment dam models, namely cohesionless (type-A) soil and cohesive soil (type-B). Henceforth the cohesionless soil and cohesive soil used for the model preparation will be referred as type-A and type-B soil respectively.

### i. Model with Cohesionless Soil

The type-A soil, cohesionless soil was collected from the river bed of Ganga near Kanpur for model preparation. With this cohesionless sand, twelve experiments were carried out with the variation of model geometry and incoming discharge to the reservoir. The volume enclosed by the flume's two side walls and the upstream of the dam model is called here as the reservoir. In all these experiments the inflow is kept constant throughout the experiment. The details of the model geometry are given in Table 3.1(a). The height of the dam ( $H_D$ ) was varied from 14.5 cm to 35 cm as shown in Table 3.1(a). Similarly the length of the dam crest is also varied from 15 cm to 156 cm, keeping the upstream and downstream slope of the dam constant to 1 vertical (V) to 2.5 horizontal (H).

TABLE 3.1a

DIMENSIONS OF DAM MODEL WITH COHESIONLESS SOIL

S. No	Run Nos.	$H_D$ (cm)	$B_L$ (cm)	$L_{TD}$ (cm)	V:H **	$L_{DB}$ (cm)	$A_D$ (cm <sup>2</sup> )	Reservoir Capacity (cm <sup>3</sup> )	$Q_{in}$ (cm <sup>3</sup> /sec)
1	1005	35.0	60	150	1:2.5	325	8312.50	2363025.0	420.00
2	0805	30.0	60	150	1:2.5	300	6750.00	2025450.0	1349.60
3	0705	25.0	60	154	1:2.5	279.0	5412.50	1687875.0	1539.70
4	0505	19.5	60	150	1:2.5	247.5	3875.63	1316542.0	569.70
5	0405	14.5	60	145	1:2.5	217.5	2628.13	978967.5	291.00
6	0305	15.0	60	156	1:2.5	231.0	2902.50	1012725.0	1586.60
7	0105	14.5	60	156	1:2.5	228.5	2787.63	978967.5	1616.40
8	3004	14.5	60	154	1:2.5	226.5	2758.63	978967.5	169.70
9	2904	14.5	60	142	1:2.5	214.5	2584.63	978967.5	1586.60
10	2804	14.5	60	60	1:2.5	132.5	1395.63	978967.5	1036.13
11	2604*	14.5	60	15	1:2.5	87.5	743.13	978967.5	336.4
12	2504*	14.5	60	45	1:2.5	117.5	1178.13	978967.5	1866.60

\* These data are not used in the analysis due to insufficient informations.

**TABLE 3.1b**  
**DIMENSIONS OF DAM MODEL WITH COHESIVE SOIL**

S. No	Run Nos	$H_D$ (cm)	$B_{CL}$ (cm)	$L_{TD}$ (cm)	V:H ••	$L_{DB}$ (cm)	$A_D$ (cm <sup>2</sup> )	Reservoir Capacity(cm <sup>3</sup> )	$Q_{in}$ (cm <sup>3</sup> /sec)
1	1203	12.0	60	15	1:2.5	75.0	540.00	$7.97 \times 10^5$	940.00
2	2703	16.9	60	15	1:2.5	99.6	968.50	$1.12 \times 10^6$	1129.85
3	0404	20.0	60	15	1:2.5	115.2	1305.80	$1.32 \times 10^6$	1082.20
4	1104	23.6	60	15	1:2.5	133.1	1750.39	$1.55 \times 10^6$	1330.00
5	2204	26.4	60	15	1:2.5	137.2	1859.20	$1.60 \times 10^6$	6088.60

Upstream & downstream slope of dam cross-section V:H

Notations used in Table 3.1(a) and (b) are explained as follows:

$H_D$  = height of the dam,

$B_{CL}$  = crest length of dam model,

$L_{DB}$  = bottom width of the embankment along the centre line of the flume.

$L_{TD}$  = top width of embankment,

V:H = bank slope of vertical : Horizontal

$A_D$  = cross - sectional area of the embankment along the centre line of the flume

Reservoir capacity = volume of water stored in the flume upstream of embankment

$Q_{in}$  = Inflow discharge into the reservoir.

This slope of the dam was chosen keeping in view, that the ratio of Vertical to Horizontal (V:H) varies from 1:2 to 1:3 in the field. In some cases the top width of the embankment dam model is not proportionate to the earthen dam geometry. Larger top width is provided in some cases, because this gives enough time for the measurement of breach process.

## ii. Embankment Dam Model with Cohesive Soil

The type-B soil, cohesive soil used for the preparation of embankment dam model was collected from the campus of Indian Institute of Technology, Kanpur. In total five experiments were carried out in this category. In case of cohesive soil embankment model the height of the dam varies from 12.0 cm to 26.4 cm, keeping the top width constant as 15 cm. The upstream and downstream slopes were maintained as V:H = 1:2.5. In this case top width was maintained proportionate to dam geometry. This is because the breaching process in cohesive soil model takes more time compared to cohesionless soil, giving sufficient time for measurement of breaching process. The details of dam models with cohesive soil is given in Table 3.1(b). The inflow was kept constant in these experiments also.



### c. Properties of Soil used in Embankment Model

Soil samples collected from each embankment of the dam were used for measurement of the angle of friction ( $\phi$ ) and cohesion ( $c$ ) by conducting undrained triaxial test in the Geotech laboratory of the Institute. These samples used for triaxial test are used for measurement of the dry density and water content of the soil after putting it inside the oven for 24 hours. The particle size distribution analysis was carried out for the soil used in the embankment fill. The type-A soil and type-B soil were subjected to sieve analysis for the size distribution. The details of soil properties are shown in Table 3.2. Moisture content was kept at 14 percentage during the construction of embankment dam model with type-A and type-B soils.

**TABLE 3.2**  
**SOIL PROPERTIES OF COHESIONLESS**  
**AND COHESIVE SOIL USED IN MODEL PREPARATION**

Type of soil	$d_{50}$ (mm)	$\phi$ (degree)	$c$ KPA	$(\gamma_b)_{av}$ 9810* N/m <sup>3</sup>
Cohesionless Soil (Type-A soil)	0.16	32.1	0	1.58
Cohesive soil (Type-B soil)	0.28	33.1	1.6	1.95

The particle size distribution curves for type-A and type-B soils are shown in the Figure3.1(c).

### d. Preparation of Embankment Dam Model

To prepare the embankment dam model the following procedures were adopted for both cohesive and cohesionless soil. The soil was mixed properly after adding water to it. The amount of water added to the soil was judged purely based on the experience for better compaction of the soil. There after this soil was laid in the layers of 5 cm thick on the dry bed of the flume. Soil was compacted well with a hand hammer uniformly over the top surface. Scratches were made on the top surface before laying another layer. The next layer of the thickness 5 cm was spread over the surface and was again compacted. This process was continued till the model dimensions were achieved. Then the top surface, upstream and downstream face of the dam were compacted uniformly. Slight depression in the centre of the top of the model along the centre line of the flume was made in order to control the position of the breach occurrence. Then the soil samples were collected from the model body for the measurements of soil properties. The positions where soil samples were removed were again filled with soil with proper compaction., The water was allowed upstream of the reservoir

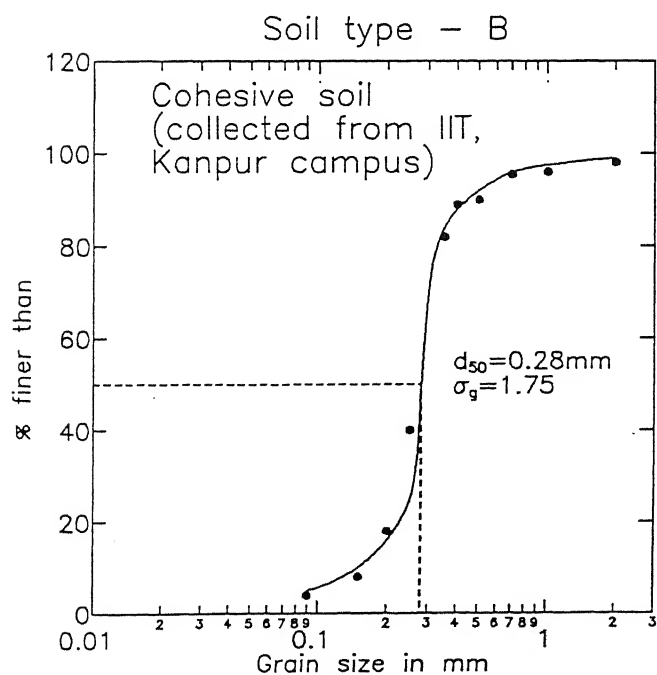
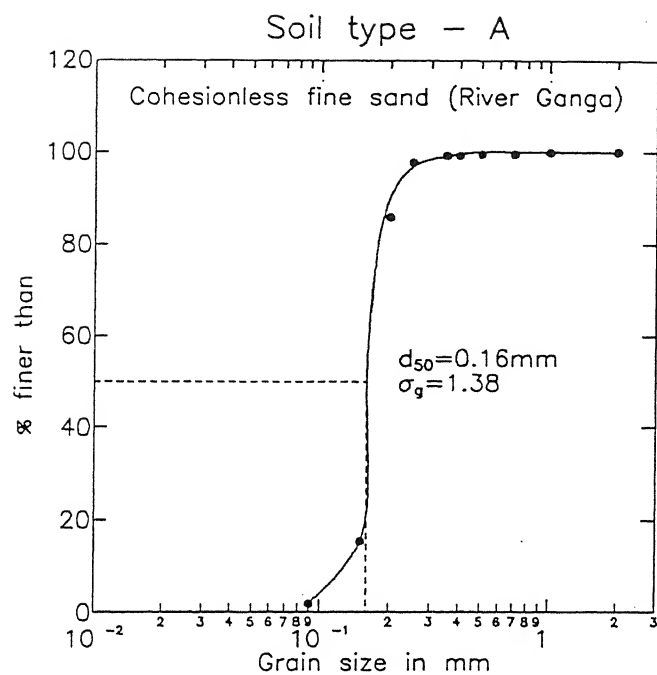


Fig. 3.1(c): Particle size distribution for soil types-A and B

keeping constant flow. As soon as the overtopping of flow occurs, the breach process sets in. Measurements of water surface levels, sediment bed levels and width of breach were carried out at prefixed positions along the breach longitudinal section. The methods adopted for the preparation of embankment dam, both for cohesive and cohesionless soil were same for all the runs conducted.

### 3.2 Some Observations of the Breach Process

Some critical observations made during the breaching process of cohesionless and cohesive soil embankment dam models are:

#### a. Observations of Erosion Process due to Overtopping of Flow in Cohesionless Soil Embankment Dam

- i. As soon as the incoming flow or reservoir water level exceeds the embankment level, water starts over flowing first on the dam crest and then on the downstream slope as indicated in the photographs, shown in Figures 3.2(a), and (b) respectively. These photographs are taken from downstream end sequentially, away from the embankment, looking in the upstream direction. The height of this model was 0.25m and top width of the crest of the embankment was 0.15m with both upstream and downstream slope equal to  $V:H=1:2.5$ .
- ii. As the flow traverses the downstream slope completely and touches the bed, the erosion near the toe of the embankment is initiated. Lateral widening of channel at the toe of the embankment and deepening of channel on the downstream face are visible as in Figures 3.2(c) and (d). Erosion on the flow path particularly in the downstream is initiated because of steep gradient associated with high shear stress.
- iii. Toe erosion starts receding upstream and by widening its path as well as having steeper vertical fall. These can be seen in Figures 3.2 (e) and (f). During this process, the flow channel formed at the dam crest and downstream face of the embankment deepens having almost v - shaped valley or narrow deep valley.



**Fig. 3.2(a) :** Flow of reservoir water on dam crest after overtopping and shows erosion of downstream top edge of the embankment



**Fig. 3.2(b) :** Flow of water on the downstream slope of the dam : overtopping



**Fig. 3.2(c) :** Initiation of erosion near toe of the dam



**Fig. 3.2(d) :** Lateral enlargement of erosion at toe of the dam and formation of gully on downstream slope of the embankment

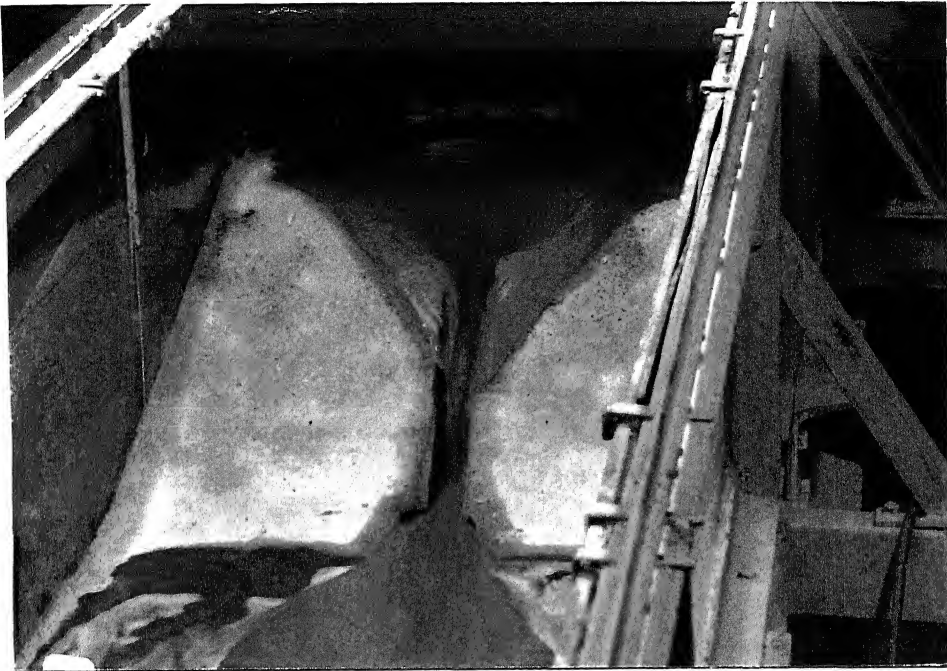


**Fig. 3.2(e) :** Receding of toe erosion in upstream direction

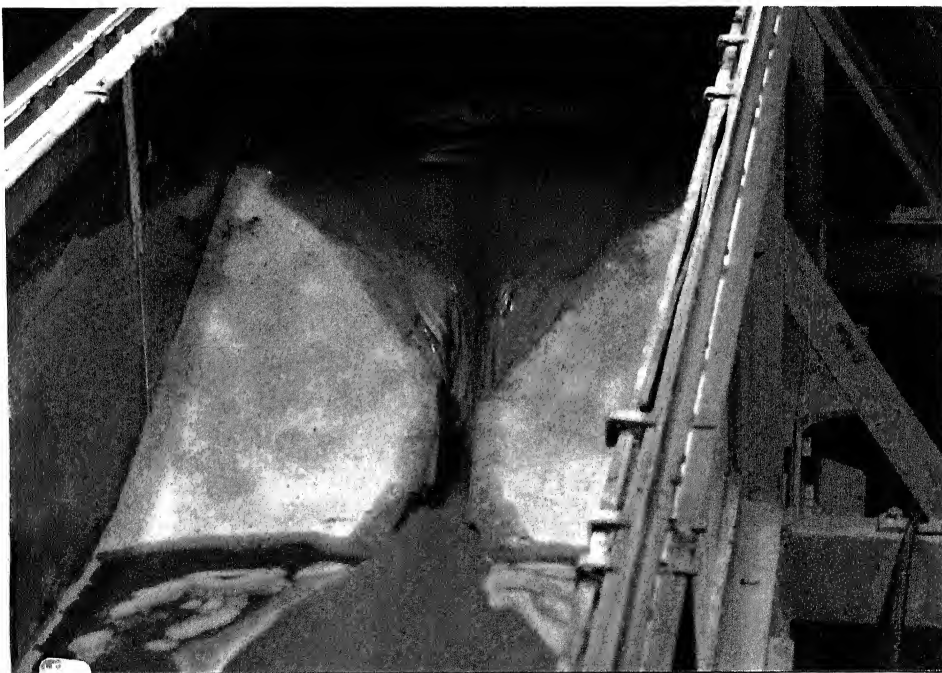


**Fig. 3.2(f) :** Deep vertical cut in the downstream face of the dam along with receding of toe erosion in upstream direction

- iv. Formation of bank collapse and washout of collapsed bank soil, formation contracting section upstream and diverging section downstream with contracted throat are seen in Figures 3.2(g) and (h).
- v. During the receding crest of the flow, the flow channel gets widened in the downstream face with possible bank collapse. This phenomenon can be seen from Figures 3.2(i), (j), (k), and (l).
- vi. During this receding process of crest, one can observe that the flow over the crest behaves like flow over a erodible weir with gradual change in water surface in the upstream and steep drop in water surface level over the crest. On the downstream end one can notice pool formation and sometimes flow associated hydraulic jump. This is shown in Figures 3.2(m), (n), and (o).
- vii. Once the receding of the crest moves in the top section of the embankment dam, the erosion process is fast, causing bank collapse and bed erosion. This can be seen from Figure 3.2(p).
- viii. As soon as the flow crest moves upstream, beyond the upstream edge of the embankment, the crest width enlarges. The alignment of the crest is curved. This causes the breach section having a large width at upstream edge, contraction at the centre and enlargement of width at down stream end. This can be seen in Figures 3.2(j) to 3.2(p).
- ix. By this time, water level in the reservoir has lowered considerably. The rate of erosion process slightly reduces. The flow at upstream face will be similar to flow over spillway with erodible crest. During this process, the crest level reduces and bank collapses causing widening of the breach. as shown in Figures 3.2 (q) to 3.2 (r).
- x. The above mentioned process continues till the crest is almost washed out and channelisation of flow through breach section forms. This is shown in Figures 3.2(q) and 3.2(r). This process continues till emptying of reservoir or occurrence of gradual varied flow having a very minimal erosion. This erosion is similar to the erosion in channel with gradually varied flow.





**Fig. 3.2(g) :** Widening of the path of erosion on downstream slope of the dam with steeper vertical fall and bank collapse



**Fig. 3.2(h) :** Under scouring on the downstream slope of the dam with breach channel having contraction section upstream and diverging section downstream with a throat are visible





**Fig. 3.2(i) :** Widening of the breach channel by bank collapse and spillway type crest formation are visible



**Fig. 3.2(j) :** Washout of soil from bank collapse with contracted throat and spillway type of crest flow at upstream are visible



**Fig. 3.2(k) :** Widening of flow path of water, contracted throat and spillway type of crest flow are visible



**Fig. 3.2(l) :** Spillway type of flow over the erodible crest with large width at upstream edge, contraction at the centre and enlargement of breach width at downstream end are visible



**Fig. 3.2(m):** Flow over the crest behaves like flow over erodible spillway



**Fig. 3.2(n):** Pool formation at downstream of erodible crest and flow associated hydraulic jump



**Fig. 3.2(o):** Widening of breach with pool formation at downstream of the crest, and hydraulic jump formation at the erodible spillway at the upstream



**Fig. 3.2(p):** Curved crest spillway type flow, hydraulic jump form at the toe of the spillway flow, more lateral erosion on side bank are visible



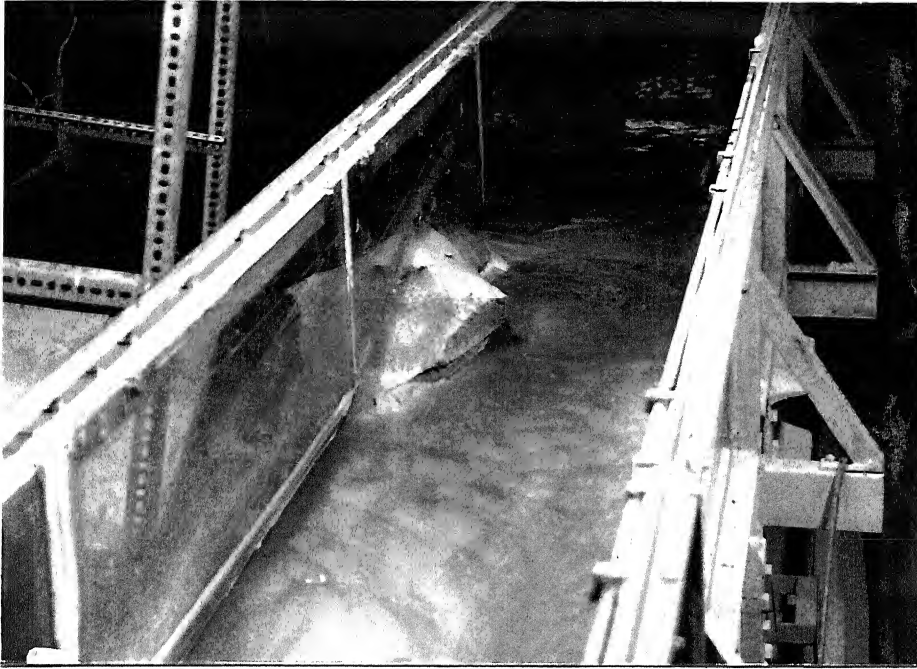


Fig. 3.2(q): Reduction in reservoir level, lateral erosion touching one side of the flume, flow concentration on one side are visible



Fig. 3.2(r): State of breach process nearing to the final state of erosion is observed

The whole process of erosion of breach occurs within around 5 to 10 minutes in laboratory for dam model with cohesionless soil.

### **b. Erosion Process due to Overtopping of Flow on the Cohesive Soil Embankment**

All the steps of erosion process indicated in cohesionless soil embankment are occurring in the erosion process of cohesive soil embankment also. The main difference in the erosion process of the embankment with cohesive soil is slower to cohesionless soil embankment erosion. Duration of breach observed for the cohesive soil embankment in the laboratory is about 20-45 minutes depending upon the intensity of inflow and channel geometry of the embankment model. The other main observation is the occurrence of the cascading of the flow near the downstream edge of the embankment during part of erosion process.

## **3.3 Data Collection**

### **a. Measurement of Basic Data During Breach Erosion**

To study the breaching process of the dam due to overtopping of the flow, it is necessary to measure the water level( $h_w$ ), bed level( $h_c$ ) and width of the breach at different longitudinal positions with respect to time. Vernier point gauge with an accuracy of 0.10mm has been used for measurements of  $h_w$ , and width of the top surface of water has been measured by an ordinary scale with an accuracy of 1.0mm. The vernier point gauge was modified for the measurement of  $h_c$  by providing a flat bottom at tip of the pointer by fixing a thin cork. From this basic data one can compute water and sediment discharge and breach geometry for given flow condition. During the measurement of these breach variables for cohesionless embankment it was observed that the erosion process was very fast. In order to increase the erosion time, the top width of the model was increased from 15 cm to 156 cm.

The position of the measurement of water surface, bed level, and breach width are indicated in Figure 3.3(a). Table 3.3(a) contains details of measured quantities at each section. Analysis of erosion process was carried out after completing the water surface, bed surface and breach width variations with time. A few shortcomings were observed during the analysis of dam breach model data with cohesionless soil fill, particularly the absence of bed level measurements at downstream end, and water surface level variations for upstream of the embankment. These shortcomings were taken care of by installing more measuring stations for the embankment models prepared out of cohesive soil.

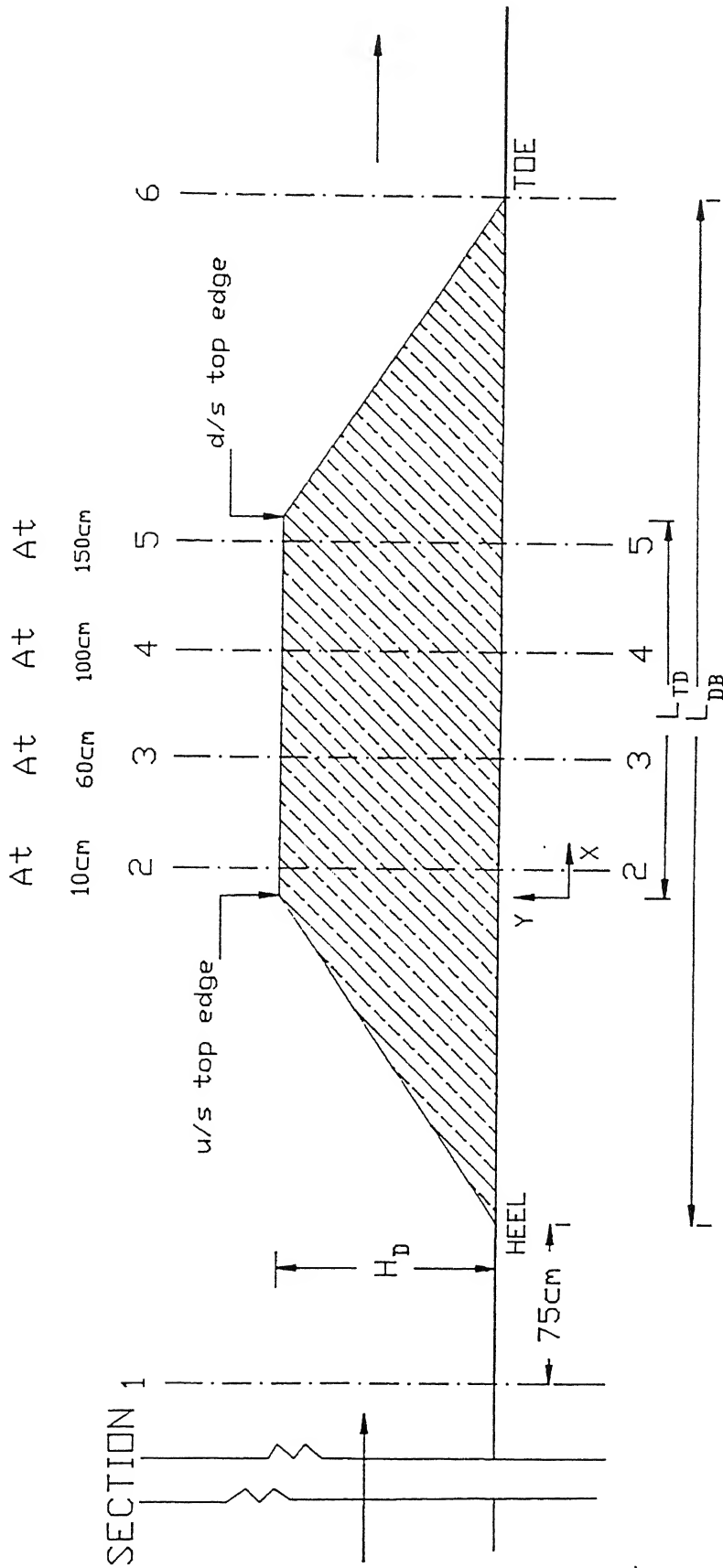


Fig 3.3a , LONGITUDINAL CROSS-SECTION OF EMBANKMENT DAM MODEL WITH COHESIONLESS SOIL INDICATING LOCATION OF SELECTED MEASURING SECTIONS

Figure 3.3(b) indicates the positions at which measurements were carried out for cohesive soil embankment models. Table 3.3(b) gives the details of measured quantities at different sections for cohesive soil embankment model.

### b. Final Measurements after the Attainment of Complete Breach Process

The bed level, water surface levels, breach width and cross-sections of the breach at different locations in addition to the specified measuring sections were carried out. By end of the breach, flow in the breach section has reached steady state. The measurement of discharge through breach was carried out by measuring the discharge over the v-notch attached to the tank located at downstream end of the outlet flume.

**TABLE 3.3a**  
**VARIABLES MEASURED DURING DAM BREACH AT DIFFERENT**  
**SECTIONS OF DAM MODELS WITH COHESIONLESS SOIL**

Section	1 (aa)	2 @ 10 cm	3 @ 60	4 @ 100	5 @ 150	6 Downstream	Remarks
1005	W	S W	S B	S B	S B	W	
0805	W	S W B	S B	S B	S B	W	
0705	W	S W B	S B	S B	S B	W	
0505	W	S W B	S B	S B	S B	W	
0405	W	S W B	S B	S B	S B	W	
0305	W	W B	-	***S B	S B	W	***@ 90 cm
0105	W	W B	S B	**S B	-	W	**@ 77 cm
3004	W	S W	W	S	-	W	
2904	W	S W	S B	S B	-	W	*@ 30 cm
2804	W	W S B	W S B	-	-	W B	

**TABLE 3.3b**  
**VARIABLES MEASURED AT DIFFERENT**  
**SECTIONS OF DAM MODELS WITH COHESIVE SOIL**

Sections / Run No	1	2 (aa)	3	4	5	6	7	8
1203	W	W	W	W S B	W S B	W S B	W S B	W S B
2703	W	W	W	W S B	W S B	W S B	W S B	W S B
0404	W	W	W	W S B	W S B	W S B	W S B	W S B
1104	W	W	W	W S B	W S B	W S B	W S B	W S B
2204	W	W	W	W S B	W S B	W S B	W S B	W S B

Where W  $\Rightarrow$  Water level

S  $\Rightarrow$  Sediment Bed level

B  $\Rightarrow$  Breach width at corresponding water surface.

Hence forth the section of measurement of water level in the reservoir, section-1 and section-2 for cohesionless and cohesive soil embankment respectively will be called as section-(aa) in the course of discussion.



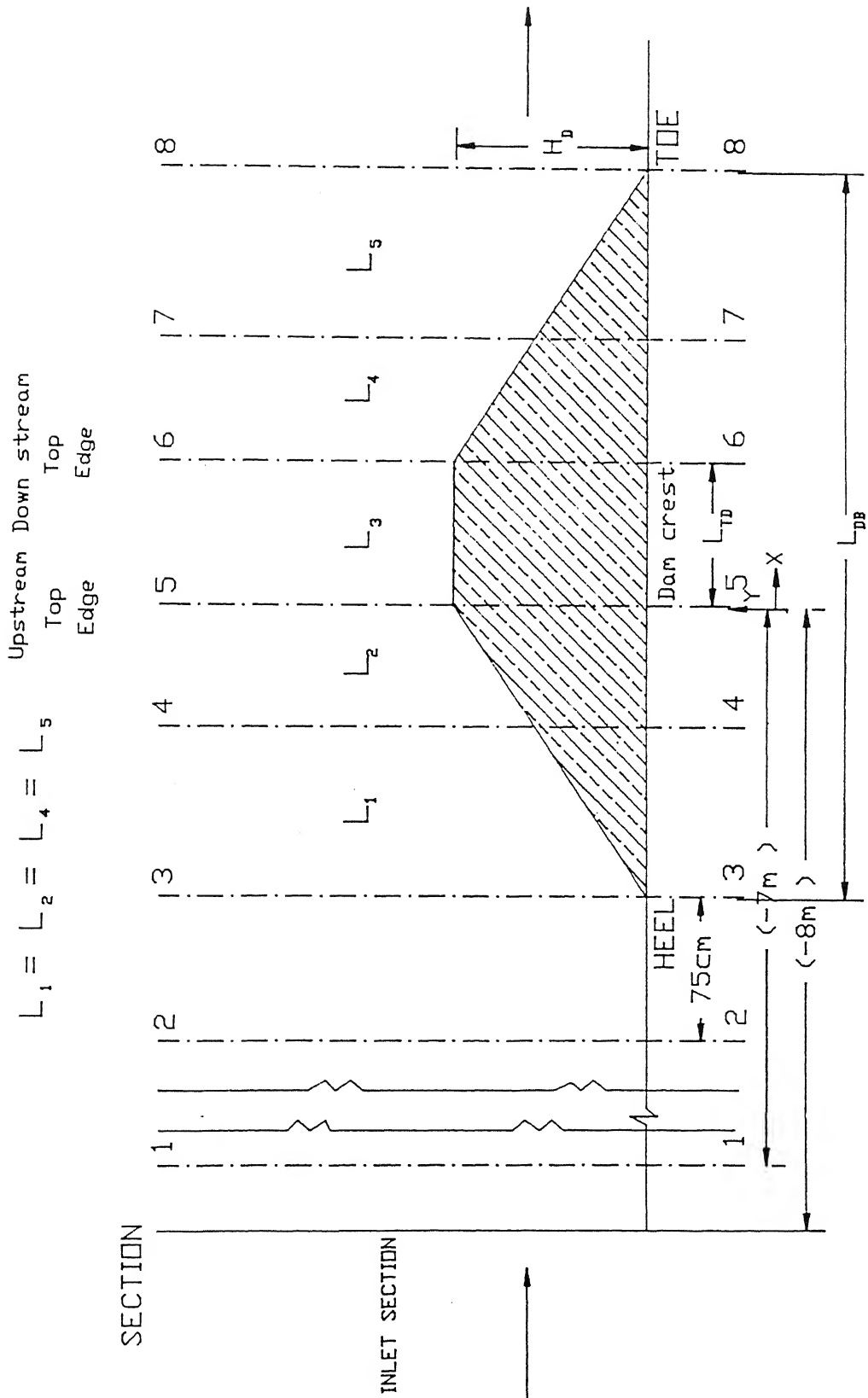


Fig 3.3b<sup>1</sup> LONGITUDINAL CROSS-SECTION SHOWING LOCATION OF SELECTED MEASURING SECTIONS FOR COHESIVE SOIL EMBANKMENT MODEL

### c. Basic Data Presentation for the Embankment Dam Model of Cohesionless Soil

Basic data collected for the run no.-1005 is shown as a typical set. The run no.- 1005 means, the experiments were carried out on the 10th day of the 5th month of the year 1995. The variation of water level in the reservoir ( $h_{wr}$ ), for section-1 and sediment bed level for the section-2 is shown in Figure 3.4(a). Variations of water level ( $h_{wc}$ ) and sediment bed level ( $h_{cm}$ ) at section - 2 are shown in Figure 3.4(b). The variation of water and sediment bed level are shown in Figure 3.4(c) for section-5. Figure 3.4 (d) shows the water level variation for section-6. The sediment bed level variations are shown in Figures 3.4(e) and (f) for sections 3 and section 4 respectively. The variation of breach width are shown in Figures 3.4(g), (h), (i) and (j) for sections-2, 3, 4 and 5 respectively.

### d. Basic Data Presentation for the Embankment Dam Model of Cohesive Soil

The basic data collected for the run no.-0404 is presented as a typical set. Here the run number 0404 means the experiment was conducted on the 4th day of the 4th month of the year 1996. Figure 3.5(a), contains the variation of reservoir levels with time for sections 1 and 2. Figure 3.5(b) contains the variation of the water surface level for section-3. The variations of water surface level and bed level are shown in Figure 3.5(c) for section-4. The Figures 3.5(d), (e), (f), and (g), contain variations of water surface level with time for sections 5, 6, 7 and 8 respectively. The breach widths at water surface level for sections 4, 5, 6, 7 and 8 are presented in the Figures 3.5(h), (i), (j), (k), and (l) respectively.

## 3.4 Computation of Parameters Controlling Breach Process

The parameters controlling the breach process can be broadly classified into two broad categories, namely flow parameters and sediment parameters. Definitions of some of these parameters are shown in Figure 3.6.

### a. Flow Parameters

The following are the flow parameters viz.,  $h_u$ ,  $Q_w$ ,  $\bar{S}_f$ ,  $\bar{V}_*$ ,  $\Delta E$ .

$h_u$  : the difference in the water level at section-(aa) to the sediment crest at breach. The reservoir level at section-a is chosen based on the water surface variation from the inlet to the breach section. It was observed in most of the cases that the maximum water level was occurring at section 1 in the case of cohesionless embankment and section 2 in the case of

cohesive embankment. This level was considered for discharge computation.

$Q_w$ : the water discharge flowed through the breach at any instant of breach process. This is computed using flow continuity equation as shown below.

$$[(Q_{in} \Delta t) - (Q_w \Delta t)] = \text{Change in volume of water in the reservoir during time } \Delta t$$

where,  $Q_w$  = Water discharge through breach section

$Q_{in}$  = Inflow discharge in to the reservoir, which is kept constant throughout the experiment and is measured after complete breaching of the embankment.

The change in the reservoir volume is computed by knowing change in water surface level from the variation of the reservoir level and multiplying it with water surface plan area.

$\Delta E$  : total energy difference between energy level at section-(aa) and downstream toe section of breach. Velocity at toe section is computed by knowing the cross-sectional flow area and its corresponding breach discharge.

$\bar{S}_f$  : Energy slope. This is the difference in total energy between the upstream section-aa to the down stream (toe) of the dam divided by the inclined sediment bed length ( $L_{is}$ ) between upstream edge of the dam to the toe of the dam. where ,

$$L_{is} = (\Delta h_c^2 + L^2)^{1/2}$$

$\Delta h_c$ : Difference in sediment bed level between the upstream edge to the toe of the embankment.

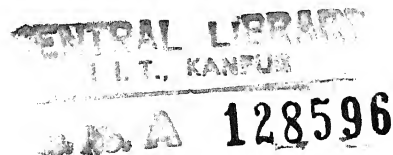
$L$  : Horizontal distance between the above mentioned sections.

In this analysis it is assumed that the energy at upstream edge of the embankment is equal to the energy at the section-(aa).

$\bar{V}_*$  : Average bed shear velocity and is computed as ,

$$\bar{V}_* = \{g \bar{R}_h \bar{S}_f\}^{1/2}$$

where,  $g$  = acceleration due to gravity



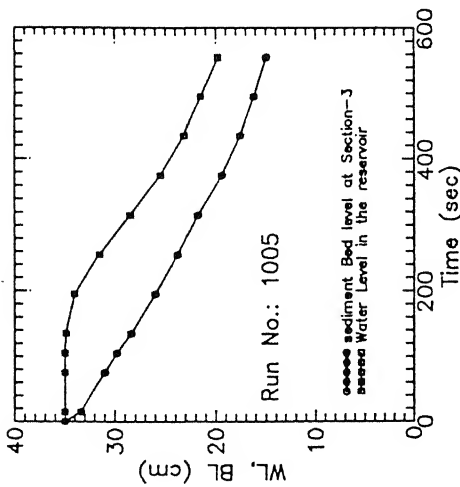


Fig.3.4a: Variation of Water level in the Reservoir, at Section-1 along with Crest Variation at Section-3 with Time

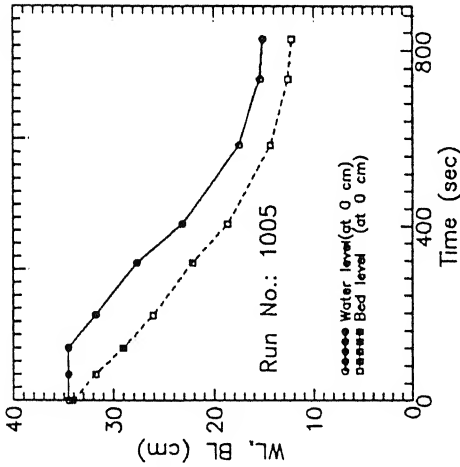


Fig.3.4b: Variation of water level and sediment bed level at section-2 with time

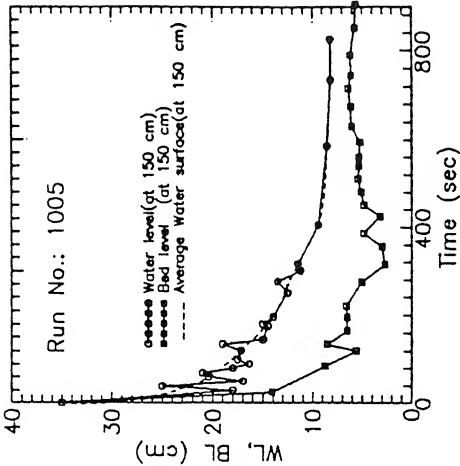


Fig.3.4c: Variation of Water level and Sediment Bed Level at Section-5 with Time

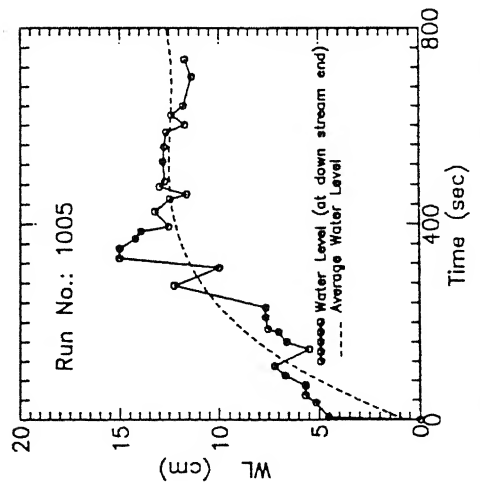


Fig.3.4d: Variation of Water level at Section-6 with Time

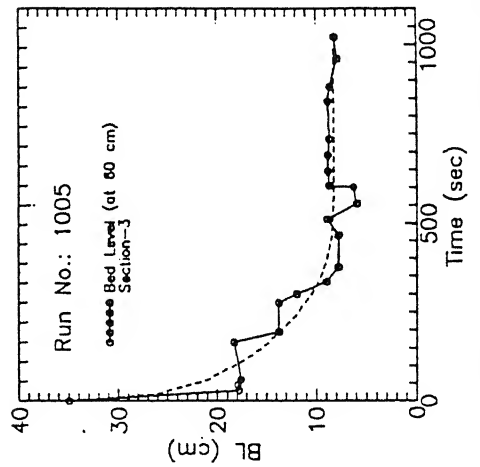


Fig.3.4e: Variation of Sediment Bed level at Section-3 with Time

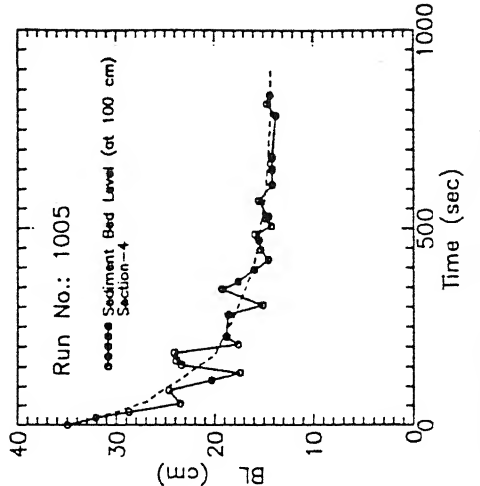


Fig.3.4f: Variation of Sediment Bed Level at Section-4 with Time

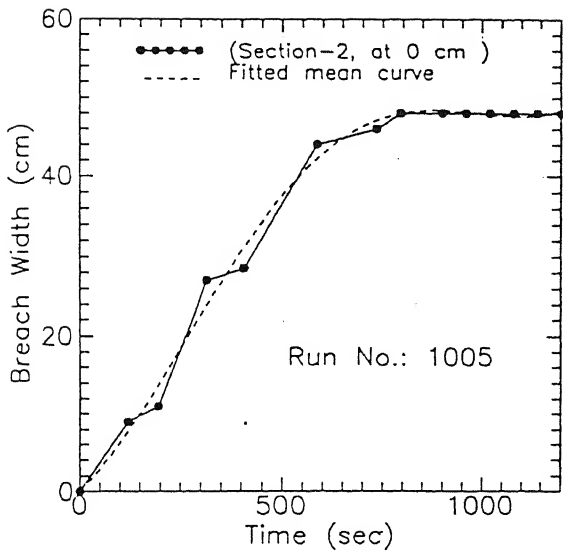


Fig.3.4g: Variation of Breach Width at Section-2 with Time

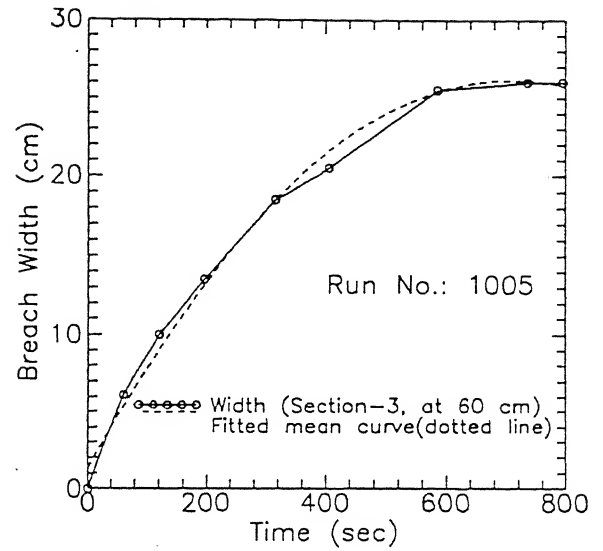


Fig.3.4h: Variation of Breach Width at Section-3 with Time

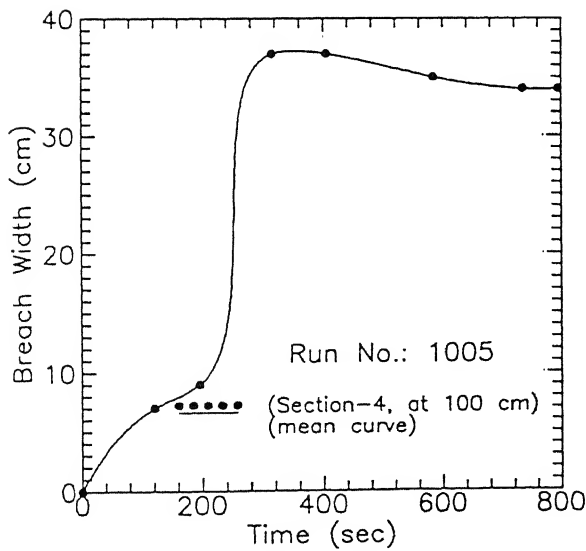


Fig.3.4i: Variation of Breach Width at Section-4 with Time

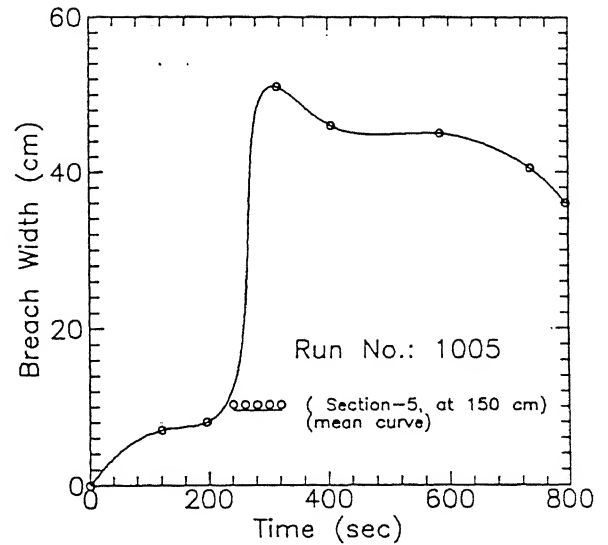


Fig.3.4j: Variation of Breach Width at Section-5 with Time

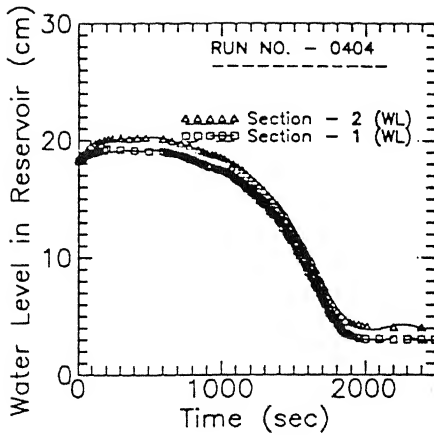


Fig.3.5a: Variation of Reservoir Water Levels with Time at Sections-1 and 2

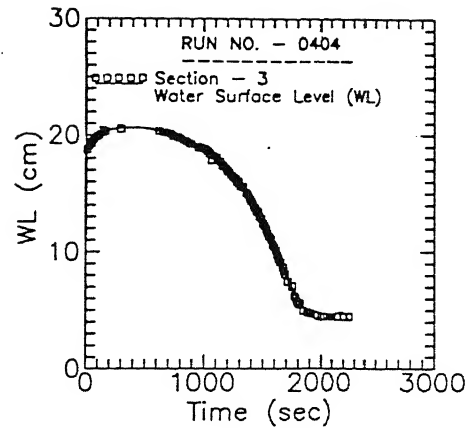


Fig.3.5b: Variation of Water Surface Levels with Time at Section-3

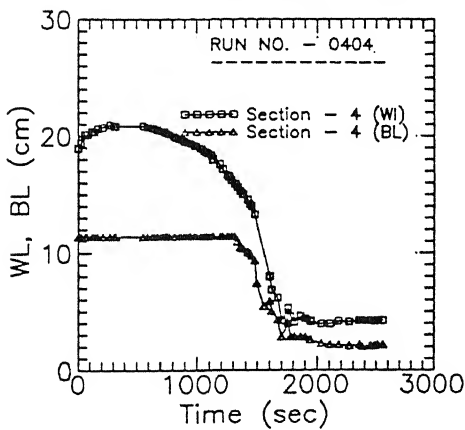


Fig.3.5c: Variation of Water Surface and Sediment Bed Levels at Section-4 with Time

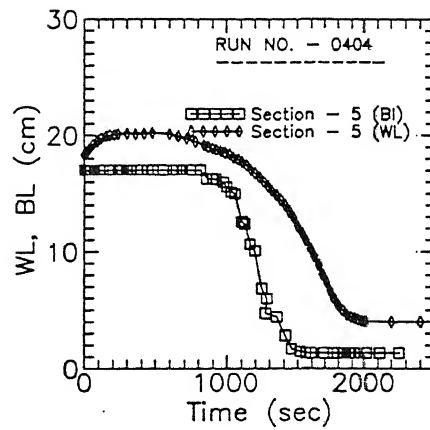


Fig.3.4e: Variation of Water Surface and Sediment Bed Levels at Section-5 with time

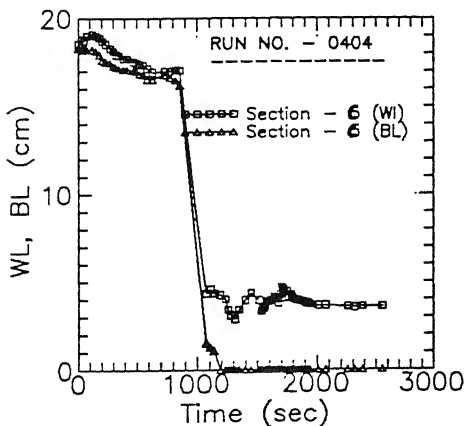


Fig.3.5e: Variation of Water Surface and Sediment Bed Levels with Time at Section-6

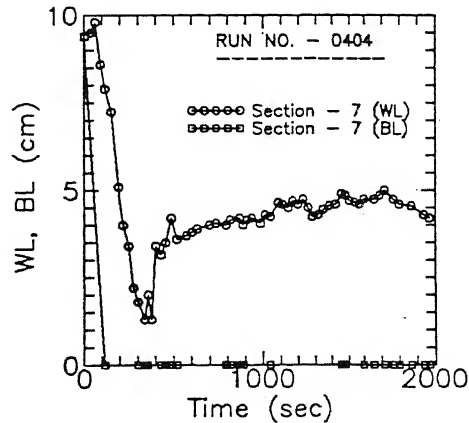


Fig.3.5f: Variation of Water Surface and Sediment Bed Levels with Time at Section-7

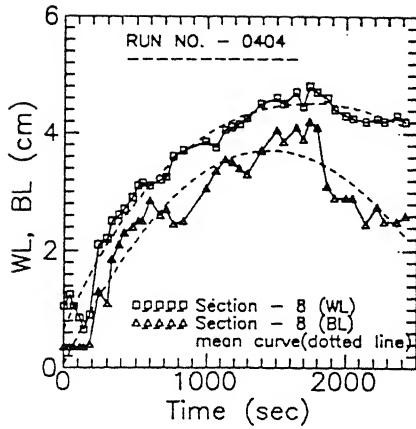


Fig.3.5g: Variation of water surface and sediment bed levels with time at section-8

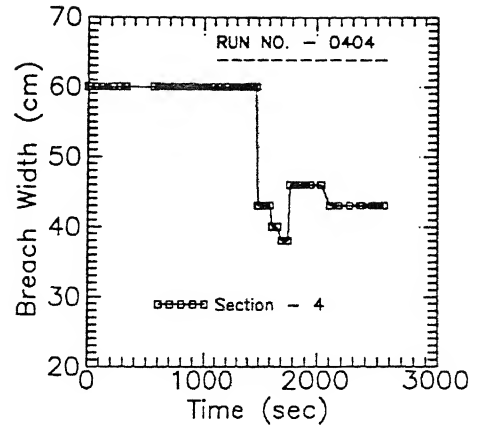


Fig.3.5h: Variation of breach width at section-4 with time

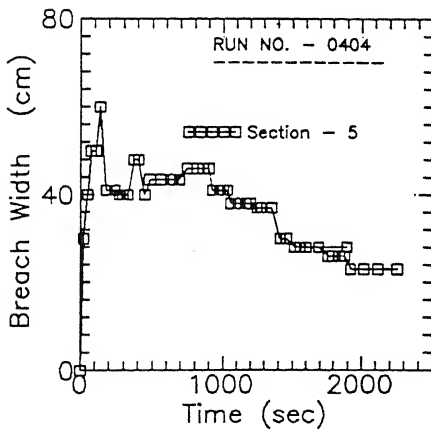


Fig.3.5i: Variation of breach width at section-5 with time

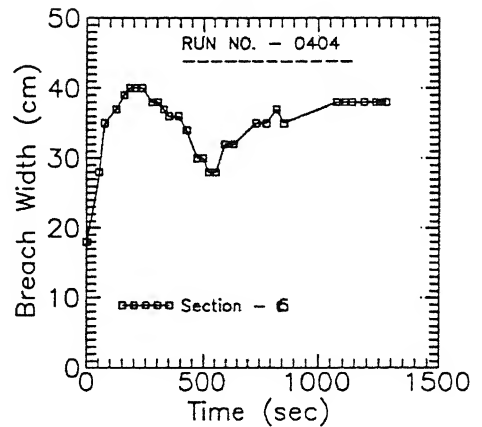


Fig.3.5j: Variation of breach width at section-6 with time

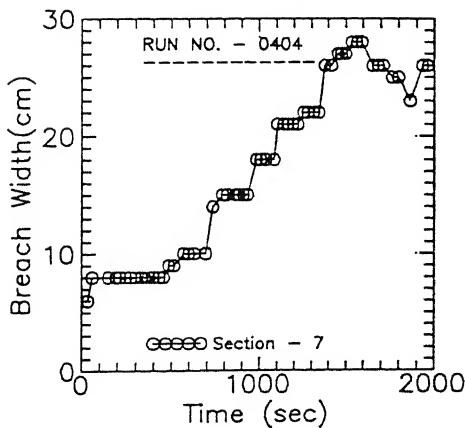


Fig.3.5k: Variation of breach width at section-7 with time

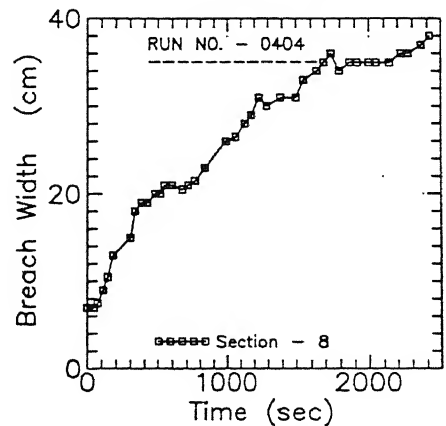


Fig.3.5l: Variation of breach width at section-8 with time

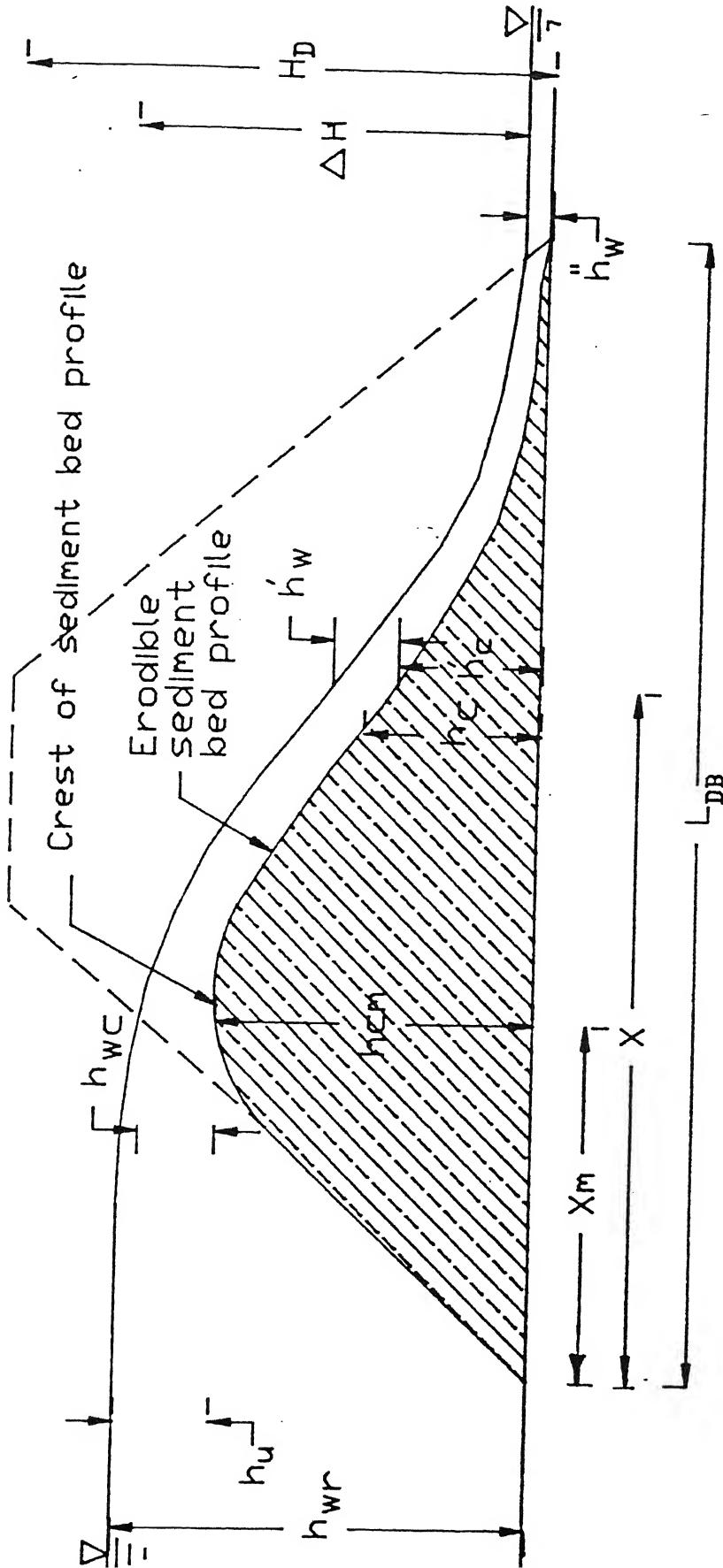


Fig. 3.6: Definition sketch for the dam breach analysis



$\bar{R}_h$ : Average value of the hydraulic radius at three sections, namely at the upstream top edge, downstream edge of the embankment and at the toe of the breach.

$\Delta H$ : Difference of water surface level between upstream of embankment (section 1, for cohesionless embankment section 2 for cohesive embankment) to the water level at downstream toe of the embankment.

$h_{cm}$ : Height of crest level measured from the bed of embankment.

$h_c$ : Height of the sediment profile at a section  $x$  measured from upstream edge of the dam.

$h'_c$ : Height of sediment profile at the downstream top edge of the embankment.

$h_{wr}$ : Reservoir level measured at section-(aa)

$H_D$ : Height of embankment dam.

### **b. Sediment Parameters**

The sediment parameters are  $A_s$ ,  $\nabla_s$ ,  $Q_s$  and  $C$ .

$A_s$ : This is defined as the eroded breach cross sectional area. This quantity is computed as the product of depth of erosion and the average width of erosion at a section considered. This quantity is computed at three sections namely upstream edge, downstream edge of the embankment and toe of the dam.

$\nabla_s$ : Volume of sediment eroded. This quantity is computed as the product of average eroded area between the two sections and the length between them. In the case of cohesive soil embankment models, more sections are used for the computation of  $\nabla_s$ .

$Q_s$ : Sediment discharge at the end of breach section. The cumulative volume of sediment eroded is plotted with time and an average curve is fitted to this data. The ratio of difference in cumulative eroded sediment volume divided by the corresponding time interval is considered as the total sediment discharge out of the breach section.

$C$ : Sediment concentration. This quantity is computed by dividing sediment discharge by breach outflow water discharge at a given time.

### 3.5 Frequency Analysis of Deviation of Data from the Mean Value

Measurement of water surface level, sediment bed level and water surface width for a section are plotted with time. Typical variations of these measurements may be seen in Figures 3.4 and 3.5. Fluctuations in data measured are clearly visible. A mean curve was drawn through these measured data using regression analysis. The data measured from this mean curve are taken for further analysis, not the actual fluctuating values. In order to see how much error one makes by using mean value instead of fluctuating values, a frequency analysis for the deviations from actual value to mean value is carried out. Typical variations of these frequency plots are shown in Figures 3.7 (a), (b), 3.8(a), (b), and 3.9(a), (b) for measurement of sediment bed level, ( $h_c$ ), water surface levels ( $h_w$ ) and width of breach at water surface level. The standard deviation indicates the average order of fluctuations associated with the measured data. The left hand side and right hand side crossed points of the dotted line in Figures 3.7(b), 3.8(b), and 3.9(b) shows  $\mu - \sigma$  and  $\mu + \sigma$  respectively. In x-axis of these figures, range means difference between the observed and fitted value of the variable. The symmetrical frequency plot with high peak and narrow base around mean indicates there is least difference between observed and fitted value of the variable. The unit of  $\mu$  and  $\sigma$  in these figures are expressed in centimeters. The magnitude of standard deviation in the measurement of sediment bed is high in comparison to other measurements. This is because erosion and deposition process associated with bank collapse and also with some uncertainty in locating sediment bed level. Since the mean curve obtained through regression analysis is used for extracting data for further analysis, error involved in the data will be minimum.

### 3.6 Concluding Remarks

In the present chapter besides describing the experimental setup and procedure in details, a typical set of measured variables like water level, sediment bed level, breach width at selected sections are presented for dam model of both cohesive and cohesionless soil fill during breach process. The approach adopted for the computation of other breach criteria variables are demonstrated. A typical frequency analysis of the deviations of experimental data from the mean curve are presented to access the order of the fluctuations associated with data.

Since the data extracted are from the mean curve, the error in the analysis of breach process is hoped to be minimum.

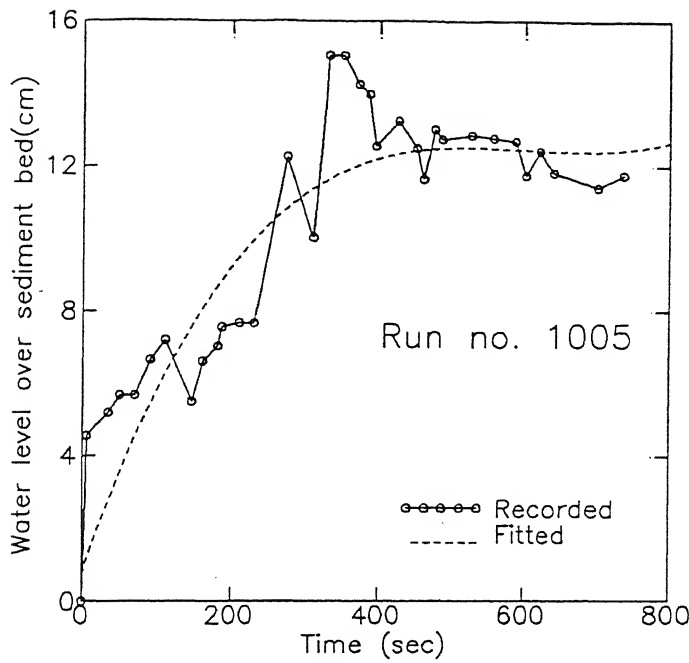


Fig. 3.7(a) : Recorded water levels at section-6 with time (sample data)

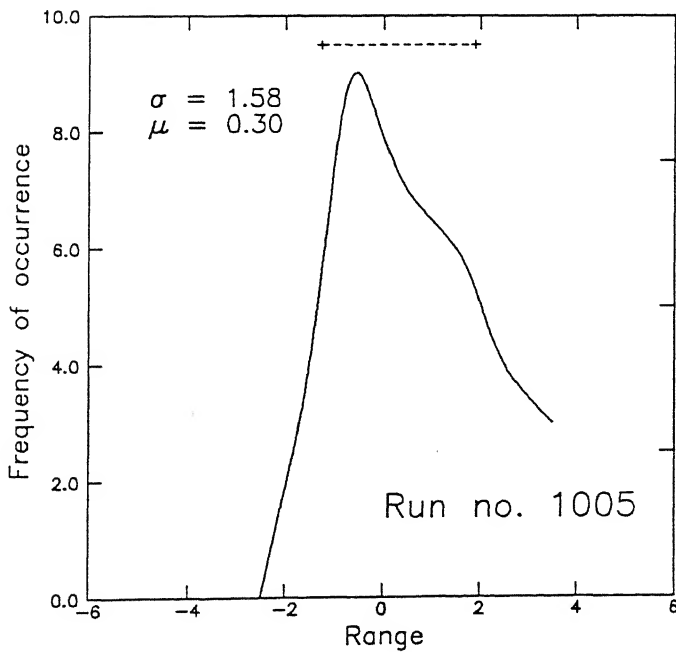


Fig. 3.7(b) : Frequency analysis for deviations in measurement of water level ( $h_w$ ) from mean curve during the breach process (for Fig. 3.7(a) )

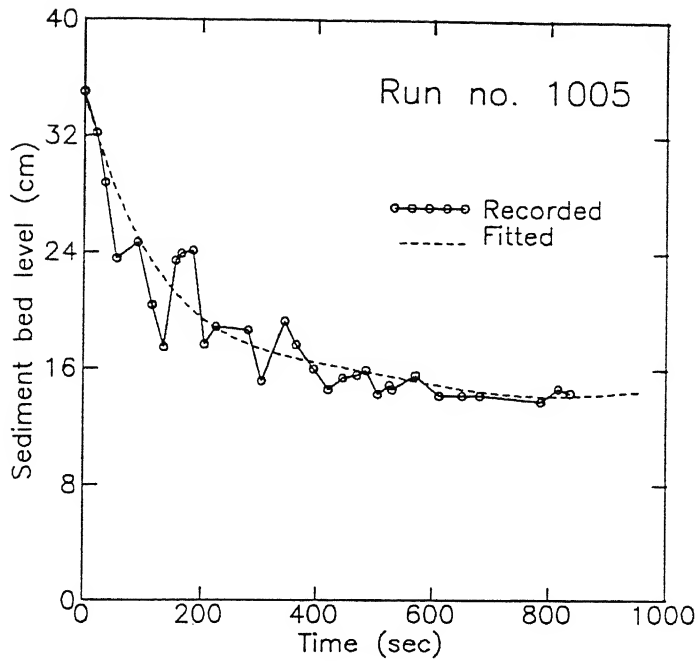


Fig. 3.8(a) : Recorded sediment bed levels at section-4 with time (sample data)

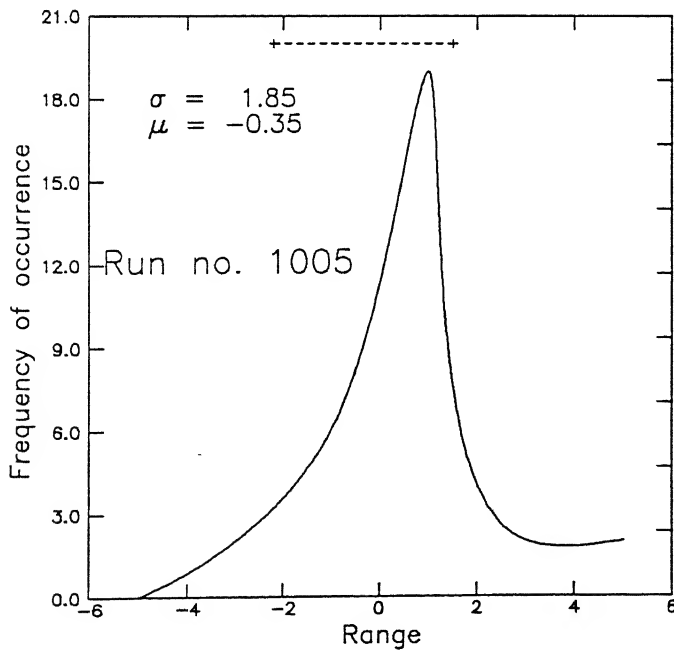


Fig. 3.8(b) : Frequency analysis for deviations of sediment bed level ( $h_c$ ) measurement from the mean curve during the breach process (for Fig. 3.8(a) )

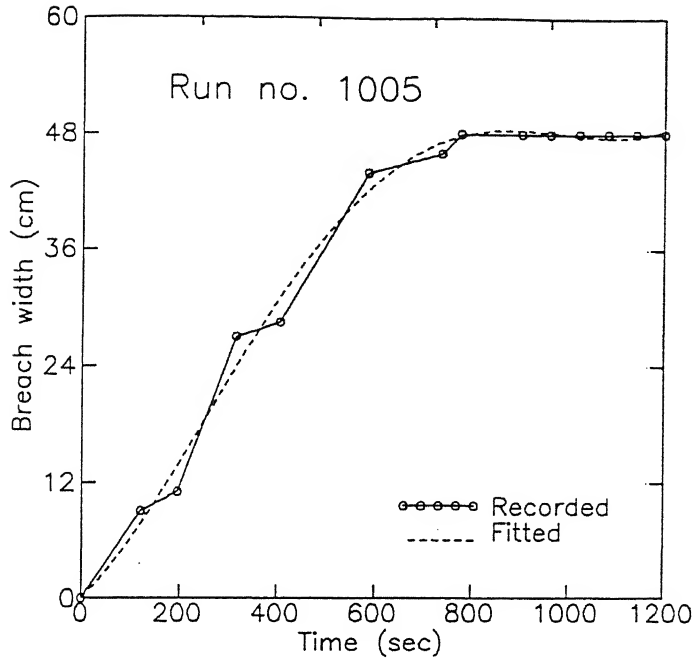


Fig. 3.9(a) : Recorded breach width at section-2 with time (sample data)

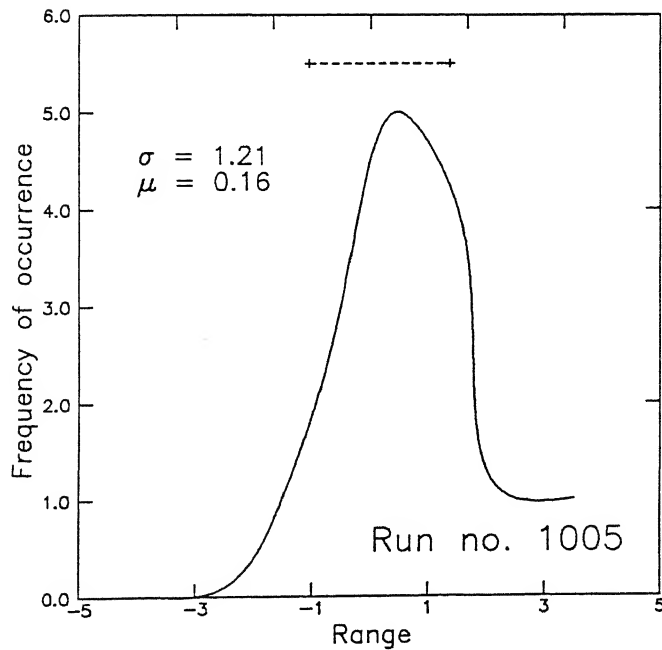


Fig. 3.9(b) : Frequency analysis for deviations of measurement of breach width from mean curve during the breach process (for Fig. 3.9(a) )

## **CHAPTER IV**

# **MECHANISM OF DAM BREACH PROCESS**

### **4.1 General**

In this chapter effort has been made to know the details about the mechanism involved in the dam breach process, with the help of experimental data obtained from the model studies. The data on water level, sediment bed levels, and width of breach are measured both in time and space during the dam breach process due to overtopping flood for the homogeneous dam models of cohesive and cohesionless soil with varying flow parameters and dam geometry. The effect of dam breach causes variation in the discharge of water and sediment at the downstream end of the dam. These two variables are very important so far their routing in the downstream of dam is concerned. To estimate these two quantities with time, it is essential to know the evolution of breach process, particularly the breach morphology and breach hydraulics with time. The study on dam breach process involves to know the dynamic variations of the following criterion variables, namely:

- a. Variation of crest and the sediment bed level in the longitudinal direction of breach.
- b. Variation of breach width at crest and at other sections along the breach.
- c. The rate of variation of crest height and its width.
- d. Water level variations at different sections of the breach.

These are the basic criterion variables to which other related criterion variables like energy loss, sediment discharge, water discharge are related.

To know these stated criterion variables, the available predictor variables in dam breach process are:

- Inflow hydrograph to the reservoir
- Capacity of the reservoir (reservoir-water elevation relation)
- Dam geometry

These two types of variables, in a more common way the input and output can be related through parametric study with the properties of the dam fill material like angle of friction, cohesion, median particle size, and bulk density of dam fill before overtopping.

In the present simulation of physical scaled model study both input and output are measurable. To study the governing mechanism involved, the cause and effect can be functionally related through suitable controlling parameters.

## 4.2 Parametric Formulation

In an experimental study one has to resort to nondimensional parametric study to take care of the scale effects. The results so obtained from the analysis of the experimental data can be applied to any prototype situation. Considering this aspect in view and knowing the possible variables controlling the dam breach process, the following nondimensional parameters are used, which can be grouped under the following head. The symbols are defined in the list of symbols.

### a. Breach Hydraulics

$$\frac{X}{X_m}, \frac{X}{H_D}, \frac{h_{cm}}{H_D}, \frac{h_c}{h_{cm}}, \frac{h_{cm}}{D_{er}}, \frac{h_u}{h_{cm}}, \frac{h_u}{h_{up}}, \frac{h_u}{H_D}, \frac{\text{Drop in water level at crest}}{H_D},$$

$$\frac{h_{cm^*}}{h_{wr^*}}, \frac{h_{wr}}{h_{wrm}}, \frac{q_w}{\sqrt{2gh_u^3}}, \frac{(dh_{cm}/dt)}{\sqrt{2gh_u}}, \frac{Q_w - \bar{Q}_{in}}{Q_{wp} - \bar{Q}_{in}}, \frac{Q_w}{Q_{wp}}, \frac{V'_w}{\sqrt{gy'_c}},$$

### b. Breach Morphology

$$\frac{D_{er}}{H_D}, \frac{B_{cr}}{H_D}, \frac{B'_{cr}}{H_D}, \frac{d\sqrt{A_{cr}}/dt}{\sqrt{2gh_u}}, \frac{B_{cr}}{D_{cr}}, \frac{dB_{cr}/dt}{\sqrt{2gH_D}}, \frac{dh_{cm}/dt}{dB_{cr}/dt},$$

### c. Time Components of Breach

$$\frac{t}{t_{50}}, \frac{t}{t_{95}}, \frac{t}{t_{wp}}, \frac{t}{t_{sp}}, \frac{t}{t_{hup}}, \frac{t-t_*}{t_{95}-t_*}, \frac{t-t_{**}}{t_{95}-t_{**}},$$

### d. Energy Loss Parameters

$$\frac{\Delta H_c}{H_D}, \frac{\Delta H}{H_D}, \frac{\Delta H}{L_{DB}}, \frac{\Delta E}{E_1}, \frac{\bar{V}_*}{\sqrt{2gH_D}}, \frac{dh_{cm}/dt}{\bar{V}_*}$$

### e. Sediment Transport Parameters

$$\frac{V'_w}{\bar{V}_*}, \frac{\Sigma \nabla_s}{\Sigma \nabla_w}, \frac{Q_s}{Q_w}, g_s^*$$

Some specially coined nondimensional numbers are used frequently in the present study.

These nondimensional quantities are presented here with an intention to acquaint them before their appearance in the analysis. The individual descriptions of these parameters are made wherever they are used.

$$Q_{PN} = \frac{Q_{wp}}{\sqrt{gH_D^5}} = Q - peak - Number$$

$$Q_{APN} = \frac{Q_{wp}}{A_D \sqrt{gH_D}} = Q - peak - Area Number$$

$$Q_{PSN} = \frac{Q_{wp}}{A_D V_{SR}} = Q - peak - soil resisting velocity Number$$

$$V_{SRN} = \frac{V_{SR}}{\sqrt{gH_D}} = Soil Resisting Velocity Number$$

$$CAP_N = \frac{\bar{Q}_{in} H_D}{Capacity V_{SR}} = Reservoir Capacity Number$$

$$\tau_{*c} = \frac{(\tau_{0c})_{Cohesion} + (\tau_{0c})_{friction}}{\Delta \rho g d_{50}} = Shield's Entrainment Number$$

Singh and Scarlotos (1986) have coined the following parameters.

$$\left. \begin{aligned} F_b &= \frac{Q_{wp}}{(B_{cr})_f \sqrt{gD_{er}^3}} = Breach Froude Number \\ S_f &= \frac{(B_{cr})_f D_{er}}{L_{TD} H_D} = Breach shape factor \end{aligned} \right\}$$



### 4.3 Analysis of Breach Process in Cohesionless Soil Embankment

Cohesionless embankment breach data are analysed first. From this analysis one gets information on the variation between the predicted and criterion variables. With this knowledge, identification of major controlling variables for the analysis of cohesive soil embankment breach data is carried out. This analysis reveals the importance of cohesion in the breach process. Finally an attempt has been made to analyse the breach process by combining both the model data on cohesionless and cohesive soil embankments. Field data available in literature are used along with laboratory data to develop the relation to predict the important variables of breach process. A method is developed to predict the breach processes for a given inflow, dam geometry reservoir capacity and embankment material properties.

Analysis of breach processes involves study of breach morphology and breach hydraulics. Breach morphology involves variation of water surface, sediment bed surface and width of the channel with time during breach process. Water discharge relations, sediment discharge computation, energy loss, bed shear stress and their internal relationships are studied in the breach hydraulics. Breach erosion involves the variation of crest height, crest width and their rate of erosion, volume of sediment eroded and transported out of breach section.

Cohesionless soil embankment model are built using river sand collected from river Ganga near Kanpur, India as detailed in Chapter III. As soon as the flow overtops the embankment, erosion of soil sets in. Erosion of the soil on the embankment body leads to development of channelisation. Erosion of the soil at the toe of the dam leads to the formation of the crest, where flow drops suddenly. With increase in the magnitude of overtopping flow, the crest starts receding upstream and finally reaching the upstream face of the embankment dam. During the receding of the crest towards upstream direction, the widening of the channel bed and bank occurs by erosion. This process of channel formation is defined here as the breach process. Development of breach is analysed by studying the morphology of the breach first and later the breach hydraulics. The formation of the eroding crest during breach development may be looked upon as a erosive crest similar to spillway or weir. Analysis of flow relation with crest geometry and flow depth are carried out. During the process of crest receding, widening of the crest and erosion of the crest occurs simultaneously. Hence, the rate at which crest erosion or widening takes place is studied further. Growth of the crest width and reduction in crest level with variation of the upstream and downstream flow conditions are analysed. The volume of water flown out of breach and the amount of the sediment

eroded in the breach are analysed next. The erosion of sediment depends mainly on the excessive erosive force caused by the flow. This aspect is analysed by computing the average shear stress ( $\tau_f$ ) of flow and relating with sediment concentration ( $C=Q_s/Q_w$ ) at a given instant of time. Work done by the flow by eroding the sediment causes loss in energy. This loss in energy is related to the flow condition upstream and downstream of the embankment. Finally, the time taken for breach process and final breach dimensions are analysed.

### a. Breach Morphology

Morphology of breach contains variation of planform of the breach, longitudinal variation of reach bed level, water level, and cross-sectional variation of breach sections.

#### i. Morphological Variations of Breach

Breach morphology is related to the variation of breach geometry with time. Variation of breach geometry depends on outflow hydrograph. For run 0405, morphology is presented for a typical outflow hydrograph as shown in Figure. 4.1.

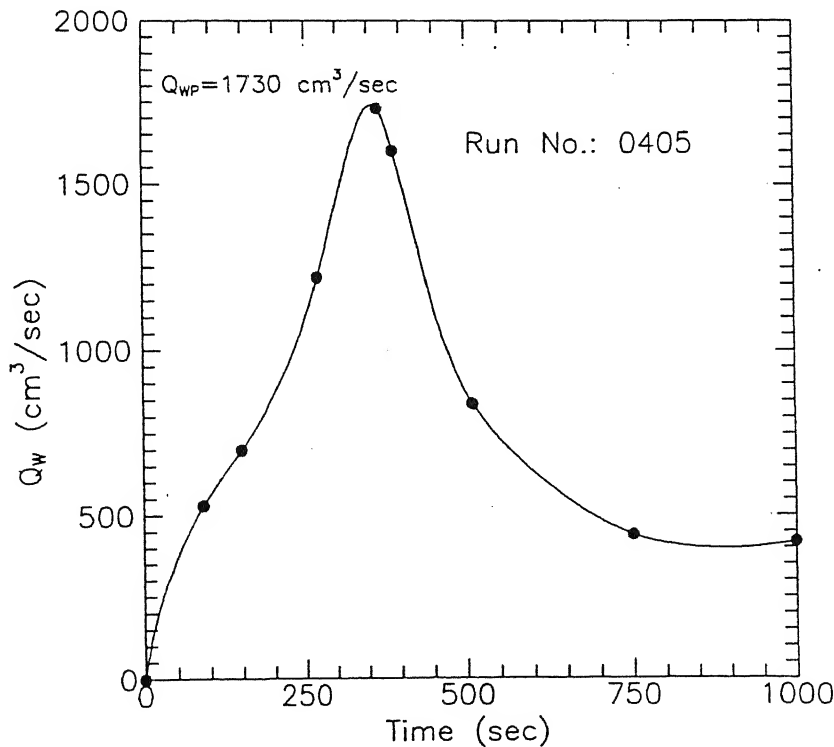


Fig. 4.1: Breach hydrograph for run no. 0405

Morphological variables like the water surface, sediment bed surface and breach width before, at and after the occurrence of the breach peak discharge are presented in Figures 4.2 (a), (b), (c) and (d) respectively as a typical set. These Figures indicate a gradual variation of the water surface upstream of the crest and rapid variation after the crest. The sediment surface level remains almost parallel to the water surface level. The gradual widening of the breach width at the upstream section, followed by a narrow channel width where water surface drops rapidly is observed. Widening of the breach width in the downstream section 6, 7 where rapid variation in the water level occurs is observed in every run. After the occurrence of peak flow, as the breach process progresses the channel contraction occurs right at or near the upstream face of the embankment. The gradual widening of the breach occurs in the downstream direction from the upstream face of embankment upto the downstream face of the embankment. These features are observed in all the cohesionless embankment models. The bed level and water surface level in the breach section at the end of breach remains similar to the gradually varied flow in the channel.

## **ii. Breach Cross Sectional Variation with Time**

The cross sectional area eroded due to breach flow at upstream edge and down stream edge of embankment dam for four different instants of time during the breach are plotted in Figure 4.3. It may be observed that the variation of cross-sectional shape during most of the breach erosion process for cohesionless soil remains rectangular. Due to the instability of the slope, banks may collapse. The bank soil collected in the breach channel due to bank collapse will get eroded quickly, retaining back the unstable rectangular shape. This process continues till the final stage of breach occurs. At this stage, the breach section remains more of trapezoidal shape. The area of erosion at the top upstream edge of the embankment is presented as a function of time for run 0405 as a typical case as shown in Figure 4.4. The volume of sediment eroded is plotted against time of erosion in Figure 4.5 for the run no. 0405. It reveals that the slope of the volume of erosion curve is steeper in the beginning and becomes fairly constant thereafter.

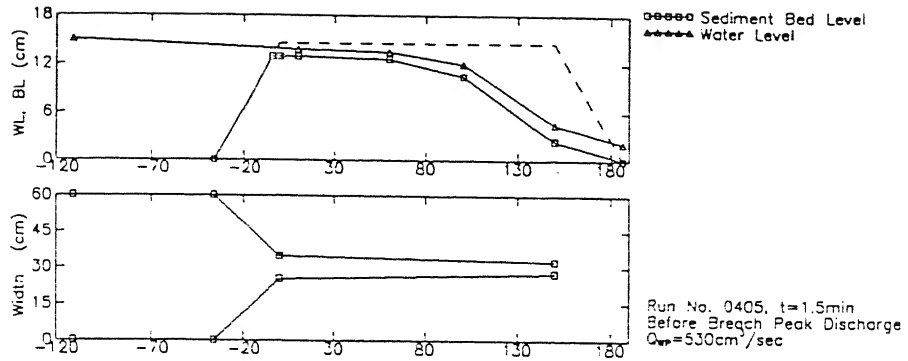


Fig. 4.2a

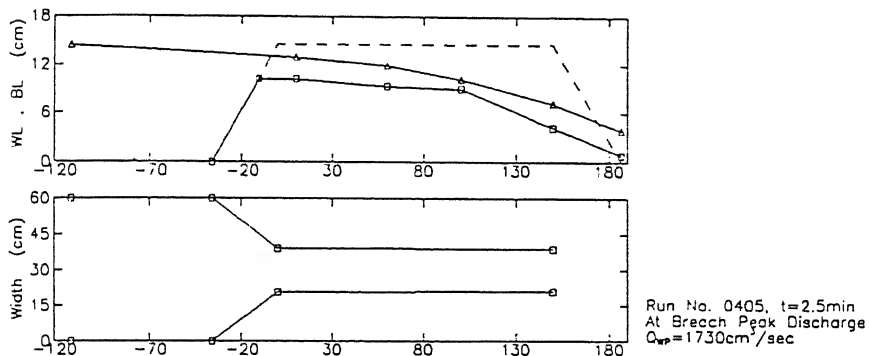


Fig. 4.2b

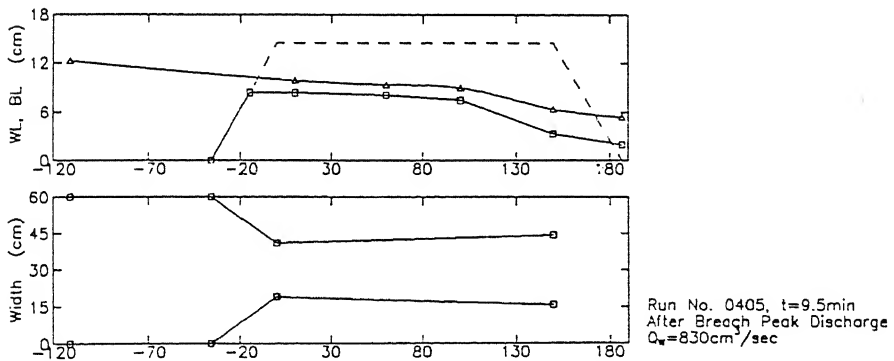


Fig. 4.2c

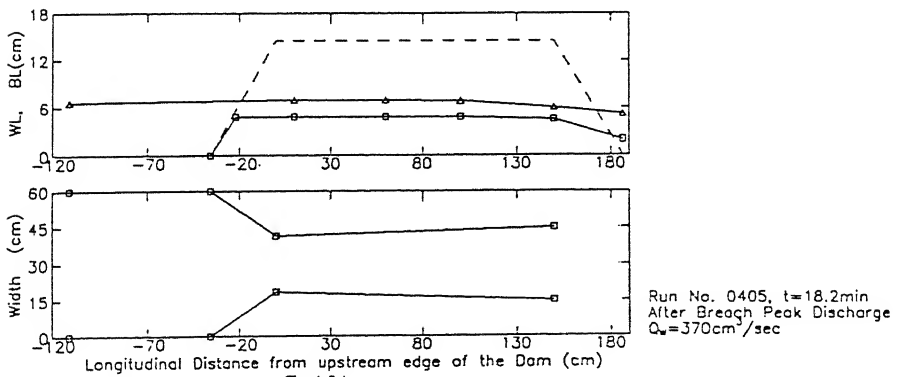


Fig. 4.2d

Fig.4.2: Variation of water surface levels, sediment bed levels and breach width along the longitudinal direction of the dam model of cohesionless soil for run no.0405: before, at and after breach peak discharge.

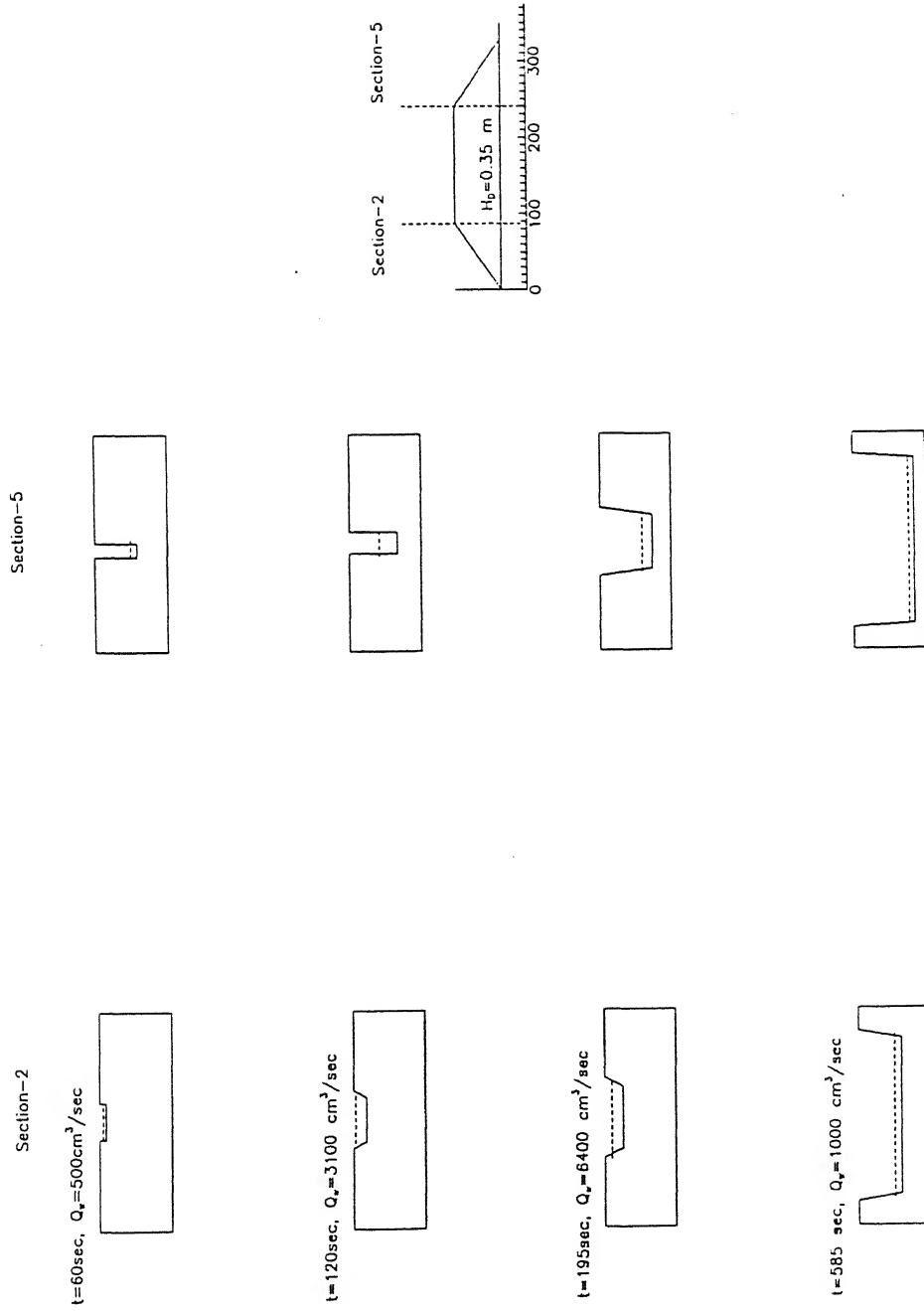


Fig. 4.3: Variation of breach cross-sectional area before, at and after peak discharge ( $Q_{wp}$ ) at sections-2 and 5 for dam model with cohesionless soil, for run no. 0405

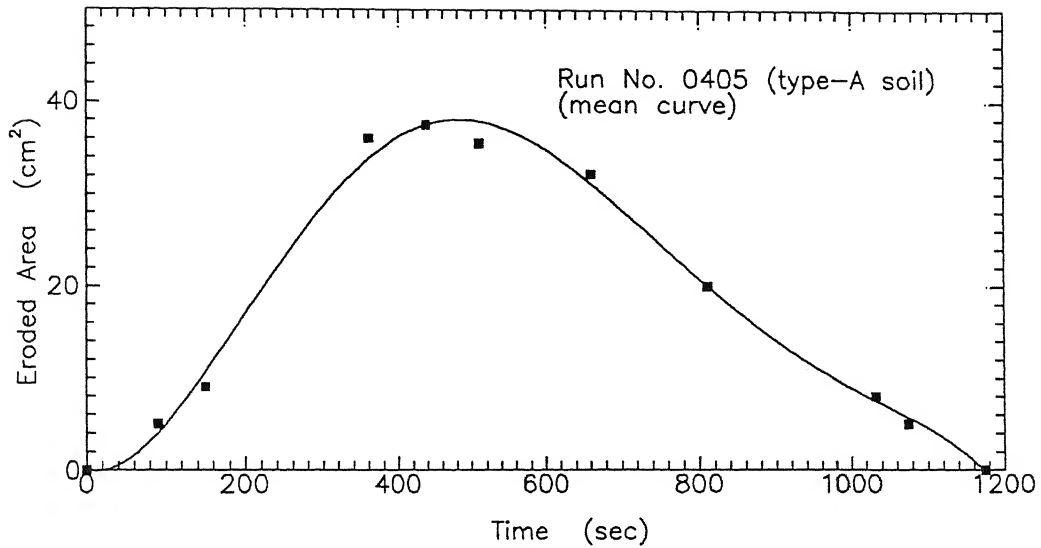


Fig. 4.4: Variation of eroded area at the upstream edge of the embankment for run no. 0405 with time.

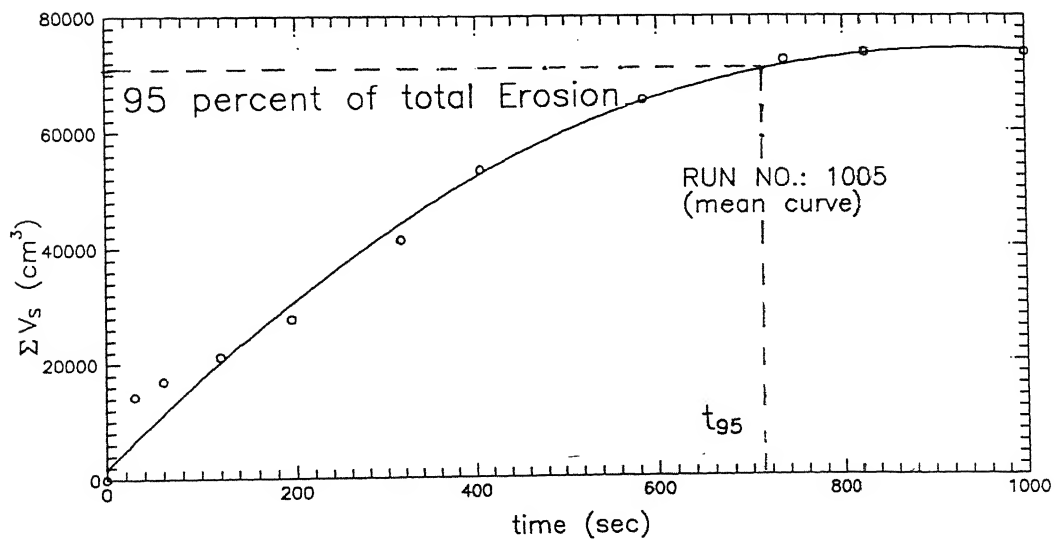


Fig. 4.5: Cumulative volume of eroded sediment from breach section of the dam body for run no.1005

## b. Breach Hydraulics

Breach hydraulics contain the discharge computation through the breach, analysis of coefficient of discharge ( $c_d$ ) of the assumed broad-crested weir type flow situation in dam breach, the analysis of head ( $h_u$ ) acting over the crest and maximum height of the erodible sediment bed. Variation of average velocity, breach hydrograph, energy loss and bed shear velocity are also analysed.

### i. Discharge Characteristics

The photos on breach process presented in Chapter III reveals that the flow through the breach behaves like flow over a spillway. From this consideration, the flow through the breach is analysed as the flow over a spillway in which crest is getting eroded. In order to study what part of time during breach process the flow behaves like flow over spillway and what part of time flow behaves like a channel flow, it is essential to analyse the variations of reservoir water level, water level at downstream (near toe of the dam), and the crest variation during the breach process. These variations are shown in Figure 4.6. From this figure one can observe, when sediment crest level equals to the downstream water level by getting eroded, till then flow can be treated as free overflow similar to spillway flow. Till the downstream water level fairly coincides with upstream water level, it can be treated as weir flow under submerged condition. After the downstream water level fairly coincides with upstream water level, the state of flow in the breach is similar to channel flow. The discharge characteristics of the overtopping flow is analysed from these considerations. Discharge intensity ( $q_w$ , discharge per unit width of breach at the upstream top edge of the dam) is plotted against  $h_u$ , the difference between upstream reservoir level and the sediment crest level as shown in Figure 4.7(a). By using the regression analysis, the power law relation is developed for this data and it indicates,

$$q_w = h_u^{1.49} \times 6.56 \quad (4.1a)$$

However the scatter of the data is quite large. The coefficient of discharge ( $c_d$ ) is computed based on the weir type flow as:

$$\frac{2}{3} c_d = \left( q_w / \sqrt{2gh_u^3} \right) \quad (4.1b)$$

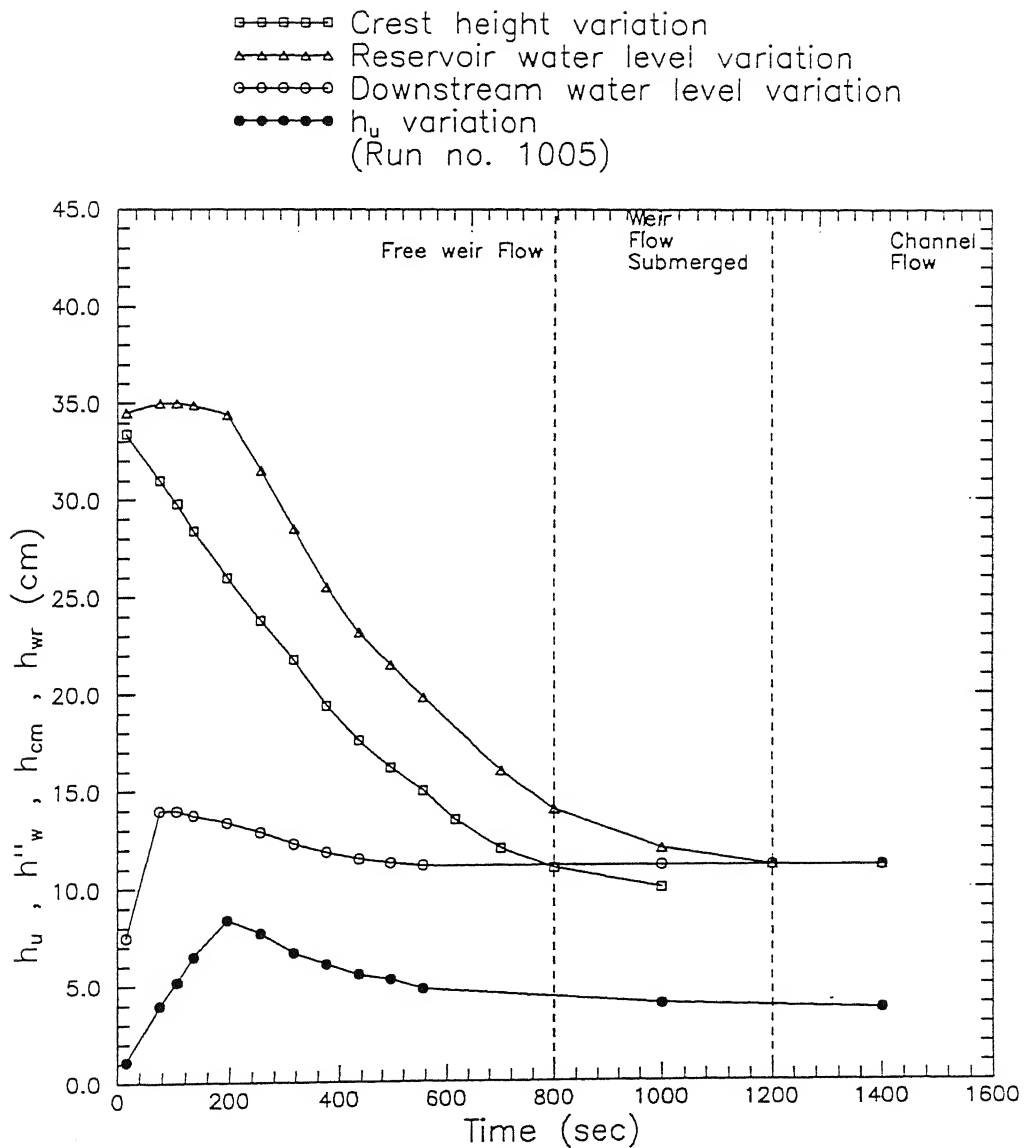


Fig. 4.6: Different phases of flow defined during the breach process



is plotted against the ratio of  $(h_u / h_{cm})$ , where  $h_{cm}$  is the height of the crest above the bed of the flume. The Figure 4.7(b) indicate that  $q_w / \sqrt{2gh_u^3}$  is inversely proportional to  $h_u / h_{cm}$ . However, its relation is given below:

$$\frac{2}{3} c_d = 0.06 \times \left( \frac{h_u}{h_{cm}} \right)^{-0.87} \quad (4.1c)$$

The frequency analysis for the data about the mean line is analysed and plotted in the Figure 4.8. The mean ( $\mu$ ) and standard deviation ( $\sigma$ ) for this frequency analysis are:

$$\mu = 0.0218$$

$$\sigma = 0.0165$$

Based on the classification of the flow as carried out in Figure 4.6, and  $c_d$  relation shown in Figure 4.7(b), it may be postulated that the free weir flow exists for  $h_u / h_{cm} \leq 0.4$ . From the Figure 4.7(b) the order of magnitude of  $c_d$  variation is 0.7-0.22 for free overflow.

## ii. Computation of Head of Water Acting Over the Weir Crest ( $h_u$ )

As a representative case, the variation of  $h_u$  with time for run-1005 is plotted in the Figure 4.9. It may be observed that  $h_u$  starts increasing with time and attains a maximum value. With further increase in time  $h_u$  starts decreasing asymptotically and reaches certain value depending on the breach geometry and amount of incoming flow to the reservoir. The variation of  $h_u$  with time is mainly during free overflow. From this observation it was planned to analyse  $h_u$  with time, as  $h_u / h_{up}$  and  $t / t_{hup}$ , where  $h_{up}$  and  $t_{hup}$  are corresponding maximum value of  $h_u$  and its time of occurrence. Using the data of all the runs for cohesionless soil embankment,  $h_u / h_{up}$  is plotted against  $t / t_{hup}$  in Figure 4.10(a). The relation between them is given as:

$$\frac{h_u}{h_{up}} = X^p e^{(1-X^p)} \quad (4.2a)$$

where  $p_r = 2.5$  (rising limb) and  $p_f = 1.0, 1.2, 1.25$  for falling limb as shown in Figure 4.10(a). As already indicated the variation  $h_u / h_{up}$  follows a steep rising limb and then gradual receding limb. The position at which the final value in the receding limb reaches depend on the magnitude of the incoming flow to the breach and breach geometry. The  $h_{up}$  is found to be

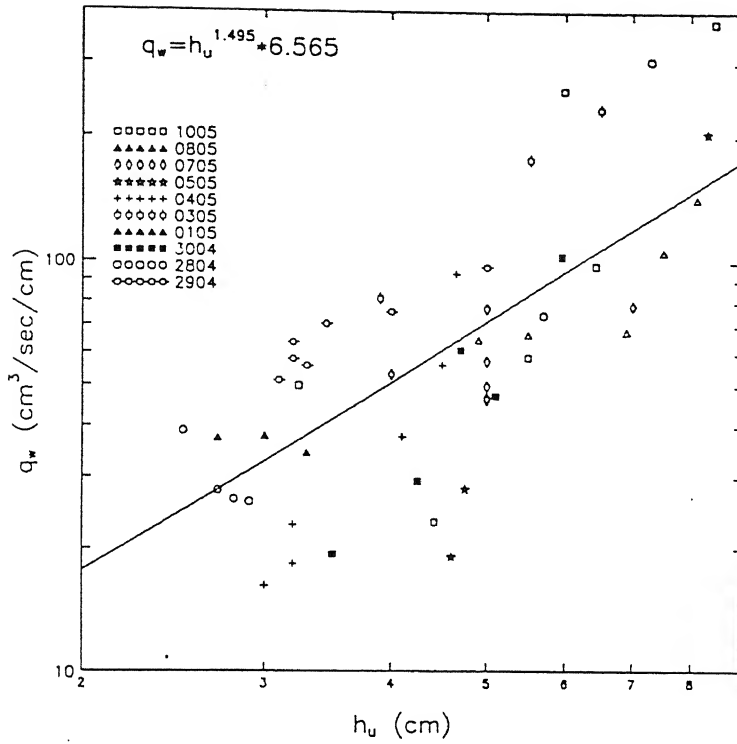


Fig. 4.7(a): Relation between head of water over the erodible crest( $h_u$ ) and breach outflow discharge intensity  $q_w$  for dam model of cohesionless soil

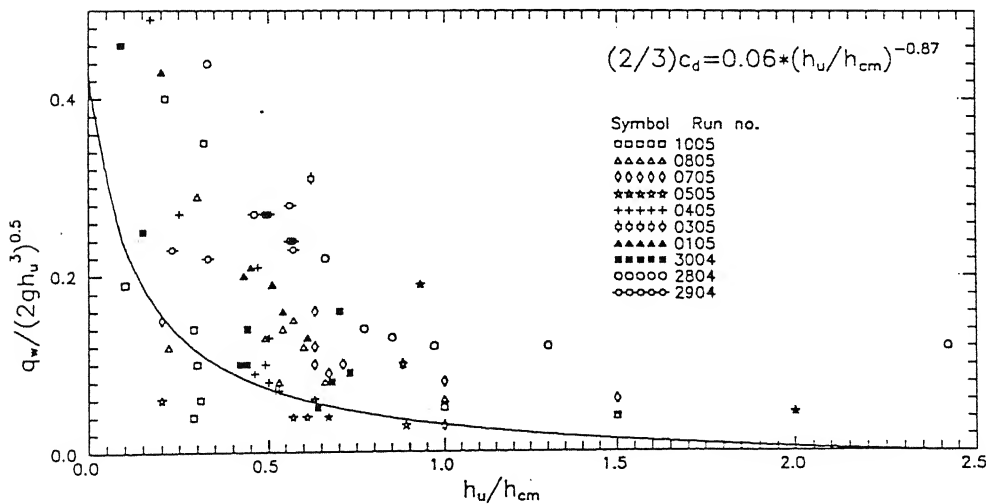


Fig. 4.7(b): Relation between discharge coefficient( $c_d$ ) and the ratio of head of water over erodible crest to the crest height at any time of breach

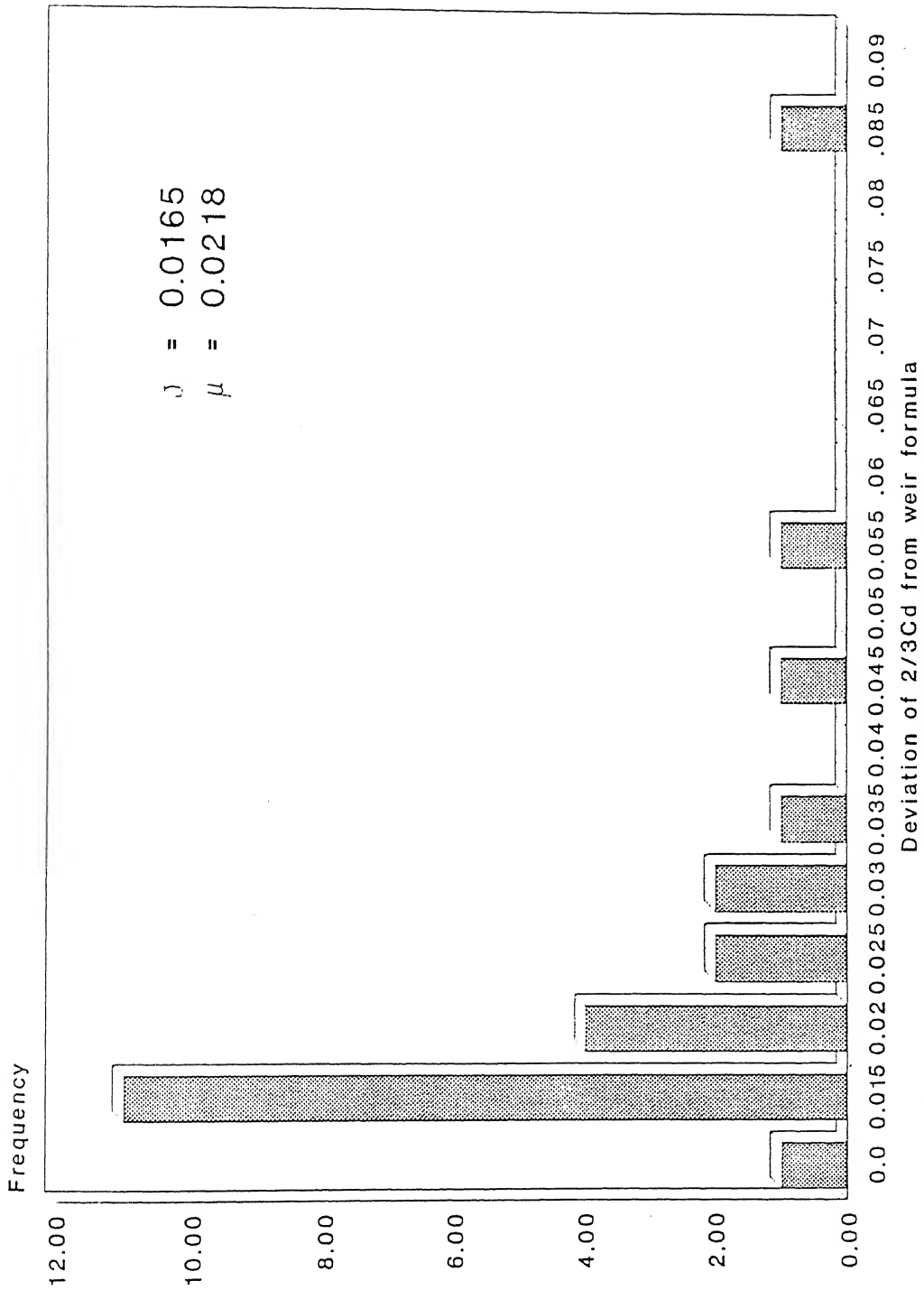


Fig. 4.8: Frequency of deviation of discharge coefficient from weir formula (Cohesionless soil)

function of height of the dam ( $H_D$ ), inflow to the reservoir ( $Q_{in}$ ) and cross sectional area ( $A_D$ ) of the embankment. Using these variables, a dimensional analysis is carried out and it is found that  $h_{up}/H_D$  is related to the  $Q_{in}/A_D\sqrt{2gH_D}$ . This relation is plotted in the Figure 4.10(b). It may be observed that the curve gradually increases with increase in X-axis value and reaches maximum value around two. It decreases very steeply with further increase in its X-axis value. Using regression analysis an equation relating these is given as:

$$(h_{up}/H_D) = 0.2068 + 288.7X - 323103X^2 \quad (4.2b)$$

$$\text{where, } X = \left( \frac{Q_{in}}{A_D\sqrt{2gH_D}} \right)$$

The time scale ( $t_{hup}$ ) is nondimensionalised with  $t_{95}$  and is plotted against nondimensional  $h_{up}$  as shown in Figure 4.10(c). The functional relation among them is written as:

$$\frac{t_{hup}}{t_{95}} = e^{1.35X} \times 0.185 \quad (4.2c)$$

$$\text{where } X = \frac{h_{up}}{H_D}$$

With computed value of  $h_{up}$  from Equation(4.2b),  $t_{hup}$  can be found out using Equation(4.2c).

With reference to Figure 4.5,  $t_{95}$  can be determined.

### iii. Breach Average Velocity

The average breach velocity ( $\bar{V}_w$ ) is defined as the breach outflow discharge ( $Q_w$ ) at any time divided by its corresponding average flow cross sectional area, ( $\bar{A}_f$ ). The average cross sectional area is the area average of the cross sectional areas computed at upstream edge, downstream edge of the embankment and at the centre of these two. This average velocity is plotted against average hydraulic radius ( $\bar{R}_h$ ) computed at three different sections is stated. It may be noted that the average velocity decreases very slowly with increasing  $\bar{R}_h$  as indicated in the Figure 4.11(a). Same average velocity is plotted against energy gradient,  $\bar{S}_f$ , computed between the upstream edge and the downstream edge of the embankment. It may be observed that average velocity increases with  $\bar{S}_f$  in Figure 4.11(b). The relations of  $\bar{S}_f$  and  $\bar{R}_h$  with average velocity ( $Q_w/\bar{A}_f$ ) does not match either Chezy's or Manning's equation.

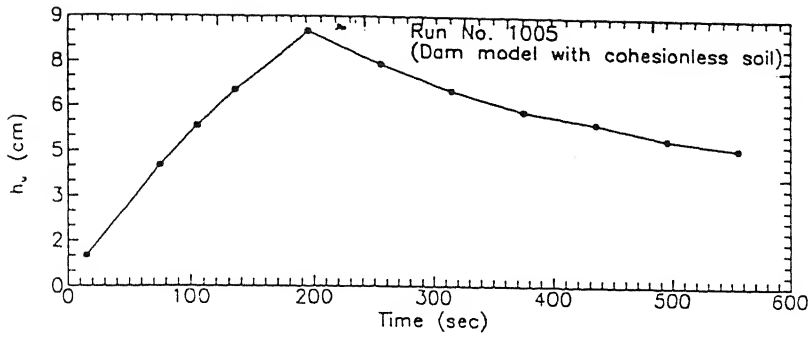


Fig. 4.9: A typical Variation of head of water( $h_u$ ) over erodible crest with time for run no.1005, dam model with cohesionless soil

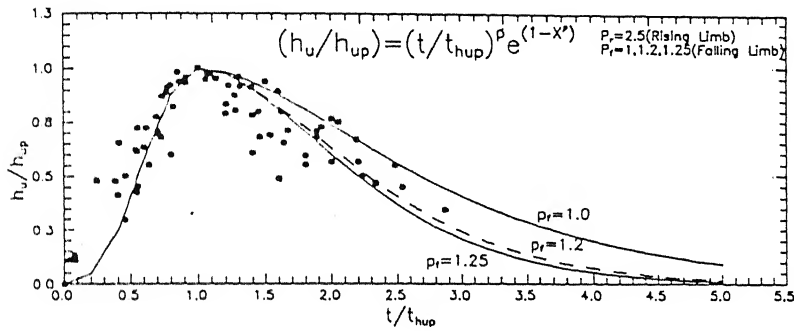


Fig. 4.10(a): Variation of normalised head of water( $h_u/h_{up}$ ) with normalised time ( $t/t_{hup}$ ).

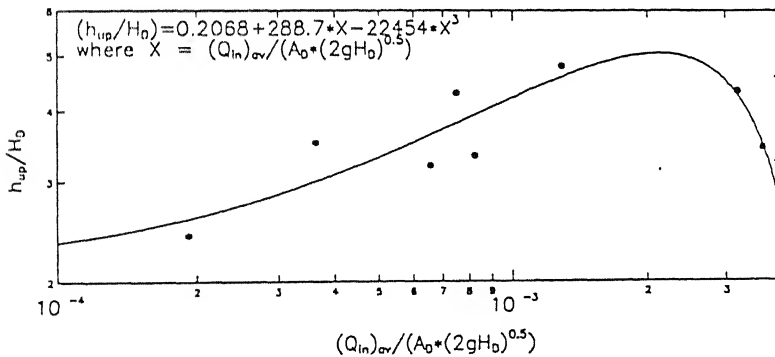


Fig. 4.10(b): Nondimensional variation of maximum water level over the erodible crest, ( $h_{up}$ ) with average inflow discharge to the reservoir, height of dam ( $H_0$ ), and dam cross-sectional area ( $A_0$ )

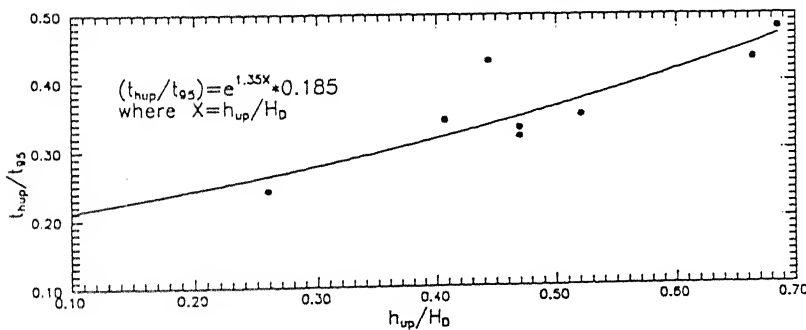


Fig. 4.10(c): Functional Relation Of  $t_{hup}$  with  $t_{g5}$ ,  $h_{up}$  and  $H_0$

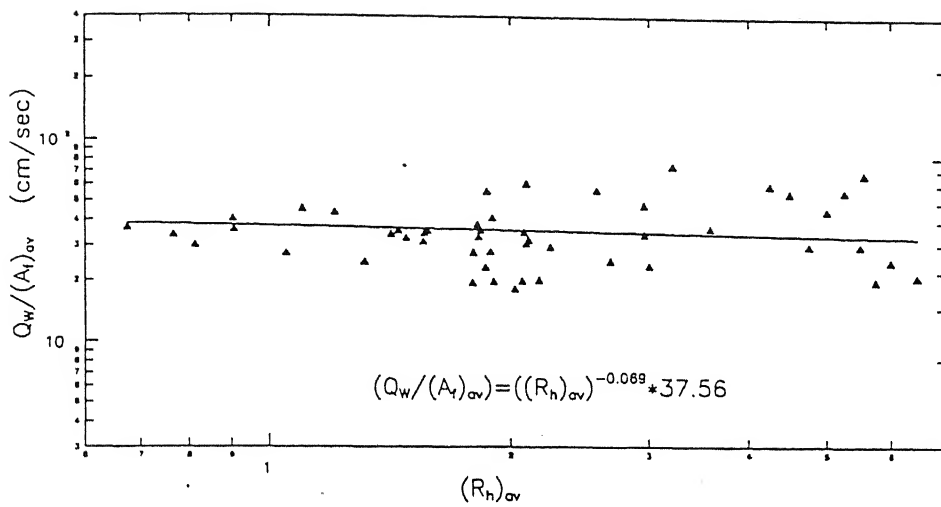


Fig. 4.11(a): Variation of average breach flow velocity  $(V_w)_{av}$  with average breach hydraulic radius  $(R_h)_{av}$

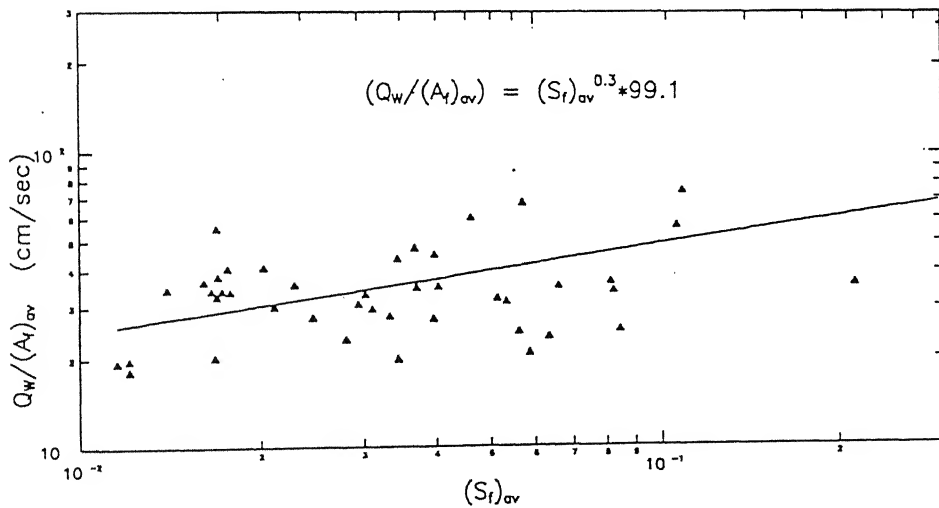


Fig. 4.11(b): Variation of average breach flow velocity  $(V_w)_{av}$  with average breach energy gradient  $(S_f)_{av}$

The average velocity in the dimensionless form as  $(Q_w / \bar{A}_f) / \sqrt{g \bar{R}_h \bar{S}_f}$  is plotted against non-dimensional water level variation at crest as shown in Figure 4.11(c). From this figure it may be observed that the dimensionless average velocity increases with increase in the magnitude of drop in the water level at the crest. The average velocity is further analysed in relation to Manning's equation. The magnitude of  $Q_w / \bar{A}_f$  is plotted against  $\bar{R}_h^{2/3} \bar{S}_f^{0.5}$  and also is plotted against  $\bar{R}_h^{-0.23} \times \bar{S}_f^{0.34}$  obtained from the regression analysis. Both the relations found to coincide each other, indicating mutual balance between  $\bar{S}_f$  and  $\bar{R}_h$ , as indicated in the Figure 4.11(d). The data as plotted in Figure 4.11(d), when reduced appropriately simplifies similar to Manning's relation:

$$\frac{Q_w}{\bar{A}_f} = \bar{R}_h^{0.152} \times \bar{S}_f^{0.1235} \times 43.8 \quad (4.3a)$$

From regression analysis,

$$\frac{Q_w}{\bar{A}_f} = (\bar{S}_f^{0.09} / \bar{R}_h^{0.074}) \times 45.35 \quad (4.3b)$$

Overall this relation indicates nonconfirmation to Manning's equation in breach flow. This may be due to flow acceleration associated during the breach.

#### iv. Flow Velocity at the Downstream Top Edge of the Embankment

The  $V'_w$  is the velocity of flow at the downstream top edge of the embankment. Analysis of  $V'_w$  is carried out by introducing critical velocity,  $(gy'_c)^{0.5}$  for nondimensionalising  $V'_w$  and is plotted against average water surface slope,  $\bar{S}_w$  with same  $Q_{wp}$  - number as shown in Figure 4.12(a). Here  $y'_c$  is the critical depth of flow at the downstream top edge of the embankment. Its magnitude is computed assuming wide rectangular flow as:

$$y'_c = \left( \frac{(q'_w)^2}{g} \right)^{\frac{1}{3}} \quad (4.4a)$$

where  $q'_w$  = water discharge intensity at downstream top edge of the dam

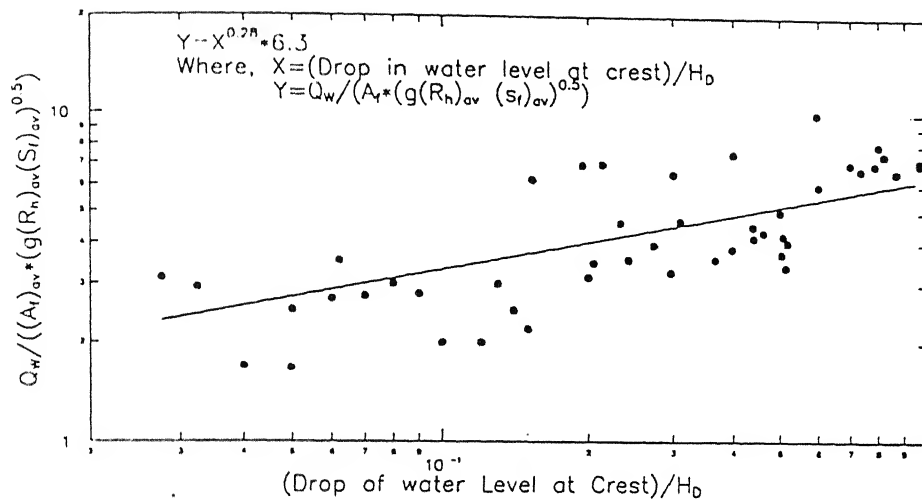


Fig. 4.11(c): Variation of nondimensional average breach flow velocity with nondimensional drop of water level at crest

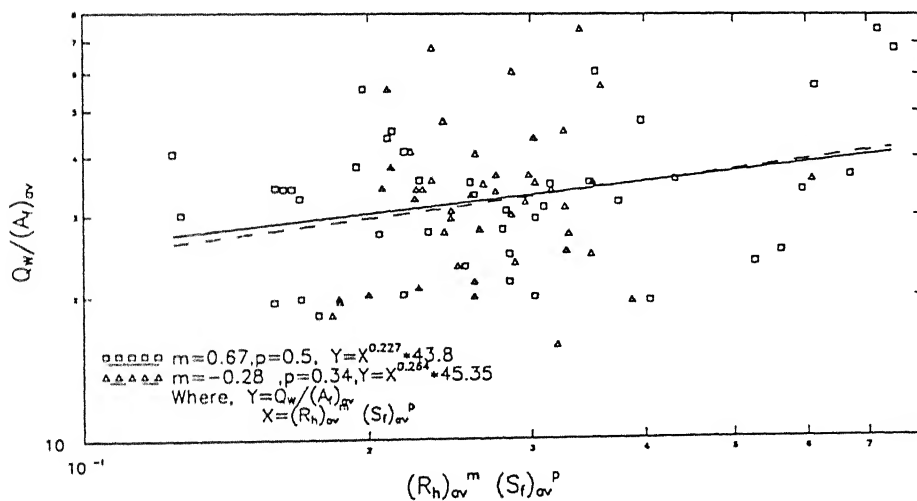


Fig. 4.11(d): Comparison of Manning's Equation in breach flow



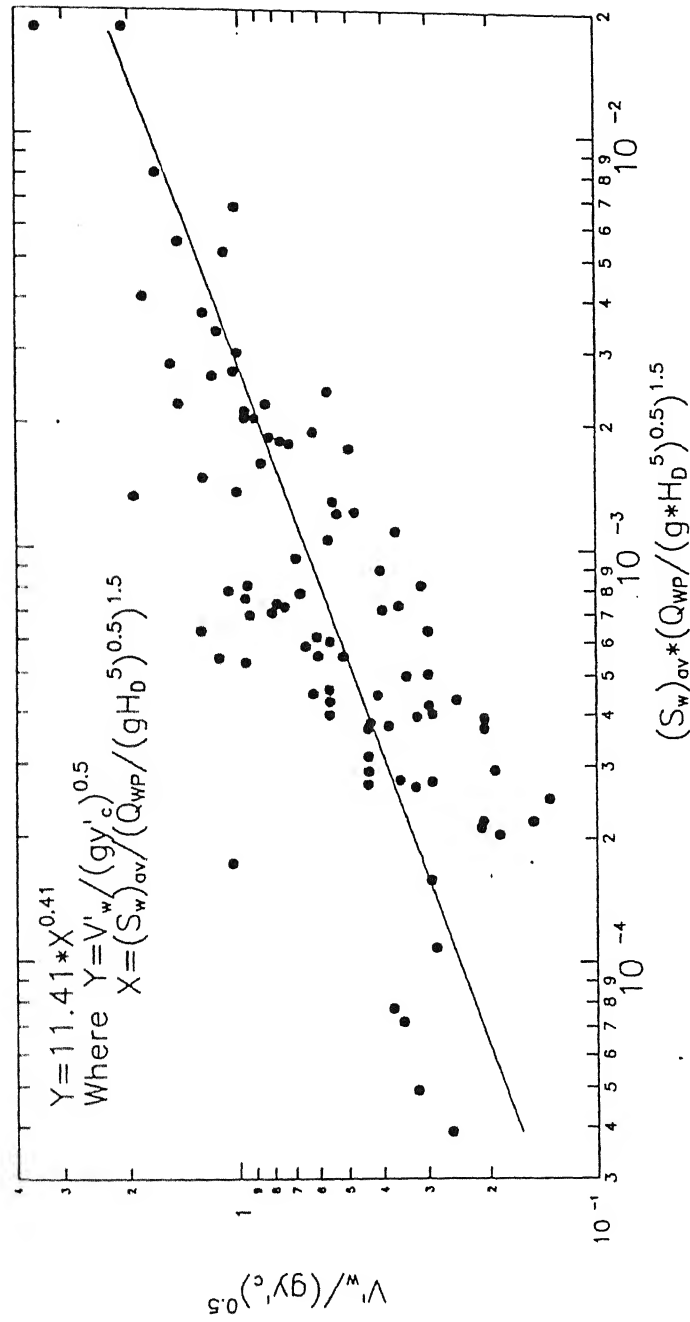


Fig. 4.12(a): Variation of nondimensional breach flow velocity at downstream edge of the dam to the critical flow velocity at that section with average water surface gradient  $(S_w)_{av}$

Relation between them is obtained from regression analysis as given below. This relation involves the knowledge of the water intensity ( $q_w$ ).

$$\frac{V'_w}{\sqrt{gY'_c}} = 11.41 \times \left[ \bar{S}_w \times \left( \frac{Q_p}{\sqrt{gH_D^5}} \right)^{2.0} \right]^{0.41} \quad (4.4b)$$

On similar lines the non-dimensional flow velocity at the downstream top edge ( $V'_w$ ) of the embankment with corresponding shear velocity at that section  $V'_s$  is plotted with  $\bar{S}_w$  as shown in Figure 4.12(b). The relation obtained from regression analysis enables to predict the shear velocity at the downstream end for a known flow condition. The functional relation among them is given as follows:

$$\frac{V'_w}{V'_s} = 161.64 \times \left[ \bar{S}_w \times \left( \frac{Q_p}{\sqrt{gH_D^5}} \right)^{2.0} \right]^{0.5} \quad (4.4c)$$

From Figure 4.12(b) it can be observed that for low values of  $\bar{S}_w$  the scattered data deviates more, whereas for higher  $\bar{S}_w$  the scatter in the data is less. This indicates that the relation is good during initial stages of breach process.

## v. Breach Hydrograph

Breach hydrograph is the relation between outflow through the breach plotted against time, as shown in the Figure 4.13(a). This hydrograph has a steep rising limb with a peak followed by a gradual receding limb. The receding limb discharge after a long duration reaches equal to the magnitude of the inflow discharge into the reservoir. Considering the variation in inflow discharge it was thought to analyse rising limb and receding limb separately. The rising limb is non-dimensionalised by peak breach outflow discharge ( $Q_{wp}$ ), whereas receding limb is non-dimensionalised by  $(Q_w - \bar{Q}_{in}) / (Q_{wp} - \bar{Q}_{in})$ . Both these magnitudes are plotted in Figure 4.13(b) with nondimensional time  $t/t_{wp}$ , where 't' is the time under consideration and  $t_{wp}$  is the time of occurrence of peak outflow discharge.

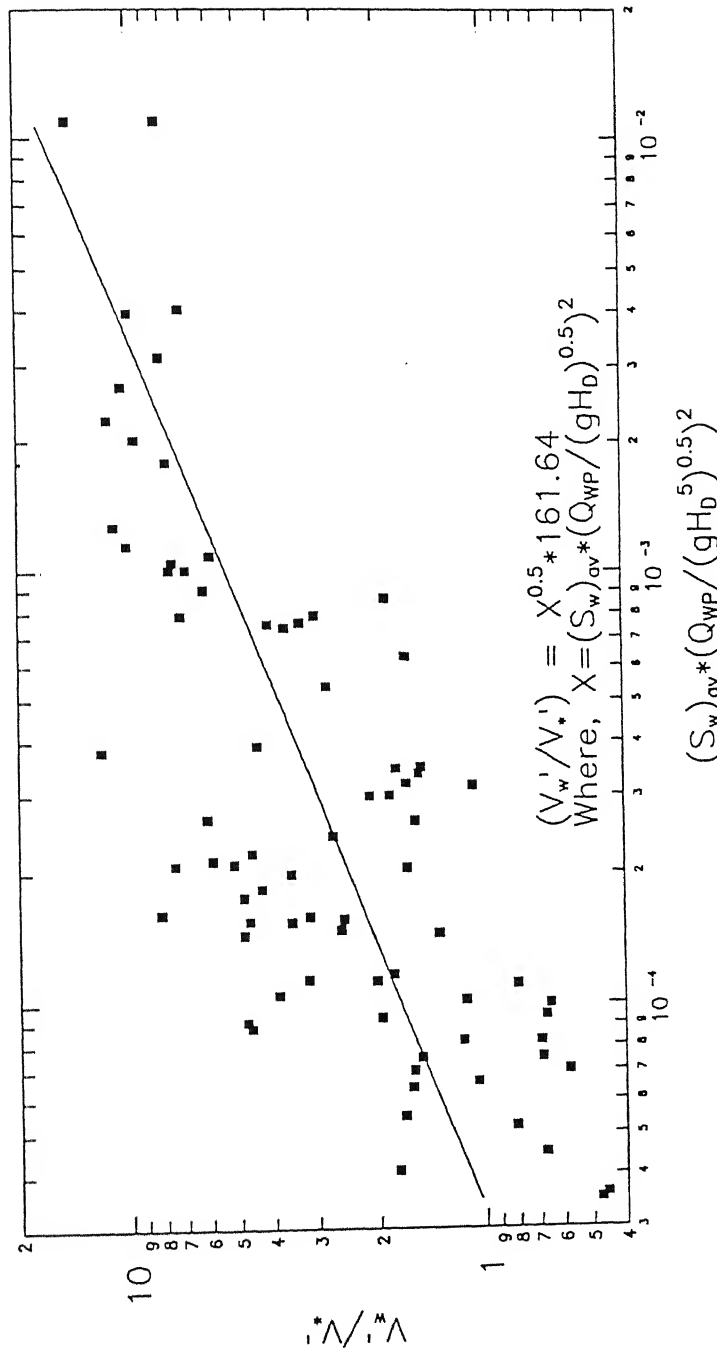


Fig. 4.12(b): Variation of the ratio of downstream top edge breach velocity to the downstream shear velocity with average water surface gradient

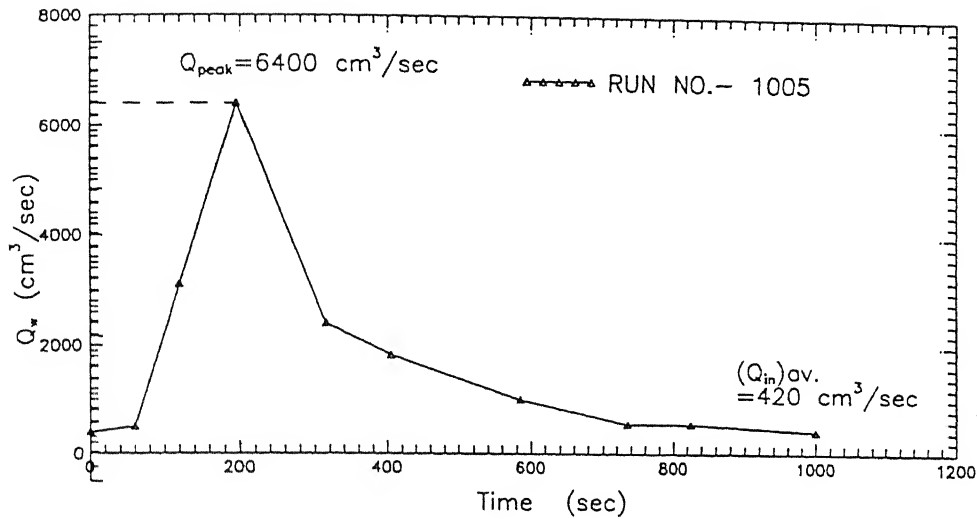


Fig. 4.13(a): A typical breach outflow hydrograph for run no. 1005

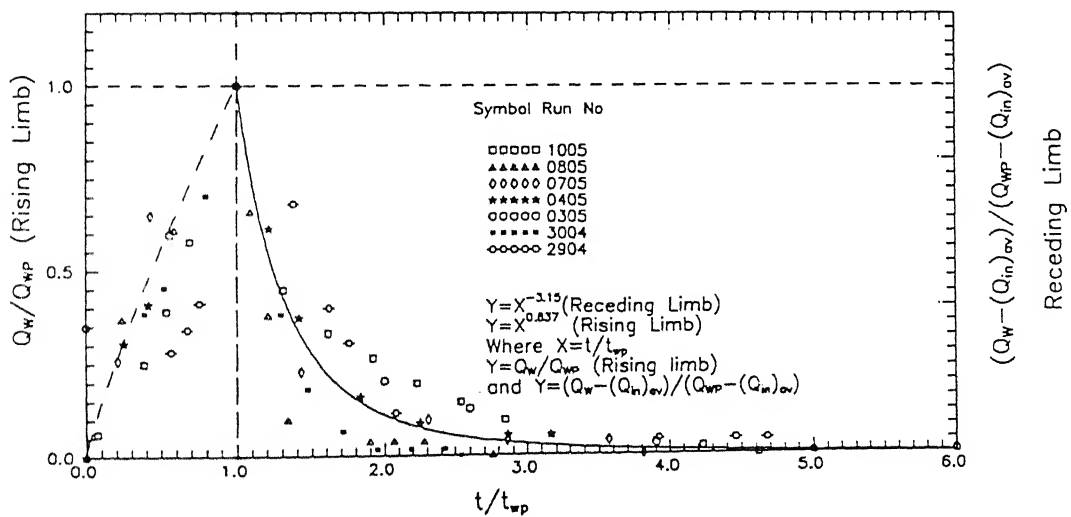


Fig. 4.13(b): Nondimensional breach outflow with nondimensional time

The relations of rising limb and receding limb are obtained by regression analysis as indicated below.

$$\frac{Q_w}{Q_{wp}} = \left( \frac{t}{t_{wp}} \right)^{0.837} \quad (\text{for rising limb}) \quad (4.5a)$$

$$\left( \frac{Q_w - \bar{Q}_{in}}{Q_{wp} - \bar{Q}_{in}} \right) = \left( \frac{t}{t_{wp}} \right)^{-3.15} \quad (\text{for receding limb}) \quad (4.5b)$$

The magnitude of peak discharge ( $Q_{wp}$ ) and its corresponding time ( $t_{wp}$ ) are related with embankment geometry and inflow characteristics in the section where the combined analysis of cohesionless fine sand and cohesive soil embankment is carried out.

#### vi. Energy Loss During the Breach Process

Energy is computed at upstream of the embankment level and at downstream end of the embankment as the sum of datum energy head, potential head (depth of water) and the velocity head. The difference in energy between these two sections is considered to be the energy loss during the breach process. This energy loss nondimensionalised with upstream energy ( $E_1$ ) at a given instant of drop of water ( $\Delta H$ ), is plotted as shown in Figure 4.14(a). Here the drop ( $\Delta H$ ) is defined as the difference in water level in the reservoir to the downstream end of the embankment. This drop is non-dimensionalised with dam base length ( $L_{DB}$ ). The relation between them is obtained from regression analysis as:

$$\frac{\Delta E}{E_1} = 6.5 \times \left( \frac{\frac{\Delta H}{L_{DB}}}{\left( \frac{Q_{wp}}{\sqrt{gH_D^5}} \right)^{0.17}} \right)^{0.66} \quad (4.6a)$$

A good correlation exists between them. To predict drop ( $\Delta H$ ) during the breach,  $\Delta H$  is nondimensionalised with  $H_D$  and is plotted against  $t/t_{95}$  as shown in Figure 4.14(b). It may be noted that drop  $\Delta H$  decreases with increase in  $t/t_{95}$  and the relation between them is given as:

$$\frac{\Delta H}{H_D} = 0.85 \times e^{-1.025 \left( \frac{t}{t_{95}} \right)} \quad (4.6b)$$

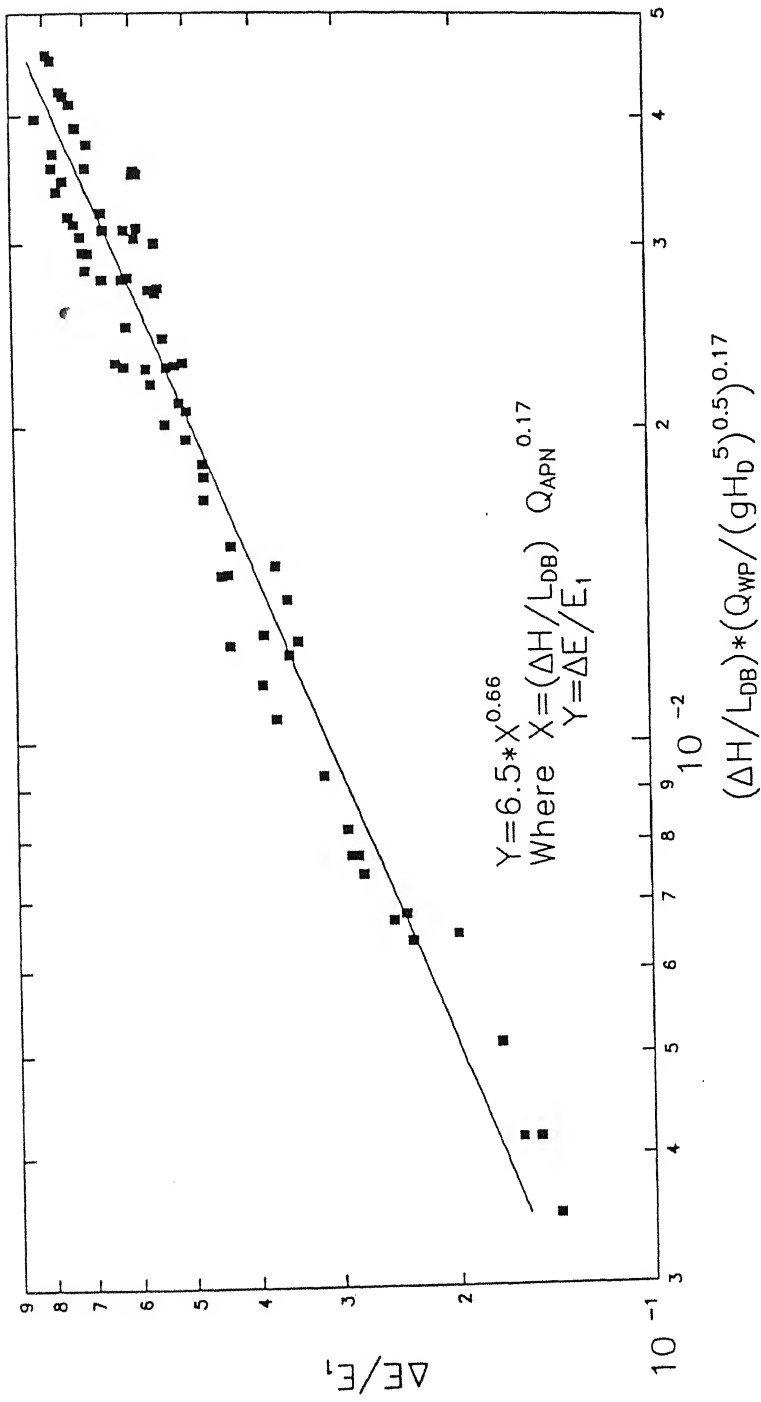


Fig. 4.14(a): variation of nondimensional breach energy loss with drop in water level between upstream and downstream of the dam( $\Delta H$ ).

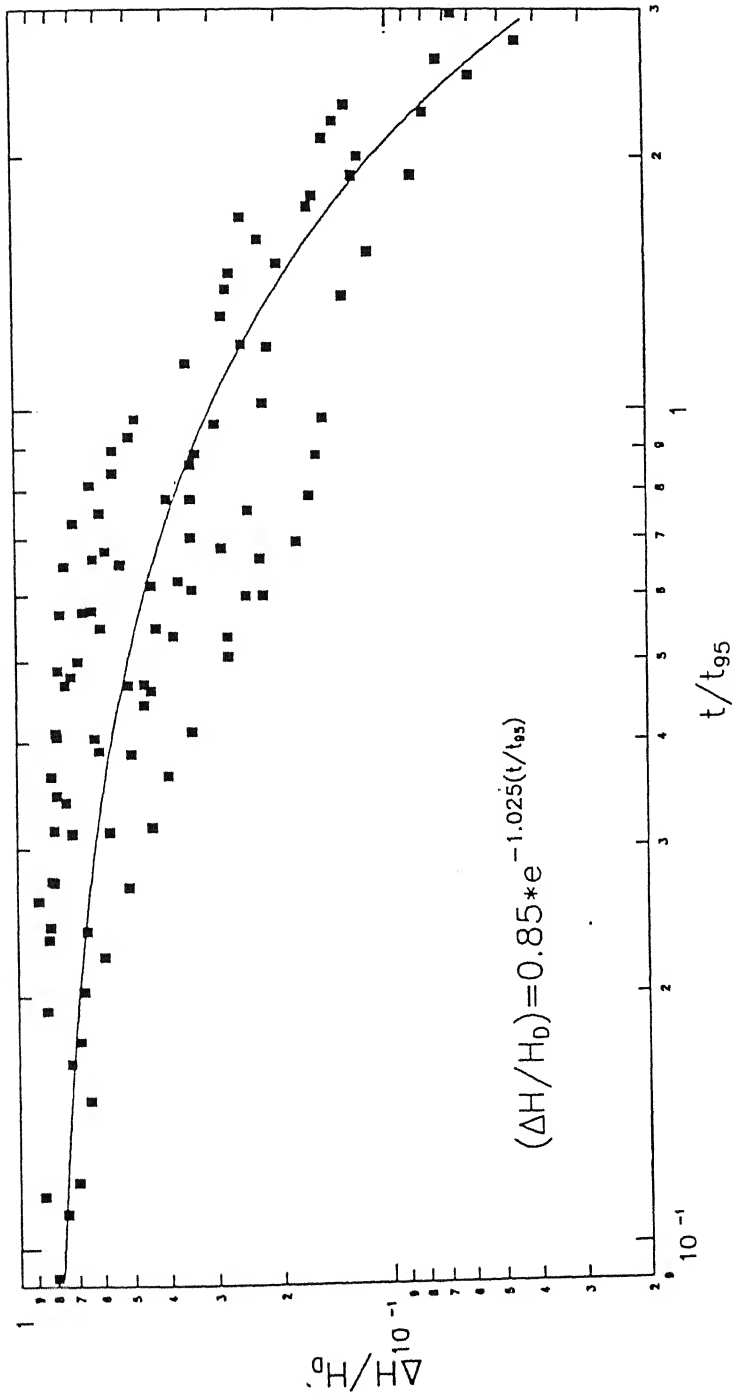


Fig. 4.14(b): Variation of nondimensional drop in water level between upstream and downstream ( $\Delta H$ ) with nondimensional time

### c. Breach Erosion

Variation of sediment bed profile, crest height and its width during breach process are analysed. Eroded sediment volume and its transport relation are analysed further.

#### i. Variation of Sediment Bed Profile with Time

As the water flows over the embankment, sediment gets eroded. Magnitude of erosion depends upon the shear stress acting on the sediment bed. It is observed that the sediment erosion starts from the downstream end of the embankment, recedes upstream within a short time. Once it reaches upstream edge of the embankment, the sediment gets eroded over the whole surface along the breach. These surfaces are measured along the centerline of the breach with time and they are plotted in Figures 4.15(a) and (b). It is observed that in the case of a dam of larger height the downstream bed profile gradually flattens with increase in time. In the case of lower height dam sediment erosion profile is slightly flatter compared to dams of larger height. These profiles are studied by nondimensionalising sediment bed level ( $h_c$ ) by its maximum level ( $h_{cm}$ ) at the crest, which is usually located at the upstream top edge of the dam. This distance ( $X$ ) along the embankment and along the flow is nondimensionalised by the value ' $X_m$ ' where  $h_{cm}$  occurs. The nondimensional plots of  $h_c/h_{cm}$  against  $X/X_m$  are plotted in Figures 4.16(a) and (b). It may be observed from nondimensional variation that for higher embankment dam model the variation for  $H_D$  19.5 cm to 35 cm is in one pattern. For lower dam models of  $H_D$  equal to 14.5 cm the variation is in a slightly different way. However in both the cases, there is a steep rise to the maximum value, then gradual decrease with increasing  $X$  values. The relation between them obtained from regression analysis is a polynomial curve and is presented in Figures 4.16(a) and (b).

#### ii. Variation of Crest Height ( $h_{cm}$ )

The sediment bed profile variation with time is of similar pattern as shown in Figures 4.16(a) and (b) for all the cohesionless embankment models. With this in view, the height of sediment crest is non-dimensionalised with final depth of erosion ( $D_{er}$ ) and plotted against the nondimensional time  $t/t_{50}$  in Figure 4.17(a). Here  $t_{50}$  is the time at which 50% of the maximum erosion depth ( $D_{er}$ ) has taken place. It was observed, the relation between



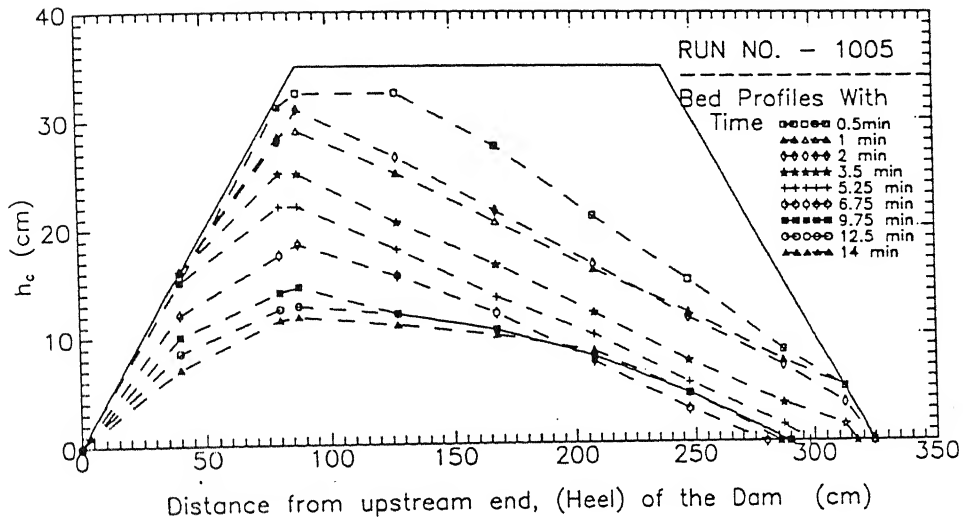


Fig. 4.15(a): A typical Variation of sediment bed profile for run no. 1005, ( $H_0=35\text{cm}$ ), dam model with cohesionless soil

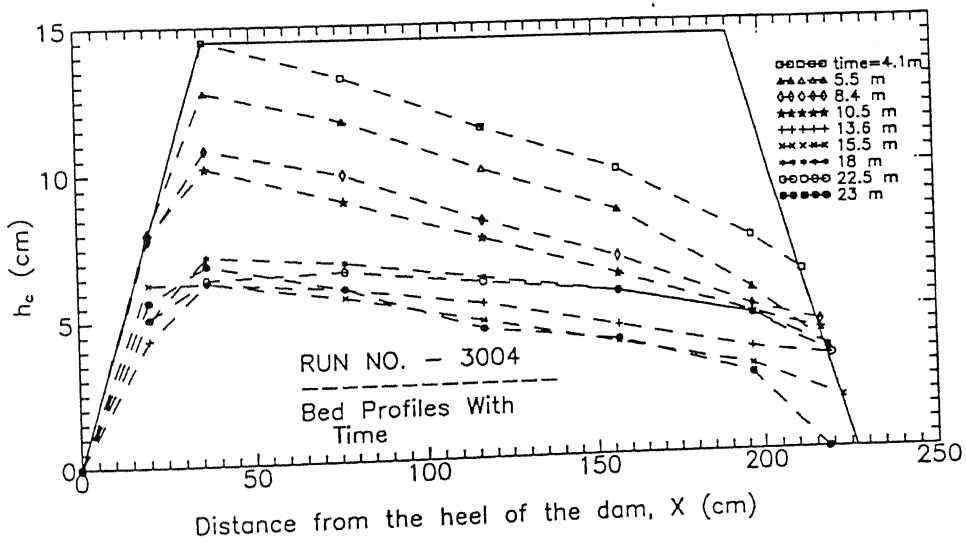


Fig. 4.15(b): A typical Variation of sediment bed profile for run no. 3004, ( $H_0=14.5\text{cm}$ ), dam model with cohesionless soil

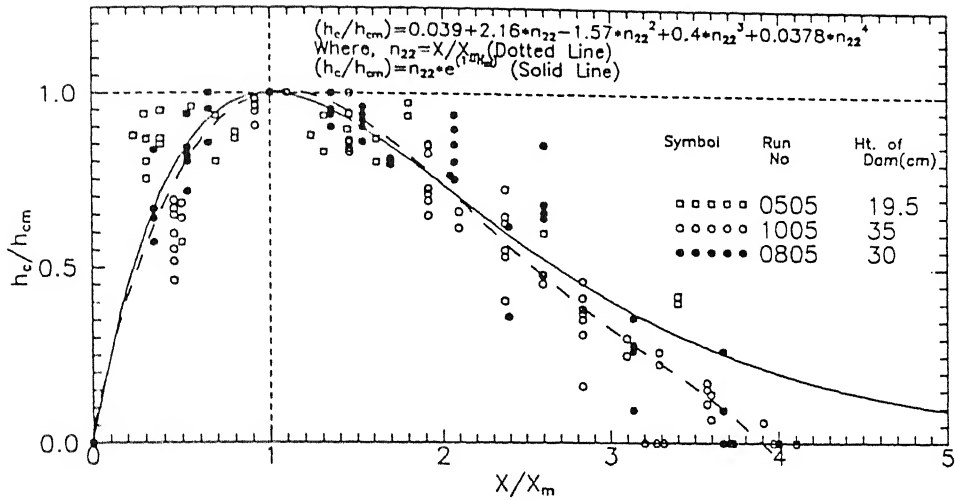


Fig. 4.16(a): Nondimensional variation of sediment bed height ( $h_c$ ) at any location of breach with its nondimensional distance,  $X$  from heel of the dam (for dams of height=19.5cm, 30 cm and 35cm)

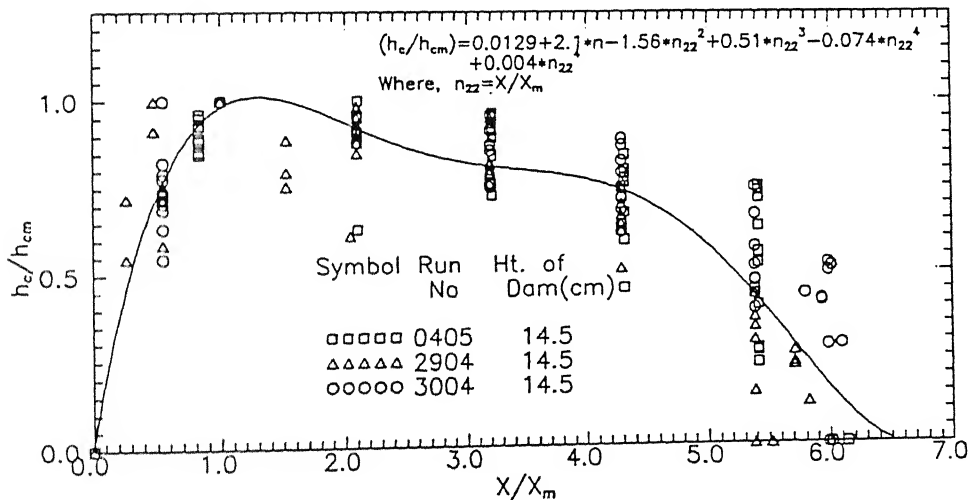


Fig. 4.16(b): Nondimensional variation of sediment bed height ( $h_c$ ) at any location of breach with its nondimensional distance,  $X$  from heel of the dam (for dams of height=14.5cm)

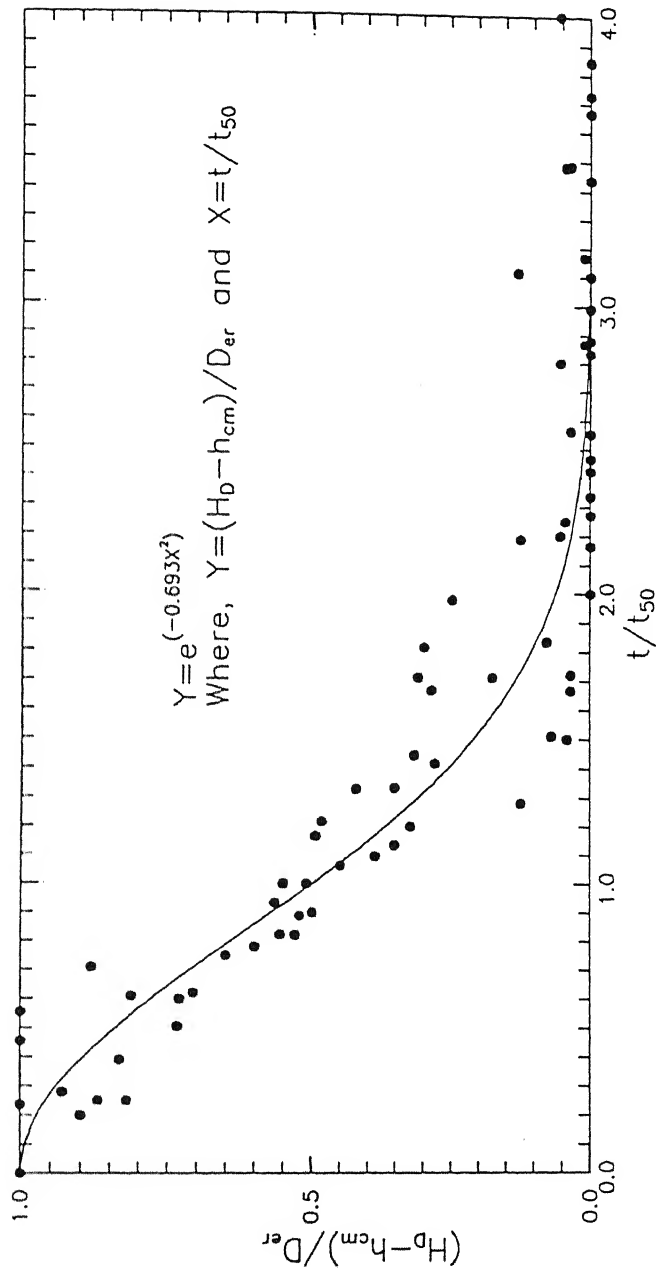


Fig. 4.17(a): Nondimensional Variation of crest of erodible sediment bed ( $h_{cm}$ ) at any time of breach with its nondimensional time of occurrence.

nondimensional depth of erosion with nondimensional time follows simple exponential decay curve as:

$$Y = e^{-0.693 X^2} \quad (4.7a)$$

Where,  $Y = (H_D - h_{cm}) / D_{er}$

$X = t/t_{50}$ , and  $D_{er}$  = final depth of erosion

The time scale  $t_{50}$  is studied by nondimensionalising it as  $t_{50} \sqrt{g / H_D}$ . This value is plotted against nondimensional  $\bar{Q}_{in}$  as shown in Figure 4.17(b). The functional relation among them is as follow:

$$t_{50} \sqrt{g / H_D} = -3194.91 + 160087 X - 9.289 \times 10^7 X^2 \quad (4.7b)$$

(This equation is not valid for  $X=0$ )

$$\text{Where } X = \frac{\bar{Q}_{in}}{A_D \sqrt{g / H_D}}$$

From the Figure 4.17(a) it will be observed that the crest height can be predicted with time of erosion which is used in predicting sediment bed profiles along the breach from Figures 4.16(a) and (b). The final breach depth of erosion at crest ( $D_{er}$ ) is related with peak outflow discharge ( $Q_{wp}$ ) and height of the dam ( $H_D$ ) in a non-dimensional form as shown in Figure 4.17(c). The functional relation developed for  $D_{er}$  with these variables may be written as:

$$\frac{D_{er}}{H_D} = 0.52 \left[ \frac{Q_{wp}}{\sqrt{g H_D^5}} \right]^{-0.043} \quad (4.7c)$$

Depth of erosion  $D_{er}$  is also correlated with inflow discharge parameter, defined as

$\bar{Q}_{in} / (A_D \sqrt{2g H_D})$  as shown in Figure 4.17(d). Using regression analysis, relation between them is written as:

$$\frac{D_{er}}{H_D} = 0.71 \left\{ \frac{\bar{Q}_{in}}{A_D \sqrt{2g H_D}} \right\}^{0.015} \quad (4.7d)$$

For prediction of  $D_{er}$ , either Figure 4.17(c) or Figure 4.17(d) can be used depending upon the availability of the information.

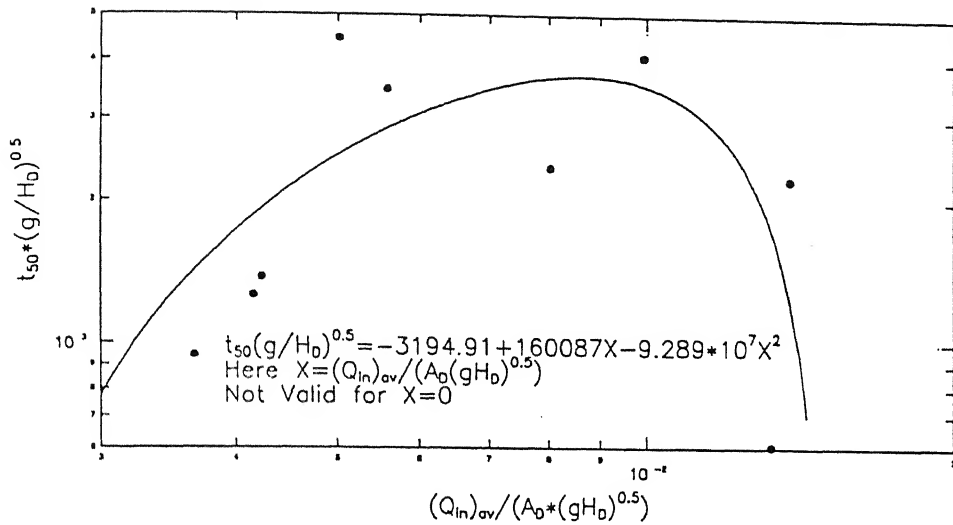


Fig. 4.17(b): Variation of time scale  $t_{50}$  in nondimensional form with  $Q_{APN}$  number

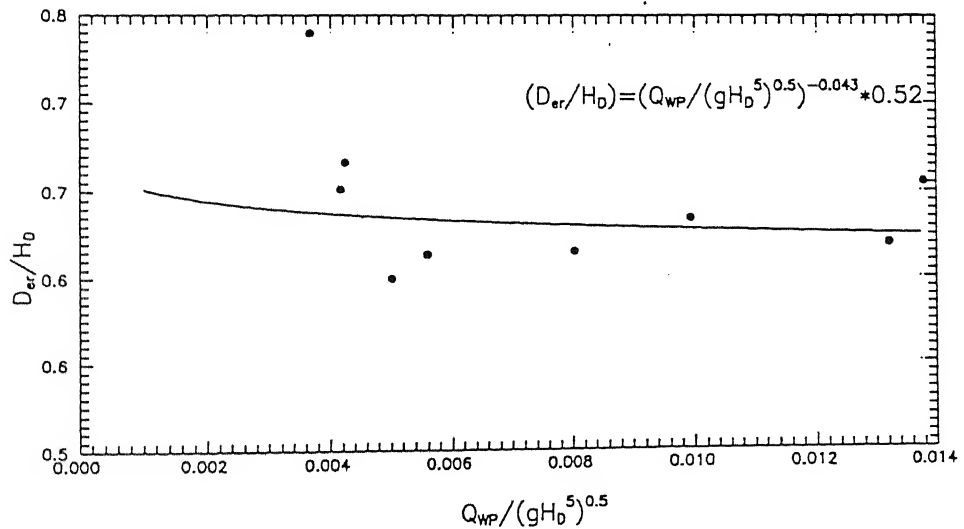


Fig. 4.17(c): Variation of final depth of erosion at crest,  $(D_{er})$  in nondimensional form with peak breach discharge ( $Q_{WP}$ ) and height of the dam ( $H_0$ )

The relation between the depth of erosion and drop of water level at crest is also presented as an alternative approach to predict crest height variation. Here depth of erosion ( $H_D - h_{cm}$ ) is non-dimensionalised with height of the dam ( $H_D$ ) and plotted against nondimensional water level drop at the crest as shown in Figure 4.17(e). Here  $h_{cm}$  is the crest height. It may be observed from this figure that there is a good agreement between sediment crest level and water level at the crest with respect to the water level in the reservoir. The relation between them is obtained from regression analysis as:

$$\frac{(H_D - h_{cm})}{H_D} = \left( \frac{\text{Drop of water level at crest}}{H_D} \right)^{0.69} \quad (4.7e)$$

From the Equation (4.7e), by knowing the water surface at the crest one can predict, crest level of the dam at any time of breach.

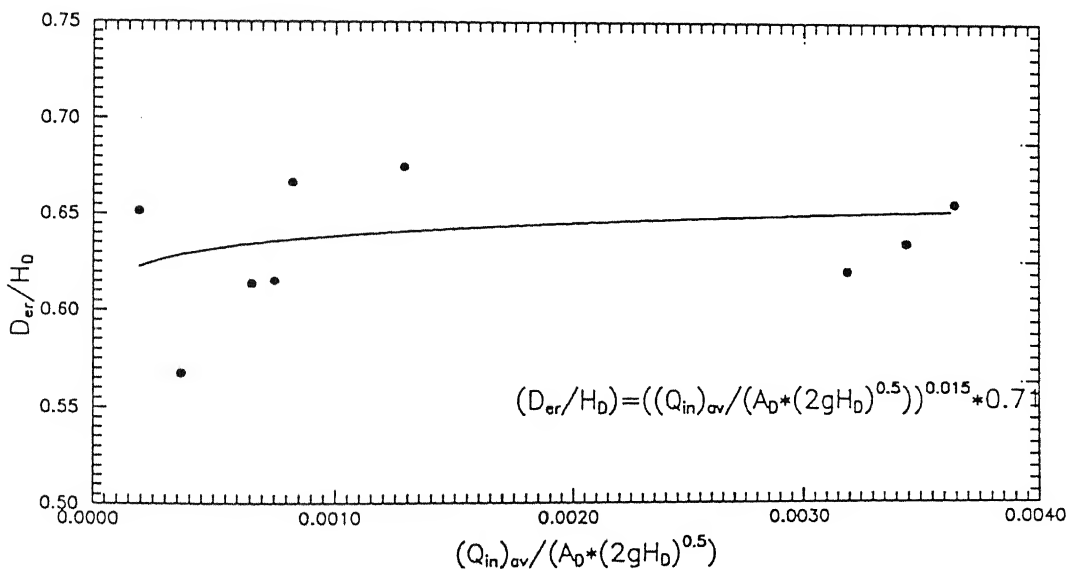


Fig. 4.17(d): Variation of final depth of erosion at crest, ( $D_{er}$ ) in nondimensional form with average inflow discharge to the reservoir, height ( $H_0$ ) and cross-sectional area ( $A_0$ ) of the dam

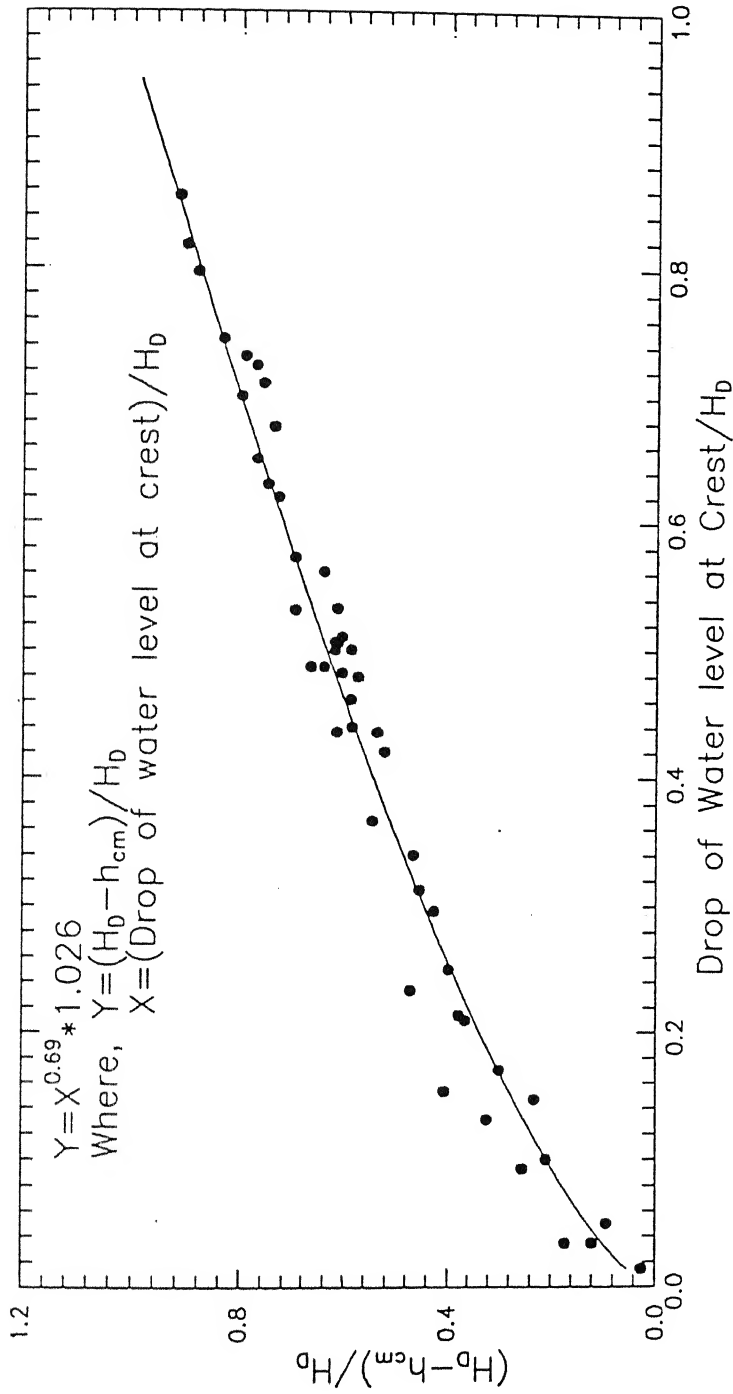


Fig. 4.17(e): Variation of nondimensional depth of erosion at any time  $(H_b - h_{cm})$  with nondimensional drop of water level at the crest

### iii. Rate of Crest Height Variation

The rate of crest variation ( $dh_{cm}/dt$ ) is plotted against crest drop flow velocity ( $\sqrt{2gh_d}$ ). This drop-flow velocity is computed based on the difference in water level upstream to the crest. The ( $dh_{cm}/dt$ ) is plotted against ( $\sqrt{2gh_d}$ ) as shown in Figure 4.18(a). There are two distinct limbs, rising and receding limb. During the rising period, the rate of crest erosion is less compare to the receding period. During the transition state from rising to receding limb, rate of crest erosion has multiple values.

Crest sediment erosion rate is also plotted with crest flow velocity ( $V_{wc}$ ) in the Figure 4.18(b). Crest erosion is a single valued function of  $V_{wc}$ . The crest flow velocity  $V_{wc}$  is also associated with peak discharge  $Q_{wp}$  and height of the dam  $H_D$ . The magnitude of  $V_{wc}$  is computed by knowing discharge over the crest  $Q_w$  and wetted flow area at the crest as:

$$V_{wc} = \frac{Q_w}{\text{Wetted flow area at the crest}} \quad (4.8a)$$

where Wetted flow area at the crest =  $B_{cr} h_{wc}$

This was studied particularly to avoid the multiple values as indicated in the Figure 4.18(a). The relation between the crest erosion rate with flow velocity obtained from regression analysis is written as:

$$\frac{dh_{cm}}{dt} = \left[ \frac{V_{wc}}{(Q_{wp} / \sqrt{gH_D^5})} \right]^{1.2} \times 1.5 \times 10^{-5} \quad (4.8b)$$

It may be noted in Figure 4.18(b) that  $V_{wc}$ , the crest flow velocity is in the same unit of measurement as that of the rate of crest erosion. These two figures involves flow velocity ( $V_{wc}$ ), crest flow velocity ( $\sqrt{2gh_d}$ ), where one is obtained from breach discharge and breach flow area at the crest and the other one from the difference in water level upstream and at the crest. The prediction of  $h_d$  is easier compared to prediction of  $V_{wc}$ . However the sediment crest erosion rate related to  $h_d$  is a multiple valued function. Whereas the sediment crest erosion rate is a single valued function of  $V_{wc}$ . It may be advocated to use single valued functional relationship. The rate of sediment crest erosion is subjected to further analysis because of its importance in the prediction of the discharge through the breach and also to study in the dimensionless form.



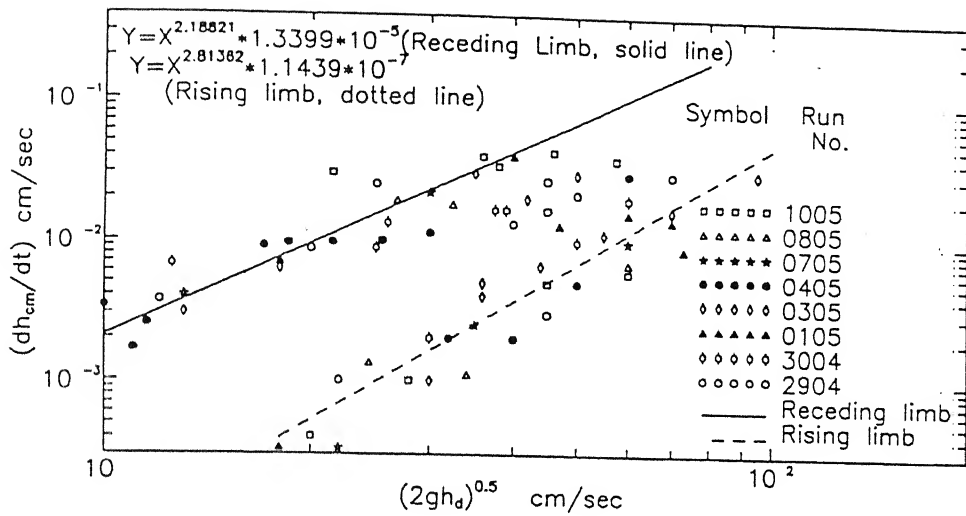


Fig. 4.18(a): Variation of rate of crest height,  $(dh_{cm}/dt)$  with drop flow velocity,  $(2gh_d)^{0.5}$

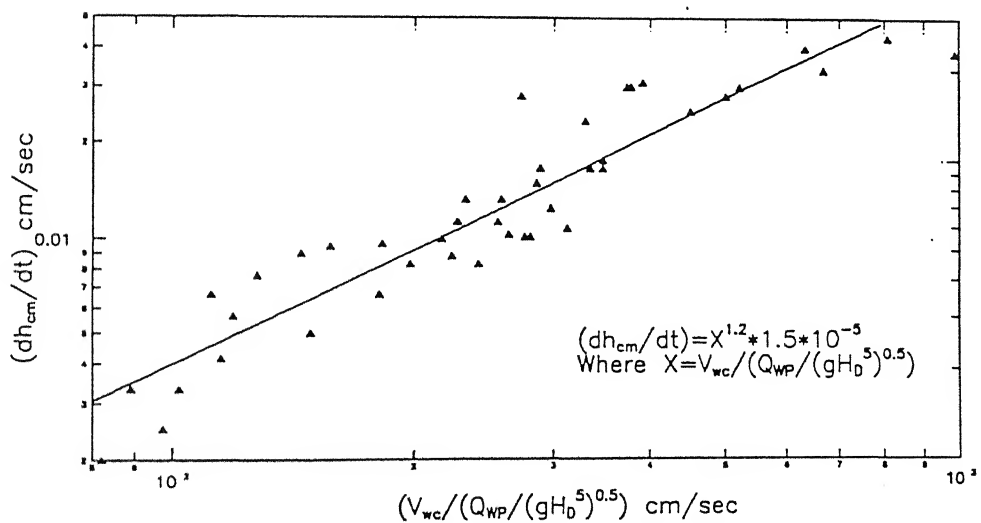


Fig. 4.18(b): Variation of rate of crest height,  $(dh_{cm}/dt)$  with crest flow velocity,  $(V_{wc})$

The rate of decrease of sediment crest is nondimensionalised with average shear velocity and  $Q_{WP} / \sqrt{gH_D^5}$  and is plotted against nondimensionalised drop in water level at the crest with respect to height of the dam  $H_D$ . These values are plotted for all the embankment models as shown in the Figure 4.18(c). It may be noted that the rate of erosion decreases with increase in drop water level at the crest. The relation between them is as follows:

$$\left[ \frac{1}{\bar{V}_s} \frac{dh_{cm}}{dt} \right] / \left( Q_{WP} / \sqrt{gH_D^5} \right) = 0.05 \times e^{-3.14 \left( \frac{H_D - h_{cm} - h_{wc}}{H_D} \right)} \quad (4.8c)$$

#### iv. Variation of Sediment Bed at the Downstream Top Edge of the Embankment

Top width in some of the embankment model varies 3 to 10 times the height of the dam. Due to longer top width, the sediment bed level variation at this section also becomes important in the sediment erosion analysis. The bed level of the eroded sediment at the downstream edge of the embankment is studied with respect to drop at the downstream edge and both the quantities are nondimensionalised with  $H_D$  as shown in Figure 4.18(d). Initial erosion is not accounted in this figure. There appears to be a good agreement between the height of sediment bed, and the drop in water level at that section. The relation is obtained through regression analysis as follows:

$$\frac{h'_c}{H_D} = 1.47 \times e^{-2.92 \left( \frac{Drop'}{H_D} \right)} \quad (4.9)$$

$$\text{Where } Drop' = H_D - (h'_c + h'_{wc})$$

Where  $h'_c$  is the sediment bed level at the downstream top edge of the dam and  $Drop'$  is the drop in water level with respect to top level of the dam.

#### v. Lateral Erosion at the Crest

Lateral erosion of the crest is considered at the upstream top edge of the embankment. Erosion of the breach section at the crest results due to the reduction in the sediment crest level and widening of breach bank simultaneously. It is observed from the experiments that the breach widens faster than the crest height erosion. This can be seen clearly from Figure 4.19(a) that the ratio of the rate of crest erosion to the rate of crest width erosion is less than unity from the starting of the breach process. This ratio remains fairly constant for longer part of the duration. Later in the final stage the rate of lateral erosion is much faster.

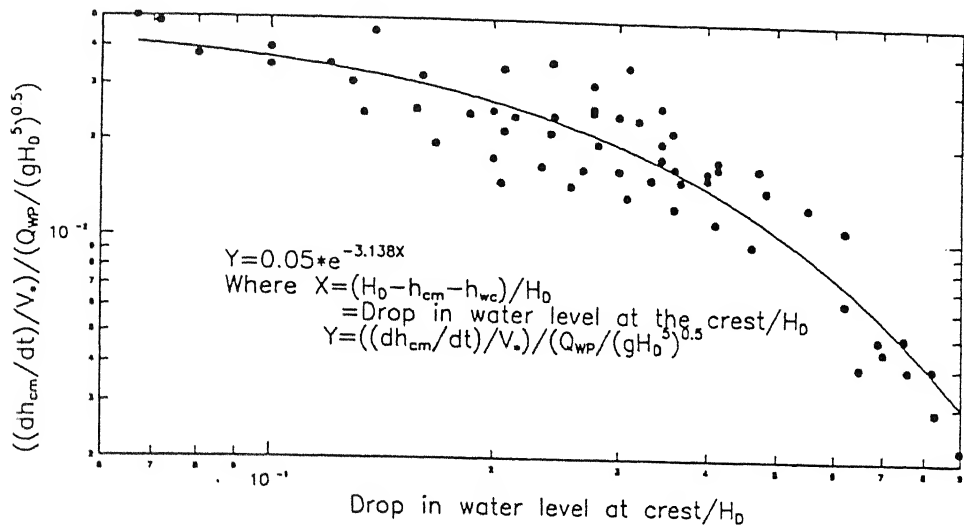


Fig. 4.18(c): Variation of rate of nondimensional rate of crest height,  $(dh_{cm}/dt)$  with nondimensional drop of water at that section

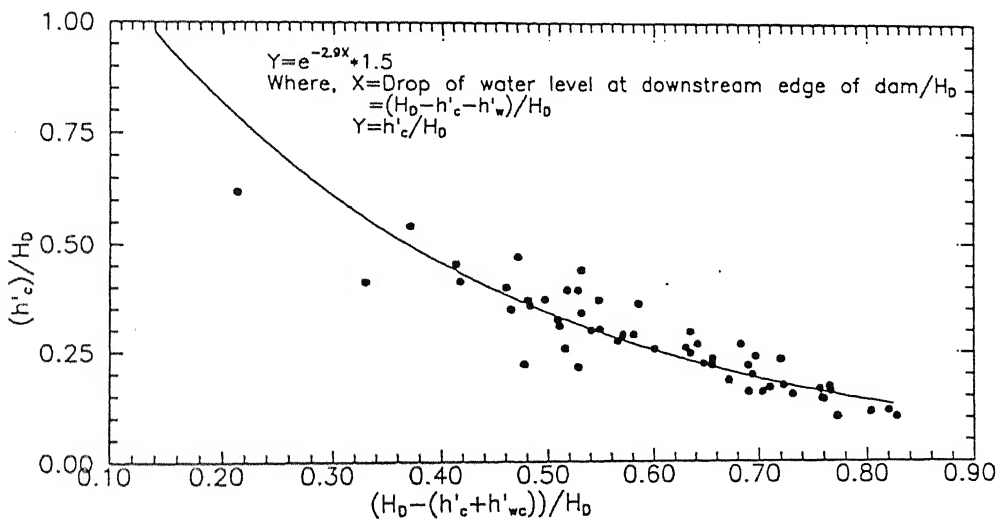


Fig. 4.18(d): Variation of sediment bed height at downstream edge of the dam with drop of water level at that section in a nondimensional form

In order to study the breach widening at crest at any time of breach, the variation of breach width with drop of water level at the crest from the reservoir level are plotted by non-dimensionalising both the quantities with  $H_D$ . It is observed that the breach crest width erodes with increase in drop as shown in Figure 4.19(b) the relation between them is given as:

$$\frac{B_{cr}}{H_D} = \left( \frac{H_D - h_{cm} - h_{wc}}{H_D} \right)^{0.57} \times 2.5 \quad (4.10a)$$

Where ,  $(H_D - h_{cm} - h_{wc})$  is called the drop of water level at the crest. This equation is obtained from regression analysis. The final magnitude of the breach width is also plotted against the maximum outflow discharge of the breach hydrograph in dimensionless form as indicated in the Figure 4.19(c). The relation between them is given as:

$$\frac{(B_{cr})_f}{H_D} = \left( \frac{Q_{wp}}{\sqrt{gH_D^5}} \right)^{0.24} \times 4.02 \quad (4.10b)$$

In order to include the effect of the downstream water level on the erosion process of the crest width the plot of  $B_{cr}/H_D$  against  $\Delta H_c/H_D$  is carried out as shown in the Figure 4.20, where  $\Delta H_c$  is water level difference between the crest and downstream end of the embankment i.e., toe of the embankment. It may be observed that  $B_{cr}/H_D$  decreases as  $\Delta H_c/H_D$  increases. The relation between them is written as per regression analysis:

$$\frac{B_{cr}}{H_D} = 712.02 e^{-1.9X} \quad (4.10c)$$

$$\text{Here } X = \left( \frac{\Delta H_c}{H_D} \right) \left( \frac{Q_{wp}}{\sqrt{gH_D^5}} \right)^{1.77}$$

Crest width ( $B_{cr}$ ) being a major breach morphological variable it is related with both drop in water level at crest in Equation (4.10a) and drop  $\Delta H_c$ . These two equations indicate  $B_{cr}$  increases with time. It increases exponentially with  $\Delta H_c$  whereas it varies in a power law form with the drop in water level at crest. But Equation (4.10c) is preferable.

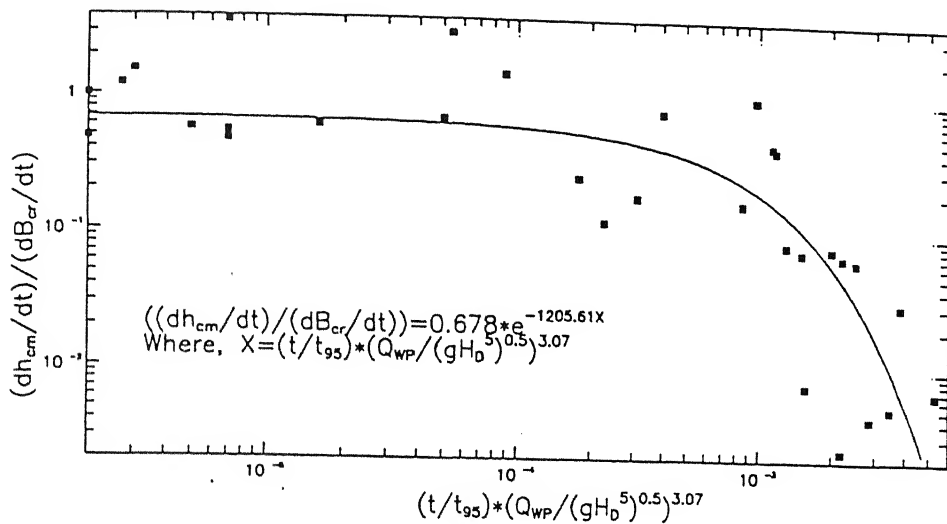


Fig. 4.19(a): Comparison of rate of crest height erosion to its lateral erosion with time in a nondimensional form

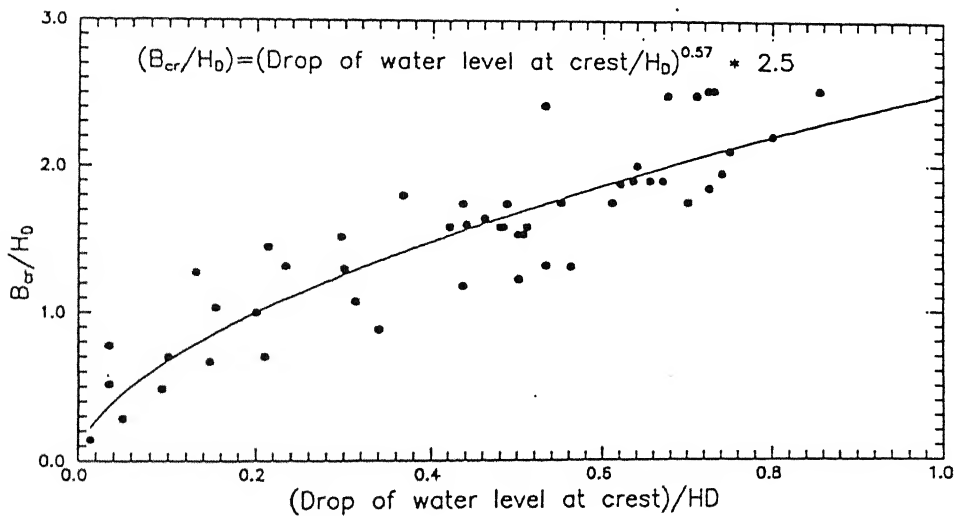


Fig. 4.19(b): Variation of nondimensional breach crest width at any time of breach, ( $B_{cr}$ ) with nondimensional drop of water at crest.

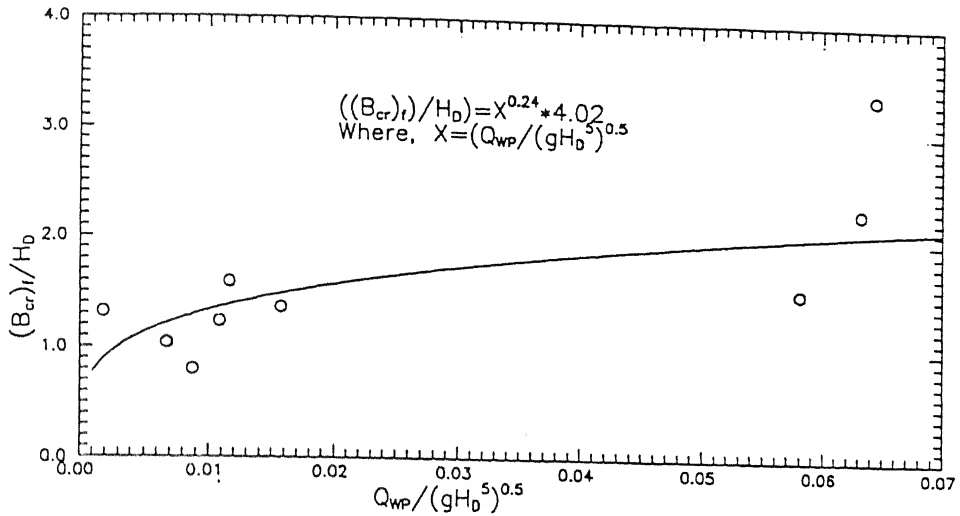


Fig. 4.19(c): Variation of nondimensional final breach crest width,  $(B_{cr})_f$  with  $Q_{PN}$  number

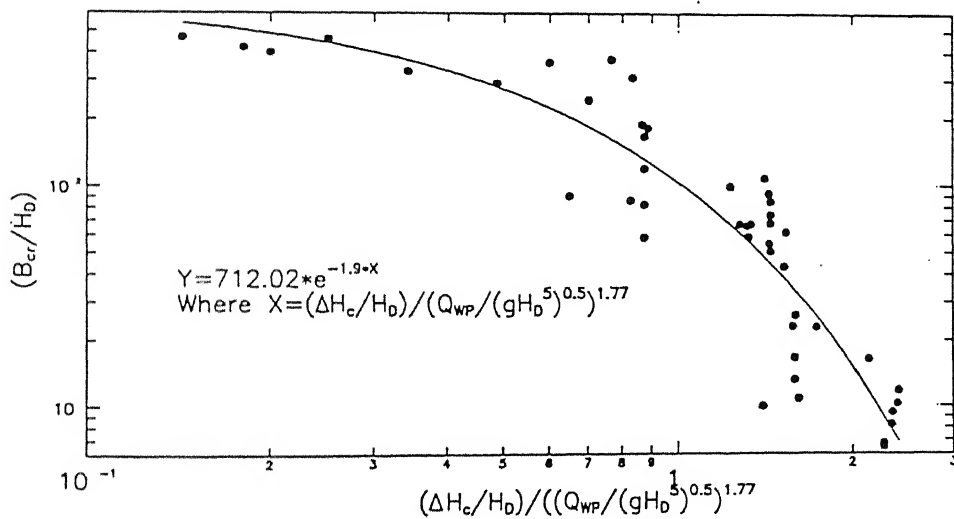


Fig. 4.20: Variation of nondimensional breach crest width at any time of breach with drop in water level between crest and toe of the dam,  $\Delta H_c$  and  $Q_{PN}$

## vi. Rate of Lateral Erosion at Crest

The rate of width erosion with time is equally important in the study of erosion process along with the rate of vertical erosion. Widening of breach width at the crest causes the change in magnitude of flow intensity at the crest. Keeping this in view, the rate of width erosion with time is plotted in the Figure 4.21(a). From this figure it may be observed that the rate of width erosion decreases with time. To represent this variation in non-dimensional form,  $dB_{cr}/dt$  is nondimensionalised with respect to  $\sqrt{2gH_D}$  and time ( $t$ ) with  $t_{95}$ . The  $t_{95}$  is defined as the time at which 95% of the sediment erosion occurs in the breach. This is plotted in the Figure 4.21(b). Using regression analysis the relation is established as:

$$\frac{(dB_{cr}/dt)}{\sqrt{2gH_D}} = \left(\frac{t}{t_{95}}\right)^{-2.08} \times 1.14 \times 10^{-5} \quad (4.11a)$$

The rate of erosion of the width at the crest is mainly a function of the magnitude of the crest flow velocity ( $V_{wc}$ ). To test this postulation, rate of erosion is again plotted against the crest flow velocity in dimensionless form. The relationship exists among them is indicated in the Figure 4.21(c). The relation obtained among them is as follows:

$$\frac{\left[ \left( \frac{dB_{cr}}{dt} \right) * \left( \frac{Q_{up}}{\sqrt{gH_D^3}} \right)^{1.62} \right]}{V_{SR}} = \left( \frac{V_{wc}}{\sqrt{2gH_D}} \right)^{1.07} \times 0.0128 \quad (4.11b)$$

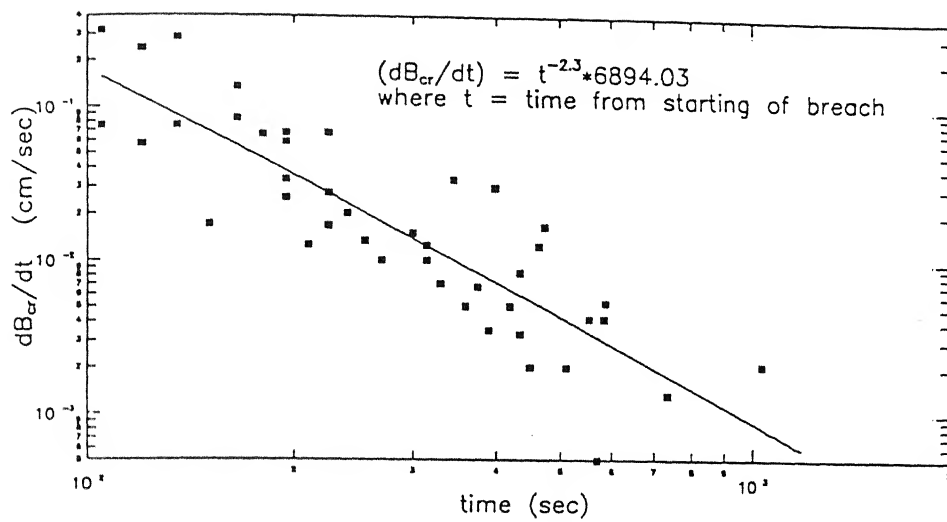


Fig. 4.21(a): Variation of rate of lateral erosion with time

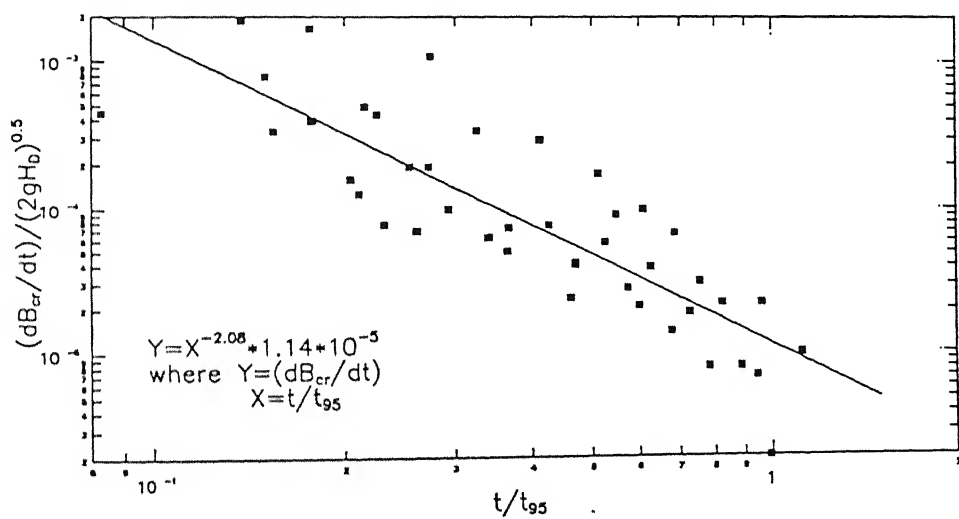


Fig. 4.21(b): Variation of rate of lateral erosion with nondimensional time ( $t/t_{95}$ )



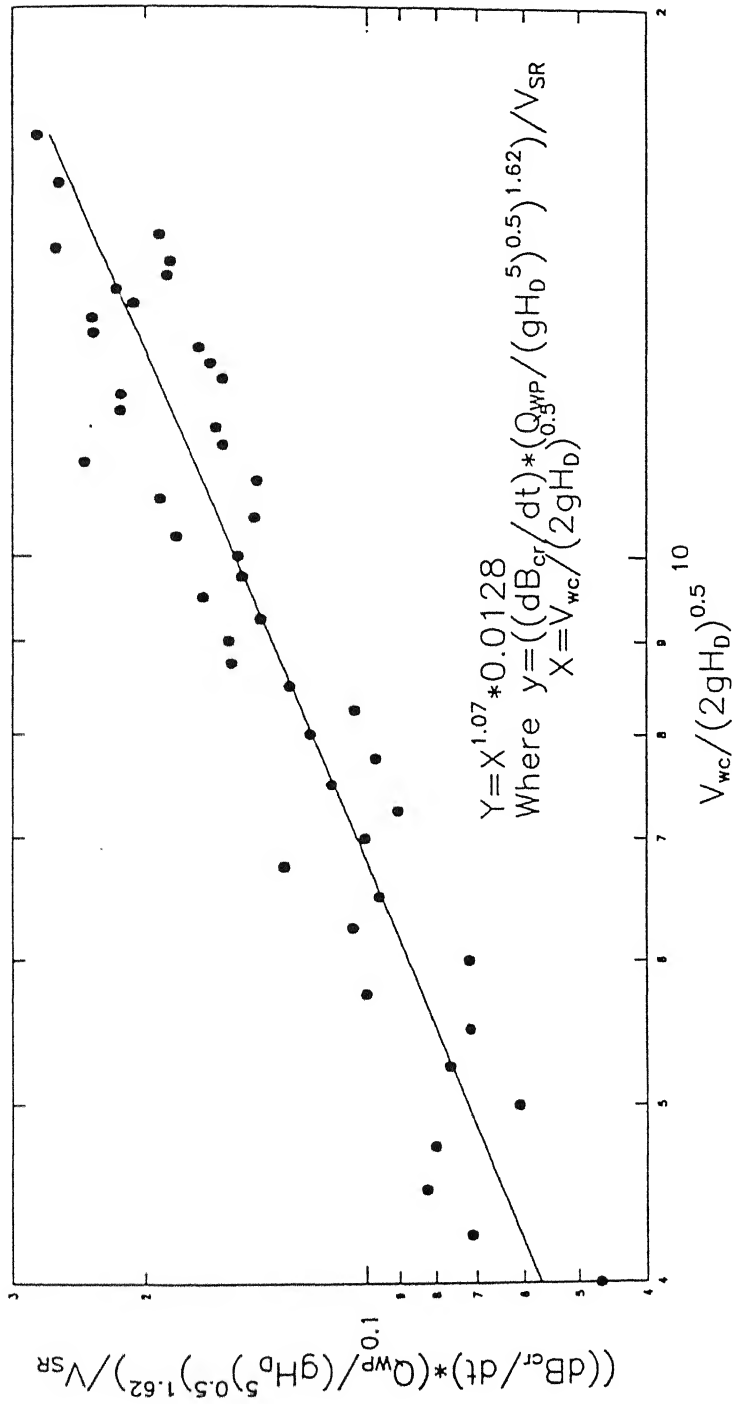


Fig. 4.21(c): Variation of nondimensional crest width erosion with its nondimensional crest flow velocity

### vii. Variation of Width at Downstream Top Edge of the Embankment

The breach width at downstream top edge of the embankment is denoted as  $B'_{cr}$ . Its qualitative variation is presented in the section containing the description of breach morphology. Its variation is studied using similar parameters that are used for the crest width study,  $B_{cr}$ . The non-dimensional variation of  $B'_{cr}$  with  $H_D$  is plotted against  $\Delta H/H_D$  in the Figure 4.22(a). The relation is given as follow:

$$\frac{B'_{cr}}{H_D} = 2.64 * e^{-1.69(\Delta H/H_D)} \quad (4.11c)$$

It may be observed that there is a sudden increase in the width at initial stages of the erosion; as erosion proceeds, width remains almost constant.

Rate of erosion of downstream width is plotted against  $V'_{wc}$  the flow velocity along with  $\frac{Q_{wc}}{\sqrt{gH_D^3}}$  as shown in Figure 4.22(b). The results indicate two distinct variations, one following the rising limb and another one with a falling limb. The rate of erosion of width is almost linear in both the states of flow, but however, there is a wide gap between both of them indicating the existence of transitional state of flow.

The relative variation of crest widths at the downstream top edge and the upstream top edge denoted as  $\frac{B'_{cr}}{B_{cr}}$  is plotted against  $\frac{t}{t_{95}}$  as shown in Figure 4.22(c). The functional relation among them is:

$$\frac{B'}{B_{cr}} = 0.067 + 3.65 \frac{t}{t_{95}} - 3.95 \times \left( \frac{t}{t_{95}} \right)^2 + 1.4 \times \left( \frac{t}{t_{95}} \right)^3, \text{ Valid up to } \frac{t}{t_{95}} \leq 1.0 \quad (4.11d)$$

The regression curve is drawn for the data. It may be observed that this ratio becomes greater than 1.0, when  $\frac{t}{t_{95}}$  is 0.4 and more. This indicates that in the beginning the crest width

erosion at the upstream edge is more compared to that at the downstream edge of the embankment. As the breach erosion continues the crest width at downstream end enlarges gradually and becomes equal to that at the upstream edge at  $t = 0.4 t_{95}$ . Later on the crest width at downstream edge widens and remains fairly constant after  $t/t_{95} = 0.8$ . Further onwards its magnitude remains constant at an average value of 1.2.

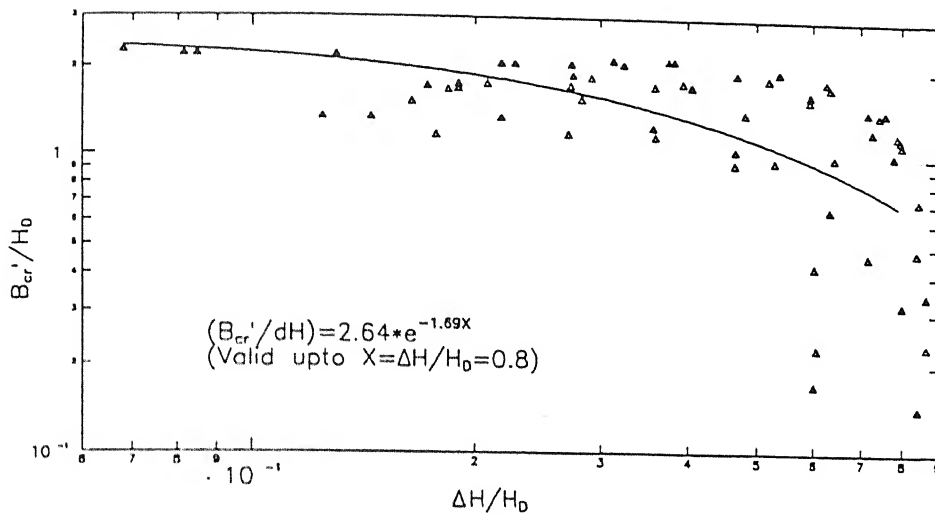


Fig. 4.22(a): Variation of nondimensional breach width erosion at the downstream top edge of the dam with nondimensional water drop between upstream and downstream of the dam,  $\Delta H$

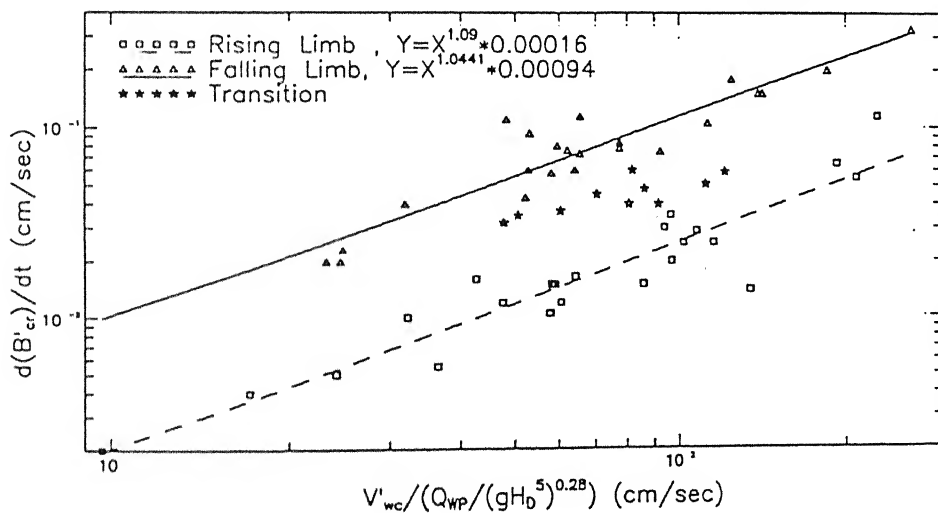


Fig. 4.22(b): Variation of rate of breach width at downstream top edge of the dam with the flow velocity at that section

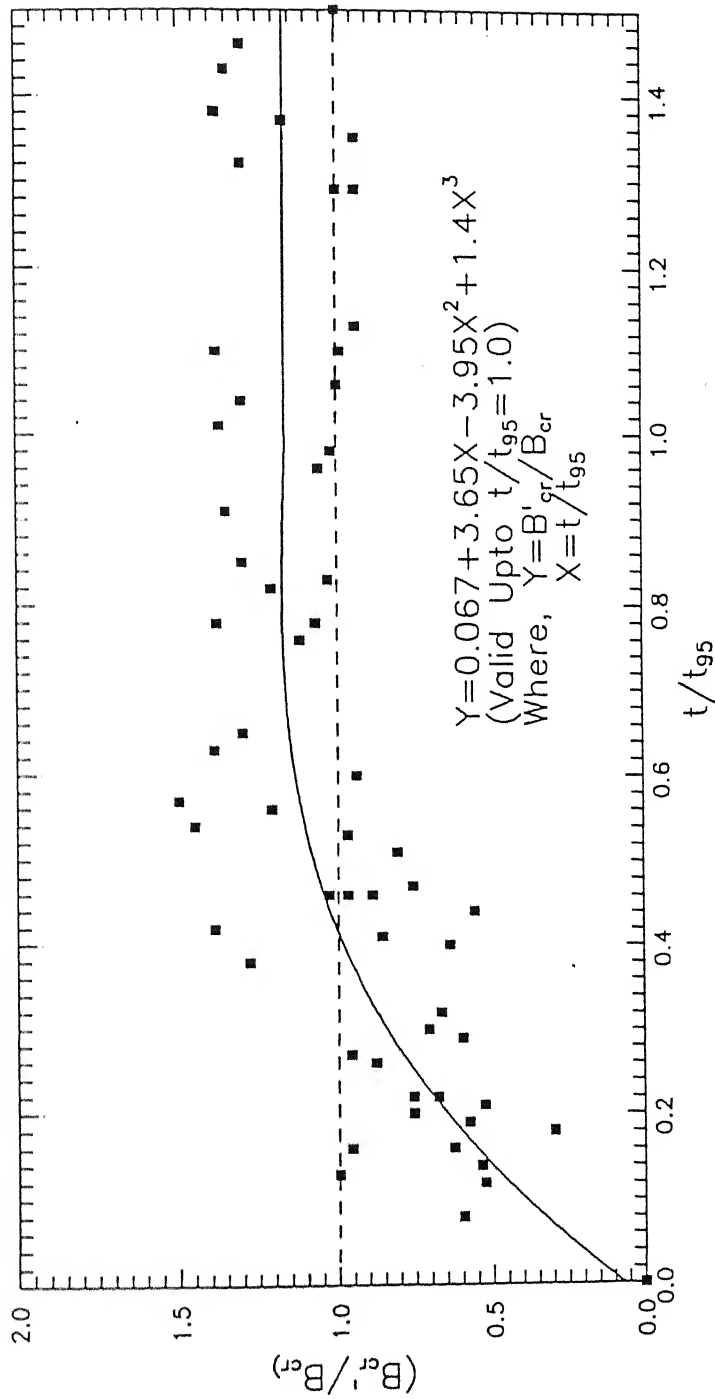


Fig. 4.22(c): comparison of variation of width of erosion at crest and at the downstream top edge of the dam with nondimensional time

### viii. Variation of Sediment Volume

The volume of sediment eroded is computed, knowing the cross - sectional area of sediment eroded at different sections along the breach sections where measurements were taken. The typical variation of cumulative volume of sediment eroded with time is shown in Figure 4.5. The rate of cumulative volume of sediment at a given time is considered as the sediment discharge ( $Q_s$ ). It is observed that the sediment erosion is a function of the magnitude of the flow discharge ( $Q_w$ ). Based on this consideration, the cumulative volume of sediment ( $\Sigma V_s$ ) is non-dimensionalised with cumulative outflow volume of water ( $\Sigma V_w$ ) at any time and is plotted against  $t/t_{95}$  as shown in Figure 4.23(a). The functional relation among them may be written from regression analysis as:

$$\frac{\Sigma V_s}{\Sigma V_w} = 0.03 \times \left( \frac{t}{t_{95}} \right)^{-0.97} \quad (4.12a)$$

Here  $t_{95}$  is the time at which 95% of the cumulative sediment eroded. The non-dimensional value of  $\Sigma V_s$  varies almost inversely with non-dimensional time variation as indicated in Figure 4.23(a). Instead of taking  $\Sigma V_s$ , the discharge ratio of sediment and water is considered for further analysis.

### ix. Variation of Sediment Discharge Intensity

In order to study sediment discharge intensity ( $q_s$ ) with flow discharge intensity ( $q_w$ ), plot of  $q_s$  versus  $q_w$  is carried out in Figure 4.23(b). Here, sediment discharge intensity ( $q_s$ ) is obtained from  $Q_s$  as  $q_s = Q_s / \text{average breach width}$ . The magnitude of  $q_s$  is plotted against the water discharge intensity  $q_w$  as shown in Figure 4.23(b). Here the water discharge intensity is obtained as  $q_w = Q_w / \text{Average breach width}$ . The average breach width is the average of the breach width at the top edge, middle of the top section and downstream top edge of the embankment. Using the regression analysis, the relation between them is as follows:

$$q_s = 9.86 \times 10^{-5} \times q_w^{1.43} \quad (4.12b)$$

It may be noted that  $q_s$  varies as  $q_w^{1.43}$ , where exponent 1.43 is much below what is observed in the sand bed stream.

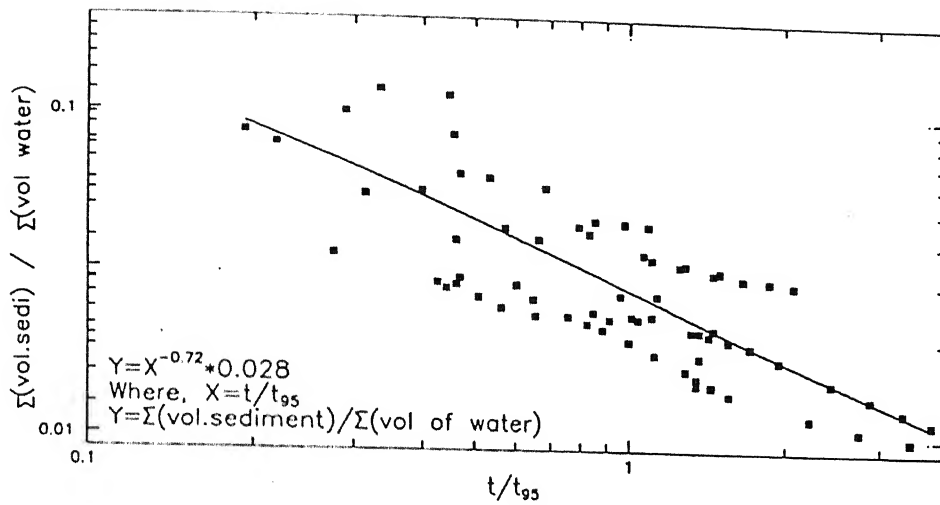


Fig. 4.23(a): Variation of nondimensionalised cumulative eroded sediment volume by cumulative flow of water in breach section with nondimensionalised time.

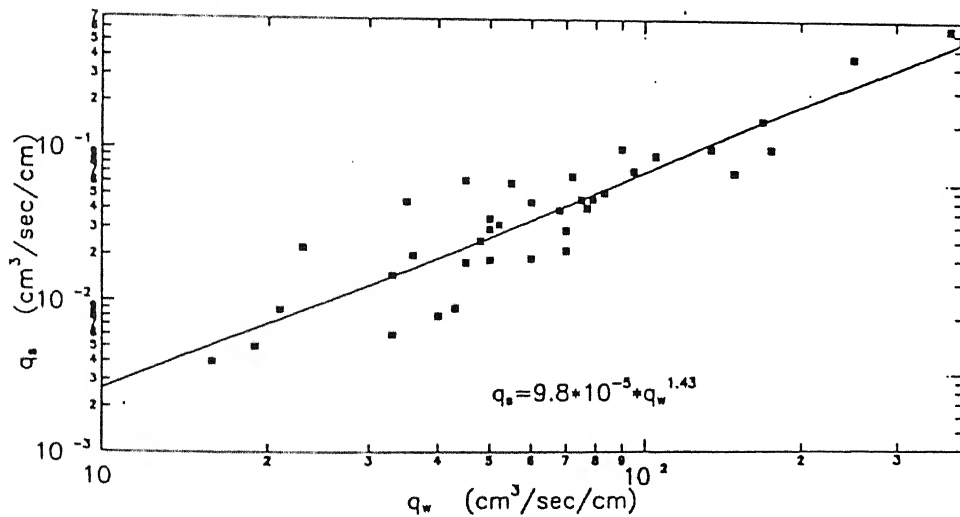


Fig. 4.23(b): Variation of sediment discharge intensity, ( $q_s$ ) with breach water discharge intensity, ( $q_w$ )

Bed shear stress is considered to be important parameter for the sediment discharge. Sediment discharge intensity ( $q_s$ ) is plotted against square of shear velocity ( $V_*^2$ ) in Figure 4.23(c), where  $V_* = (\tau_0/\rho_w)^{0.5}$ ,  $\tau_0$  = bed shear stress,  $\rho_w$  = density of water. The relation between  $q_s$  and  $V_*^2$  indicates a well defined relation for the value of  $V_* = 7.0$  cm/sec and above in a power law form,  $q_s \propto (V_*^2)^{1.928}$  as given below,

$$q_s = (V_*^2)^{1.928} \times 6.1725 \times 10^{-6} \quad (4.12c)$$

On the same plot, polynomial variation between  $q_s$  and  $V_*^2$  is plotted. This relation is shown in the following equation.

$$q_s = -0.0456 + 0.00179X - 1.25 \times 10^{-6} \times X^2 \quad (4.12d)$$

$$\text{where } X = (V_*^2)$$

In Figure 4.23(c), it is clearly shown that there is a deviation from the power law relation for  $V_* \leq 7.0$  cm/sec. This situation occurs at the final stage of breach process.

#### x. Variation of Sediment Concentration

The ratio  $Q_s/Q_w$  can also be termed as the sediment concentration. By plotting  $Q_s/Q_w$  with non-dimensional variation in water surface level between upstream reservoir level and downstream end of the embankment  $\Delta H$ , is shown in Figure 4.23(d). Sediment concentration is high during the initial phase of the erosion and gradually reduces with decrease in  $\Delta H/H_D$  values. The maximum concentration reaches around ten percent (10%), which is considered to be hyper concentrated level. The magnitude of hyper-concentration is 8 percent and above. The concentration study involves for the whole breach section. The relation obtained through regression analysis is as follows:

$$\frac{Q_s}{Q_w} = -0.0051 + 0.145X - 0.38X^2 + 0.345X^3 \quad (4.12e)$$

$$\text{Here } X = \frac{\Delta H}{H_D}$$

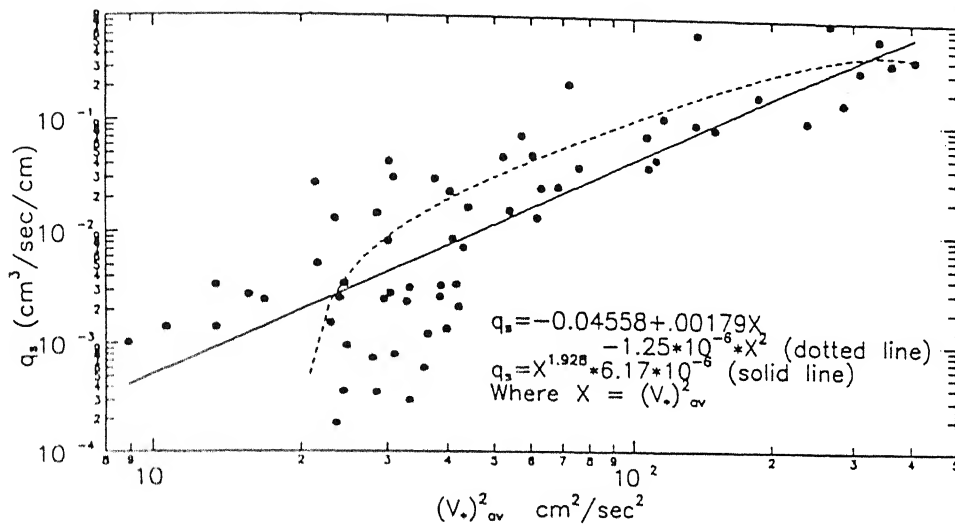


Fig. 4.23(c): Variation of sediment discharge intensity, ( $q_s$ ) with square of the average shear velocity ( $V_*^2$ )

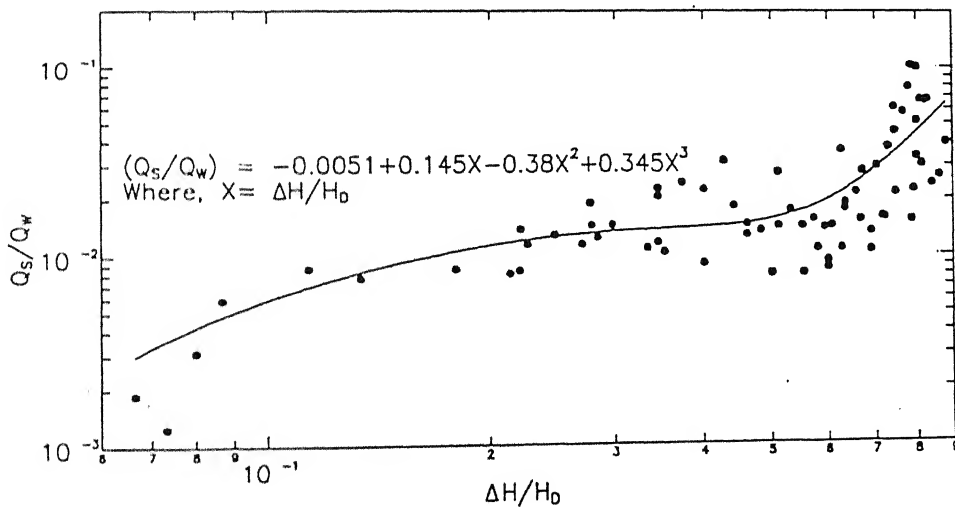


Fig. 4.23(d): Variation of sediment concentration with drop in water level  $\Delta H$



### xi. Sediment Load Computation

The product of  $q_s$  with bulk density of sediment ( $\gamma_b$ ) of the embankment soil is considered as the sediment load. It is non-dimensionalised with  $\gamma_s$ ,  $d_{50}$  and  $V_{SR}$ , where  $\gamma_s$  = unit weight of sediment,  $d_{50}$  = median size of particle,  $V_{SR}$  = sediment resisting velocity, defined as:

$$V_{SR} = \sqrt{\left( \frac{\Delta\rho_w}{\rho_w} * d_{50} * \tan\varphi + \left( \frac{c}{\rho_w} \right) \right)} \quad (4.12f)$$

$$\text{where, } \frac{\Delta\rho_w}{\rho_w} = \left( \frac{\rho_s - \rho_w}{\rho_w} \right)$$

$\varphi$  = angle of repose

$c$  = cohesive stress, obtained from triaxial undrained shear test

$\rho_s$  = density of sediment particle

The dimensionless sediment load is plotted against non dimensional shear velocity,  $\bar{V}_*^2 / V_{SR}^2$  in Figure 4.24. The relation between them is obtained from regression analysis and is given as:

$$g_s^* = 0.0082 * \left( \frac{\bar{V}_*^2}{V_{SR}^2} \right)^{1.938} \quad (4.12g)$$

It can be observed that for smaller values of  $\bar{V}_*^2 / V_{SR}^2$ , there is a considerable scatter in the sediment load.

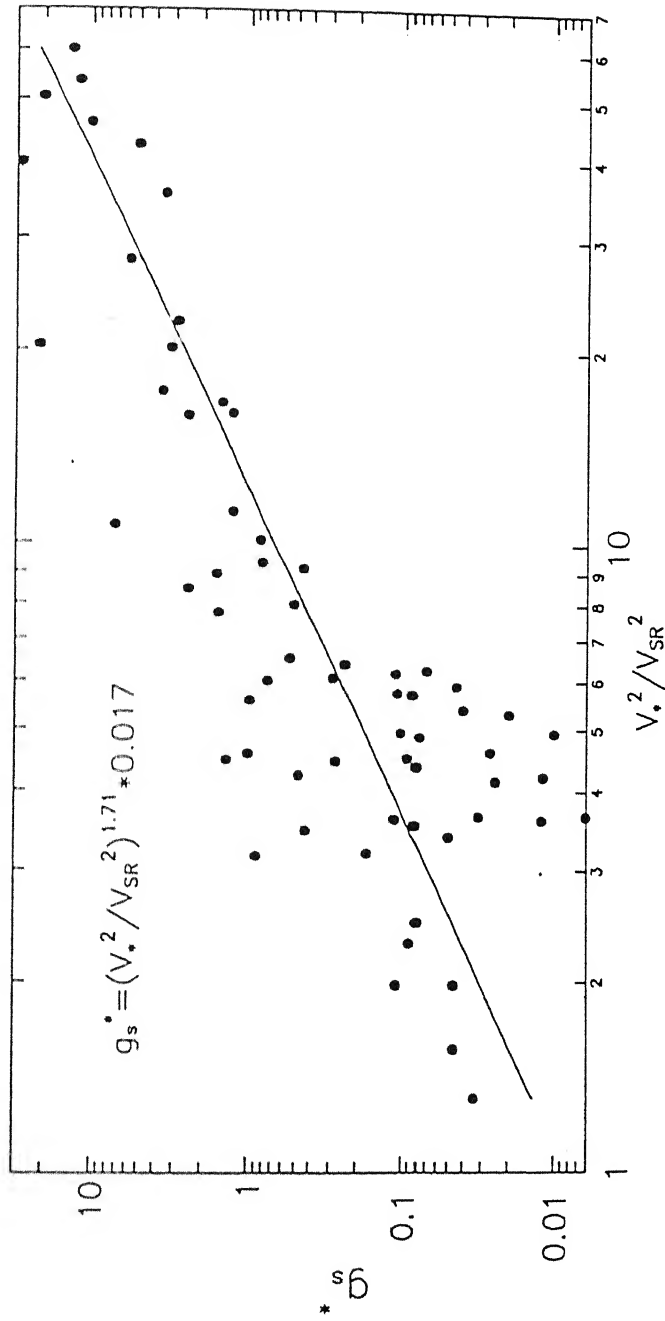


Fig. 4.24: Variation of sediment load with shear velocity in a nondimensional form

## 4.4 Analysis of Cohesive Soil Embankment

In the previous section, the analysis of cohesionless soil embankment has been reported. It may be noted that the variation of flow parameters, geometric parameters and sediment parameters are interrelated to bring an insight into the breach processes of cohesionless soil embankment. In the present section the analysis of cohesive soil embankment is carried out in the light of cohesionless soil approach.

The basic data comprises of variation of water level, variation of sediment bed level and the corresponding breach flow width at different time along the longitudinal section of the breach which are presented in Chapter III, Figures 3.4(a) to 3.4(m). These figures contain the data for the run number 0404 for the sections 1 to 8. Only water levels are presented for the sections 1, 2 and 3 which are in the reservoir, upstream of the embankment. For other sections all the three data are presented. Using these basic information further analysis on breach morphology, breach hydraulics and breach erosion are carried out.

### a. Breach Morphology

The variations of breach planform, bed and flow profiles along the flow in the breach and breach cross-sections are analysed.

#### i. Breach Planform Variations

During the breach erosion, it was observed that the crest of the erodible bed profile is moving from the downstream towards the upstream as the erosion progress. Also widening of breach section follows a particular pattern during the breach process. In order to study the variation of depth of flow at crest and its corresponding width variation during the breach process, four situations namely two situations before the occurrence of breach peak outflow ( $Q_{wp}$ ), one at the time of  $Q_{wp}$  and other after peak outflow are shown in the Figures 4.25(a), (b), (c), and (d) respectively. It may be observed that the position of crest is very near the upstream edge of the embankment. The width is contracting slowly from upstream to the downstream edge. As the discharge increases the crest moves upstream and reaches upstream face of the embankment before the attainment of peak flow. By the time peak flow is attained, the exposure of the hard bed occurred due to erosion. After the peak flow occurrence, width reduces upto the upstream top edge of the dam and remains fairly constant further onward.

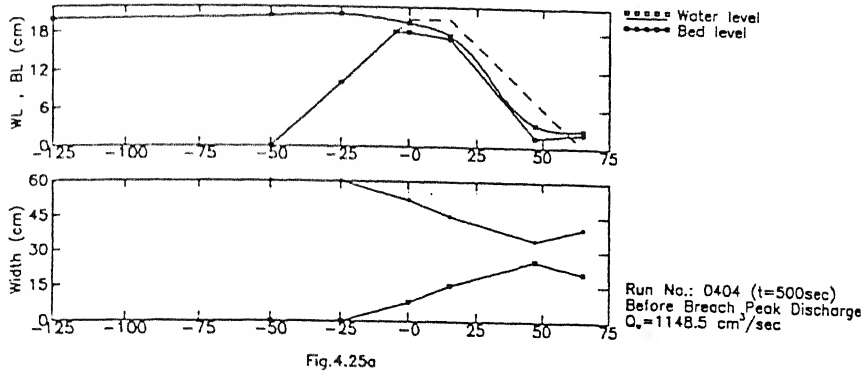


Fig. 4.25a

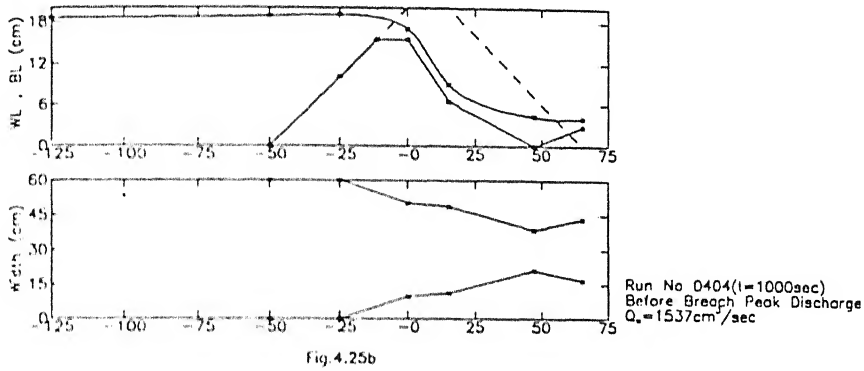


Fig. 4.25b

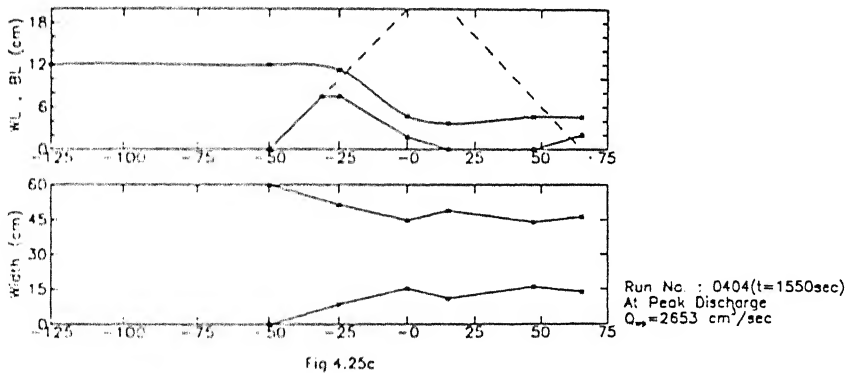


Fig. 4.25c

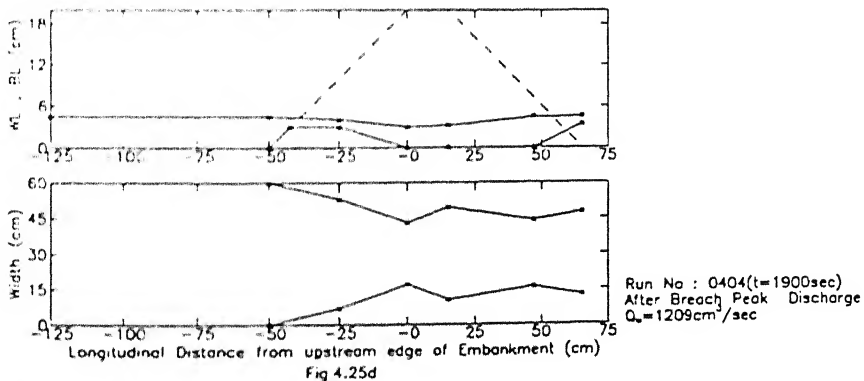


Fig. 4.25d

Figs. 4.25a, b, c and d: Variations of Water levels, sediment Bed Levels and Breach Width along the Longitudinal direction of Dam breach at different time for Cohesive Soil embankment model

The constriction of the width causes accelerated flow as indicated in Figures 4.25(a), (b), and (c).

## ii. Variations of Bed and Flow Profiles Along the Flow in the Breach

The variation of water level and width variation at sections, the downstream edge (section - 6) and section in between downstream edge and downstream end, denoted as section - 7 follows slightly different variation compared to other. Water level and bed level fall very rapidly in these two sections compared to other sections like sections 4, 5 and 6. This is due to steep erosion in the bed causing a valley like flow. This type of channel formation starts from downstream end as can be seen from the Figures 4.25(a), (b), (c), and (d) which indicates around 500 seconds at section - 7 and at 1000 seconds at section - 6 for the given run. The width variation at sections 6 and 7 is more like a rectangular section. At the *section - 5* width variation increases rapidly and later decreases gradually after the peak outflow discharge. The shape of the cross-section remains trapezoidal during the erosion process. Figures 4.25(a), (b) and (c) indicates free weir flow situation in which gradual drop in water surface is upto the crest and from the crest downstream the steep reduction of water surface profile occurs. Almost same water surface level between upstream and downstream indicate submerged weir type flow for Figure 4.25 (d). Slope of the downstream eroded sediment surface is steeper initially and as the breach process continues its magnitude decreases.

## iii. Breach Cross-Sectional Variation

The flow cross sectional profiles for sections 5, 6 and 7 are plotted for run no.0405 in the Figure 4.26. Here section 5 indicates section at upstream top edge of the embankment, section 6 is at downstream top edge of the embankment and section 7 is nearer to the downstream end of the embankment. Water surface level is shown with dotted line and solid line for the bed level. When time ( $t$ ) is equal to 500 seconds from start of overtopping of flow, cross sections at 5 and 6 are more or less trapezoidal in nature, but in section 7 it is almost like a rectangular narrow valley. At time ( $t$ ) equal to 1000 seconds, the cross sectional shape at section 5 continues as trapezoidal but at section 6 it becomes almost rectangular. This trend in variation in cross sectional shapes at sections 5, 6 and 7 continues at the time of peak flow and after peak flow as indicated for  $t = 1550$  seconds and  $t = 1900$  seconds respectively. It may be

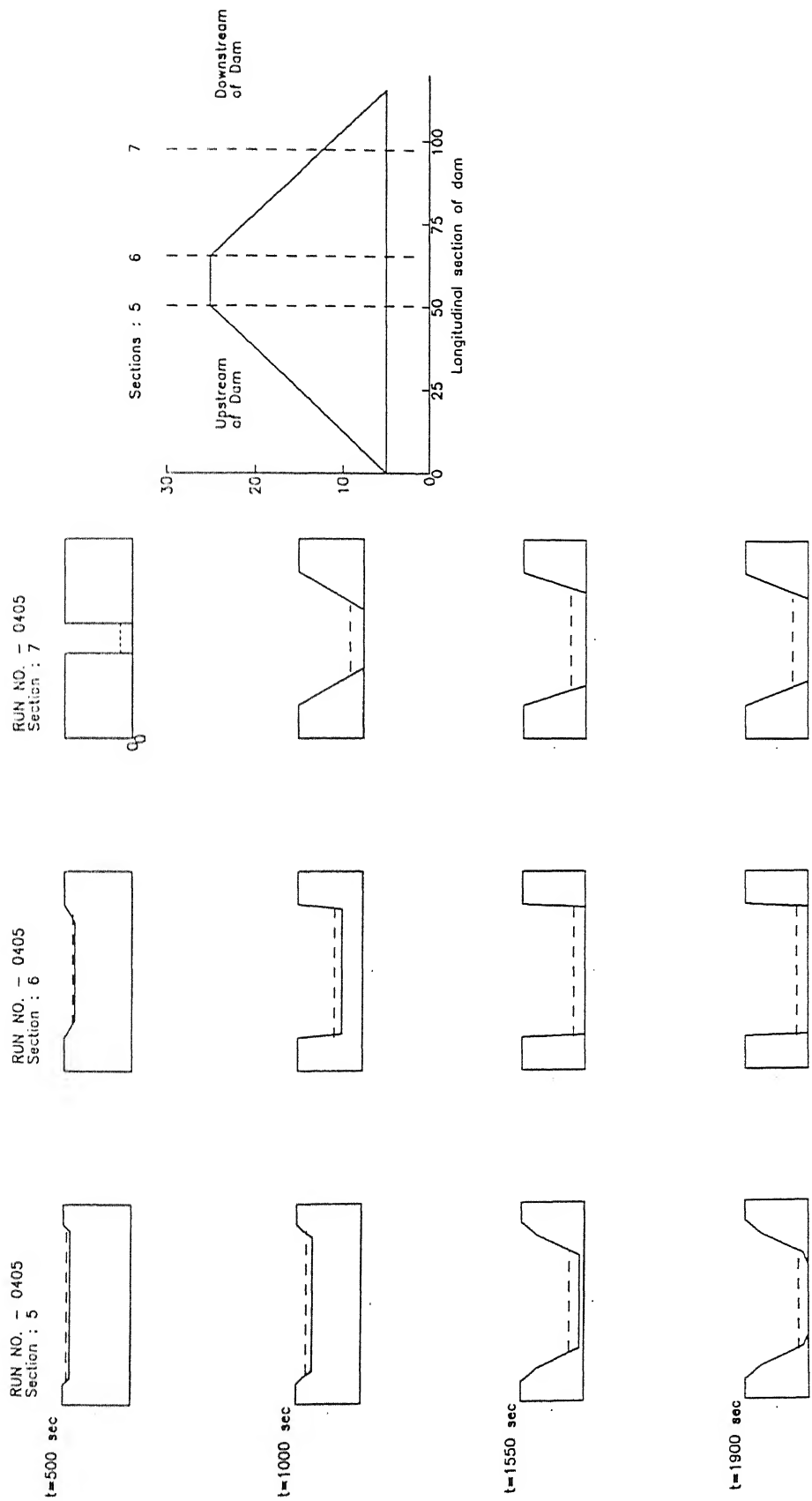


Fig. 4.26: Variation of eroded cross-sectional area of measuring sections--5,6 and 7 before, at and after breach peak discharge for dam model with cohesive soil for run no 1404

observed in the beginning of erosion that at the downstream end a narrow steep rectangular shape of cross-sectional erosion takes place but at the upstream end it is more like a trapezoidal shape of erosion. Later on as the erosion process continues, the widening of downstream section occurs and it becomes more like trapezoidal shape. However, in the upstream edge, section 5 the cross sectional shape remains almost same with a magnitude of side slope remaining constant. At the section 6 after initiation of breach, the cross sectional shape becomes more rectangular in shape.

### b. Breach Hydraulics

Computation of discharge over the breach section is carried out on the line of analysis of cohesionless embankment by plotting discharge intensity ( $q_w$ ) against head acting over the crest ( $h_u$ ) as shown in Figure 4.27(a). Using regression analysis, the relation between them is written as:

$$q_w = 5.45 \times h_u^{1.467} \quad (4.13a)$$

The exponent of  $h_u$  is nearly equal to the discharge over the spillway. There is a wide scatter observed in the relation. With this scatter in view,  $q_w$  is nondimensionalised with respect to head acting  $h_u$  as  $\frac{q_w}{\sqrt{2gh_u^3}} = \frac{2}{3} c_d$ , which is a function of discharge coefficient for weir flow, ( $c_d$ ). This is plotted against the ratio of depth of flow acting on the crest to the height of the crest from the bed level as indicated in Figure 4.27(b). It may be observed that  $q_w / (2gh_u)^{3/2}$  decreases with increase in the value of  $(h_u / h_{cm})$ . This decrease is rapid upto  $(h_u / h_{cm}) < 0.4$ . For higher values it remains fairly constant. As observed in the discharge analysis of cohesionless soil embankment, free weir flow occurs at the crest for  $(h_u / h_{cm}) \leq 0.4$ ; for higher values the flow becomes submerged weir flow and later on open channel flow. The steep drop in the values of  $q_w / (2gh_u)^{3/2}$  for  $(h_u / h_{cm}) < 0.4$  indicates the effect of crest erosion, even though discharge relationship behaves similar to weir flow. For the comparison of the variation of  $c_d$  with  $(h_u / h_{cm})$  the relationship obtained for cohesionless soil embankment is incorporated in the form of dotted line. Observing the scatter in the discharge relationship data, it was thought, a statistical representation of the deviation is needed. With this in view the statistical deviation from mean value is plotted against the frequency of

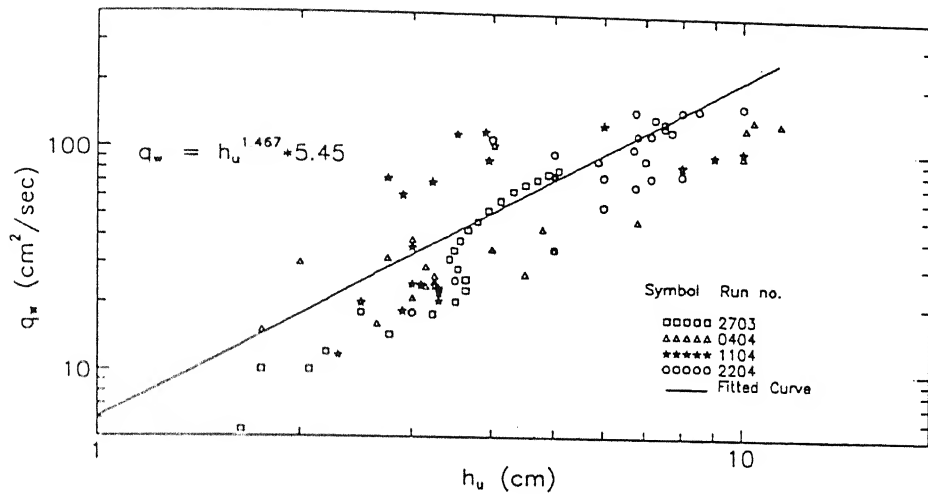


Fig. 4.27(a): Relationship between head of water ( $h_u$ ) over crest of erodible sediment bed with breach outflow discharge ( $Q_w$ )

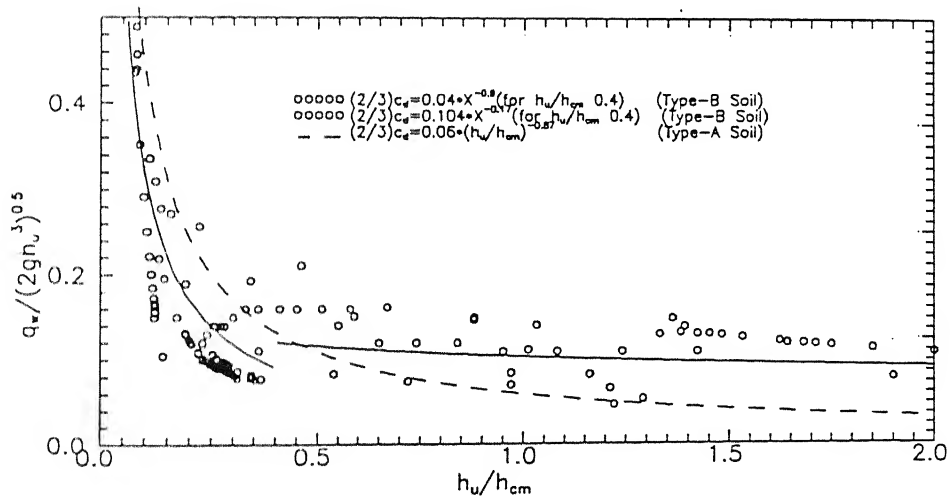


Fig. 4.27(b): Variation of discharge coefficient ( $c_d$ ) with the ratio of erodible crest to its height at any time of breach



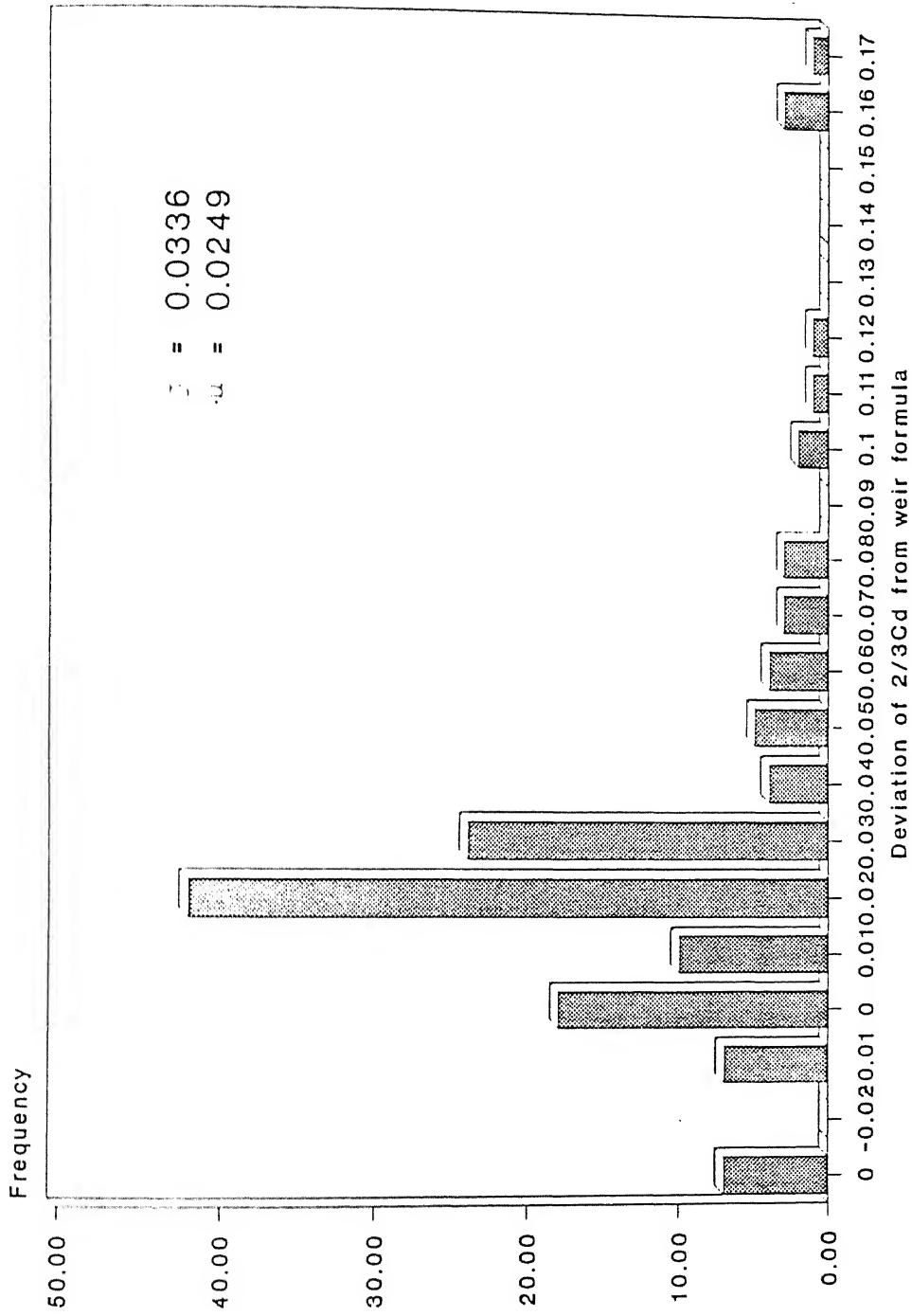


Fig. 4.27(c): Frequency of deviation of discharge coefficient from weir formula (Cohesive soil)

occurrence as shown in the Figure 4.27(c). The high frequency are observed around the deviation of the magnitude of  $\pm 0.04$ , having two peaks.

### c. Breach Erosion

The variation of rate of crest height, width at crest, rate of width erosion and rate of cross sectional area at crest are presented for cohesive soil embankment breach.

#### i. Rate of Crest Variation ( $dh_{cm}/dt$ )

Rate of crest variation is represented as  $dh_{cm}/dt$ . It is nondimensionalised with upstream flow velocity,  $\sqrt{2gh_u}$  along with  $Q_{PSN}$ , and is plotted against  $t/t_{95}$  as shown in Figure 4.28(a). The relation between them is given by polynomial function as:

$$\xi_{11} = 9.8 \times 10^{-4} - 6.4 \times 10^{-3} \left( \frac{t}{t_{95}} \right) + 2.3 \times 10^{-4} \left( \frac{t}{t_{95}} \right)^2 \quad (4.14a)$$

$$\text{where } \xi_{11} = \left( (dh_{cm}/dt) / \sqrt{2gh_u} \right) / (Q_{PSN})^{1.2}$$

It can be seen from Figure 4.28(a) that there is a steep reduction in the rate of crest erosion towards the end of breach process.

Rate of crest variation is also related with drop in water level between upstream and downstream of embankment ( $\Delta H$ ). The nondimensionalised rate of crest erosion  $\left[ (dh_{cm}/dt) / \sqrt{2gh_u} \right] / (Q_{PSN})^{1.2}$  is plotted against nondimensional drop in water levels  $\Delta H / H_D$  as shown in Figure 4.28(b). The functional relation among them can be written as:

$$\xi_{11} = \left( \frac{\Delta H}{H_D} \right)^{0.57} \times 0.00879 \quad (\text{Power law relation}) \quad (4.14c)$$

$$\xi_{11} = 7.86 \times 10^{-4} + 0.02035 \left( \frac{\Delta H}{H_D} \right) - 0.015 \left( \frac{\Delta H}{H_D} \right)^{2.0} \quad (\text{Polynomial functional Relation})$$

Two curves, one from power law relation and another from polynomial fit are obtained. The polynomial functional relation appears to be better representation of the data. From Figure 4.28(a) and (b) the rate of variation of crest height of sediment bed can be obtained in any time during the breach for the corresponding drop in water level ( $\Delta H$ ).

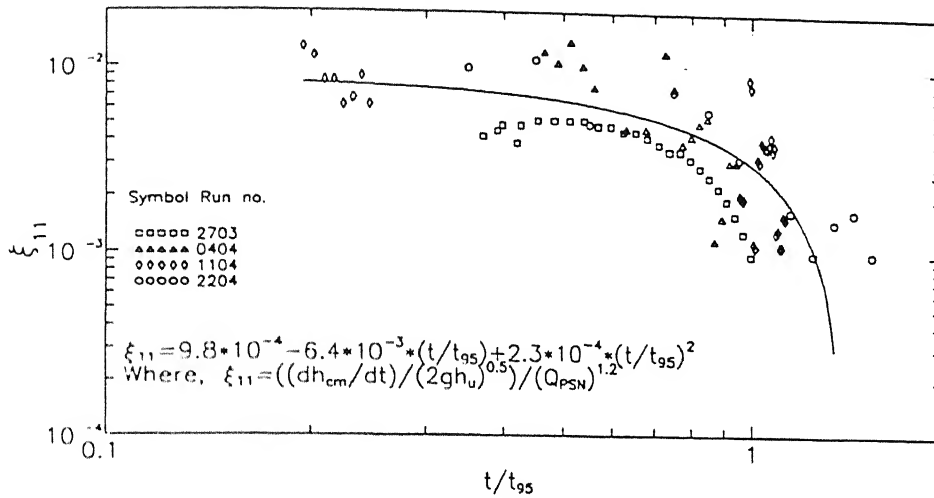


Fig. 4.28(a): Variation of rate of crest height with time in a nondimensional form

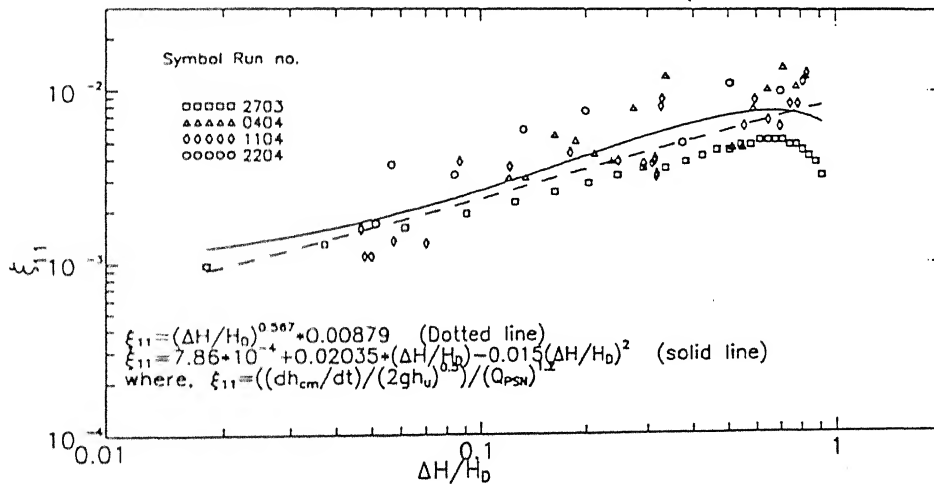


Fig. 4.28(b): Variation of crest height with drop in water level between upstream and downstream of the dam,  $\Delta H$  in a nondimensional form

## ii. Variation of Crest Width

Qualitative description on the variation of crest width is described under the breach morphology section. It is necessary to know quantitative variation of width at the crest position also. Breach width at crest ( $B_{cr}$ ) is nondimensionalised with height of the embankment ( $H_D$ ) and is plotted against the drop of water level at the crest which is also nondimensionalised with  $H_D$ . It may be observed that the breach width attains its maximum, almost equal to the 1.9 times  $H_D$  and decreases linearly with the drop in water level crest. This observation can be seen in the Figure 4.29(a). The functional relation among them is,

$$\frac{B_{cr}}{H_D} = 1.896 - 0.058X \quad (4.15a)$$

Where  $X = (\text{Drop of water level with respect to } H_D) / H_D$

The relation between the breach width ( $B_{cr}$ ) at the crest (section 5) and the breach width ( $B_7$ ) at section 7 located near the downstream end of the embankment are studied. The breach width ratio ( $B_7 / B_{cr}$ ) is plotted with  $t/t_{95}$  in Figure 4.29(b). The functional relation among them is obtained from regression analysis as:

$$\left( \frac{B_7}{B_{cr}} \right) \left( \frac{Q_{wp}}{\sqrt{gH_D^3}} \right)^{0.44} = 0.112 - 26.02X + 17992.9X^2 - 1979090X^3 + 6408 \times 10^7 X^4 \quad (4.15b)$$

$$\text{where } X = \frac{t}{t_{95}} \left( \frac{Q_{wp}}{\sqrt{gH_D^3}} \right)^{1.61}$$

During initial phase of erosion, ( $B_7 / B_{cr}$ ) is small, as erosion continues this ratio of width attains high value (0.3) at  $X = 0.07$  and there after remain constant. This can also be observed in Figures 4.25(a), (b), (c) and (d).

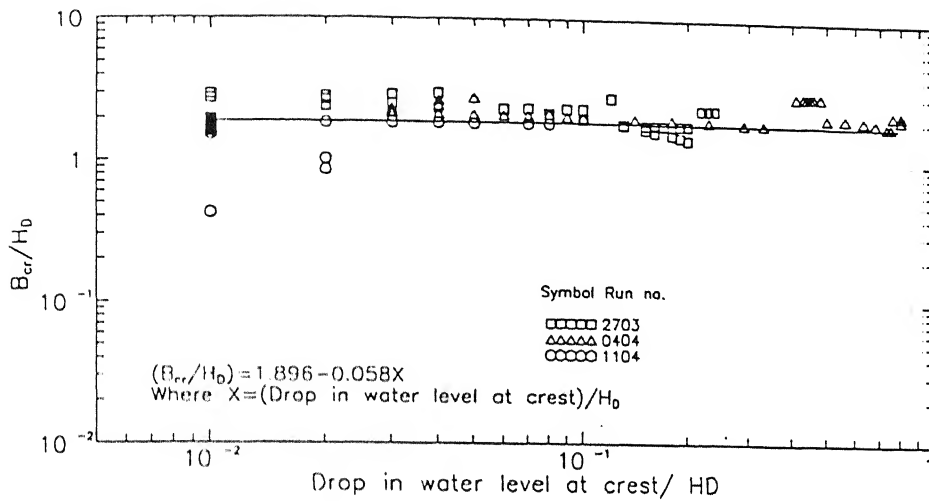


Fig. 4.29(a): Variation of the ratio of crest width to height of dam with nondimensional drop of water at crest

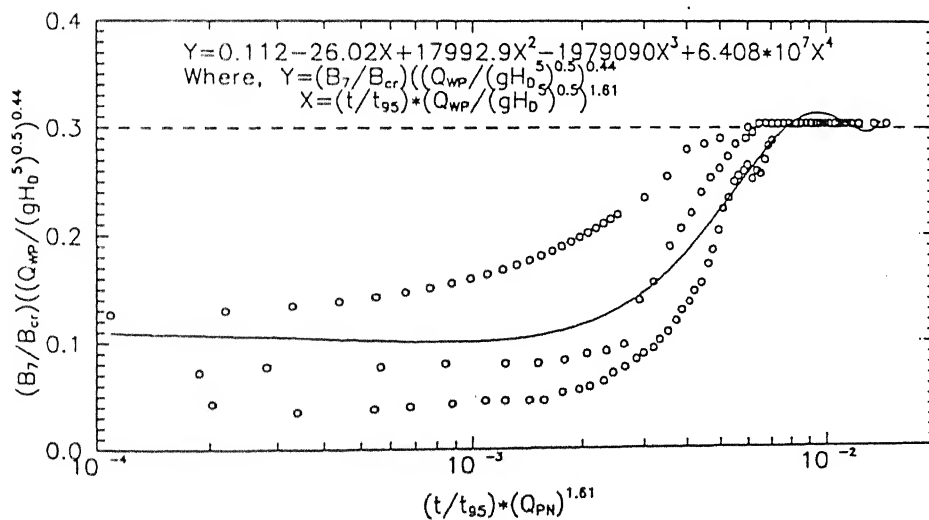


Fig. 4.29(b): Relative variation of breach crest width to breach width at section-7 with time in nondimensional form

### iii. Rate of Width Erosion of Cohesive Soil Embankment Model

The rate of width erosion at section 5, the upstream edge of the embankment top is analysed by plotting  $dB_{cr}/dt$  against time ( $t$ ) as shown in Figure 4.30(a). It may be observed that the rate of width erosion increases very steeply within a short period and remains fairly constant with magnitude zero throughout the breach process. This indicates that the dimension of the breach width attains maximum in the initial process of breach erosion and remains althrough constant during the remaining part of the breach erosion. Nondimensionalised rate of width of erosion is plotted against non-dimensionalised time,  $t/t_{95}$  as shown in Figure 4.30(b). The dimensionless rate of width erosion as shown in Figure 4.30(b) attains peak very soon after initiation of the breach process and remains zero althrough. It is found in the breach process that there are few cases of sudden fluctuation in rate of breach width erosion. This may be due to collapse of the banks.

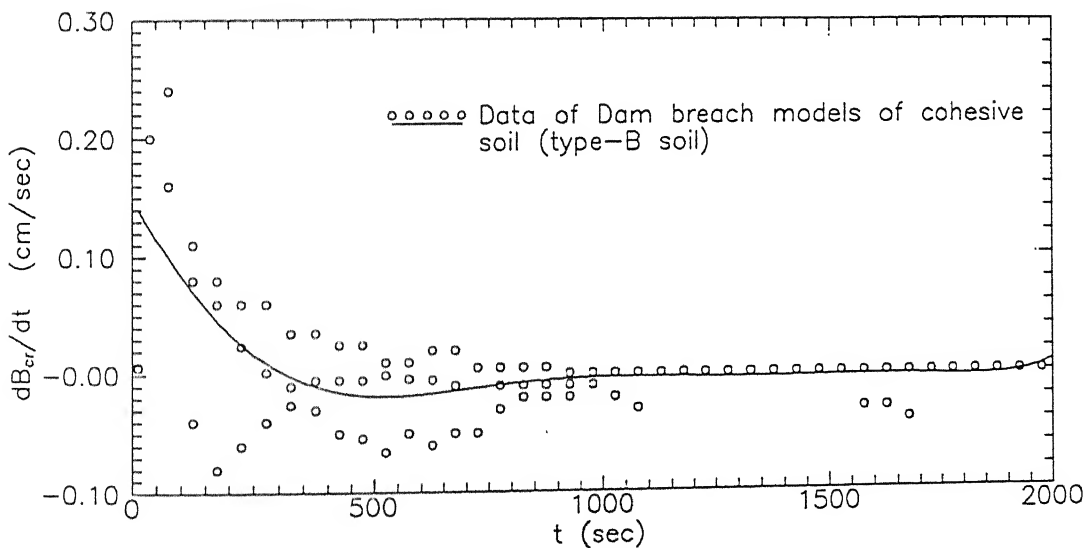


Fig. 4.30(a): Variation of rate of width erosion at crest for dam model of cohesive soil with time

#### iv. Rate of Variation of Cross-Sectional Area at Crest ( $A_{cr}$ )

In the last subsection the rate of depth and width erosion at crest are analysed. Taking together, the depth and width of erosion into account, the rate of variation of eroded crest cross-sectional area is analysed with drop in water level between the upstream and downstream of the dam. This is carried out in nondimensional way as shown in Figure 4.31. The functional relation among them is as follows.

$$\xi_{22} = 0.00196 - 0.01366X + 0.0419X^2 - 0.03657X^3 + 0.0066X^4 \quad (4.16)$$

$$\text{where } \xi_{22} = ((d\sqrt{A_{cr}} / dt) / \sqrt{2gh_u}) / (Q_{PSN})^{0.54} \quad \text{and } X = \Delta H/H_D$$

It may be observed that the rate of erosion of crest cross-sectional area increases and attains a peak near  $\Delta H/H_D \cong 0.7$  and then decreases upto  $\Delta H/H_D \cong 0.3$ . Before discussing the combined analysis of breach process for the embankments consisting of cohesionless and cohesive soil separately, the variation of the variables like head acting over the crest ( $h_u$ ), height of crest ( $h_{cm}$ ), width of crest ( $B_{cr}$ ), the rate of erosion of crest and rate of width erosion at crest are presented for both cohesionless and cohesive soil dam model together for comparison.

#### d. Comparative Study Between Cohesionless and Cohesive Soil Embankment Breach Observations

The presence of cohesion in the soil adds more resistance to the erosion. This increase in resistance causes the decrease in the rate of crest erosion and rate of width erosion compared to cohesionless soil. With this observation, the head acting over the crest ( $h_u$ ), height of crest ( $h_{cm}$ ) and width of crest ( $B_{cr}$ ) are nondimensionalised with height of the dam ( $H_D$ ) and plotted against  $t/t_{95}$  as shown in Figures 4.32(a), (b) and (c), respectively where  $t$  is time at any instant from the beginning of the erosion and  $t_{95}$  is the time by which 95% of the breach erosion has taken place. These data are chosen for nearly same height of the embankment dam, however, there is variation in the magnitude of inflow to the reservoir. Still these plots give a qualitative comparison in behaviour of breach process with cohesive and cohesionless soil embankment dam models.

The Figure 4.32(a) indicates the variation of  $h_{cm}/H_D$  with  $t/t_{95}$  for the embankment models built using cohesionless soil (type-A soil) and cohesive soil (type-B soil). The  $h_{cm}/H_D$  for cohesionless soil decreases from start of the overtopping of the flow, whereas in cohesive

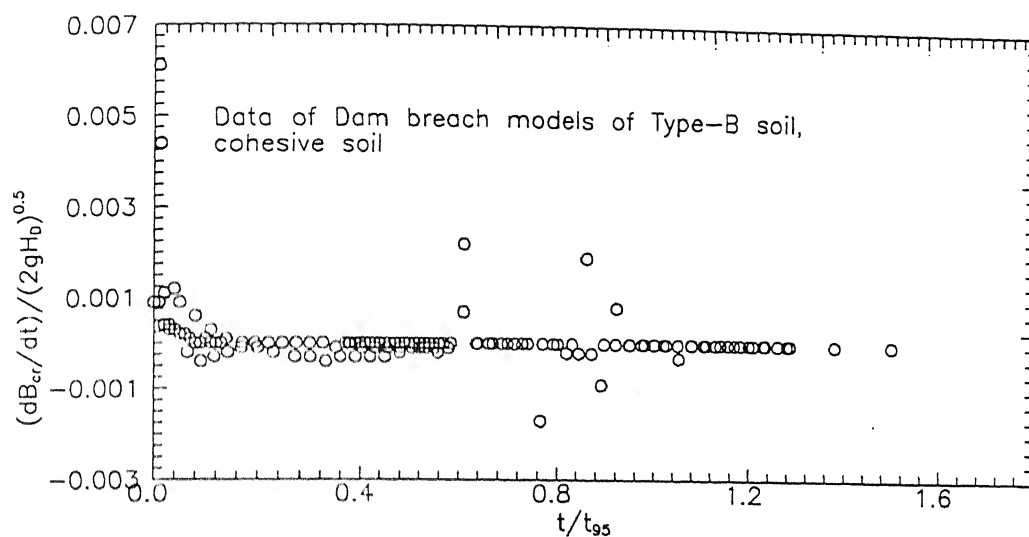


Fig. 4.30(b): Variation of nondimensional rate of breach width with nondimensional time for cohesive soil embankment dam

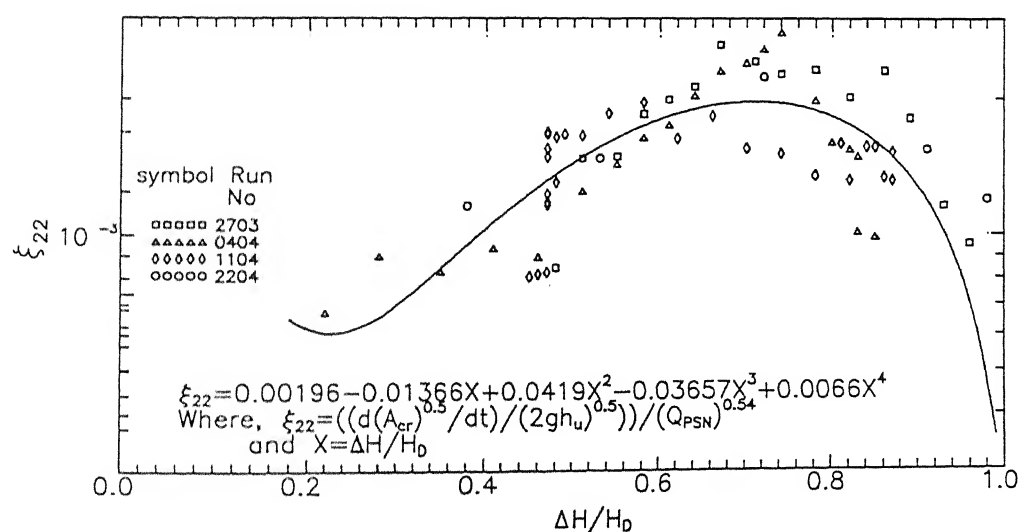


Fig. 4.31: Variation of nondimensional eroded crest area ( $A_{er}$ ) with nondimensional drop in water level ( $\Delta H/H_0$ ) between upstream and downstream of the dam.



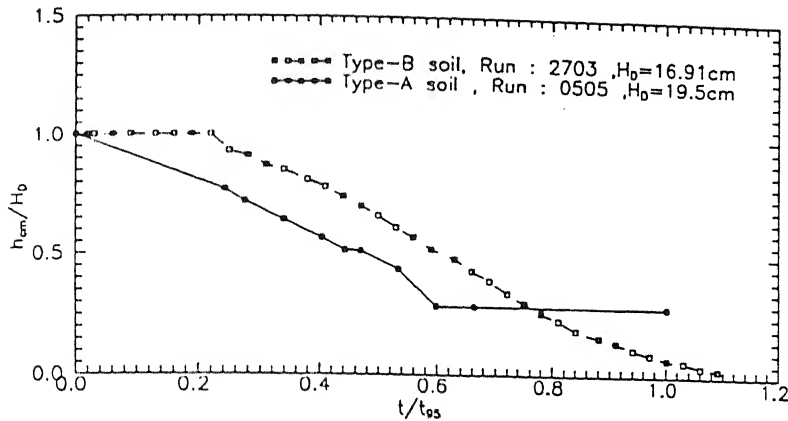


Fig. 4.32(a): Comparison of the variations of crest level of erodible sediment bed for the breach model of cohesive and cohesionless soil embankment dams

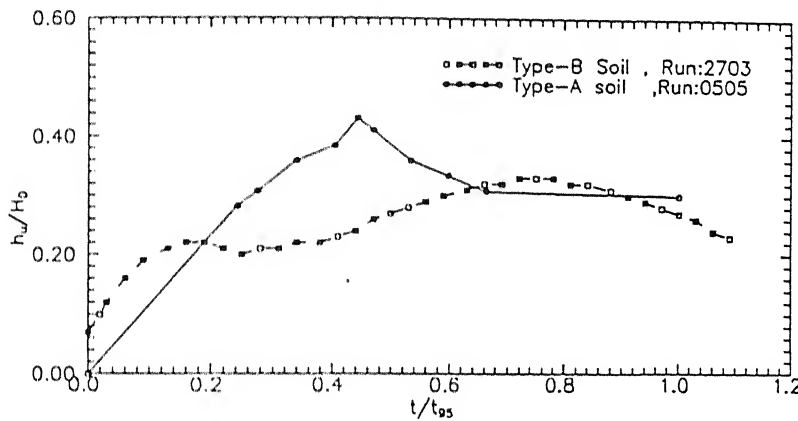


Fig. 4.32(b): Comparison of the variations of head of water level over the crest of erodible sediment bed for breach model of cohesionless and cohesive soil

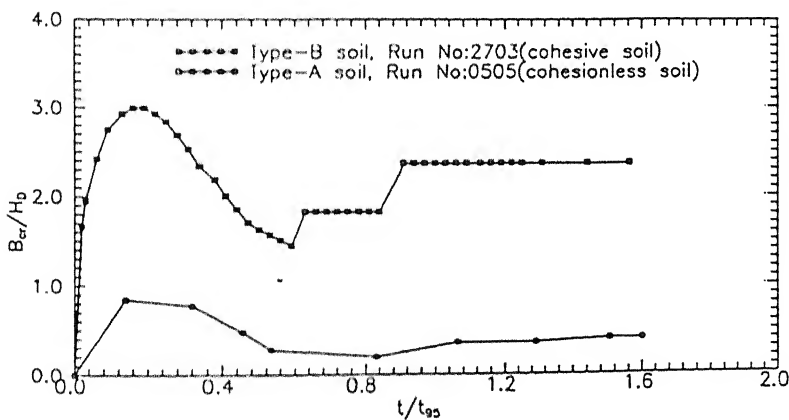


Fig. 4.32(c): Comparison of the variations of crest width of erodible sediment bed for the dam breach model of cohesionless and cohesive soil embankment dams

soil it starts slightly later. However, their decreasing relation as observed is fairly parallel to each other indicating the crest erosion is similar in nature.

The variations of the head acting over crest ( $h_u$ ) for both the soil are shown in Figure 4.32(b). The maximum magnitude of  $h_u/H_D$  occurs in early phase of the breaching for cohesionless soil (type-A soil) compared to cohesive soil (type-B soil) and also the magnitude of the peak values are different.

The comparison of width variation for both the soil is shown in the Figure 4.32(c). It may be observed that width enlarges faster initially, attains peak and starts decreasing then slowly increases and reaches constant as the end of the breach process approaches for cohesive soil (type-B soil). The increase crest width for cohesionless soil (type-A soil) occurs during  $t/t_{95} < 0.15$ , reaches a peak with a magnitude of  $B_c/H_D = 0.8$ , then decreases with increase in  $t/t_{95}$  upto 0.55 and remains fairly constant thereafter. The magnitude of peak of the breach width for cohesive soil is of the order of three times  $H_D$ , whereas in the case of cohesionless soil it is of the order of  $H_D$  for this particular chosen run. The sudden rise in the width in case of cohesive soil is an indication of collapse of the bank at that time. In the computation of the sediment volume eroded at any instant of time the average of width at that instant is considered, not the abrupt deviation in this value because it was very difficult to take into account the bank collapse and its erosion at any instant of time.

The rate of erosion of the crest height and the width are non-dimensionalised with  $H_D$  and are plotted in the Figures 4.33(a), (b) respectively. The magnitude of the non-dimensional crest erosion for cohesionless soil is much higher compared to its corresponding value for cohesive soil. The values of  $t/t_{95}$  for peak rate of crest erosion are almost equal for both cohesive and cohesionless soil. The magnitude of non-dimensional rate of crest erosion for cohesionless soil is of the order of 0.012 whereas for cohesive soil is of the order of 0.00008.

The variation of the rate of crest width indicates that most of the erosion occurs in the initial period of the breach in case of cohesionless soil (type-A soil), whereas in cohesive soil (type-B soil) it occurs in the later stages of the breach. The magnitude of its peak for cohesionless soil is of the order of  $\cong 0.00013$ , whereas for cohesive soil it is  $\cong 0.0044$ .

It may be summarised that the magnitude of the rate of erosion of crest height and crest width is higher in cohesionless soil compared to cohesive soil embankment breach. This is due to extra resistance offered by cohesion in cohesive soil.

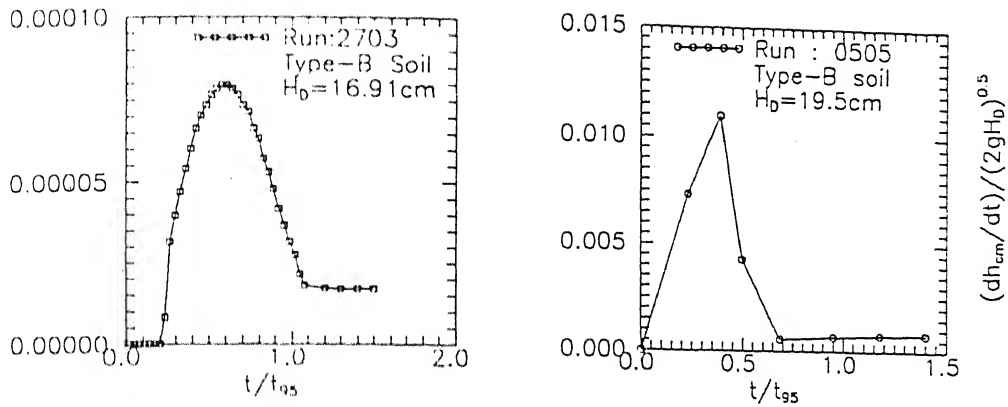


Fig. 4.33(a): Comparison of the rate of variations of crest height of erodible sediment bed for the dam breach model of cohesionless (type-A) and cohesive (type-B) soil

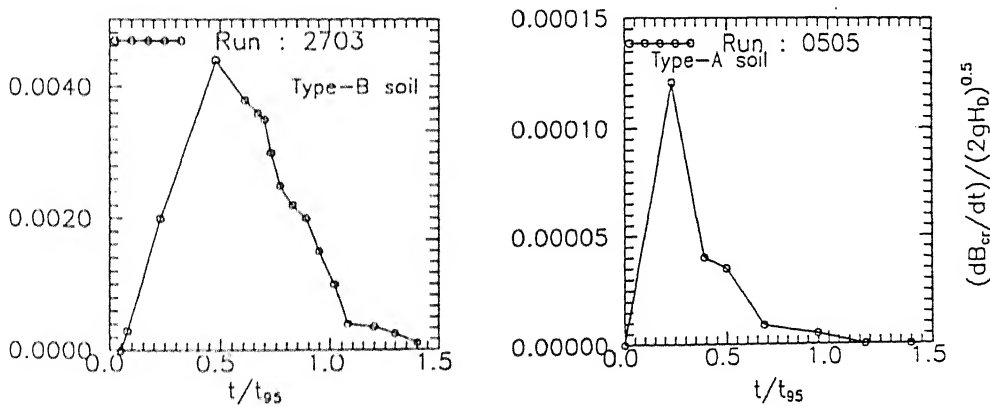


Fig. 4.33(b): Comparison of the rate of variations of crest width of erodible sediment bed for the dam breach model of cohesionless (type-A) and cohesive soil (type-B)

## 4.5 Analysis of Breach Process for Cohesive and Cohesionless Soil Embankments

In the section 4.4d, comparison of the breach process was carried out for cohesionless and cohesive soil embankments. In the present section it is planned to analyse the combined data taking soil properties into consideration. In this section the analysis contain variation of water surface ( $h_{wr}$ ) in the reservoir, head acting on the crest ( $h_u$ ) and crest height ( $h_{cm}$ ), energy variation ( $\Delta E$ ), sediment concentration ( $Q_s/Q_w$ ) and sediment load( $g_s$ ) along with time scales. After this, the final values of breach width, final depth of breach erosion, duration of breach are analysed. The occurrence of peak outflow discharge ( $Q_{wp}$ ) and its corresponding time ( $t_{wp}$ ) are also analysed. From this combined analysis it is hoped to evolve a general method of prediction and evaluation of the breach process.

### a. Variation of Water Surface in the Reservoir ( $h_{wr}$ )

Water surface level measured at a section 75 centimeters upstream of the embankment is plotted against time taken in the form  $(t-t_*)/(t_{95}-t_*)$ , where  $t_*$  is the time at which maximum water level ( $h_{wrm}$ ) in the reservoir occurred during the breach process. The ratio of  $h_{wr}/h_{wrm}$  is plotted against  $(t-t_*)/(t_{95}-t_*)$  as shown in the Figure 4.34(a). It may be seen that the gradual reduction in water level as the duration of the breach process increases. In the final stage of erosion the water level in the reservoir attains certain magnitude after which the reduction in the reservoir level is almost negligible. This variation is mainly due to the intensity of inflow discharge ( $Q_{in}$ ) to the reservoir. If  $Q_{in}$  is large the erosion in the breach is higher and final stage of water in the reservoir is lower. This variation can be seen in Figure 4.34(a) for both the embankment breach processes. As is obvious from the Figure 4.34(a) there is wide distribution in  $h_{wr}/h_{wrm}$  with  $(t-t_*)/(t_{95}-t_*)$ . In order to fit a single curve to these scattered points, the modification of X-axis is considered. The value on X-axis ( $\beta$ ) for  $h_w/h_{wrm} = 0.7$  is read and subjected to regression analysis. From regression analysis the

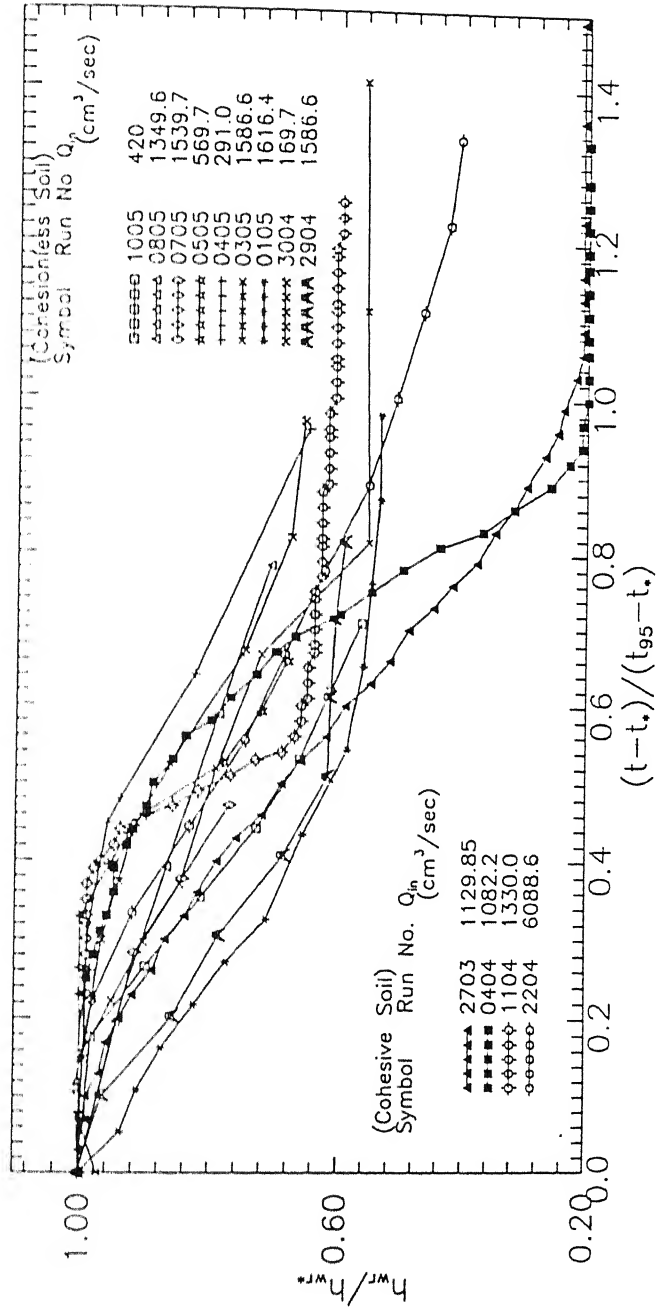


Fig. 4.34(a): Variation of normalised reservoir water level ( $h_{wr}$ ) by its maximum value with normalised time

relation between  $X$  intercept for  $h_w/h_{wrm} = 0.7$  is correlated with  $V_{SRN}^{0.514}$  and  $Q_{PSN}^{-0.514}$  as:

$$\beta = 2.037\lambda \quad (4.17a)$$

$$\text{where, } \lambda = (V_{SRN} / Q_{PSN})^{0.514}$$

This relation is shown in Figure 4.34(b). Time scale  $t_*$ , time at which maximum value of  $h_{wr}$  occurs from the start of the flow overtopping, is nondimensionalised with soil resisting velocity ( $V_{SR}$ ) and plotted against  $Q_{APN}$  number as shown in Figure 4.34(c). Polynomial functional relation is obtained from regression analysis and is written as :

$$Y = 119503 + 3.04 \times 10^7 X - 1.02 \times 10^8 X^2 \quad (4.17b)$$

$$\text{Where } Y = \frac{(t_{95} - t_*)g}{V_{SR}}$$

$$\text{and } X = \frac{Q_{WP}}{A_D \sqrt{gH_D}} = Q_{APN}$$

Using results of Figures 4.34(b) and 4.34(c), the results presented in Figure 4.34(a) are replotted as  $(h_w/h_{wrm})$  against  $\left(\frac{t - t_*}{t_{95} - t_*}\right) \left(\frac{Q_{PSN}}{V_{SRN}}\right)^{0.514}$  in the Figure 4.34(d). The relation shown in Figure 4.34(d) shows a fairly good agreement and is represented in polynomial functional form as:

$$\frac{h_w}{h_{wrm}} = 1.0 - 0.0289\alpha - 0.084\alpha^2 + 0.01\alpha^3 \quad (4.17c)$$

$$\text{Where, } \alpha = \frac{(t - t_*)}{(t_{95} - t_*)} \times \left(\frac{Q_{PSN}}{V_{SRN}}\right)^{0.514}$$

## b. Variation of Reservoir Water Level in relation to Downstream Water Level

$\Delta H$  is the difference in water level upstream of the embankment, in the reservoir and the downstream end of the breach channel. The variation of this quantity is non-dimensionalised with its maximum value, denoted as  $\Delta H_*$  and is plotted against  $(t - t_{**}) / (t_{95} - t_{**})$  as shown in Figure 4.35(a) for all the runs, where  $t_{**}$  corresponds to the time of occurrence of  $\Delta H_*$ . It may be observed that as the breach process continues the magnitude of  $\Delta H$  decreases and reaches almost 0.1 at final stage. The values of X-axis ( $\Omega$ ) in Figure 4.35(a) are obtained with intercept

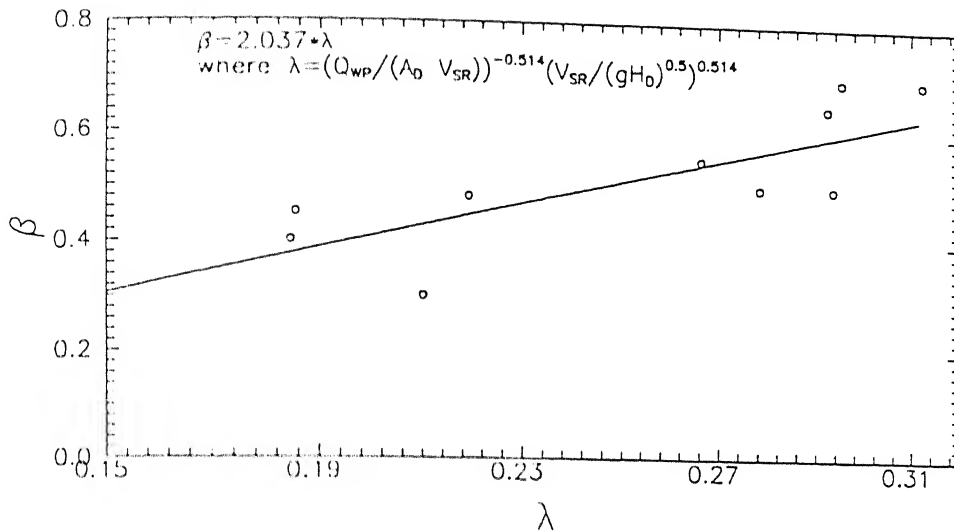


Fig. 4.34(b): Variation of  $\beta$ , the X-intercept at  $y=0.7$  in the fig. 4.34a for different runs of experiments on dam breach model of cohesive and cohesionless soil with  $\lambda$ , a function of peak outflow discharge, soil resisting velocity and the height of dam

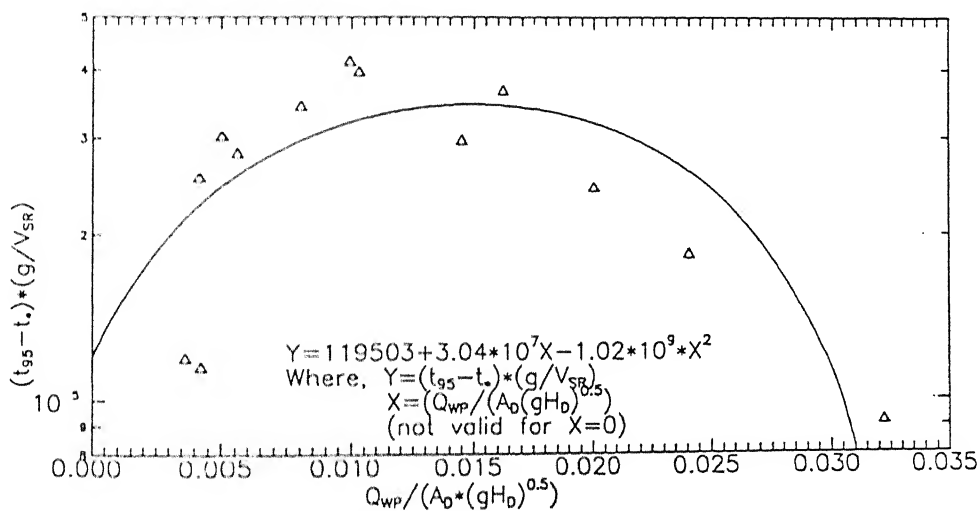


Fig. 4.34(c): Variation of reservoir time scale ( $t_*$ ) with peak breach outflow discharge, height of the dam and its cross sectional area.

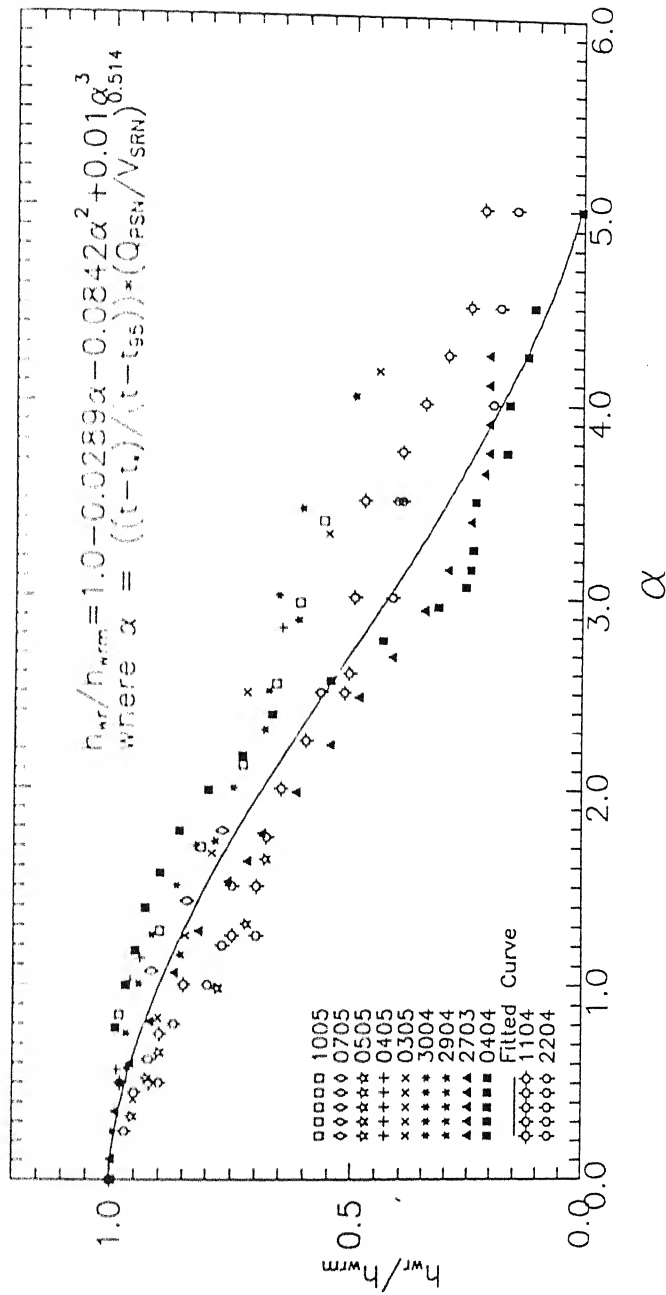


Fig. 4.34(d): Variation of reservoir water level ( $h_{wr}$ ) with time in a nondimensional form along with  $V_{SRN}$  and  $Q_{PSN}$  numbers



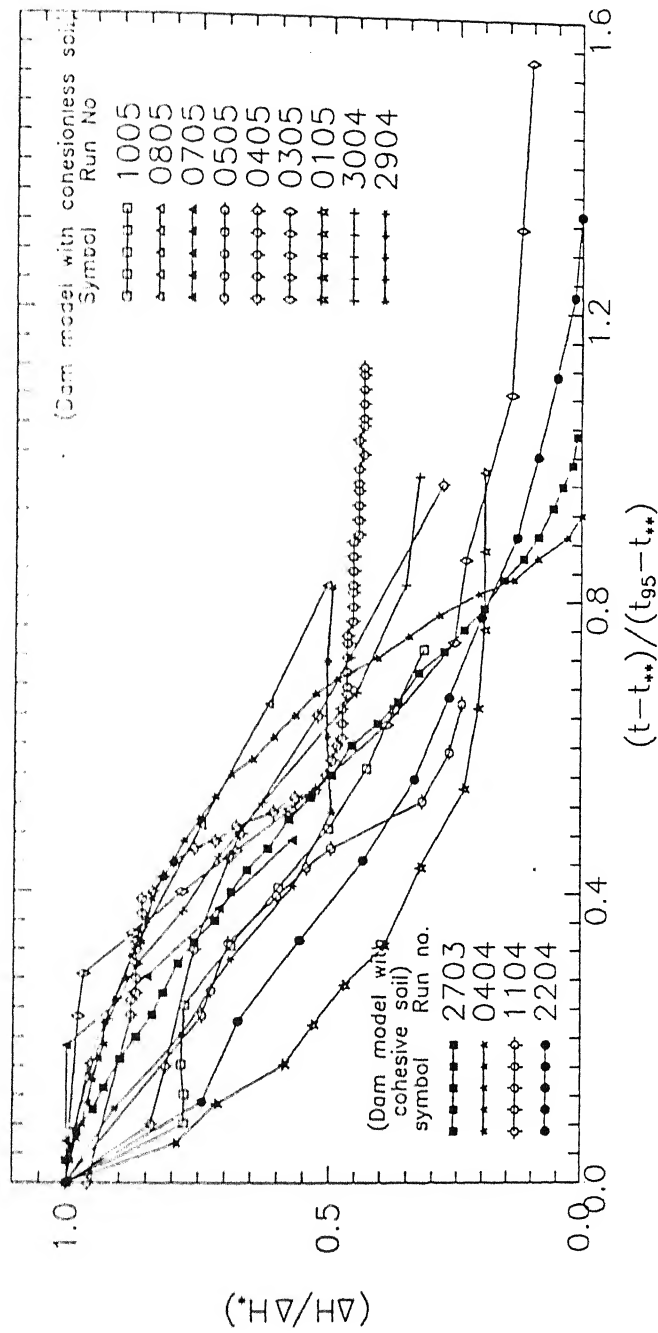


Fig. 4.35(a): Variation of normalised water level difference ( $\Delta H$ ) between upstream and downstream of the dam model with time in nondimensional form

of  $y$ -axis  $\cong 0.7$ , in Figure 4.35(a). This intercept is analysed further. It may be observed that the intercept varies with  $Q_{PSN}$  and  $V_{SRN}$  number as indicated in the Figure 4.35(b). The relation of  $\Omega$  with  $Q_{PSN}$  and  $V_{SRN}$  obtained from regression analysis is as follows:

$$\Omega = 2.02K^{0.489} \quad (4.18a)$$

$$K = [Q_{PSN}^{-0.67} \times V_{SRN}]$$

The reservoir drop time scale,  $t_{..}$ , corresponding to the maximum difference of water level,  $(\Delta H_*)$ , between upstream and downstream of the dam is plotted in the form  $\frac{(t_{95} - t_{..})g}{V_{SR}}$  against  $Q_{APN}$  number as shown in Figure 4.35(c). The functional relation between them in the form of quadratic equation obtained from regression analysis may be written as:

$$Y = 84610.2 + 3.83 \times 10^7 X - 1.192 \times 10^9 X^2 \quad (4.18b)$$

$$\text{where } Y = \frac{(t_{95} - t_{..})g}{V_{SR}} \text{ and } X = \frac{Q_{WP}}{A_D \sqrt{gH_D}}$$

Using correlated parameters for  $X$ -axis from Figures 4.35(b) and (c) the data shown in Figure 4.35(a) is replaced as  $\frac{\Delta H}{\Delta H_*}$  against  $\left(\frac{t - t_{..}}{t_{95} - t_{..}}\right) \left(\frac{V_{SRN}}{Q_{PSN}^{0.67}}\right)^{0.469}$  in Figure 4.35(d). The agreement between the data and curve obtained from regression can be considered to be good. The relation between them is represented in polynomial functional form as:

$$\frac{\Delta H}{\Delta H_*} = 0.968 + 0.056\varepsilon - 0.17\varepsilon^2 + 0.026\varepsilon^3 \quad (4.18b)$$

$$\text{where, } \varepsilon = \left(\frac{t - t_{..}}{t_{95} - t_{..}}\right) * (Q_{PSN}^{-0.67} * V_{SRN})^{0.469}$$

### c. Variation of Crest Height

The magnitude of water flowing in the breach depends on the head acting over the crest ( $h_u$ ). Magnitude of  $h_u$  is the difference in water level in the reservoir and sediment bed level at crest. Variation of sediment bed level at the crest is important for further analysis. With this in view, crest level ( $h_{cm}$ ), is measured from bed of the flume to the crest level of the sediment bed, which is nondimensionalised with height of dam ( $H_D$ ) and plotted with  $(1 - (\Delta H / \Delta H_m))$

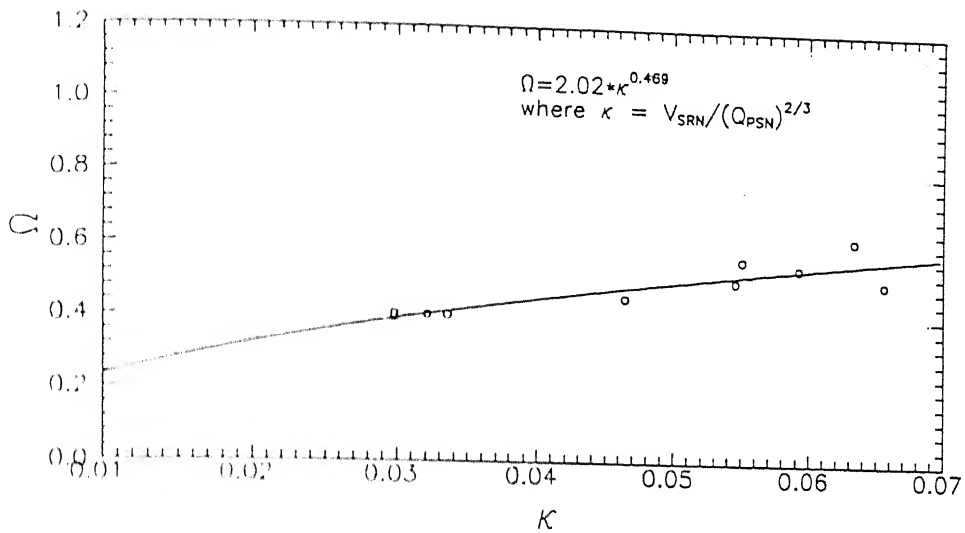


Fig. 4.35(b): Variation of  $\Omega$ , (x-intercept at  $y=0.7$  in the Fig. 4.35(a) with  $\kappa$

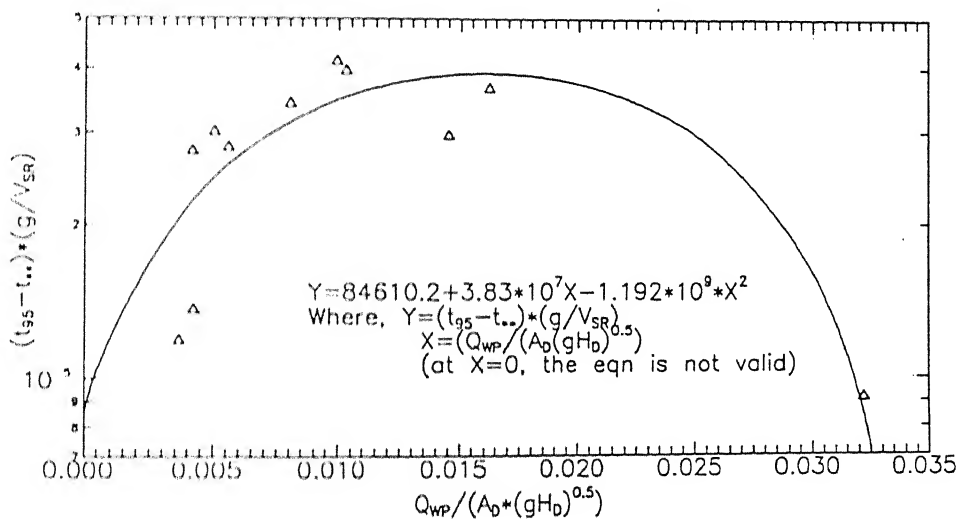


Fig. 4.35(c): Variation of reservoir drop time scale( $t_{**}$ ) with peak breach outflow discharge, height of the dam and its cross sectional area

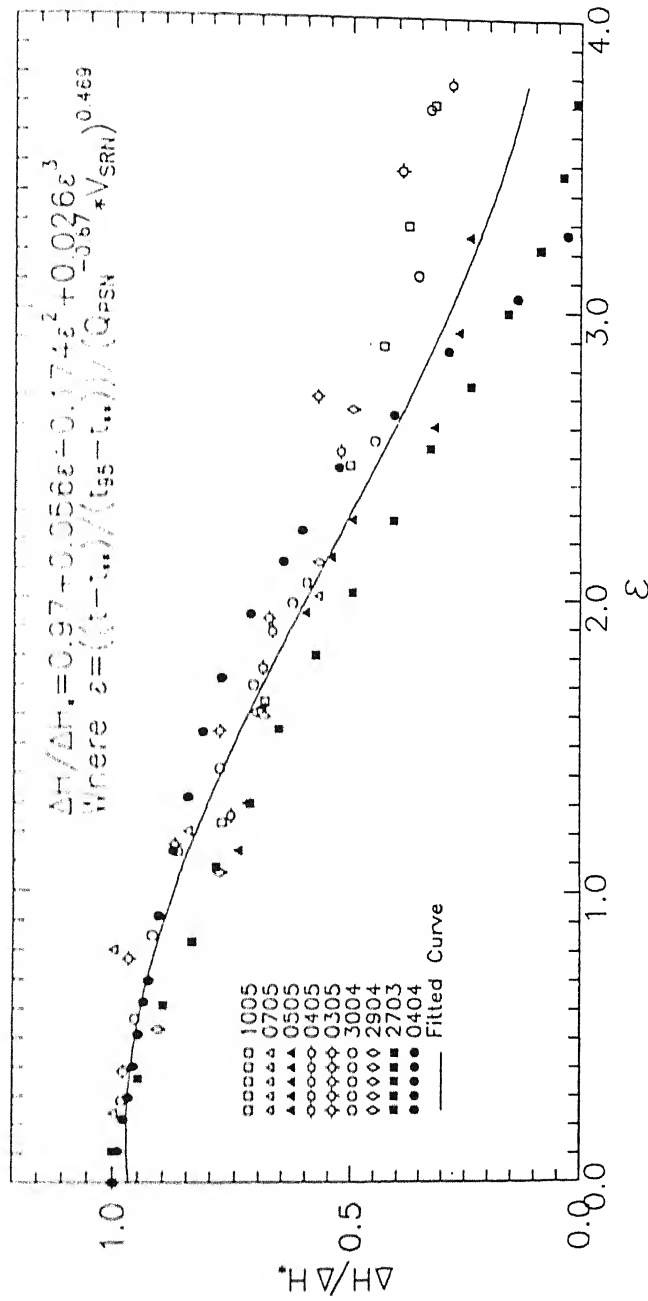


Fig. 4.35(d): Variation of water level difference ( $\Delta H$ ) between upstream and downstream of the dam with time in a nondimensional form along with  $Q_{PSN}$  and  $V_{SRN}$  numbers

along with  $Q_{PSN}$  as shown in Figure 4.36. Crest level decreases with increase in  $(1 - (\Delta H / \Delta H_m))$ . From the regression analysis, polynomial functional relation is obtained as:

$$\frac{h_{cm}}{H_D} = 0.91 - 16.65\chi + 190\chi^2 - 868.4\chi^3 \quad (4.19a)$$

$$\text{where, } \chi = \left(1 - \frac{\Delta H}{\Delta H_m}\right) * V_{SRN}^{0.6}$$

The scatter in the data about the mean curve obtained from regression analysis is high. It may be noted that the variation of  $h_{cm}/H_D$  for water level rising from overtopping level to the maximum level on the embankment is not included in the analysis. By the time  $\Delta H$  attains  $\Delta H_m$ , the erosion process is already started and nearly 5% of embankment height must have eroded by that time. This observation can be seen in the Figure 4.36.

#### d. Rate of Crest Height Erosion ( $dh_{cm}/dt$ )

The rate of crest erosion along with time is essential for the breach process study. Rate of crest erosion is nondimensionalised with velocity of flow approaching the crest, denoted as  $\sqrt{2gh_u}$ . Dimensionless rate of crest erosion is plotted against difference in water level between the upstream and downstream of the embankment and nondimensionalised with  $L_{DB}$ , the base length of the embankment. These values are plotted individually for each run. Power law relation is fitted with regression analysis. The exponent and multiplying constant of the power law  $n_{22}$  and  $K_{22}$  are analysed with the  $V_{SRN}$  as indicated in Figures 4.37(a) and (b). Using related values of  $n_{22}$  and  $K_{22}$ , the rate of crest erosion is plotted again as shown in Figure 4.37(c). It may be observed that the scatter in data is high, but there is a general variation of increasing trend of  $dh_{cm}/dt$  with  $\Delta H/L_{DB}$  as:

$$\frac{\left(\frac{dh_{cm}}{dt}\right)}{\sqrt{2gh_u}} = k_{22} \left(\frac{\Delta H}{L_{DB}}\right)^{n_{22}} \quad (4.19b)$$

Incorporating the values of  $k_{22}$  and  $n_{22}$  in Equation (4.19 b), the relation may be simplified as:

$$\frac{\left(\frac{dh_{cm}}{dt}\right)}{\sqrt{2gh_u}} = 0.15^{0.7} \quad (4.19c)$$

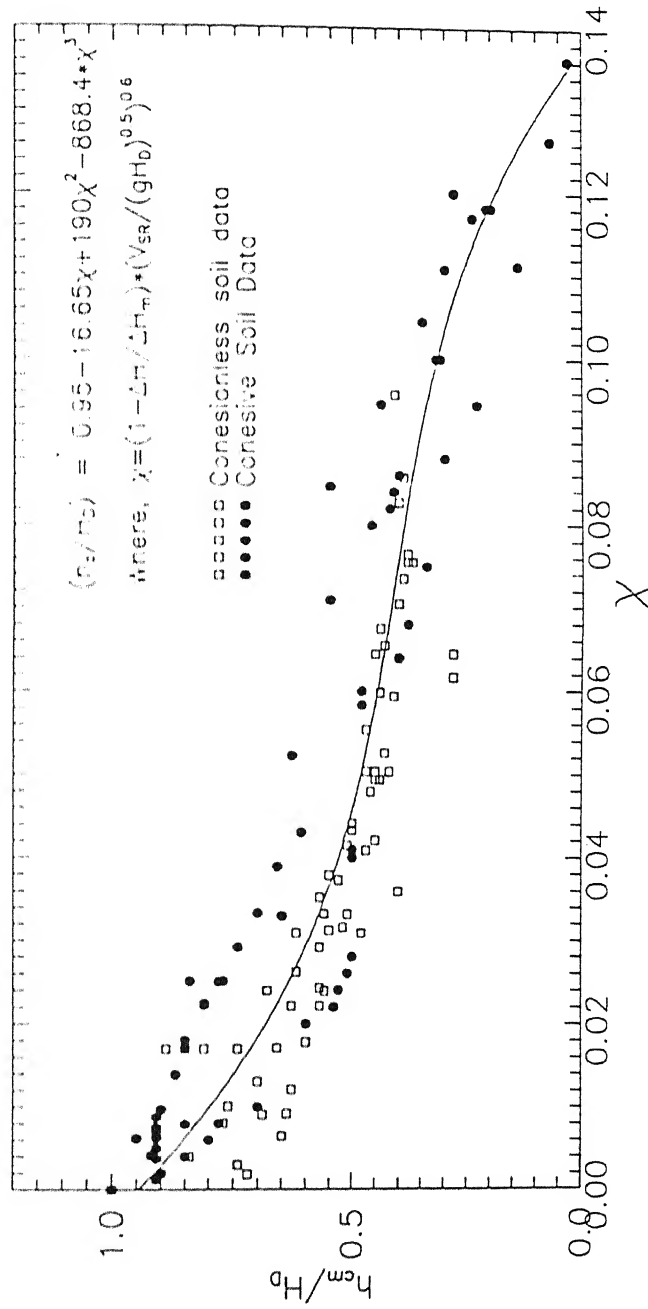
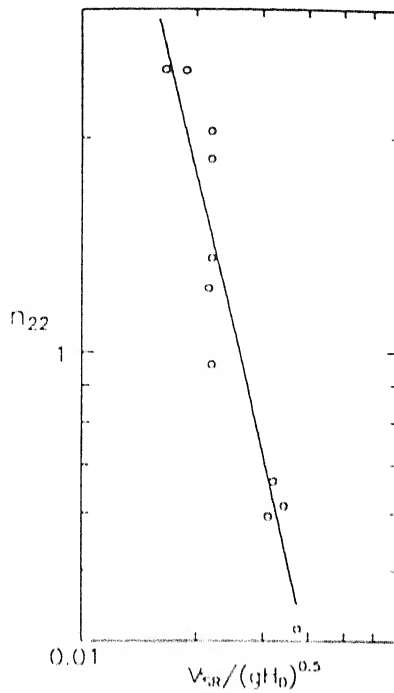


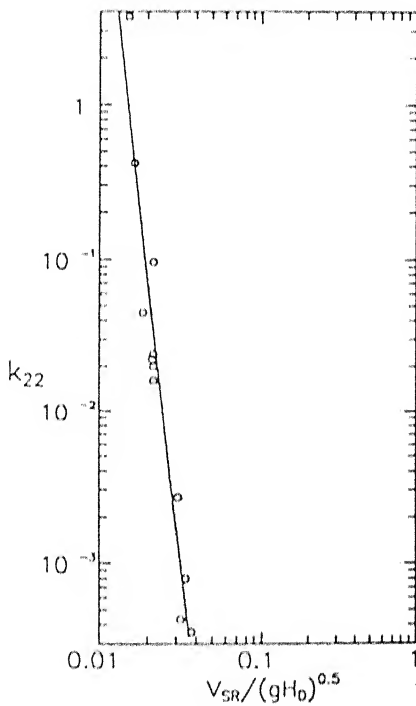
Fig. 4.36: Variation of nondimensional crest height of erodible sediment bed at any time ( $h_{cm}$ ) with  $\chi$ , a function of nondimensional drop in water level,  $\Delta H$  and soil resisting velocity number,  $V_{SR}$



$$n_{22} = 0.0003 * (V_{SRN})^{-2.22}$$

Where,  $n_{22}$  is the exponent of the power law relation between individual run of  $((dh_{cm}/dt)/(2gh_u)^{0.5})$  Versus  $dH/L_{DB}$

Fig. 4.37(a): Variation of exponent  $n_{22}$  with soil resisting velocity number ( $V_{SRN}$ )



$$k_{22} = 1.8 * 10^{-17} * (V_{SRN})^{-9.18}$$

Where,  $k_{22} = ((dh_{cm}/dt)/(2gh_u)^{0.5}) / (dH/L_{DB})^{0.0003 * (V_{SRN})^{-2.22}}$

Fig. 4.37(b): Variation of  $k_{22}$ , sediment erosion coefficient with soil resisting velocity number ( $V_{SRN}$ )

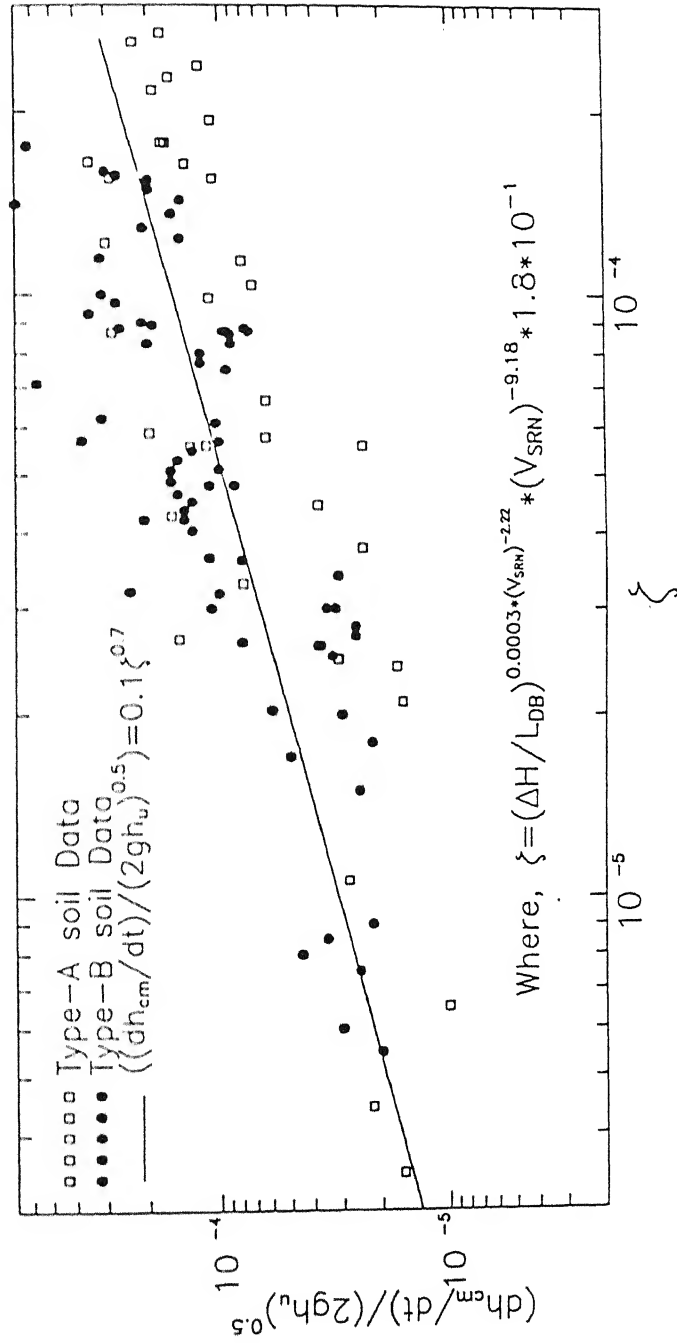


Fig. 4.37(c): Variation of nondimensional rate of erosion of crest height( $h_{cm}$ ) with  $\Delta H$  and  $V_{SRN}$



$$\text{where, } \zeta = \left( \frac{\Delta H}{L_{DB}} \right)^{(0.0003 / V_{SRN}^{2.22})} \times V_{SRN}^{-9.18} \times 1.8 \times 10^{-17}$$

It may be observed here that the data of both types of the embankment merged together, as can be seen from Figure 4.37(c).

#### e. Variation of Head of Water Over the Crest ( $h_u$ )

The head of water over crest of sediment bed during dam breach is noted as  $h_u$ . This is the difference between reservoir level( $h_{wr}$ ) and crest of sediment bed profile( $h_{cm}$ ) as:

$$h_u = h_{wr} - h_{cm}$$

In the analysis of cohesionless and cohesive embankment separately,  $h_u$  is non-dimensionalised with  $h_{up}$  and plotted against  $t / t_{hup}$  in Figure 4.38(a). The value of  $h_u$  for breach discharge calculation can be obtained at any time of breach, if the scales  $h_{up}$  and  $t_{hup}$  can be estimated. Attempt to correlate  $t_{hup}$  for combined data was not successful. Instead, the analysis of  $h_{up}$  based on reservoir level variation is attempted here.

It is realised for the computation of  $h_u$  using the breach variables like reservoir level( $h_{wr}$ ) and crest of sediment bed( $h_{cm}$ ) will be more appropriate compared to time as shown in Figure 4.38(a). Prior to this in sections 4.5a and 4.5b the method to predict  $h_{wr}$  and  $h_{cm}$  is discussed. One can directly use Equations (4.17c) and (4.19a) for  $h_u$  computation.

In another way of analysis  $h_u$  is related to reservoir level ( $h_{wr}$ ) in a normalised form, for both the cohesive and cohesionless embankments data as:

$$\frac{h_u}{h_{up}} = x^\eta \times e^{\eta(1-x)} \quad (4.20a)$$

$$\text{where, } x = \frac{(h_{wrm} - h_{wr})}{(h_{wrm} - h_{wr*})}, \text{ where } h_{wr*} \text{ is the reservoir water level}$$

corresponding to  $h_{up}$ .

In this equation to predict  $h_u$  at any time of breach reservoir level  $h_{wr}$  to be known for the estimated exponent and scales like:  $\eta$ ,  $h_{wrm}$ ,  $h_{wr*}$  and  $h_{up}$ . The variation of  $h_u/h_{up}$  is plotted for combined analysis of both the cohesive and cohesionless embankments with normalised reservoir water level ( $h_{wr}$ ) as shown in Figure 4.38(b). Even though the trend in variation is same but large scatter can be seen in both rising and falling limbs. Falling limb data is further analysed using the relation given as equation (4.20a). The value of exponent ( $\eta$ ) of the

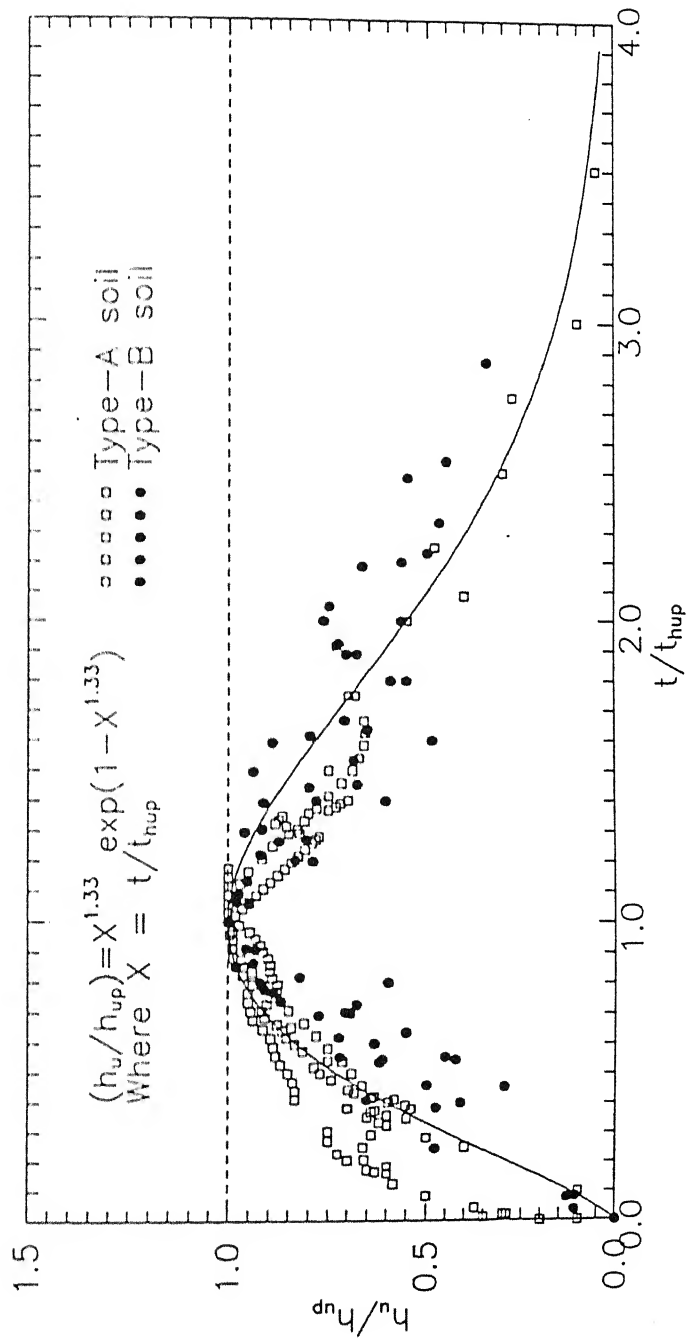


Fig. 4.38(a): Variation of normalised head of water over erodible crest of sediment bed with corresponding normalised time

Equation (4.20a) varied from 0.06 to 0.68 as indicated in Figure 4.38(b). All the data fall in the range of exponent  $\eta$  variation between 0.06 to 0.68. The  $h_{wrm}$  is the reservoir level corresponding to top of the dam, ( $h_{wr}$ ) is the reservoir level acting at any time under consideration, and  $h_{wr*}$  is the reservoir level correspond to  $h_{up}$ .

1. The variation of  $\eta$  is plotted against  $V_{SRN}$  as indicated in Figure 4.38(c) using regression analysis, a power law relation is given as:

$$\eta = V_{SRN}^{1.492} \times 84.1 \quad (4.20b)$$

2. It was observed in the experiments that the magnitude of  $h_{wrm}$  is slightly higher than the height of the dam. Since the difference in their magnitude is not appreciable, an assumption of  $h_{wrm} \cong H_D$  is considered as very close to the reality.

3. The  $h_{wr*}$  plotted against  $V_{SRN}$  by nondimensionalising with maximum water level ( $h_{wrm}$ ) in the reservoir. There is a good agreement between these two variables as can be seen from Figure 4.38(d). A polynomial relation is obtained based on regression analysis.

$$\frac{h_{wr*}}{h_{wrm}} = 1 - 0.49V_{SRN} - 40.5V_{SRN}^2 - 4039.4V_{SRN}^3 \quad (4.20c)$$

4. The magnitude of  $h_{up}$  is the maximum value of  $h_u$  occurring during the erosion process. The value is needed to predict the variation of  $h_u$  as indicated in Figure 4.38 (b). The magnitude of  $h_{up}$  is computed as:

$$h_{up} = h_{wr*} - h_{cm*} \text{ (value of } h_{cm*} \text{ corresponding to } h_{wr*} \text{)} \quad (4.20d)$$

The value of  $h_{cm*}$  is non-dimensionalised with reservoir level at that time  $h_{wr*}$  is plotted against  $V_{SRN}$  as shown in Figure 4.38(e). The functional relation among them is obtained by regression analysis as:

$$\left( \frac{h_{cm*}}{h_{wr*}} \right) = 0.443 e^{21.1V_{SRN}} \quad (4.20e)$$

The magnitude of head acting over the sediment crest  $h_u$  of breach can be computed by knowing  $h_{wrm}$ ,  $h_{wr*}$  and  $h_{up}$  from Figure. 4.38(b). The magnitude of  $h_{wr*}$ ,  $h_{up}$  and  $\eta$  can be found from the relations developed in Figures 4.38(c), (d) and (e).

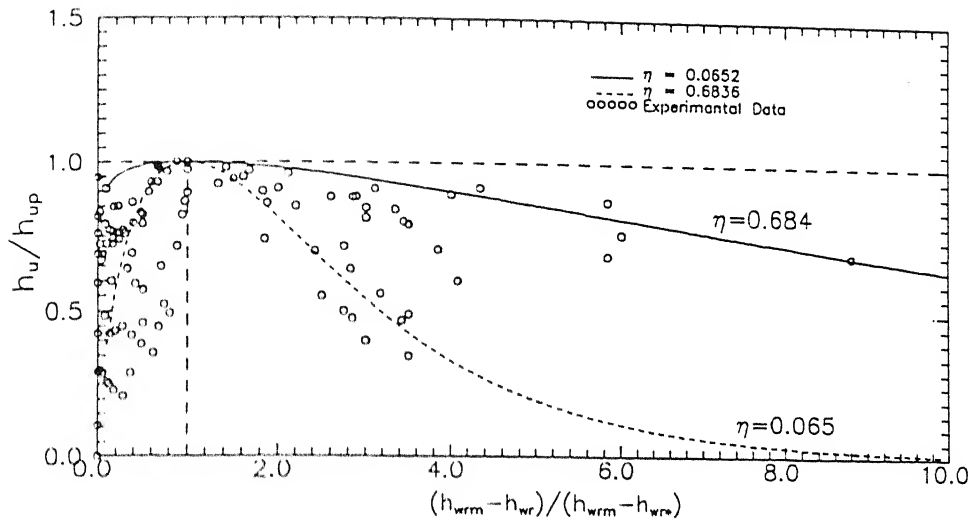


Fig. 4.38(b): Variation of normalised head of water over erodible crest of sediment bed with normalised reservoir water level

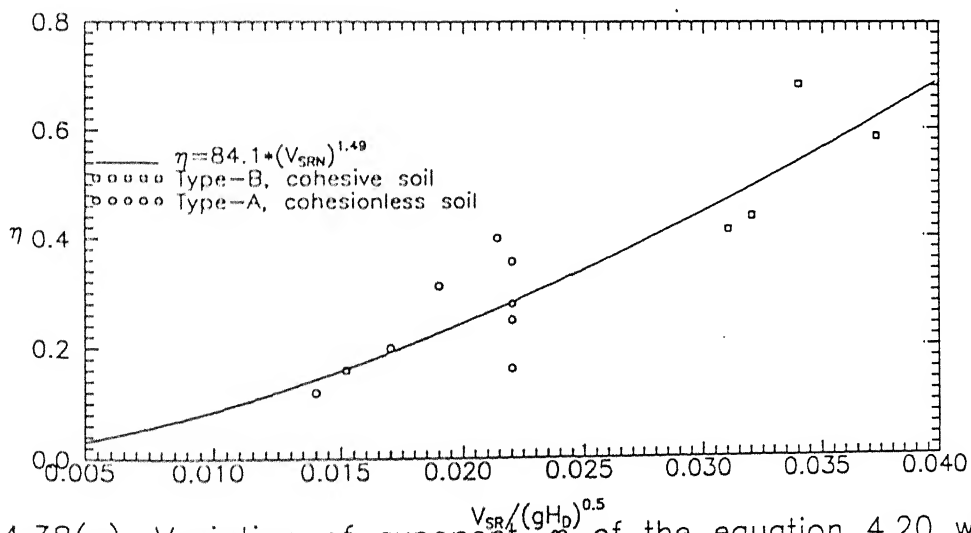


Fig. 4.38(c): Variation of exponent,  $\eta$  of the equation 4.20 with soil resisting velocity number ( $V_{SRN}$ )

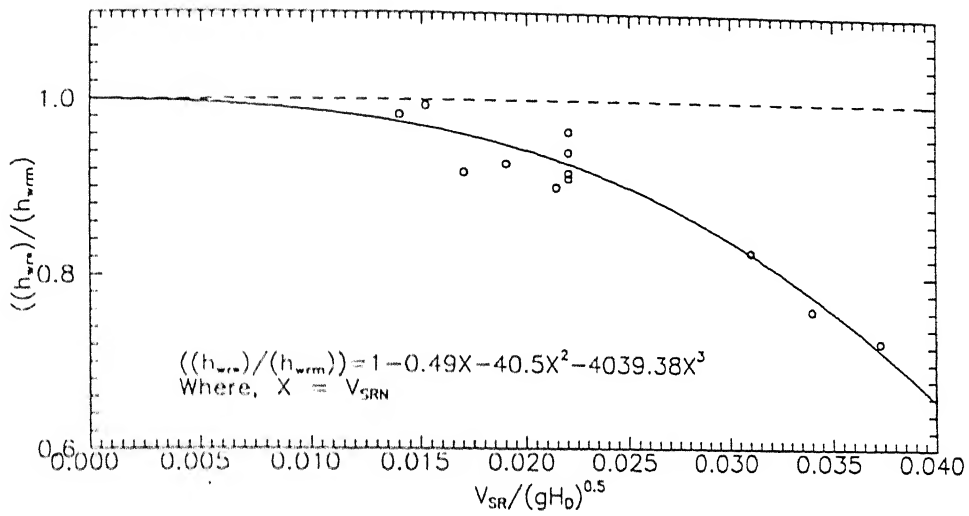


Fig. 4.38(d): Variation of scale  $h_{wre}$  with soil resisting velocity number ( $V_{SRN}$ )

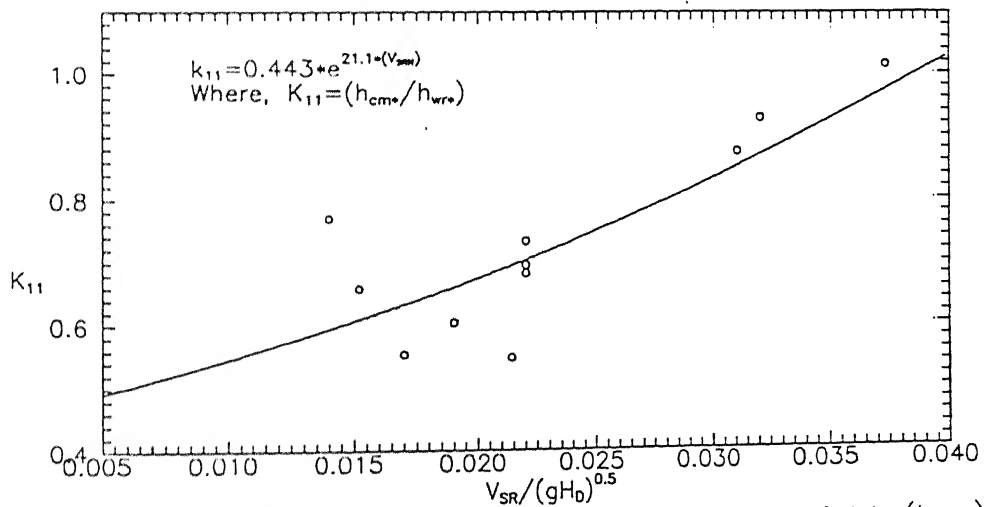


Fig. 4.38(e): Variation of ratio of crest height ( $h_{cme}$ ) to reservoir level  $h_{wre}$ , (at value of  $h_{up}$ ) with soil resisting velocity number,  $V_{SRN}$

### f. Variation of Energy Loss During the Breach Process

The modes of energy dissipation during the breach process can be categorised in the following headings:

- a. Energy spent in eroding and transporting the sediment.
- b. Due to formation of hydraulic jump intermittently.
- c. Due to boundary friction.
- d. Water fall occurring particularly in the cohesive embankment.

It was difficult to compute energy loss under the above sub items. Combined energy loss is computed as the difference in energy between the upstream of the embankment ( $E_1$ ) to the downstream of embankment ( $E_2$ ) is denoted as  $\Delta E$ . This energy loss  $\Delta E$  is non-dimensionalised with upstream energy ( $E_1$ ) and is plotted against the variation in water level in the upstream and downstream of the embankment ( $\Delta H$ ) as shown in Figure 4.39. This  $\Delta H$  value is non-dimensionalised with the base length of the embankment ( $L_{DB}$ ). Using the ratio of average shear velocity ( $\bar{V}_*$ ) with sediment resisting velocity ( $V_{SR}$ ) along with  $Q_{PSN}$ , the regression analysis is carried out. The polynomial relation between  $\Delta E/E_1$  and  $\Delta H/L_{DB}$  is written as:

$$\frac{\Delta E}{E_1} = -0.017 + 0.87\delta - 0.23\delta^2 \quad (4.21)$$

$$\text{where } \delta = \left( \frac{\Delta H}{L_{DB}} \right)^{0.41} \times \left( \frac{\bar{V}_*^2}{V_{SR}^2} \right)^{0.24} \times Q_{PSN}^{0.51}$$

This functional relation for  $\delta$  was obtained from regression analysis of the data. Energy loss will be higher during the initial stage of erosion and it decreases as the breach erosion reaches final stage.

### g. Sediment Load Variation

Volume of sediment eroded is computed from breach geometry at any given instant during breach. The bulk density of compacted soil in the embankment is known by measurement from the sample collected from the embankment. The product of volume rate of sediment discharge,  $Q_s$ , with bulk density ( $\gamma_b$ ) is considered to be sediment load ( $g_s = Q_s \gamma_b$ ). Sediment load,  $g_s$  is non-dimensionalised with ( $\gamma_s d_{50} V_{SR}$ ) and is plotted against non-dimensionalised

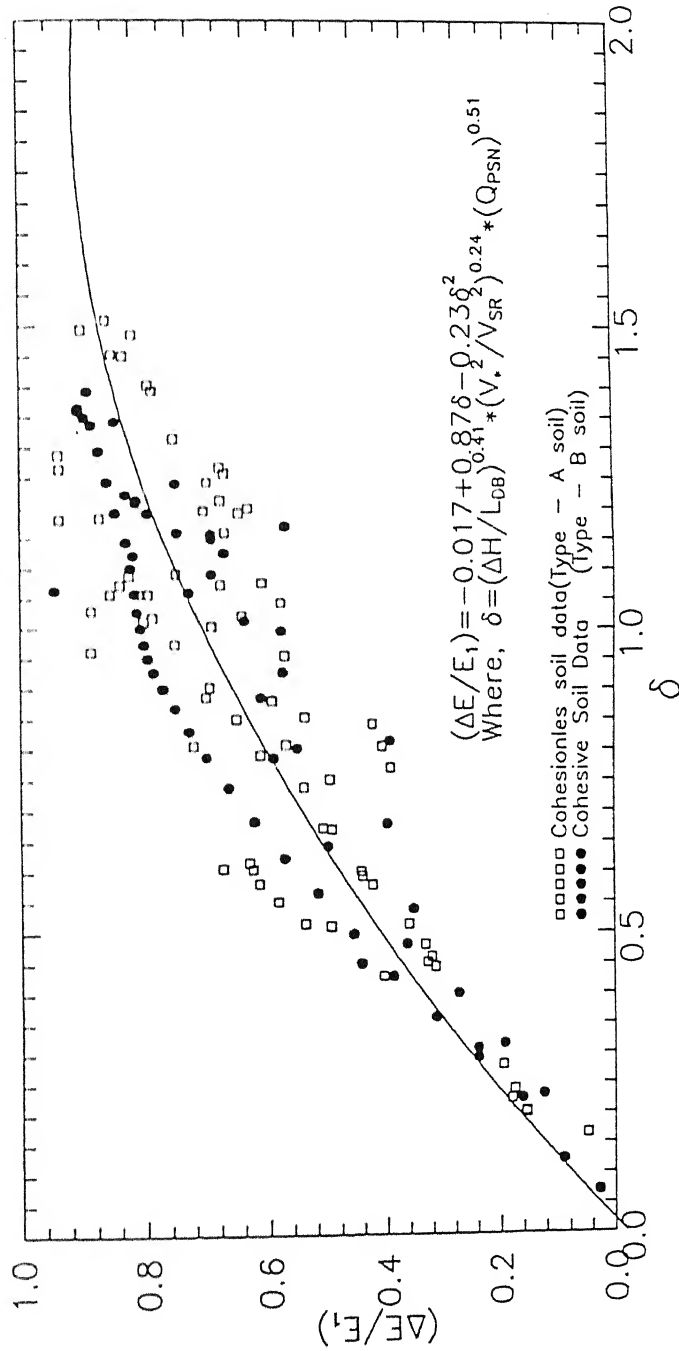


Fig. 4.39: Variation of nondimensional energy loss,  $\Delta E$  with nondimensional  $\Delta H$

average shear velocity( $\bar{V}_*$ ) as  $\bar{V}_*^2 / V_{SR}^2$  along with  $Q_{PSN}$  and  $V_{SRN}$  as shown in Figure 4.40. Using the regression analysis, relation between them is written as:

$$g_s^* = -2.12 + 4.3\psi - 0.17\psi^2 \quad (4.22)$$

$$\text{where } \psi = \left( \frac{\bar{V}_*^2}{V_{SR}^2} \right) \times Q_{PSN}^{0.64} \times V_{SRN}^{0.42}$$

This equation is valid for  $\psi > 0.48$ . Wide scatter in the data indicates a poor agreement. The relation shows that  $g_s$  varies almost square of the shear stress.

#### h. Variation of Sediment Concentration

Sediment discharge ( $Q_s$ ) is nondimensionalised with water discharge ( $Q_w$ ), denoted as sediment concentration ( $C$ ) at a given instant of breach time. Using regression analysis between the variables  $h_u/H_D$ ,  $\Delta H/L_{DB}$ ,  $\bar{V}_*^2 / V_{SR}^2$  and  $Q_{PSN}$  and  $V_{SRN}$ , a relation is obtained as indicated in Figure 4.41. The exponent of the variables are obtained from the regression analysis. Separate curves are fitted for cohesive soil and cohesionless soil and also for combined data. Power law relation of the type given below in Equations (4.23 a), (4.23b), and (4.23c) respectively for cohesionless soil, cohesive soil and combined one are obtained.

$$C_* = \xi^{0.38} \times 0.071 \text{ (Fine Cohesionless Sand - Type A)} \quad (4.23a)$$

$$C_* = \xi^{0.39} \times 0.073 \text{ (Cohesive Soil - Type B)} \quad (4.23b)$$

$$C_* = \xi^{0.38} \times 0.067 \text{ (Combined Data)} \quad (4.23c)$$

$$\text{where, } \xi = \left( \frac{h_u}{H_D} \right)^{-0.95} \times \left( \frac{\Delta H}{L_{DB}} \right)^{0.46} \times \left( \frac{\bar{V}_*^2}{V_{SR}^2} \right)^{0.15} \times Q_{PSN}^{0.16}$$

$$\text{and } C_* = \left( \frac{Q_s}{Q_w} \right)^{0.404} \times V_{SRN}^{0.222}$$

It may be observed that the power of the variable  $\xi$  and multiplying constant for both soils data and for combined data remains fairly constant. The scatter of data is very high. Hence these relation must be used with caution.



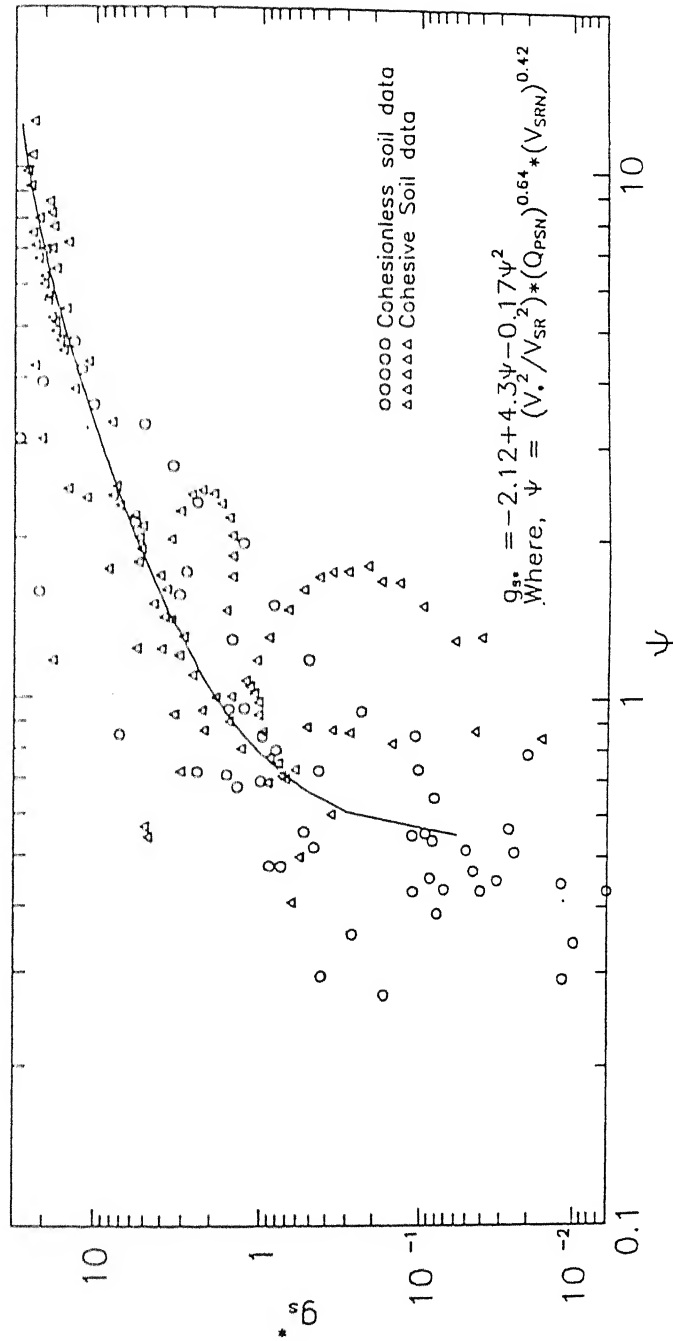


Fig. 4.40: Variation of nondimensional sediment load  $g_s^*$ , with nondimensional bed shear stress

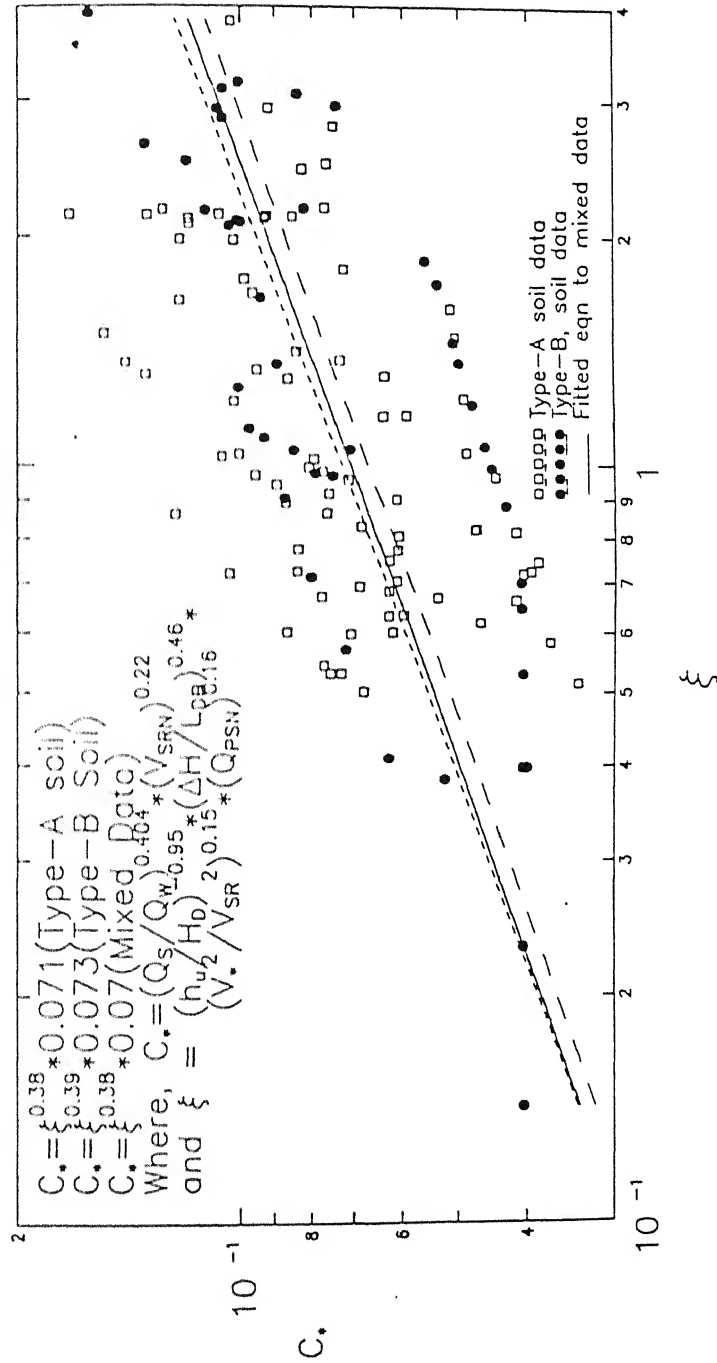


Fig. 4.41: Variation of nondimensional sediment concentration with  $h_u$ ,  $\Delta H$ ,  $L_{DB}$ ,  $V_*$  and  $Q_{PSN}$

## 4.6 Analysis of Laboratory Data Along with Field Data

It was necessary to verify the trend and order of magnitude of some of the parameters evolved from the laboratory data, with the field data. These evolved parameters are: peak outflow discharge ( $Q_{wp}$ ), erosion of breach width ( $B_{cr}$ ), depth of erosion ( $D_{er}$ ). These parameters are non-dimensionalised using flow and geometric parameters. Field data are collected from the book on 'Dam Breach Modelling Technology' by Vijay P. Singh. This book contains the data of 85 dam breaches all over the world. Data contains year of construction and failure along with the information on dam geometry and storage capacity of the reservoir. For these dams when breach occurs, the final dimensions of the breach geometry like depth of erosion, top width of erosion, and duration of erosion along with maximum outflow discharge are recorded. These field data on dam breach contain part of the information and only a few dam breaches contain all the required information. These data are used along with experimental data for analysis of breach parameters.

### a. Peak Outflow Breach Discharge ( $Q_{wp}$ )

The maximum discharge of outflow is related to capacity of the reservoir and height of the dam as indicated in the Figure 4.42. The relation between them is as follows:

$$\frac{Q_{wp}}{\sqrt{gH_D^5}} = 0.00215 \times \left( \frac{Capacity}{H_D^3} \right)^{\frac{2}{3}} \quad (4.24a)$$

The magnitude of the inflow into the reservoir is not considered in this analysis because of its non-availability. Also the dam fill material properties are not known in most of the cases. The analysis of the model data indicates that the soil properties are also important variables in the prediction of  $Q_{wp}$ .

### b. Depth of Erosion ( $D_{er}$ )

The final depth of erosion is plotted against  $H_D$  in a dimensional form and with capacity of reservoir in a nondimensional form shown in Figures 4.43(a) and 4.43(b). The figure shows that height of dam ( $H_D$ ) and capacity of the reservoir are very important variables in the prediction of final depth of erosion. The relation between them is written as:

$$D_{er} = 0.737 H_D^{1.03} \text{ or } D_{er} = 0.74 H_D \quad (4.24b)$$

$$\text{and } (gD_{er}^5/Q_{wp}^5) = 33719.7 \times ((H_D^3/Capacity)^{5/3})^{1.345}$$

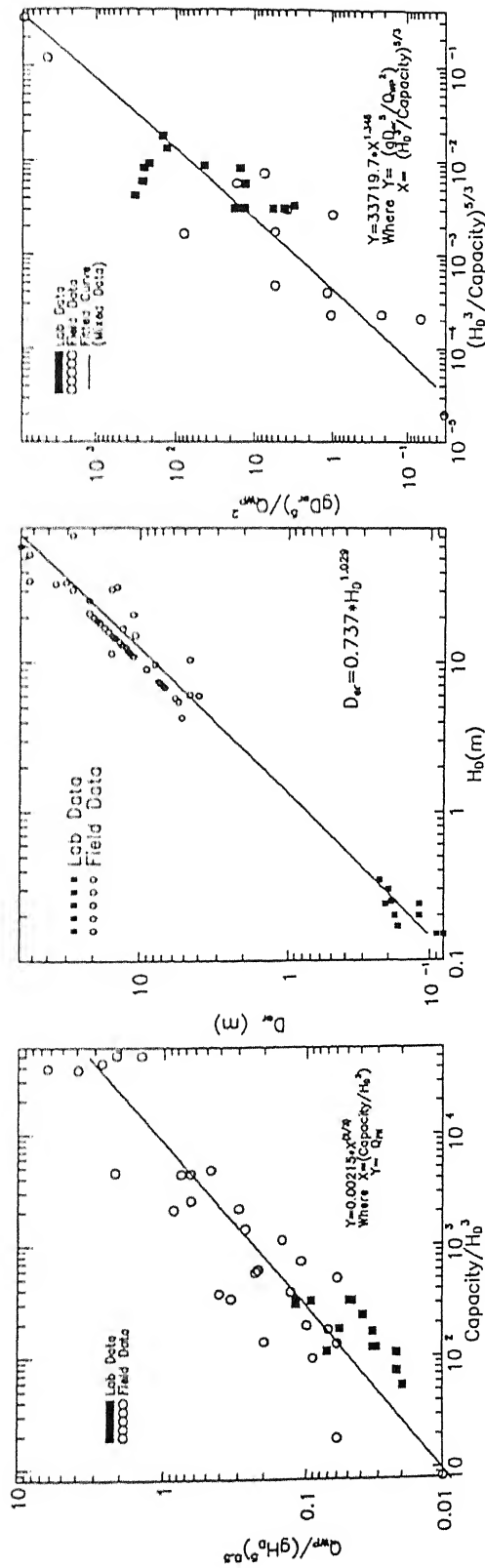


Fig. 4.42: Variation of peak breach water discharge ( $Q_{wp}$ ) with capacity of the reservoir and height of the dam ( $H_0$ ) for both lab and field data

Fig. 4.43(a): Variation of final depth of erosion with height of the dam

Fig. 4.43(b): Relation between nondimensional  $D_{er}$  with nondimensional reservoir capacity

### c. Top Width of Erosion $(B_{cr})_f$

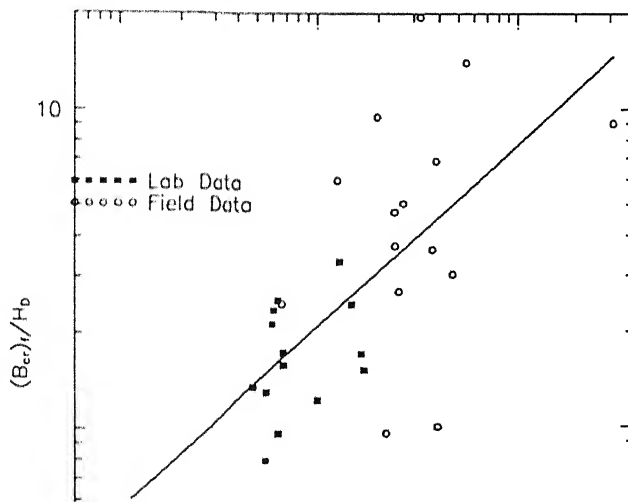
Width of erosion is plotted against peak discharge ( $Q_{wp}$ ), keeping regime flow analysis in the rivers in view. Regime flow analysis indicates that width of the river is a function of the maximum discharge passing through. The final breach width is plotted against peak discharge for both laboratory and field data. The relation between them indicates that  $(B_{cr})_f$  is proportional to the  $(Q_{wp})^{0.4}$ . Lai and Shen (1996) showed from their experiments that the equilibrium width ( $B_e$ ) of the channel is related to the dominant discharge  $Q_d$  as:

$$B_e = 10.91 Q_d^{0.5} \quad (4.24c)$$

Where  $B_e$  is measured in meters and  $Q_d$  is in cubic meters per second. These experiments were conducted for the study on the flushing of sediment through reservoir. The magnitude of the exponent observed for the breach of a dam is very near to the exponent observed for the channel formation. In the present mixed data analysis of both field and laboratory, final width is non-dimensionalised with height of the dam and is plotted against dimensionless  $Q_{wp}$  in terms of  $H_D$  and capacity of the reservoir as shown in the Figure 4.44. The relation between them is as follow:

$$\frac{(B_{cr})_f}{H_D} = 28.4 \left[ \frac{Q_{wp}}{\sqrt{g H_D^{2.6} \text{Capacity}^{0.8}}} \right]^{0.57} \quad (4.24d)$$

There is a wide scatter in the data due to the exclusion of inflow and soil properties.



#### d. Relation Between Breach Froude Number ( $F_b$ ) and Breach Shape Factor ( $S_f$ )

The breach Froude number is defined as:

$$F_b = \frac{Q_{wp}}{(B_{cr})_f \sqrt{g D_{er}^3}} \quad (4.25a)$$

and breach Shape factor is defined as:

$$S_f = \frac{(B_{cr})_f D_{er}}{L_{TD} H_D} \quad (4.25b)$$

These parameters are coined by Vijay P. Singh and P. D. Scarlatos (1989). They showed the Breach Froude number is related to  $S_f$  as:

$$F_b = 0.2 S_f^{-0.39} \quad (4.25c)$$

This analysis is carried out using laboratory and field data and the relation among them is shown in Figure 4.45 and in a functional form may be written using regression analysis as:

$$F_b = 0.048 S_f^{-0.52} \quad (4.25d)$$

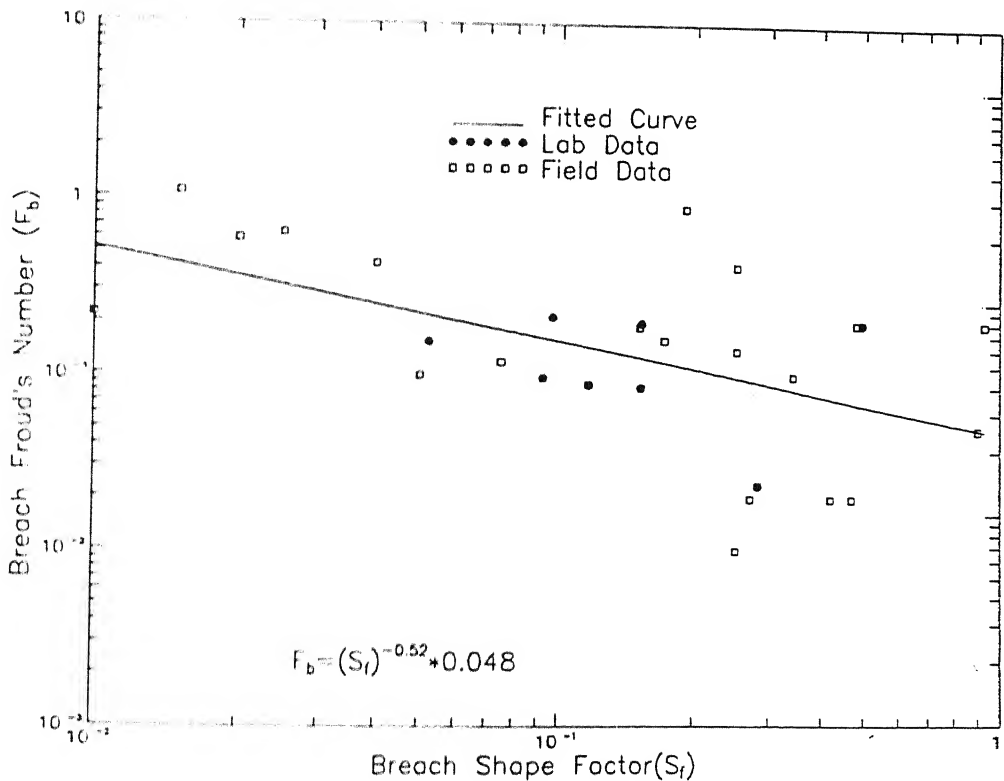


Fig. 4.45: Relation between breach Froude number ( $F_b$ )

## 4.7 Discussion of the Results

In this chapter efforts has been made to know the details about the mechanism involved in the dam breach process, with both cohesive and cohesionless soil models by varying both flow parameters and embankment geometry. Required variables are measured with respect to time at suitable location along the dam body and in the reservoir. The dynamic nature of the breach problem is analysed using these data.

The mechanism involved in this problem can be broadly categorised into three domain namely,

- a. Breach Morphology.
- b. Flow Hydraulics.
- c. Breach Erosion.

### a. Breach Morphology

- i. From the experiments, it is observed that the breach cross-sectional area does not remain same along the breach at any time of breach, except towards the end of the breach. This is shown in Figures 4.1(a) and (b) for cohesionless soil and in Figures 4.25(a), (b), (c), and (d) and 4.26 for cohesive soil embankments. This needs to be taken appropriately in using the routing procedure for flow through breach channel. This variation of breach geometry implies that there will be no uniform erosion along the length.
- ii. The cross-sectional area of the breach changes from trapezoidal at the upstream edge (or near crest) of the dam, to rectangular (or steep side slope) at the downstream edge, where discontinuity of surface slope occurs. Again the shape modifies to trapezoidal shape upto downstream end of the dam. The computation of sediment load eroded at any time is done through taking the average of cross-sectional area between any two measuring sections.
- iii. At the initial phase of breach there is cascading of flow particularly in cohesive soil.
- iv. The limitation or the shortcomings of the present study mostly goes to lack of automation in recording of the bed profiles both in longitudinal and lateral direction and water surface profile along breach with time. During the initial period of breach the water will be turbid, particularly near the sections 6 and 7 (as shown in photographs attached in Chapter III), near the downstream top edge and at the section between downstream edge and toe of the dam. So the bed level measurement with time by the help of point gauge or even with suitable modification to point gauge as described in Chapter III may not be error free. To

overcome this limitation, actual values of water level, bed level and water surface widths are plotted with time. An average curve passing the points is fitted. The readings corresponding to this average curve are used as data points in the analysis.

v. Collapsing of breach banks are not analysed explicitly. Corresponding width enlargement due to side collapse is considered in computation of sediment volume. Conditions under which banks are collapsing is not considered in the present analysis.

### **b. Breach Hydraulics**

i. From the measured  $h_u$  and  $Q_w$ , it is confirmed that the broad-crested weir formula can suitably be used in the dam breach hydraulics. The magnitude of discharge coefficient varies with the height of sediment crest level and head acting over it.

ii. The effect of tail-water is not considered in the analysis.

As observed from the experiments and also from the historical dam failure cases, dam body never gets eroded vertically upto its bottom. It can be seen from Equation (4.24b),  $Der \cong 0.74 H_p$  for both lab and field data. So the chances of submergence of flow for very low  $h_u/h_{c_m}$  value is rare and even if it happens, that will be towards the end of the breach. By that time the flow in the breach channel will be of channel type flow without much further erosion either in vertical or lateral direction. So one may fairly assume free weir flow situation without undue loss of accuracy.

iii. An interesting observation about the breach crest is that it moves in upstream direction, particularly the flow crest moves very fast near the zone of downstream top edge of the dam, where there is discontinuity of slope surface. Though the crest moves in upstream direction, it is observed during most of the time of the breach process, the crest lies near the upstream top edge of the dam. Though it depends on the top width of the dam section, still, it will be appropriate to locate the crest near the upstream top edge of the dam without substantial error.



### c. Breach Erosion

- i. Erosion in the breach section occurs both in vertical and lateral directions. Vertical erosion is mainly due to erosion caused by flow velocity. Lateral erosion or widening of breach is due to bank collapsing. Bank collapsing occurs due to caving of the banks at the corner of the base. Caving causes hanging of banks, with water flowing below resulting in their collapse. Permeability of soil fill plays a dominating part in the erosion process. Soil fill having less permeability is more resistant to vertical erosion. In the present analysis, explicitly the effect of permeability of the soil fill is not considered.
- ii. The dominating factor in breach erosion is the acceleration of flow. This is controlled particularly by the magnitude of water level drop between the upstream and downstream of the dam.
- iii. Cascading and water fall types of flow occur along the breach in cohesive soil embankment. These are absent in cohesionless soil embankment breach. Cause for these types of flow is mainly due to presence of cohesion.
- iv. The flow during initial phase of erosion appears like dense muddy flow in cohesionless soil embankment.

## 4.8 Concluding Remarks

- a. In the breach hydraulics, reservoir water level ( $h_{wr}$ ), head over crest ( $h_u$ ), water level difference ( $\Delta H$ ) are suitably non-dimensionalised and analysed for their variations.
- b. The corresponding scales for the above variables are obtained for the use at any other given situations. The scales are related with known parameters of dam geometry and properties of its fill materials; reservoir size and breach peak outflow discharge.
- c. The related time component associated in these variables are also analysed. In the breach morphology, width and depth of erosion are studied extensively along with their rate of variation.
- d. The photographs are taken at different stages of the cohesionless embankment breach which indicates the process involved in breaching of the embankment.
- e. Though photographs give qualitative information about the changing nature of morphology with time during the breach process, the rate of variation of depth of erosion of crest ( $h_{cm}$ )

of sediment bed and width of erosion at crest ( $B_{cr}$ ) reveal quantitative information about their mutual relation.

- f. Erosion of sediment and its transport occurs mostly with accelerated flow conditions in the dam breach process. Sediment transport relations available in literature are developed for the uniform flow condition. Due to this basic change in flow condition, transport formula used in most of the numerical modelling of dam breach is not used in present analysis.
- g. The average shear velocity ( $\bar{V}_*$ ) in breach channel along with water drop ( $\Delta H$ ) and the soil resisting velocity ( $V_{SR}$ ) are used in developing functional relationship between sediment transport and flow properties.
- h. There is a strong relationship between the peak water discharge and peak sediment discharge and their corresponding times of occurrence during the breach process.
- i. The maximum depth of erosion and maximum width of erosion at crest are interrelated to each other.

Now with this background of dam breach analysis, the functional relations developed can be used to validate the field data.

## **CHAPTER V**

# **COMPARISON OF DAM BREACH RESULTS WITH TETON AND HUACCOTO DAMS**

### **5.1 Introduction**

The developed functional relations among the system parameters from the analysis of experimental data need to be tested with prototype data for their validations. As any numerical model heavily relies on the experimental observation to test the validity of the methodology adopted in computational algorithm, the experimental results similarly needs a well accepted numerical model for its comparison . Sometimes the system is so complex and dynamic in its behaviour, like the present problem of dam breaching, it is not easy to get the process information easily. This compels the investigators to bank upon the systematic, well planned experimentation on scaled models. In open literature very few experimental results are documented in this topic. Those which are available do not deal so much on the mechanism of dam breach process behaviour to bring much light on the subject. Immense effort has been made in the development of numerical solution to dam breach problem. Very few approaches have attempted with a proper perspective insight into the basic mechanism. Due to this, many numerical approaches become invalid for a given situation. A few approaches, to some extent, like BEED model are successful to a fair degree of acceptance. The knowledge on mechanism of breach process from the experimental studies will be helpful immensely in further improving the numerical approach to solve real life problem on dam breaching. However, it is necessary to validate how far the functional relationships developed from the model experiments will predict prototype behaviour for their authentication and further use . Almost

none of prototype data is available during the breach process. This gap may be filled by both qualitative and quantitative observations of the breach process by the model study in a laboratory set-up. The final verdict on the laboratory data is only how close they predict final breach geometry of the prototype dam failure. For the validation of the present study, two prototype dam failures information are used as reported by Singh (1996) namely:

- a. Teton Dam
- b. Huaccoto Dam.

Ponce and Tsivoglou (1980), Singh and Scarlatos (1989) have verified their result with these two observed dam failure data . The present laboratory analysis result is compared with the result of BEED (Breach Erosion of Earth-Fill Dams), a numerical model for the breach associated with Teton dam and Huaccoto dam. Before going into the validation of the result, a brief note on Teton dam, Huaccoto dam and BEED model will enable one to know their background.

#### **a. Teton Dam**

Teton dam, Idaho, U.S.A. an earthfill structure of height 93m, experienced failure on 5th June' 1976. The details of the dam geometry and the properties of its fill material are given in Table 5.1. The dam had a crest width of 10.5m. Clay, silt, sand and rock fragments were used as dam fill. The full reservoir capacity was  $3.1 \times 10^3 \text{ m}^3$ . The dam cross-section is shown in Figure 5.1(a).

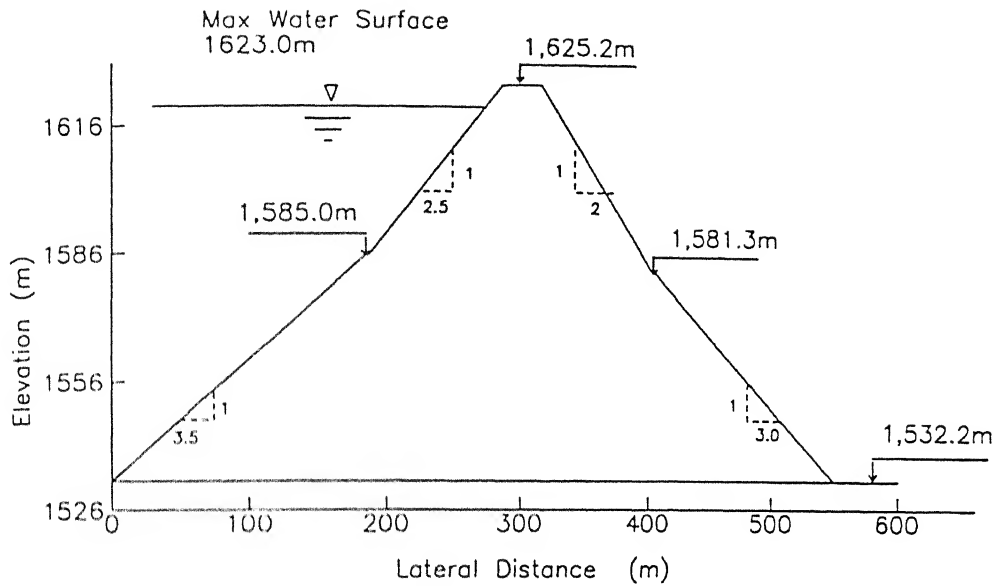


Fig. 5.1(a): Cross-sectional details of Teton dam

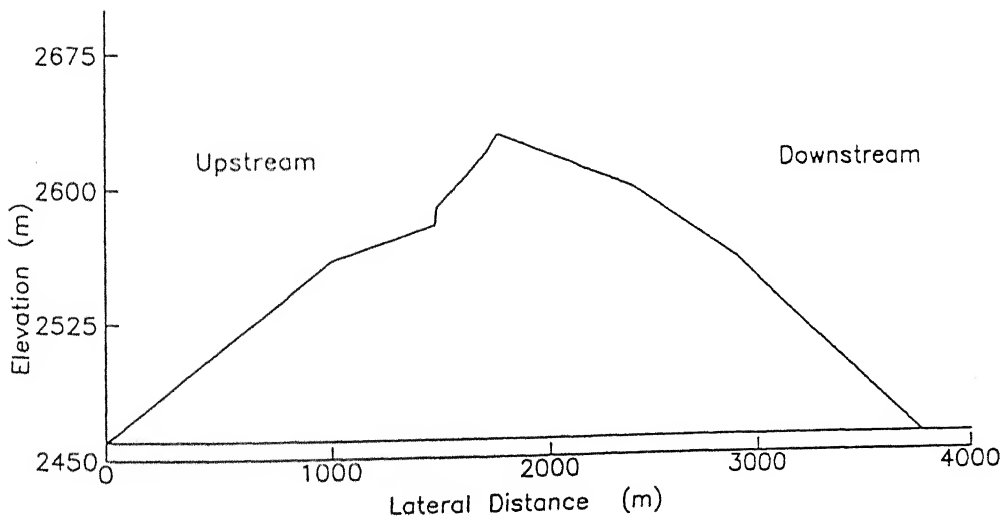


Fig. 5.1(b): Cross-sectional view of Huaccoto natural dam built by landslide material.

**TABLE 5.1**  
**CHARACTERISTICS OF DAM GEOMETRY, AND SOIL FILL**  
**PROPERTIES OF TETON DAM AND HUACCOTO DAM**

S. No	Description		Teton Dam	Huaccoto Dam
1	Reservoir Capacity	(m <sup>3</sup> )	3.1×10 <sup>3</sup>	8.87×10 <sup>8</sup>
2	Dam Height	(m)	93	≅ 170
3	Lateral Length of Embankment L <sub>DB</sub>	(m)	550	3800
4	Crest Elevation above mean Sea level			2630
5	Top width of Dam	(L <sub>DT</sub> )	29.6	
6	A <sub>D</sub> (cross-sectional area)	(m <sup>2</sup> )	24,986.71	≅ 43,6500
7	d <sub>50</sub> (median size of soil)	(mm)	3	11
8	φ (frictional angle)	(degree)	40	40
9	C (cohesive strength)	(KPA)	49	40
10	γ <sub>s</sub> (unit weight of dam fill)	kg/m <sup>3</sup>	2300	2300
11	$\bar{Q}_m$ average inflow - Q <sub>wp/2</sub>	(cumec)	106.2	
12	Type of Soil			Silty sand and some clay

### b. Huaccoto Dam

The Huaccoto natural dam was created due to landslide that occurred in Cochacay Creek, a tributary of the Montaro River in Peru on April 25, 1974. The landslide had a volume of  $15.8 \times 10^4 \text{ m}^3$  approximately, made this artificial dam and created a huge reservoir of depth nearly 168 meters which took nearly sixty days to fill. It can be quoted from the report,

“ .... Indeed, the volume of the material was so high that it would be enough to build an engineered dam about three times at the same location ...”

The overall geometric characteristics of Huaccoto dam are shown in Table 5.1 and the dam cross-section in Figure 5.1(b). The dam was overtopped during June 6-8, 1974 (Lee and Duncan, 1975). The length of the downstream slope length was around 1.069km. The overtopping flow during the first two days eroded gradually, a small channel along its downstream slope surface. Then after 6-10 hours, there was an increase in the breach channel resulting in a trapezoidal shape approximately 105m in depth and 195-225m in top width with side slopes of about 1:1. The breach did not extend up to the bottom of the embankment. As

a result, a large lake remained after the breach had subsided. The estimated breach related characteristics as mentioned by Vijay P. Singh were :

Maximum flow depth = 15 ~ 20 m

Time for discharge  $0 \text{ m}^3/\text{sec}$  to  $100 \text{ m}^3/\text{sec}$  = 16hr

Time for discharge  $100 \text{ m}^3/\text{sec}$  to peak discharge = 10hr

hydrograph duration from  $100 \text{ m}^3/\text{sec}$  rising to  $400 \text{ m}^3/\text{sec}$  receding = 32hr

### c. BEED Model

There are various numerical models on dam breaching problem as listed in chapter - 2. BEED (Breach Erosion of Earth Fill Dams) model is the recent one (1989), encompassing most of the features of dam breaching. Since then no further numerical studies on this subject have been published and tested on any historical event to the knowledge of author. Seemanpali and Singh (1992) have approached this problem using variational calculus but still BEED model seems to be more appealing and elegant and widely accepted for application. Hydraulic Research Wallingford Limited, Wallingford, U.K. (1995) have carried out large scale model study in sand berms, however, the numerical model based on these test data are still in the developing stage as reported. So keeping in view this status of knowledge in numerical modelling on this topic, BEED model has been chosen for the comparison of the present experimental results.

### i. Background of BEED Model

This model is developed by Singh and Scarlatos (1986, 1987a), Louisiana State University, Baton Rouge for Department of the Army of Engineers, Washington. This model has been tested with four historical earth dam failures namely,

1. South Fork Dam, Pennsylvania (1989)
2. Buffalo Creek Dam, West Virginia (1992)
3. Teton Dam, Idaho (1976)
4. Huaccoto Natural Dam, Peru (1976)

Some salient features in this numerical model and the methodology involved in its evolution are presented here. At this stage, it is worth to quote the statement of Singh and Scarlatos (1989) about this numerical modeling in the report to understand the inherent limitation associated with this problem :

“ Simulation of the total earth fill dam-breach erosion process is a combination of hydrologic events, hydrodynamics, sediment transport mechanics and geotechnical aspects. The real life problem is unsteady, non-homogeneous, non-linear, and three dimensional, which is not theoretically well understood. Mathematical modelling of the phenomenon requires idealisation of the real-life situation so that the leading physical processes can be described by a set of governing equations ..... For practicality, there is always a trade-off involving complexity, accuracy, and efficiency of the model “

Keeping the above statement in mind and the necessary idealisation of the system, one should look into the five components of the model namely,

- i. reservoir water balance
- ii. breach geometry
- iii. breach hydraulics
- iv. flood routing
- v. sediment routing

Among the above stated five components, present study is only concerned first three features of the BEED model. In reservoir water balance, the discharge through spillway and any other structural outlet like sluice gate, during the breach process if any can be accommodated in the model. In this model, the longitudinal flow direction is demarcated into two distinct sections namely breach section and breach channel. The flow over breach section is similar to flow over a broad crested weir. It assumes the validity of Manning's Equation in breach channel. In the breach enlargement, the Einstein-Brown formula is used for the transport of sediment in the breach. The sudden breach enlargement is taken care of by slope stability of breach channel by contour method. But in the BEED model it is difficult to predict a priori the time at which stability will overtake breaching. After instability occurs erosion again predominates until another slope stability occurs.

#### **d. Breach Variables to be Compared**

In the validation of the present experimental results, following parameters are compared with observed data of Teton Dam and Huaccoto Dam and simulated results of BEED model. There is no observational information on sediment related data like peak sediment discharge



intensity ( $q_{sp}$ ) and time of occurrence of peak sediment discharge ( $t_{sp}$ ). Hence, results on  $q_{sp}$  and  $t_{sp}$  are compared only with the simulated result of BEED model.

Major influencing parameters of breach process to be validated are:

- i. Peak outflow water discharge ( $Q_{wp}$ ).
- ii. Time of occurrence of peak outflow water discharge ( $t_{wp}$ ).
- iii. Peak sediment discharge intensity ( $q_{sp}$ ).
- iv. Time of occurrence of peak sediment discharge intensity ( $t_{sp}$ ).
- v. Final maximum top breach width ( $B_{cr}$ )<sub>f</sub>.
- vi. Final depth of erosion ( $D_{er}$ ).
- vii. Final side slope of the breach cross section (1V:zH).

In addition to the prediction of these parameters, the total outflow hydrograph is compared with observed and simulated results of BEED model for both Teton Dam and Huaccoto Dam in nondimensional form,  $Q_w/Q_{wp}$  versus  $t/t_{wp}$ . As the observed information of sediment discharge with respect to time is not available, it is compared with the simulated result of BEED model for the Teton Dam only.

Before discussing about the validated result of above parameters, it is necessary to introduce again at this stage the various nondimensional numbers used in the present analysis (which are introduced in Chapter-IV) namely:

1. Q-peak number ( $Q_{PN}$ )
2. Q-peak-sediment number ( $Q_{PSN}$ )
3. Q-peak-cross-sectional number ( $Q_{APN}$ )
4. Sediment resisting velocity number ( $V_{SRN}$ )
5. Capacity-inflow number ( $CAP_N$ )
6. Shield's entrainment number ( $\tau_{*c}$ )

**TABLE 5.2a**  
**VARIOUS NON-DIMENSIONAL NUMBERS FOR THE EXPERIMENTS**  
**CONDUCTED ON DAM MODELS (Dam Models with Cohesionless Soil)**

S. No	Run Nos.	$Q_{PN}$	$Q_{APN}$	$Q_{PSN}$	$V_{SRN}$	$CAP_N$	$(\tau_c)$
1	1005	0.02820	0.00416	0.296	0.0140	0.00239	0.0729
2	0805	0.03170	0.00423	0.279	0.0152	0.00769	0.0729
3	0705	0.03167	0.00366	0.220	0.0166	0.00880	0.0729
4	0505	0.08170	0.00802	0.427	0.0188	0.00324	0.0729
5	0405	0.06980	0.00560	0.256	0.0218	0.00166	0.0729
6	0305	0.17040	0.01320	0.616	0.0214	0.00903	0.0729
7	0105	0.13160	0.00990	0.455	0.0218	0.00921	0.0729
8	3004	0.06580	0.00500	0.230	0.0218	0.00970	0.0729
9	2904	0.16950	0.01378	0.632	0.0217	0.00904	0.0729
10	2804	0.36700	0.05530	2.540	0.0217	0.00590	0.0729
11	2604	0.34300	0.09700	4.450	0.0217	0.00190	0.0729
12	2504	0.37100	0.06620	3.040	0.0217	0.01060	0.0729

**TABLE 5.2b**  
**VARIOUS NON-DIMENSIONAL NUMBERS FOR THE EXPERIMENTS**  
**CONDUCTED ON DAM MODELS (Dam Models with Cohesive Soil)**

S. No	Run No.	$Q_{PN}$	$Q_{APN}$	$Q_{PSN}$	$V_{SRN}$	$CAP_N$	$(\tau_c)$
1	1203	0.1060	0.028	0.640	0.0440	0.00295	0.1612
2	2703	0.0550	0.016	0.436	0.0372	0.00350	0.1612
3	0404	0.0449	0.014	0.404	0.0342	0.00330	0.1612
4	1104	0.0441	0.032	0.446	0.0315	0.00410	0.1612
5	2204	0.1000	0.111	1.037	0.0310	0.01880	0.1612

$$(\tau_c) = \frac{(\tau_{0c})_{cohesion} + (\tau_{0c})_{friction}}{\Delta \rho \, g d_{50}}$$

The calculated numerical values of these numbers for Teton Dam and Huaccoto dam are given in table 5.2(c).

TABLE 5.2c  
VARIOUS NONDIMENSIONAL  
NUMBERS FOR TETON AND HUACCOTO DAMS

Number	Teton Dam	Huaccoto Dam
$Q_{PN}$	0.2488	0.1161
$Q_{PSN}$	9.1325	0.13259
$Q_{APN}$	0.086	0.000768
$V_{SRN}$	0.00943	0.005796
$CAP_N$	11.185	-
$(\tau_{*c})$	0.162	0.0703
$V_{SR}$ (cm/sec)	28.48	23.679
$A_D \sqrt{g(B_{cr})_f}$		
$Q_{in}$	10421.59	-
$A_D \sqrt{gD_{cr}}$		
$Q_{in}$	6549.87	-
$A_D \sqrt{g \sqrt{A_{cr}}}$		
$Q_{in}$	7550.39	-

$$\text{where } Q_{PN} = \frac{Q_{wp}}{\sqrt{gH_D^5}} \quad CAP_N = \frac{\bar{Q}_{in} H_D}{\text{Capacity} * V_{SR}}$$

$$Q_{PSN} = \frac{Q_{wp}}{A_D V_{SR}}$$

$$Q_{APN} = \frac{Q_{wp}}{A_D \sqrt{gH_D}} \quad \tau_{*c} = \frac{(\tau_{oc})_{combined}}{\Delta \rho g d_{50}}$$

$$V_{SRN} = \frac{V_{SR}}{\sqrt{gH_D}} \quad V_{SR} = \sqrt{\frac{\Delta \rho}{\rho_w} g d_{50} \tan \phi + \frac{c}{\rho_w}}$$

## 5.2 Comparison of Estimated Breach Variables

### a. Duration of Breach ( $t_{95}$ )

Duration of breach is taken as the time taken for the 95% of the soil to be eroded by the overtopping flood and denoted as  $t_{95}$ . The multiple regression analysis is carried out with the present experimental data and field data of Teton Dam for different possible parameters and finally it was found that the  $V_{SRN}$  is the dominant parameter which correlate with magnitude of the breach duration well. Since there is an inconsistency in the duration of Huaccoto dam breach, as reported in literature, this data is not used in the analysis. From the regression result of laboratory data and Teton Dam data it is found that the non-dimensional duration of breach time ( $t_{95}$ ) taken as  $t_{95} \left( \frac{g}{H_D} \right)^{0.5}$  varies proportional to  $V_{SRN}^{1.67}$ . Then the functional relation among them is found out to be with regression coefficient,  $R = 0.896$  as:

$$t_{95} \sqrt{\frac{g}{H_D}} = V_{SRN}^{1.67} \times 4328650 \quad (5.1)$$

Figure. 5.2 shows a good correlation between experimental data and observed data of Teton dam in the form of Equation (5.1). Table 5.3 shows comparison of estimated breach duration with observed and BEED simulated result for Teton dam failure.

TABLE 5.3  
COMPARISON OF ESTIMATED DURATION OF BREACH ( $t_{95}$ )  
WITH OBSERVED TETON DAM DATA

Output Variable	Regression Scenario	Teton Dam			
		Estimated	Observed	BEED	%error
Breach duration	Lab Data alone	1.46	1.5	1.35	2.7
$t_{95}$ (hours)	Lab+Teton dam data	1.5	1.5	1.35	0

The percentage of error listed in Table 5.3 for the estimated value of the variable is with respect to its observed value.

### b. Peak Breach Outflow Discharge ( $Q_{WP}$ )

Peak outflow discharge of a breach ( $Q_{WP}$ ) is one of the important parameters used in the analysis of breach process and in estimation of breach dimensions. Regression analysis is carried out to find major influencing parameters in developing relation for  $Q_{WP}$ . Major influencing parameters are  $A_D$ ,  $\bar{Q}_{in}$ ,  $H_D$ , Capacity of the reservoir,  $V_{SR}$  and  $\tau_{*c}$ .

$$\tau_{*c} = [(\tau_{oc})_{cohesive} + (\tau_{oc})_{cohesionless}] / (\Delta \rho g d_{50})$$

where  $\tau_{oc}$  is the tractive shear resistance offered by the sediment bed. The  $(\tau_{oc})_{cohesionless}$  can be found from Shield's diagram knowing  $d_{50}$ ,  $\gamma_s$  and  $\gamma_w$ . But there is no direct approach to get the tractive shear stress for cohesive soil. So with this limitation, to get  $(\tau_{oc})_{cohesive}$ , it is taken to be 15% higher than shear strength of soil as reported by Raudkivi (1990) in the book 'Loose Boundary Hydraulics', (page-318). Hence  $(\tau_{oc})_{cohesive} = 1.15 c$ . The calculation of  $\tau_{*c}$  is shown in appendix , where  $c$  is cohesive stress of the soil. Here again, in the case of Huaccoto Dam, inflow information is not available. From multiple regression of experimental result it is found that  $Q_{WP}$  depends on  $\bar{Q}_{in}$  along with height of the dam, capacity of the reservoir, cross-sectional area of the dam, Shield's parameter and soil resisting velocity ( $V_{SR}$ ). Since average inflow into the reservoir of Huaccoto dam is not available, its data is not used in regression analysis. Data of Teton dam and the laboratory experimental data are taken for regression analysis. The functional relation obtained as per regression analysis is indicated in Figure 5.3 and given in Equation (5.2) as:

$$\frac{Q_{WP}}{A_D \sqrt{g H_D}} = \left[ \tau_{*c}^{2.78} \times \left( \frac{\bar{Q}_{in} H_D}{Cap V_{SR}} \right)^{0.22} \right]^n \times k \quad (5.2)$$

The values of  $n$  and  $k$  along with estimated values of  $Q_{WP}$ , and their corresponding observed value and simulated value are also listed in Table 5.4. Figure 5.3 contains only the second case as indicated in Table 5.4.

TABLE 5.4

COMPARISON OF THE PRESENT ESTIMATED VALUE OF  $Q_{WP}$  FOR TETON DAM BREACH WITH OBSERVED AND COMPUTED VALUE BY BEED MODEL

Regression Scenario	Values of n, k in Eqn 5.2		$Q_{WP}$ ( $m^3/sec$ ) For Teton Dam breach			
	n	k	Estimated	Observed	BEED	% Error
Present Exp. data	0.89	5.07	67,028	65,000	68,581	3.12
.Present + Obsv.	0.89	4.93	66,390	65,000	68,581	2.1
Teton Dam Data						

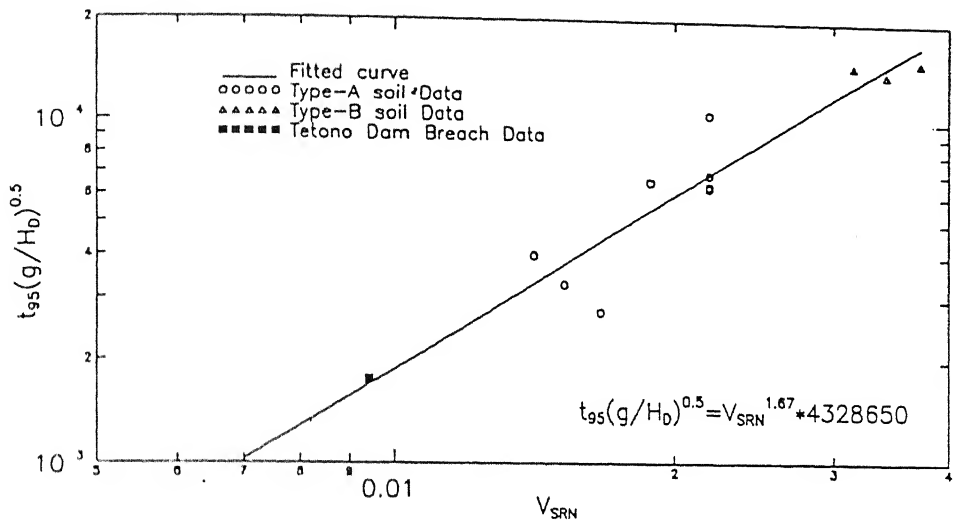


Fig. 5.2: Variation of nondimensional duration of breach ( $t_{95}$ ) with soil resisting velocity number ( $V_{SRN}$ )

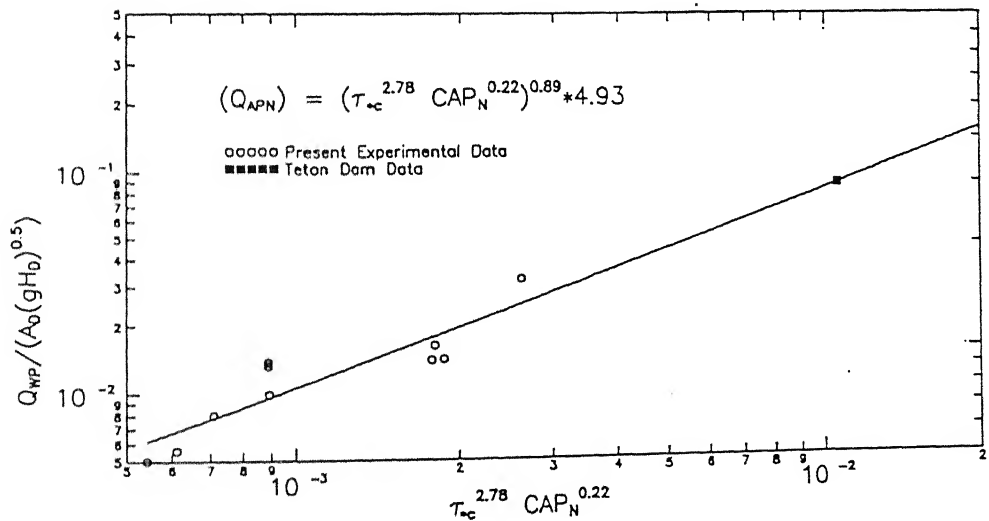


Fig. 5.3: Variation of nondimensional breach peak discharge ( $Q_{WP}$ ) with Shield's entrainment number ( $\tau_{*c}$ ) and reservoir capacity number ( $CAP_N$ )

From the above observation of the value of 'n' and 'k', it may be recommended for further use of the Equation (5.2) with  $n=0.9$  and  $k=5.0$ .

### c. Time of Occurrence of Peak Outflow Discharge ( $t_{wp}$ )

It is essential to know the time required for the maximum breach outflow to occur in a given condition to monitor the flood downstream. Regression of lab data, Teton dam and Huaccoto dam data indicates that  $t_{wp}$  is a function of  $t_{95}$ ,  $V_{SRN}$ , Shield's entrainment number ( $\tau_{*c}$ ) and peak outflow number ( $Q_{PN}$ ). The relation is given in functional form as indicated in Equation (5.3).

$$\frac{t_{wp}}{t_{95}} = 0.035 \Phi_1^{1.2} \quad (5.3)$$

$$\text{where } \Phi_1 = \left[ (V_{SRN})^{1.67} \times (\tau_{*c})^{-0.36} * Q_{PN} \right]$$

The results are also shown in Figure 5.4. The relation developed for  $t_{wp}$  in Equation (5.3) includes the Huaccoto dam data. A comment on the inclusion of Huaccoto dam data in the analysis is necessary. Since the ratio  $t_{wp}/t_{95}$  is used for regression analysis, any errors in  $t_{wp}$  and  $t_{95}$  may cancel out to certain extent. This can be observed from Figure 5.4. Error in estimation of  $t_{wp}$  is shown in Table 5.5. Large error in the estimation of Huaccoto dam is an indication of uncertainty of the observation of  $t_{wp}$ .

**TABLE 5.5**  
**COMPARISON OF ESTIMATED TIME OF OCCURRENCE OF PEAK OUTFLOW DISCHARGE ( $t_{wp}$ ) FOR TETON DAM AND HUACCOTO DAM WITH OBSERVED AND SIMULATED VALUE BY BEED MODEL**

Output Variable	Regression Scenario	Teton Dam				Huaccoto Dam			
		Estimated	Observed	BEED	%error	Estimated	Observed	BEED	%error
Time to Peak outflow Discharge ( $t_{wp}$ ) hour	Lab + Teton + Huaccoto Dam	1.27	1.5	1.35	15.3	22.8*	≈17.5	N.A	30.3

\* Observed value of  $t_{95}$  is used in the calculation.  
N.A = Not available

### d. Width of Breach ( $B_{cr}$ )<sub>f</sub>

Final breach width is one of the major breach morphological features. It represents erosive power of the breach flow discharge in embankment fill. It also gives a qualitative picture of the breach process. From the regression study of Teton dam data and present experimental

data the functional relationship among  $(B_{cr})_f$ ,  $Q_{PN}$  and  $\tau_{*c}$  is shown in Equation (5.4). The relation among them is shown in Figure 5.5.

$$\frac{(B_{cr})_f}{H_D} = f \left\{ \tau_{*c}^{0.5} \times Q_{PN}^{0.35} \right\} \quad (5.4)$$

Here  $\tau_{*c}$  contain both the component of tractive shear stress, due to the effect of cohesion ( $c$ ) and friction( $\phi$ ) of the soil. The functional relation for different situations are presented below.

$$\left. \begin{aligned} \frac{(B_{cr})_f}{H_D} &= 1.2 \ln(\tau_{*c}^{0.5} \times Q_{PN}^{0.35}) + 3.9 \text{ (Only lab data)} \\ \frac{(B_{cr})_f}{H_D} &= 0.99 \ln(\tau_{*c}^{0.5} \times Q_{PN}^{0.35}) + 3.56 \text{ (Lab and Teton dam data)} \\ \frac{(B_{cr})_f}{H_D} &= 0.74 \ln(\tau_{*c}^{0.5} \times Q_{PN}^{0.35}) + 3.0 \text{ (Lab, Teton dam and Huac cot o dam data)} \\ \frac{(B_{cr})_f}{H_D} &= 0.87 \ln(\tau_{*c}^{0.5} \times Q_{PN}^{0.35}) + 3.5 \text{ (Re commended)} \end{aligned} \right\} \quad (5.5)$$

Final estimated breach width for Teton and Huaccoto dam is compared with observed value and that of BEED model simulation value in Table 5.6.

**TABLE 5.6**  
**COMPARISON OF ESTIMATED FINAL TOP BREACH WIDTH  $(B_{cr})_f$**   
**FOR TETON DAM AND HUACCOTO DAM WITH OBSERVED AND**  
**SIMULATED VALUE BY BEED MODEL**

Output Variable	Regression Scenario	Teton Dam				Huaccoto Dam			
		Estimated	Observed	BEED	%error	Estimated	Observed	BEED	%error
Final top Breach	Only Lab Data	206.0	200	295	+3	72	200~230	298.5	66
Width $(B_{cr})_f$ (m)	Lab+Teton Data	202.0	200	295	+1	77	200~230	298.5	64
	Lab+Teton +Huaccoto	182.9	200	295	-2.2	146.8	200~230	298.5	38.6
	Recommended	212.5	200	295	+6.3	168	200~230	298.5	22

From the comparison of the estimated result with observed, the one which gave least percentage error is recommended for use. The recommended equation for the computation of final breach width is:



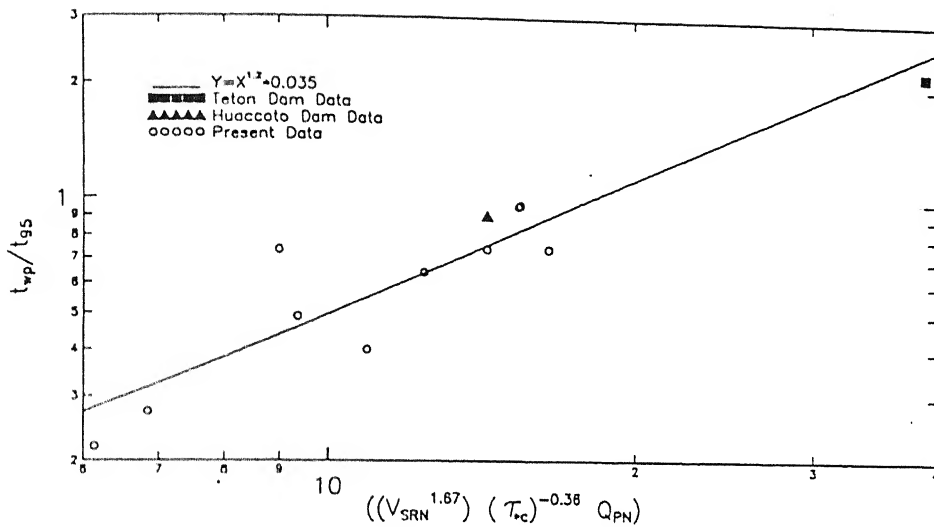


Fig. 5.4: Variation of nondimensional time of occurrence of breach peak discharge ( $t_{wp}$ ) with Shield's entrainment number,  $\tau_{*c}$  and  $Q_{PN}$ , soil resisting velocity number,  $V_{SRN}$

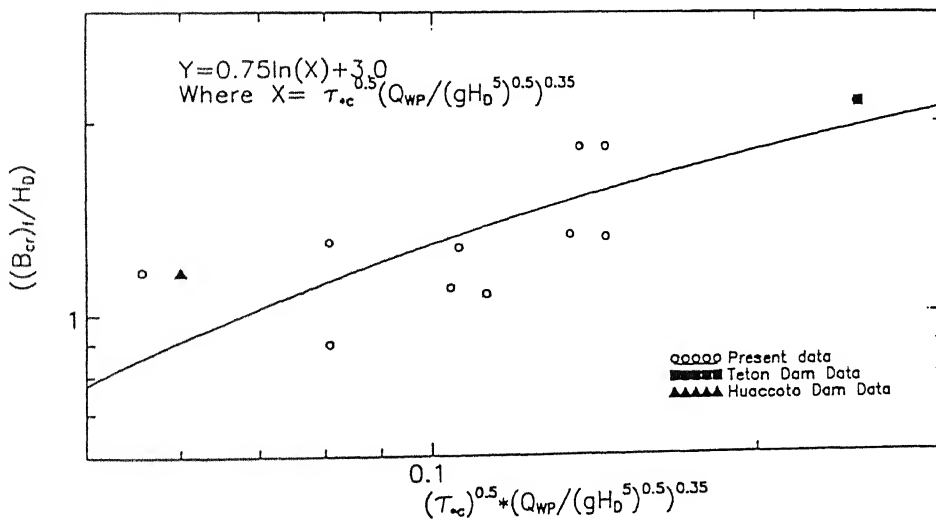


Fig. 5.5: Variation of nondimensional final top breach crest width,  $(B_{cr})_f$  with Shield's entrainment number,  $\tau_{*c}$  and  $Q_{PN}$

$$\frac{(B_{cr})_f}{H_D} = 0.87 \ln(X) + 3.5 \quad (5.6)$$

$$\text{where, } X = \tau_{*c}^{0.5} \times Q_{PN}^{0.35}$$

In the recommended relation slightly higher value of  $(B_{cr})_f$  for Teton dam is accepted to get a nearer value to Huaccoto Dam data.

#### e. Depth of Breach ( $D_{cr}$ )

From the observation of the results obtained from regression analysis of the experimental data, it is found that the  $(B_{cr})_f$ , the maximum lateral erosion is closely related with maximum vertical erosion ( $D_{cr}$ ) and the relation among them is shown in Figure 5.6 and the functional relation between them may be written as:

$$\frac{(B_{cr})_f}{D_{cr}} = [Q_{PSN} \times V_{SRN}^{3.32}]^{0.053} * 4.47 \quad (5.7)$$

TABLE 5.7  
COMPARISON OF FINAL BREACH DEPTH ( $D_{cr}$ )  
FOR TETON AND HUACCOTO DAM BREACH

Output Variable	Regression Scenario	Teton Dam				Huaccoto Dam			
		Estimated	Observed	BEED	%error	Estimated	Observed	BEED	%error
Final Depth of	Lab+Teton	90.6	79	93	+14.7	97.8	107	85	-8.6
	Eqn 5.7								
Breach ( $D_{cr}$ ) (m)	Recommended	84.6	79	93	+7.1	91.1	107	85	-14.8
	Eqn 5.8								

Equation (5.7) is slightly modified as Equation (5.8) and it is recommended for use.

$$\frac{(B_{cr})_f}{D_{cr}} = [Q_{PSN} \times V_{SRN}^{3.0}]^{0.05} \times 4.42 \quad (5.8)$$

Recommendation is based on minimum error indicated in Teton dam breach.

#### f. Side Slope of the Final Breach Cross-section (z)

During the experiments it is observed that the breach flow cross section remains trapezoidal at the crest for most of the breach duration. The side slope of the final breach cross-section is expressed as one vertical: z horizontal (1V:zH). Crest being the controlling section of flow through the breach, it is essential to predict the final possible side slope of the breach cross

section for a given condition. From the regression analysis of the present experimental data some field data including Teton dam data, it is found that the side slope of the cross section is a function of maximum lateral and vertical breach erosion dimensions as well as height of the dam and peak breach discharge ( $Q_{WP}$ ). Their relation is shown in Figure 5.7 and the relation between them be written as:

$$z = e^{2.523\psi_1} \times 0.107 \quad (5.9)$$

$$\text{where, } \psi_1 = \left[ \frac{D_{er}}{H_D^{0.65} (B_{cr})_f^{0.35}} \right]^{1.49} \times Q_{PN}^{-0.06}$$

Using Equation (5.9) and the calculated value of  $D_{er}$  and  $(B_{cr})_f$  from recommended relations, the final side slope of breach section is compared with the observed and the result of the BEED model in Table 5.8 as shown below.

**TABLE 5.8**  
**COMPARISON OF ESTIMATED SIDE SLOPE OF BREACH CROSS-SECTION FOR TETON DAM AND HUACCOTO DAM FAILURE**

Output Variable	Regression Scenario	Teton Dam				Huaccoto Dam			
		Estimated	Observed	BEED	% error	Estimated	Observed	BEED	% error
Final Slope of Breach Cross Section (Z)	Equation 5.9	0.57	0.5	0.675	10	$\cong 0.52$	1.0	1.67	48

It may be noted here that the percentage error for Teton dam is on higher side. Estimation of side slope for Huaccoto dam is relatively very high.

#### g. Peak Sediment Discharge Intensity ( $q_{sp}$ )

Sediment erosion in a breach depends on the magnitude of water discharge and soil properties of embankment. Eroded sediment volume distribution in a breach is studied by nondimensionalising it by its peak value. The magnitude of sediment peak discharge intensity ( $q_{sp}$ ) is computed from the erodible sediment volume and its bulk density. Magnitude of ( $q_{sp}$ ) is never measured in the field during breach. It is always computed using some numerical models. This value for Teton dam breach is computed from BEED model.

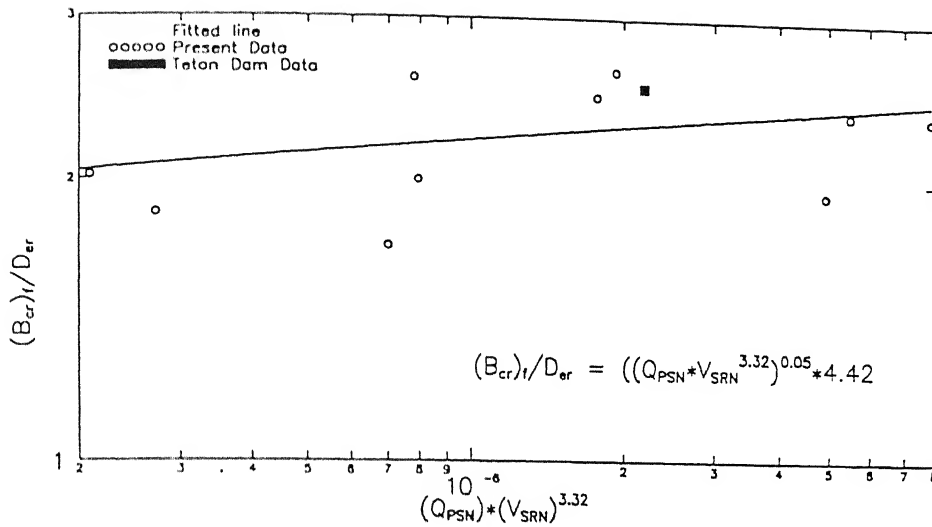


Fig. 5.6: Variation of final breach width to depth ratio at crest with  $Q_{PSN}$  and  $V_{SRN}$  numbers

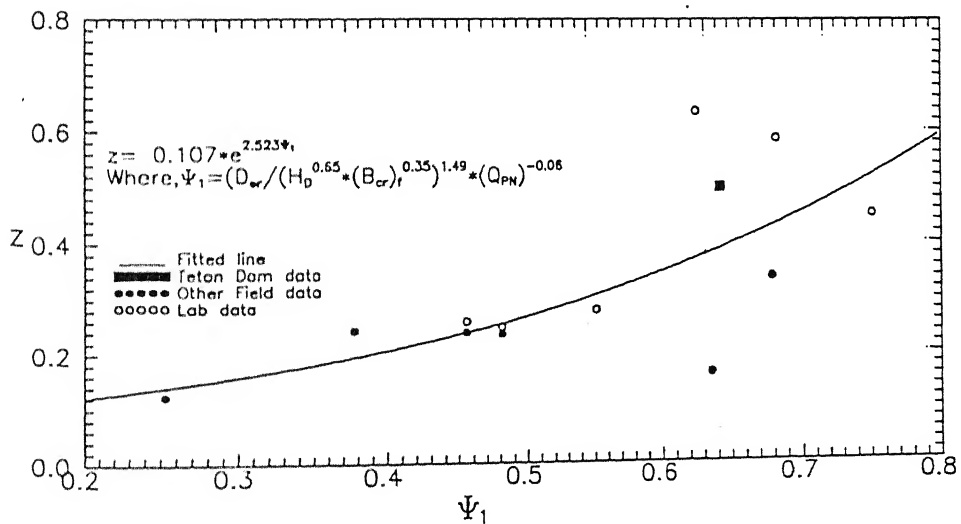


Fig. 5.7: Variation of side slope ( $z$ ) of breach cross section with final depth and width of erosion at crest

The BEED model has numerically simulated the sediment discharge and has found for Teton Dam failure that  $Q_{SP} = 70.53 \times 10^6$  kg/sec. This  $Q_{SP}$  is based on predicted final top breach width of 295m. Based on this peak sediment discharge intensity by BEED model ( $q_{sp}$ ) is worked out to be  $103.95 \text{ m}^3/\text{sec}/\text{m}$ , with average specific weight of soil used for that dam,  $\gamma_b$  is  $2300 \text{ kg}/\text{m}^3$ . The peak sediment discharge intensity is found to be the function of  $Q_{WP}$ , height of the dam ( $H_D$ ) and soil resisting velocity number ( $V_{SRN}$ ) as shown in Figure 5.8(a). The functional relation based on regression analysis of both lab and BEED model's simulated data carried out separately and combinedly, is given as:

$$\frac{H_D q_{SP}}{Q_{WP}} = V_{SRN}^{-2.0} \times 10^{-5} \text{ (for only lab data)} \quad (5.10a)$$

$$\frac{H_D q_{SP}}{Q_{WP}} = V_{SRN}^{-2.2} \times 3.687 \times 10^{-6} \text{ (for lab and Teton Dam data)} \quad (5.10b)$$

In Table 5.9 the sediment peak discharge ( $q_{sp}$ ) of Teton Dam by the present method of estimation is compared with that of simulated BEED result. Percentage of error is quite high. The relation is modified as indicated in Equation (5.10c) to reduce the magnitude of error. The recommended Equation (5.10c) is as follows:

$$\frac{H_D q_{sp}}{Q_{WP}} = V_{SRN}^{-2.25} \times 3.67 \times 10^{-6} \quad (5.10c)$$

**TABLE 5.9**  
**COMPARISON OF ESTIMATED AND SIMULATED BEED**  
**RESULT AND SEDIMENT PEAK DISCHARGE FOR TETON DAM**

		Teton Dam			Huaccoto Dam		
Out put Variables	Regression Scenario	Estimated $10^6$	Simulated BEED Result	% error	Estimated $10^6$	Simulated BEED Result	% error
$q_{sp}$	Only lab Data	79.6	103.95	23	-	-	-
( $\text{cm}^3/\text{sec}/\text{cm}$ )	Lab+Teton Data	74.6	103.95	28	-	-	-
	Recommended	93.8	103.95	9.78	31.9	-	-

\* for the calculation of  $q_{sp}$ ,  $B_{cr} = 295\text{m}$  is used, simulated result of BEED model

Analysis is not carried out for Huaccoto dam breach because of nonavailability of information on simulated value of  $q_{sp}$ .

The simulated sediment discharge  $Q_{SP}$  for Teton dam by BEED model is obtained based on computed final top breach crest width 295m. Hence for the validation of present functional relation for  $q_{sp}$ , the same  $(B_{cr})_f$  value of 295m is chosen instead of the value estimated from the present method.

### h. Time of occurrence of Sediment Peak Discharge ( $t_{sp}$ )

Like  $q_{sp}$ ,  $t_{sp}$  is also another scaled parameter which is to be estimated for sediment discharge prediction with time. From the regression analysis of present data it is noticed that  $t_{sp}$  is closely related to  $t_{wp}$ ,  $Q_{WP}$ ,  $A_D$ , and  $V_{SR}$ . Two different regression scenarios one with only laboratory data and the other with laboratory data and Teton Dam data are undertaken. The functional relations obtained from these two scenarios are as follow:

$$\frac{t_{sp}}{t_{wp}} = 0.27 \ln(Q_{PSN}) + 0.68 \quad (\text{only lab data}) \quad (5.11a)$$

$$\frac{t_{sp}}{t_{wp}} = 0.18 \ln(Q_{PSN}) + 0.56 \quad (\text{lab and Teton Dam data}) \quad (5.11b)$$

In Figure 5.8(b), lab data and Teton dam data are fitted with the Equation (5.11b). A comparative study is presented in the Table 5.10. The estimated value of  $t_{sp}$  in both cases predicts less than BEED simulated value. Equation (5.11b) is modified slightly as given below and recommended for use.

$$\frac{t_{sp}}{t_{wp}} = 0.2 \ln(Q_{PSN}) + 0.6 \quad (5.11c)$$

**TABLE 5.10**  
**COMPARISON OF ESTIMATED TIME OF OCCURRENCE OF SEDIMENT**  
**PEAK DISCHARGE FOR TETON DAM AND HUACCOTO DAM BREACH**

$t_{sp}$ in hours				
Functional Relation from Regression Analysis	Teton dam		Huaccoto dam	
	Present		Present	
	BEED	Estimated	Estimated	Regression Scenario
$\frac{t_{sp}}{t_{wp}} = 0.18 \ln(Q_{PSN}) + 0.56$	1.35	1.22		Lab and Field Data
$\frac{t_{sp}}{t_{wp}} = 0.27 \ln(Q_{PSN}) + 0.68$	1.35	1.56		
Recommended				
$\frac{t_{sp}}{t_{wp}} = 0.2 \ln(Q_{PSN}) + 0.6$	1.35	1.32	4.45	

For Huaccoto dam breach the simulated value of  $t_{sp}$  from BEED model is not available for comparison with present estimated result. From the laboratory embankment breach analysis it is observed that  $t_{sp}$  is always less than  $t_{wp}$ . It means that sediment peak discharge reaches its peak value before the peak water discharge. This observation is in agreement with the findings of Graf and Song (1995) in the study of bed shear stress in non-uniform and unsteady open channel flows.

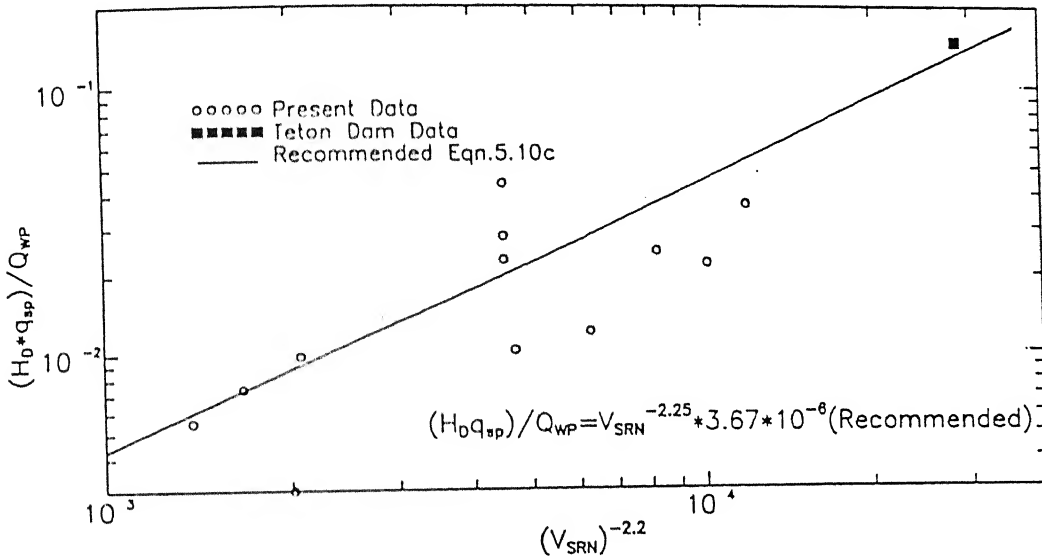


Fig. 5.8(a): Variation of nondimensional sediment peak discharge intensity ( $q_{sp}$ ) with soil resisting velocity number,  $V_{SRN}$

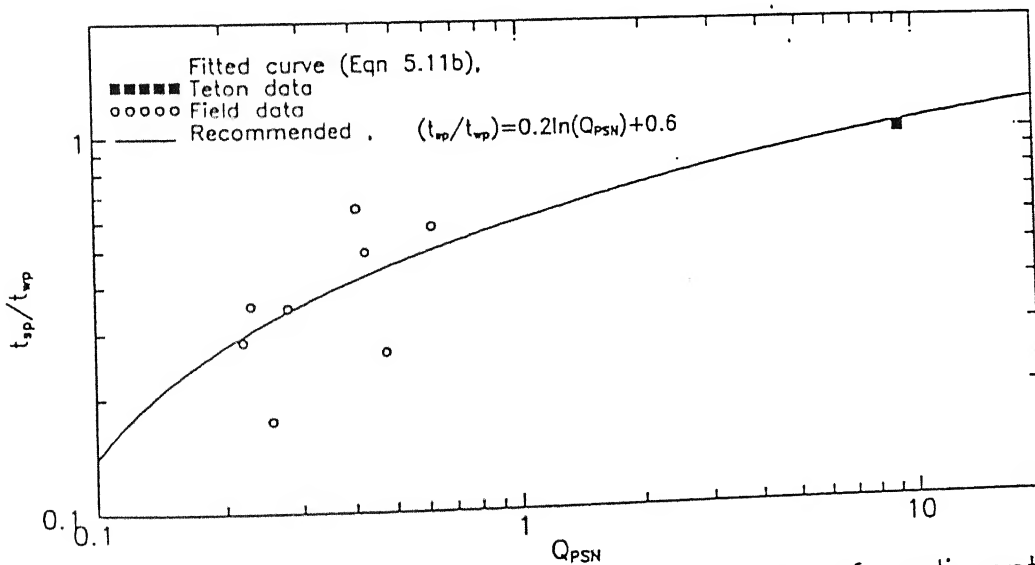


Fig. 5.8(b): Variation of time of occurrence of sediment peak discharge intensity, ( $t_{sp}$ ) in a nondimensional form with  $Q_{PSN}$  number

### 5.3 Influence of Average Inflow Discharge( $\bar{Q}_{in}$ ), Capacity of Reservoir (Cap), and Cross-Sectional area of Embankment ( $A_D$ ) on Final Breach Morphological Parameters

In the comparison of some of the important parameters in dam breach process in last section, it is found that the developed functional relations for Teton dam are in good agreement with these parameters. To improve these relations further the effect of capacity of the reservoir(cap) and the average inflow( $\bar{Q}_{in}$ ) into the reservoir are included in the analysis of final morphological breach parameters like  $(B_{cr})_f$ ,  $D_{er}$ ,  $A_{er}$ , and  $Q_{WP}$ . These final breach parameters are suitably nondimensionlised with  $A_D$  and  $\bar{Q}_{in}$  and plotted against  $V_{SRN}$  as shown in Figures 5.9(a), (b), (c), and (d) respectively. To validate these functional relations again Teton dam is taken into consideration. In case of Huaccoto Dam  $Q_{in} \cong 0$ , as reported (Singh, 1995), hence it is not included in the analysis. The  $\bar{Q}_{in}$  for Teton dam is taken as half of the peak inflow discharge to the reservoir instead of average  $Q_{in}$ . This assumption is used because inflow hydrograph was not available for Teton dam. But one should take average  $Q_{in}$  as:

$$(\bar{Q}_{in}) = \frac{\text{Volume of inflow water}}{\text{Total base time of hydrograph}}$$

In Table 5.11, a comparison between actual and present estimated values of  $(B_{cr})_f$ ,  $D_{er}$ ,  $A_{er}$  and  $Q_{WP}$  is made.

TABLE 5.11  
COMPARISON OF ESTIMATED VARIABLES OF FINAL BREACH  
GEOMETRY FOR TETON DAM BREACH

Equation Used	$\frac{A_D \sqrt{g(B_{cr})_f}}{\bar{Q}_{in}}$	$\frac{A_D \sqrt{gD_{er}}}{\bar{Q}_{in}}$	$\frac{A_D \sqrt{g\sqrt{A_{er}}}}{\bar{Q}_{in}}$	$Q_{PSN}$
Observed	10,421.6	6549.87	7550.89	9.133
With Lab Data Regression	4,688.99	3834.57	4138.11	6.2
Lab+Teton Data Regression	6,576.9	4173.8	5350.54	8.8
Modified	10,301.2	5,984.2	7432.3	9.06



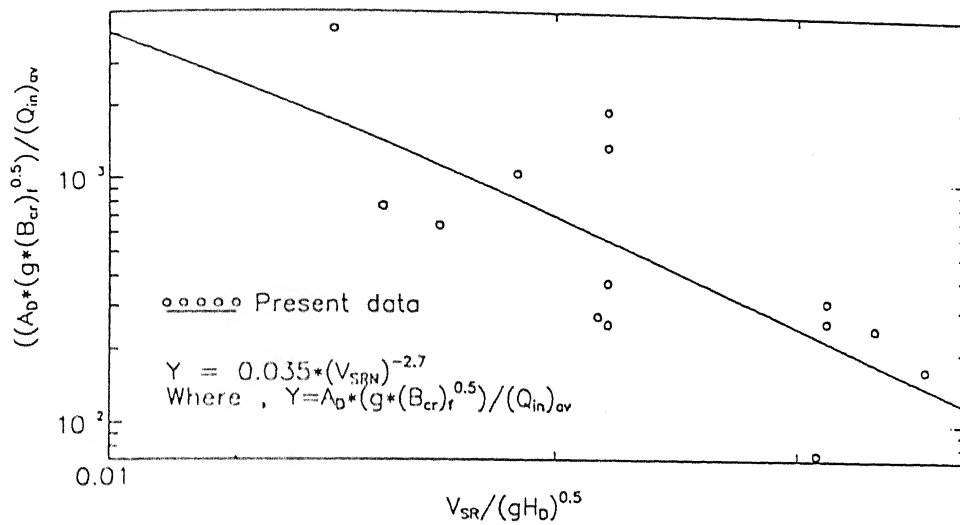


Fig. 5.9(a): Variation of nondimensional final breach crest width by average inflow discharge with soil resisting velocity number( $V_{SRN}$ )

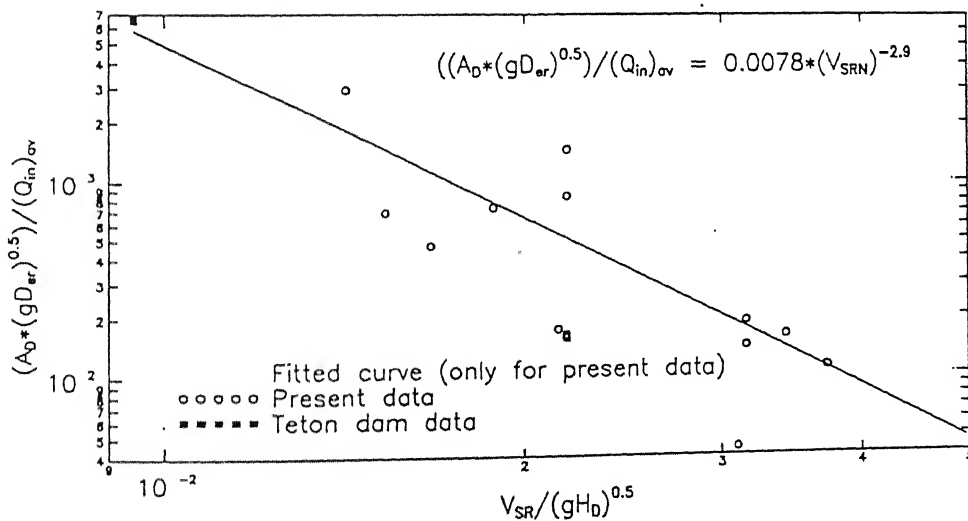


Fig. 5.9(b): Variation of nondimensional final depth of erosion at crest( $D_{er}$ ) by average inflow discharge with soil resisting velocity number( $V_{SRN}$ )

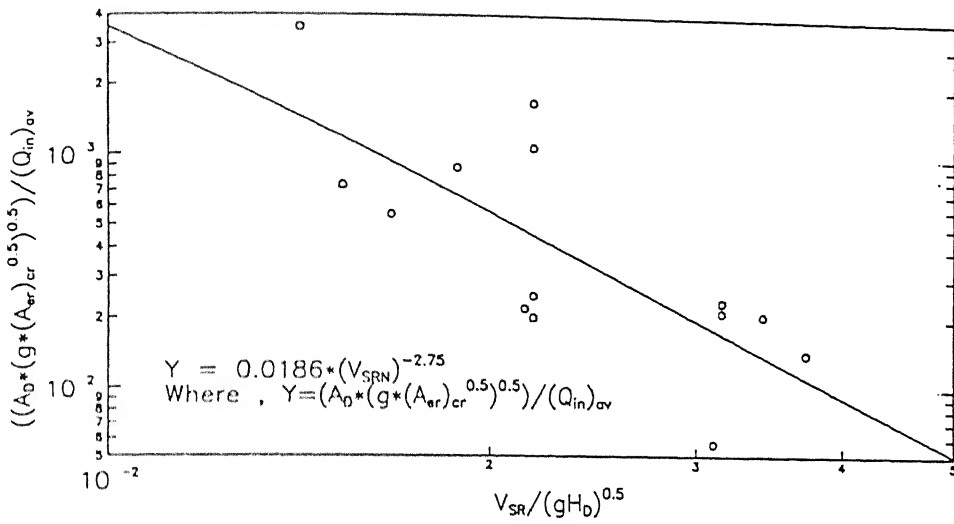


Fig. 5.9(c): Variation of nondimensional final eroded crest area ( $A_{er}$ ) by average inflow discharge with soil resisting velocity number ( $V_{SR}$ )

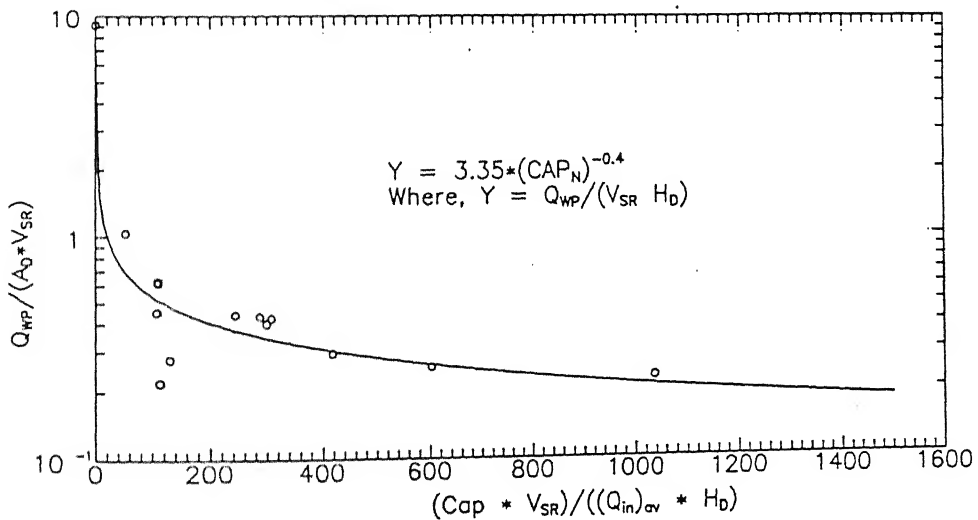


Fig. 5.9(d): Variation of nondimensional peak breach discharge ( $Q_{WP}$ ) with capacity number ( $CAP_N$ )

**TABLE 5.12**  
**FUNCTIONAL RELATIONS FOR FINAL BREACH GEOMETRY**  
**WITH DIFFERENT REGRESSION SCENARIO**

	From Lab Data Only	Lab data with Teton Dam Data	Modified
$\frac{A_D \sqrt{g(B_{cr})_f}}{\bar{Q}_{in}} =$	$V_{SRN}^{-2.87} \times 0.01$	$V_{SRN}^{-2.54} \times 0.0336$	$V_{SRN}^{-2.7} 0.035$
$\frac{A_D \sqrt{gD_{cr}}}{\bar{Q}_{in}} =$	$V_{SRN}^{-3.0} \times 0.0035$	$V_{SRN}^{-2.81} \times 0.078$	$V_{SRN}^{-2.9} \times 0.008$
$\frac{A_D \sqrt{g} \sqrt{A_{cr}}}{\bar{Q}_{in}} =$	$V_{SRN}^{-2.89} \times 0.0076$	$V_{SRN}^{-2.64} \times 0.0186$	$V_{SRN}^{-2.75} \times 0.02$
$Q_{PSN} =$	$CAP_N^{-0.4} \times 3.35$	$CAP_N^{-0.353} \times 2.64$	$CAP_N^{-0.4} \times 3.4$

The functional relationship evolved from regression analysis for the final morphology are as shown in Table 5.12. Three different regression scenarios belonging to: only with laboratory data, laboratory data and Teton dam data together, and the modified relationship are presented. Modified functional relationship is recommended for use.

## 5.4 Breach Hydrograph

The basic aim of this study is to know the variation of the breach discharge with time in addition to the morphological features of the dam breach. Keeping this in mind the breach outflow hydrograph is computed as stated earlier for each experimental run both for cohesive and cohesionless soil model. In those cases, dam geometry and inflow into the reservoir are varying along with the properties of dam fill materials. From the earlier analysis it is quite evident that the flow through the breach of the dam is controlled by breach morphology. Again the breach morphology is itself a function of dam geometry, inflow condition and the properties of the dam fill like soil resisting velocity ( $V_{SR}$ ) and Shield's entrainment number ( $\tau_{*c}$ ). But, the overall the trend of the flow hydrograph is more or less same, having a rising limb, peak and then a falling limb, though the shape of the rising and falling limb of the

hydrograph are different, depending on the above three influencing parameters. The rising limb reaches its peak very steeply whereas falling limb comes to a equilibrium level gradually. To fit a curve to the hydrograph and to generalise the equation to the fitted curve the following approach has been adopted.

- i. Time versus discharge hydrograph for all the runs are normalised with  $t_{wp}$  and  $Q_{wp}$  as shown in Figure 5.10.
- ii. For the values of  $Q_w/Q_{wp}$ , 0.8, 0.7, 0.6 and 0.4,  $t/t_{wp}$  values are obtained for rising limb and falling limb separately for all the runs of experiment conducted including cohesive and cohesionless soil models.

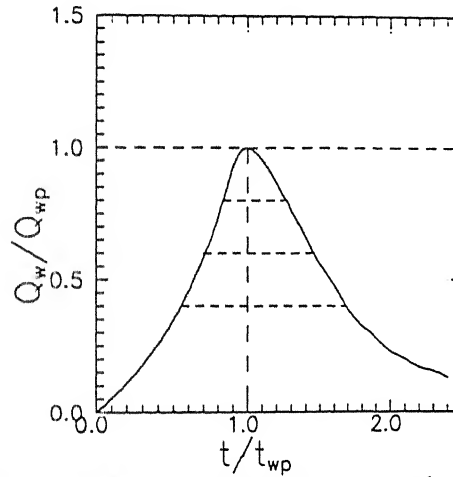


Fig. 5.10: Definition Sketch showing how  $m_{wr}$  and  $m_{wf}$  are computed

- iii. From the observation it is found that this non-dimensional  $t/t_{wp} \sim Q_w/Q_{wp}$  plots follows a curve of the nature:

$$Y = x^m e^{(1-x^m)} \quad (5.12)$$

$$\text{where } Y = \frac{Q_w}{Q_{wp}} \text{ and } x = \frac{t}{t_{wp}}$$

The 'm' value is different for rising ( $m_{wr}$ ) and falling ( $m_{wf}$ ) limb for a particular run and magnitudes of  $m_{wr}$  and  $m_{wf}$  depend on inflow characteristics, dam geometry and the properties of dam fill materials.

Figures 5.11(a) and (b) are developed as an aide to compute directly the magnitude of  $m_{wr}$  and  $m_{wf}$  by knowing  $t/t_{wp}$  and their corresponding  $Q_w/Q_{wp}$ . These curves are developed from Equation (5.12). These average values of  $m_{wr}$  and  $m_{wf}$  controls the shape and nature of flow

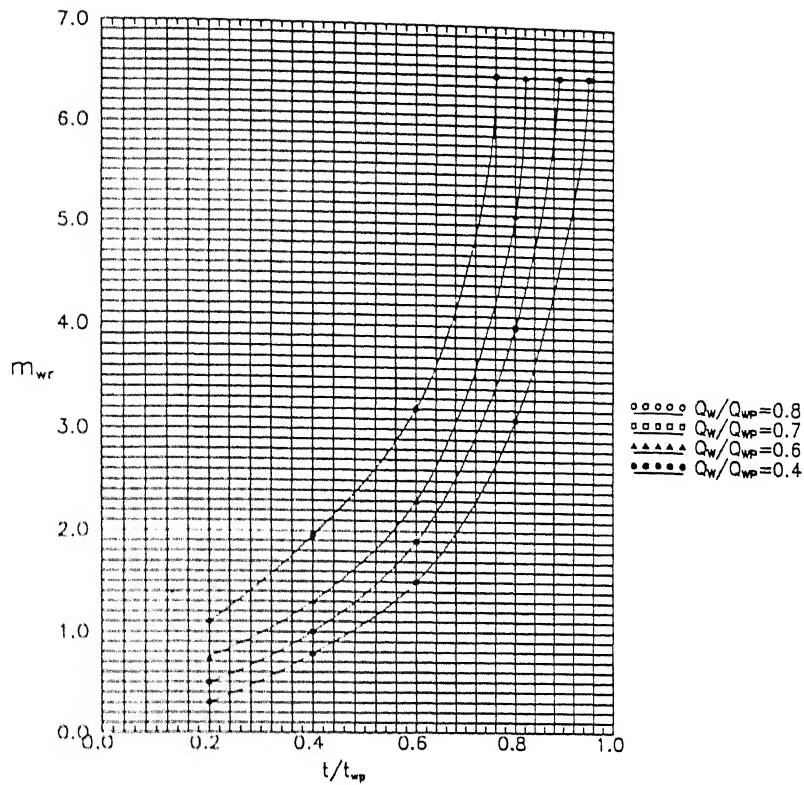


Fig. 5.11(a): An aid to compute  $m_{wr}$  for known  $Q_w/Q_{wp}$  and its corresponding  $t/t_{wp}$

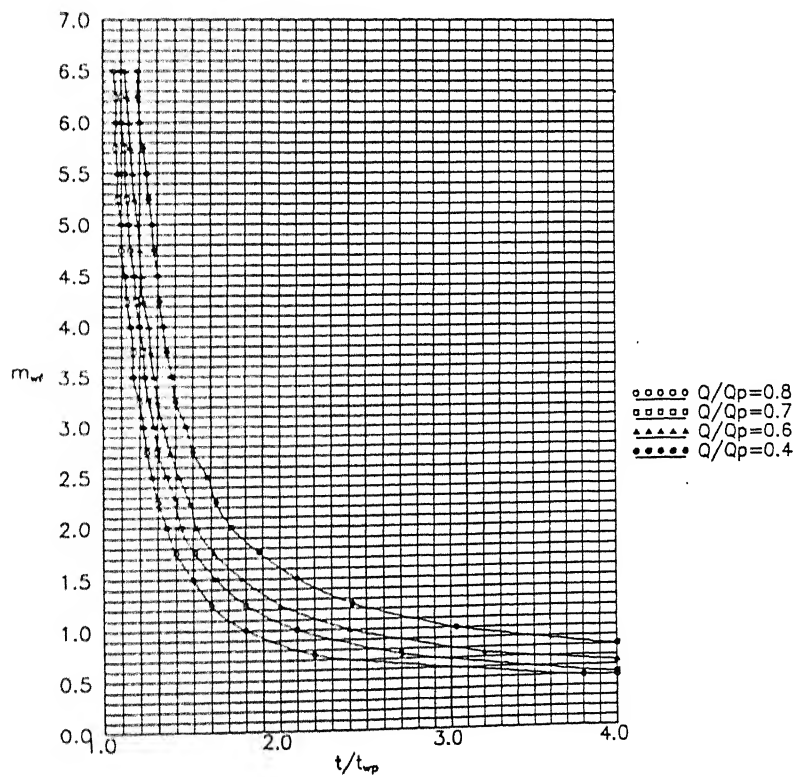


Fig. 5.11(b): An aid to compute  $m_{wf}$  for a known  $Q_w/Q_{wp}$  and its corresponding  $t/t_{wp}$

hydrograph. The average values of  $m_{wr}$  and  $m_{wf}$  are also obtained for two field data, Teton Dam and Huaccoto Dam. These average  $m_{wr}$  and  $m_{wf}$  values are found to be the function of  $\tau_{*c}$  and  $V_{SRN}$  from regression analysis. From regression analysis the following relations are developed:

$$\left. \begin{aligned} m_{wr} &= 0.0415(\tau_{*c}^{0.615} \times V_{SRN}^{0.72})^{-1.0} \\ \text{and } m_{wf} &= 0.0078(V_{SRN})^{-1.454} \end{aligned} \right\} \quad (5.13)$$

The functional relations in Equation (5.13) are shown in Figures 5.12(a) and (b) respectively.

For the validation of this methodology, two sample hydrograph of run no. 2703 (dam model with cohesive soil) and run no. 1005 (dam model with cohesionless soil) are tested with the observed hydrograph as shown in Figures 5.13(a) and (b). The agreement is encouraging. Applying the same approach to the observed outflow hydrograph of Teton dam and Huaccoto dam breach shown in Figures 5.14(a) and (b),  $m_{wr}$  and  $m_{wf}$  are computed using Equation (5.13). These values are listed below.

	Average $m_{wr}$	Average $m_{wf}$
Teton Dam	3.66	3.03
Huaccoto Dam	6.00	7.25

Comparison of normalised outflow hydrograph predicted from the present analysis with observed data and BEED model for Teton Dam is carried out in Figure 5.15(a). It may be observed that predicted rising limb from the present analysis is not in close agreement with observed data. The falling limb of the present analysis predicts fairly close to the observed value. Further it may be observed that the BEED model data predicts rising limb in close agreement with observed data whereas its falling limb deviates considerably.

Similar comparison for normalised outflow hydrograph for Huaccoto dam is shown in Figure 5.15(b). It may be observed that the predicted rising limb deviates slightly from both observed and BEED model data, whereas the falling limb agrees fairly close with observed and BEED model data. In the Huaccoto dam out flow hydrograph analysis, the value of  $t_{wp}$  used in the predicted curve is taken from the observed value.

From the validation of  $Q_{wp}$  with time in the present approach, nonconformity of the present result in rising limb may be observed. This is because of the nonavailability of more

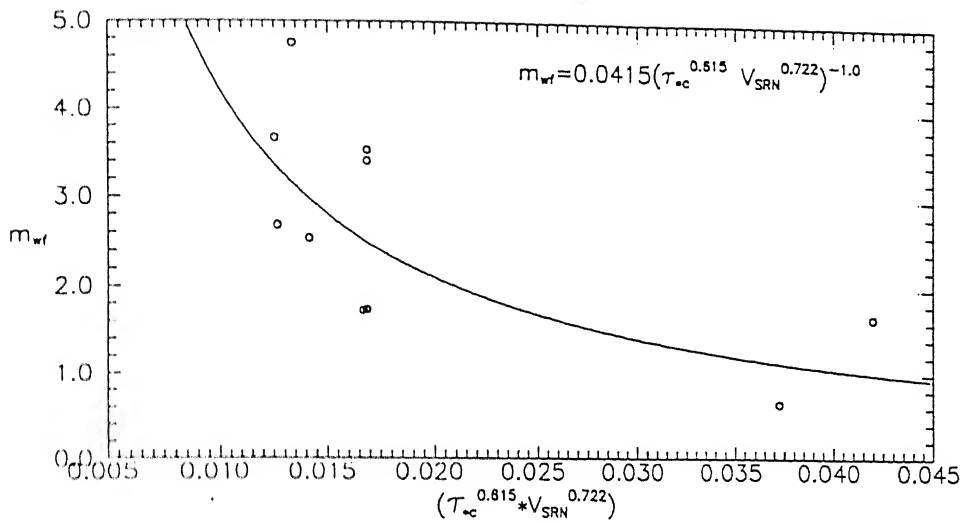


Fig. 5.12(b): Variation of exponent ( $m_{wf}$ ) for falling limb of normalised hydrograph as per eqn 5.12 with Shield's entrainment number and soil resisting velocity number ( $V_{SRN}$ )

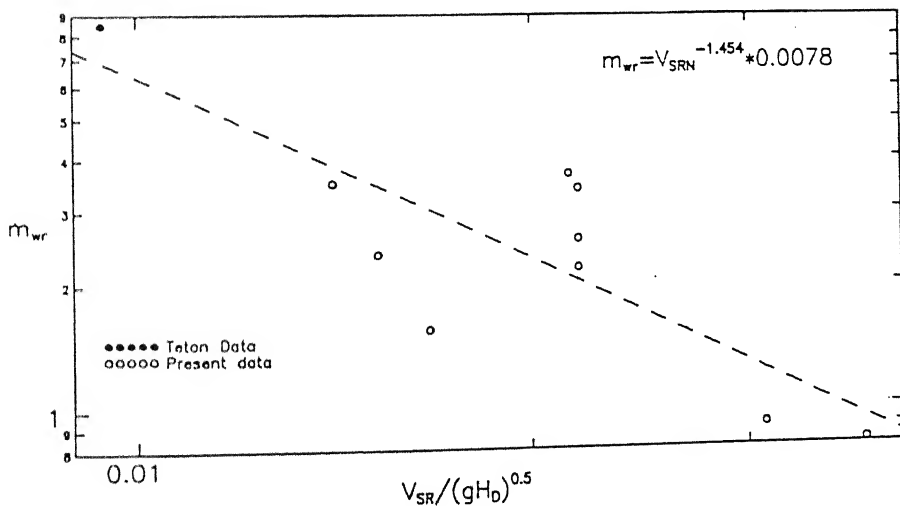


Fig. 5.12(a): Variation of exponent ( $m_{wf}$ ) for rising limb of normalised hydrograph as per eqn 5.12 with soil resisting velocity number

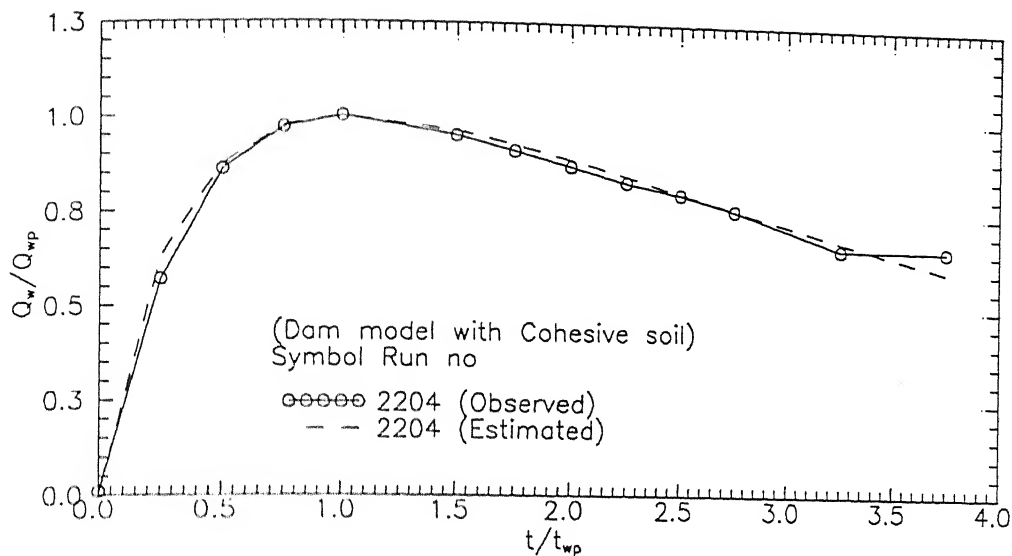


Fig. 5.13(a): Comparison of observed normalised hydrograph with its estimated value for run no. 2204, dam model with cohesive soil

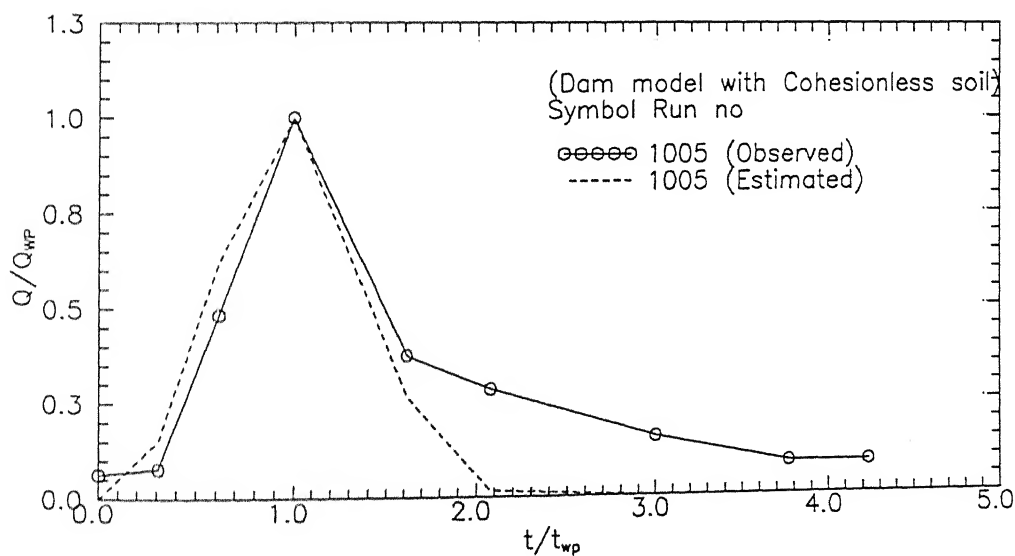


Fig. 5.13(b): Comparison of observed normalised hydrograph with its estimated value for run no. 1005, dam model with cohesionless soil



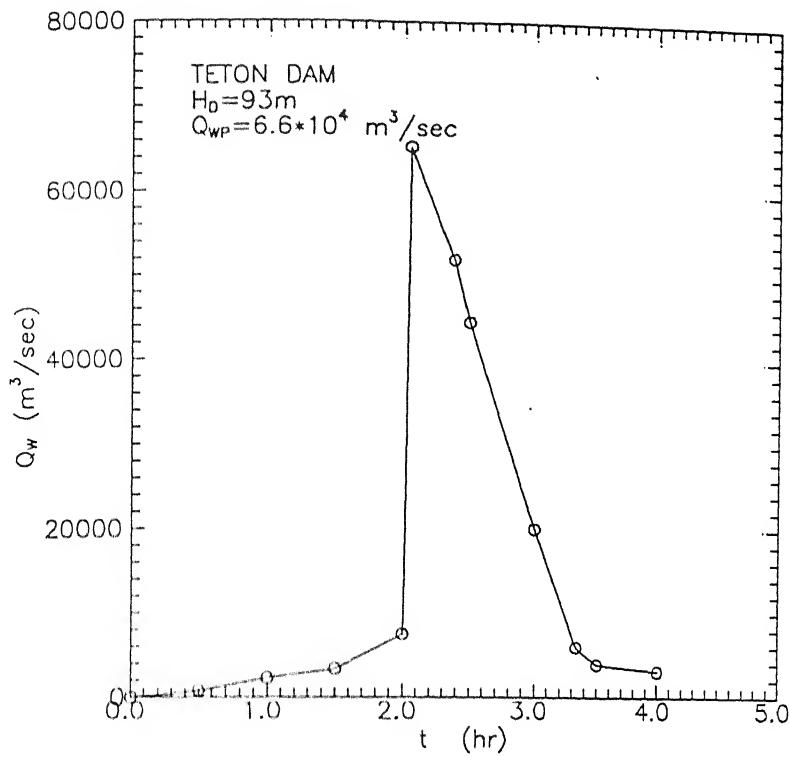


Fig. 5.14(a): Observed breach hydrograph for Teton dam

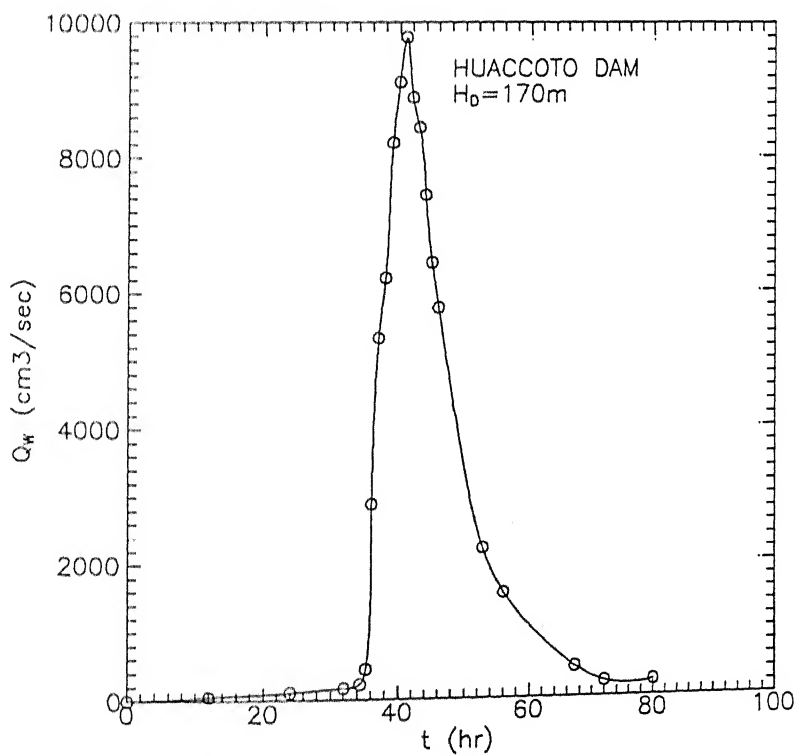


Fig. 5.14(b): Observed breach hydrograph for Huaccoto dam

field data for prediction of  $m_w$  exponent appropriately. Considering the non-availability of proper data for rising limb of the outflow hydrograph, present result may be accepted with some reservation.

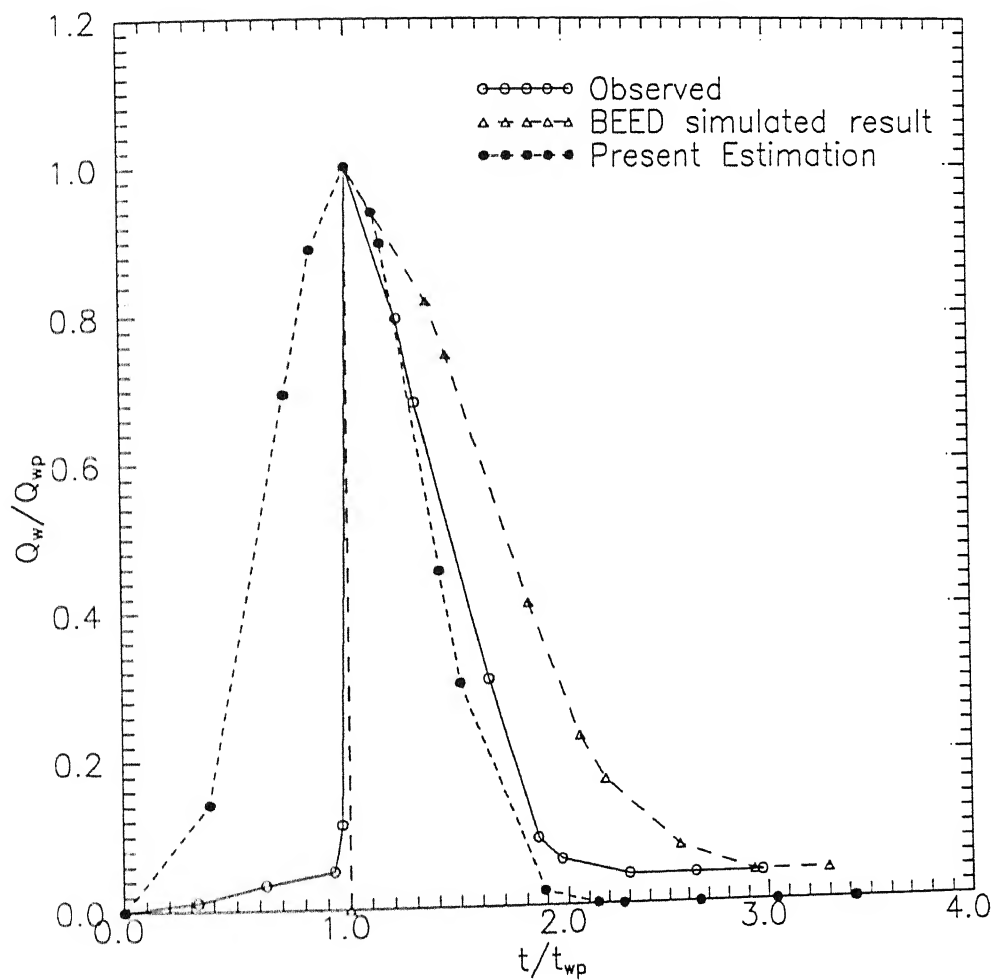


Fig. 5.15(a): Comparison of estimated normalised hydrograph with observed and simulated BEED model's result for Teton dam breach by overtopping flow

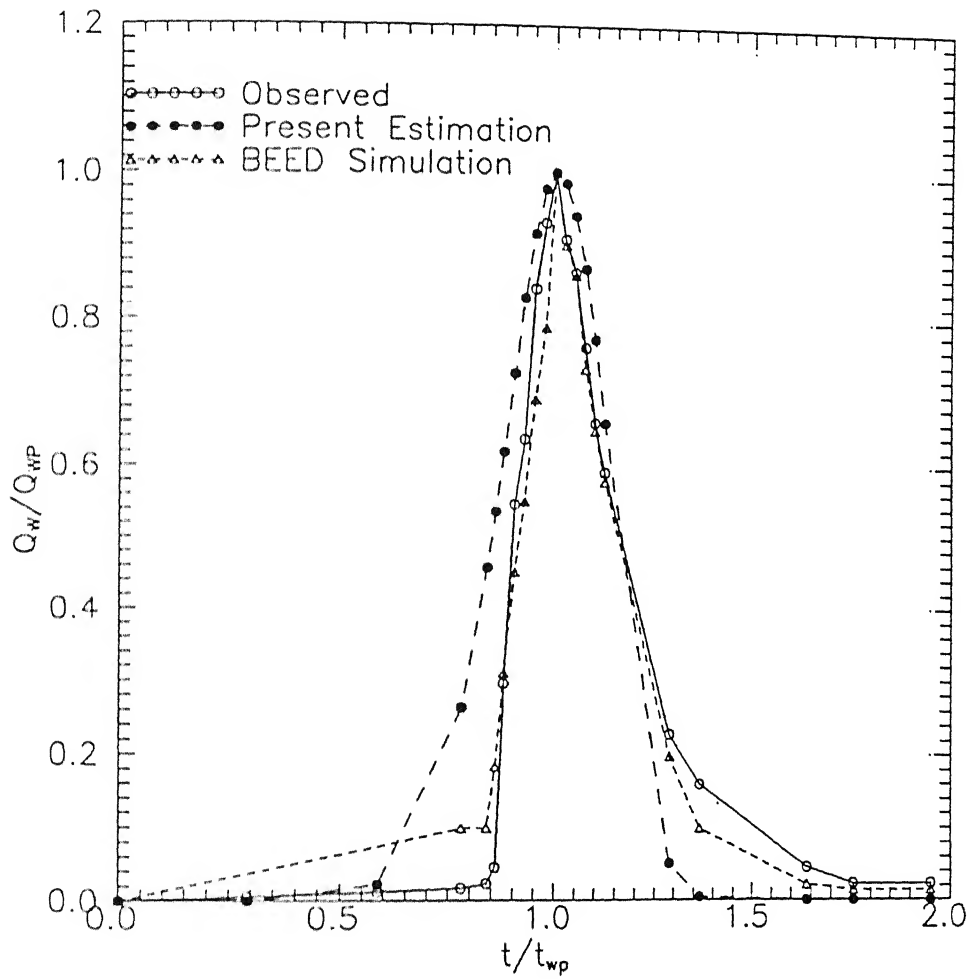


Fig. 5.15(b): Comparison of estimated normalised hydrograph with observed and simulated BEED model result for Huaccoto Dam breach by overtopping flow

## 5.5 Breach Sediment Discharge With Time

The computation of sediment discharge graph due to the dam breach erosion is essential along with water discharge for their downstream routing. The variation of sediment discharge curve with time have very steep rising limb and steep falling limb in cohesionless soil dam model whereas in cohesive soil models, the rising limb and falling limb of sediment discharge with time are gradual. Analysis of sediment discharge variation with time is carried out on similar lines of breach out flow hydrograph.

Adopted procedure to compute  $Q_s$  :

- First, time versus  $Q_s$  graphs for different experimental data are normalised with  $t_{sp}$  and  $Q_{SP}$  respectively.
- For the values of  $Q_s/Q_{SP}$ , 0.8, 0.7, 0.6, and 0.4,  $t/t_{sp}$  values are obtained for both rising and falling limb separately for all the runs conducted in the laboratory.
- Knowing  $t/t_{sp}$  values for different  $Q_s/Q_{SP}$  i.e. at 0.8, 0.7, 0.6 and 0.4 the corresponding 'm' values i.e.,  $m_{sr}$  (for rising limb)  $m_{sf}$  (falling limb) are obtained using Equation (5.12). Then the average  $m_{sr}$  and  $m_{sf}$  for each set is used for further analysis.

The  $m_{sr}$  and  $m_{sf}$  values controls the shape of sediment discharge graph with time. There is no field data information on sediment discharge with time. So only lab data are used to develop the functional relation among  $Q_{APN}$ ,  $\tau_{*c}$ ,  $Q_{PN}$ ,  $CAP_N$ , as shown in Figure 5.16(a). The relation among them can be written as:

$$m_{sf} = 12153.7 \xi_{33} \quad (5.14)$$

$$\text{where } \xi_{33} = \left[ Q_{APN}^{3.2} \times \tau_{*c}^{2.33} \times Q_{PN}^{-1.77} \times CAP_N \right]$$

As in most of the experimental runs the rising limb in sediment discharge curve with time is steep, the numerical values of  $m_{sr}$  are almost same. So instead of developing a functional relation among its controlling dam breach parameters, the average value of all  $m_{sr}$  for different runs are taken. This average value works out to be 2.57. Here with caution, it may be noted that this recommended value of  $m_{sr}$  is based on limited experimental observations.

To test this approach, the sediment discharge of Teton dam breach as shown in Figure 5.16(b), simulated by BEED model is considered. From Equation 5.14,  $m_{sf}$  value for Teton Dam is equal to 8.96 and assuming  $m_{sr} \approx 2.57$ , the non-dimensional plot of  $t/t_{sp}$  versus  $Q_s/Q_{SP}$

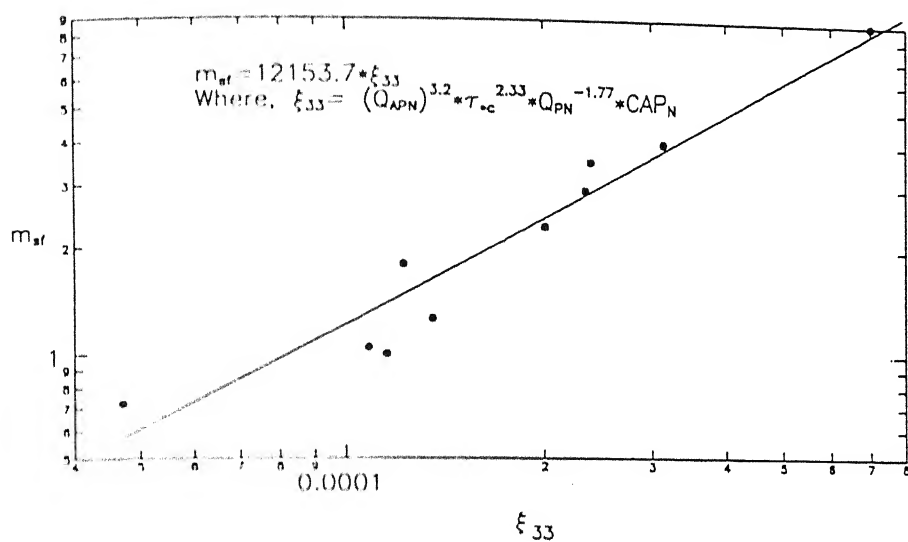


Fig. 5.16(a): Variation of exponent,  $m_{sf}$  in eqn 5.12 for falling limb of normalised sediment discharge graph with Shield's entrainment number, capacity number,  $Q_{PN}$  and  $Q_{APN}$

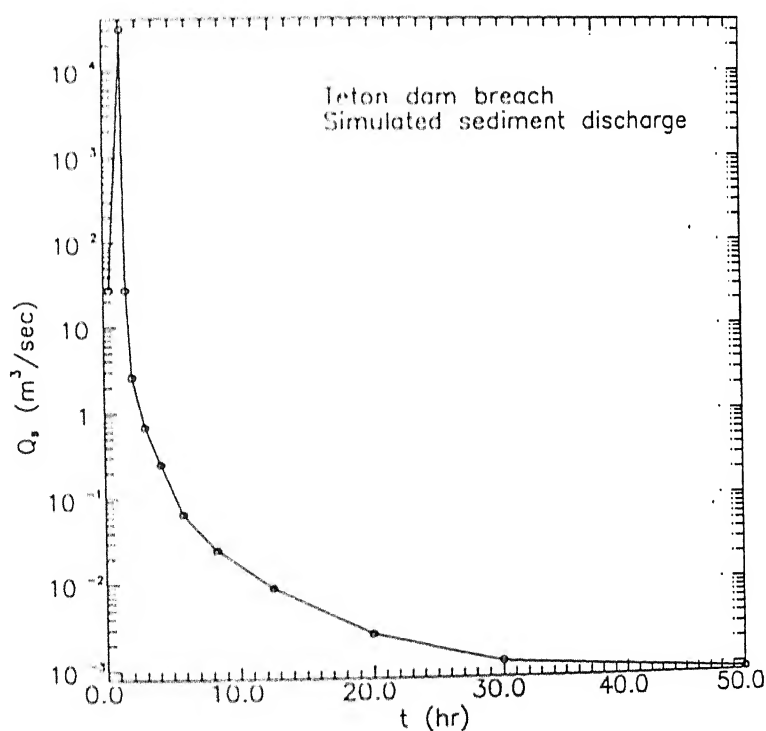


Fig. 5.16(b): Simulated sediment discharge by BEED model with time for Teton dam breach

is plotted in Figure 5.16(c). The present result is superimposed with the simulated result of BEED model for Teton dam breach. The agreement with BEED model data is fairly close except towards the end of the breach process. As there is no observed information on  $Q_s$  for Teton dam, it can not be concluded about the accuracy of the present result.

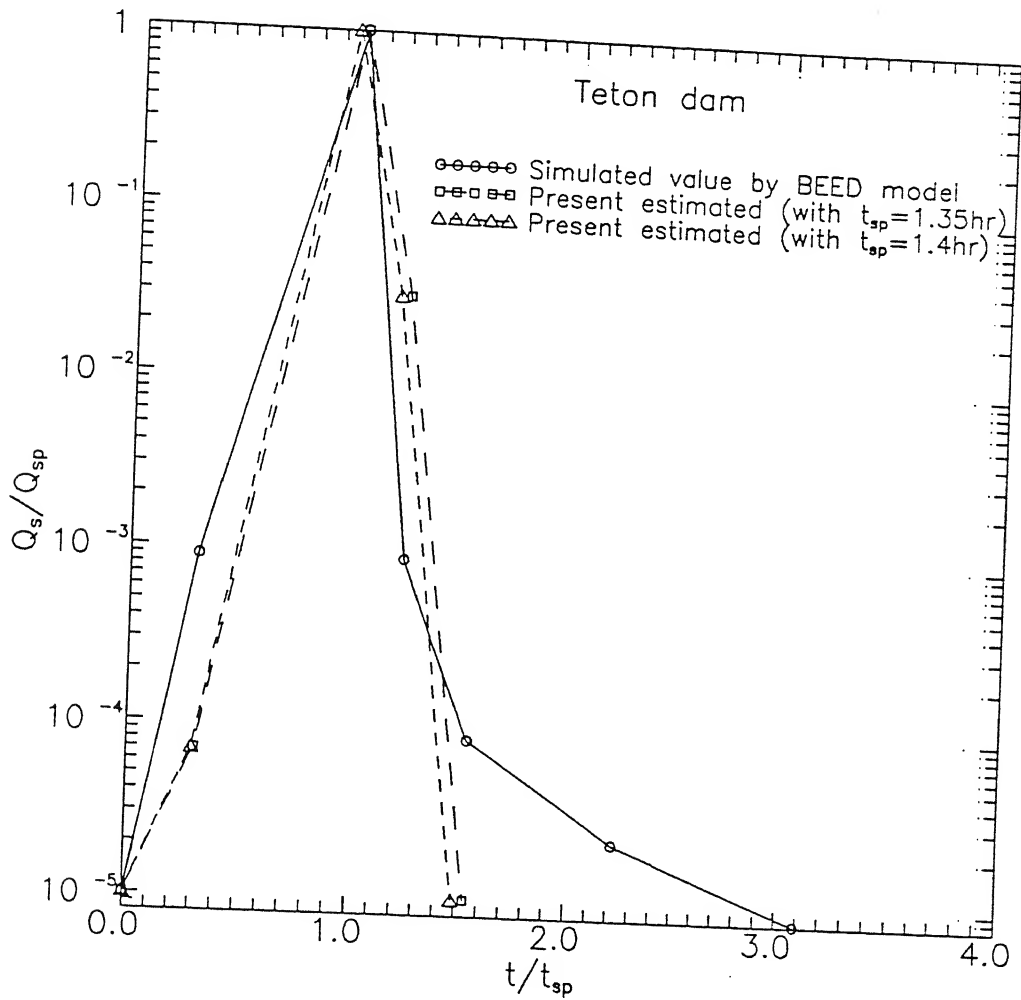


Fig. 5.16(c): Comparison of present estimated normalised sediment discharge graph with simulated result of BEED model for Teton dam

## 5.6 Suggested Procedure to Compute the Dam Breach Process

From the analysis and discussion in the previous chapter and present chapter, it is understood that the dam breach process can be seen from three broad angles, i.e. breach morphology, breach hydraulics and breach erosion. for a given condition. All of them are implicitly related. To express the breach criterion variables like water discharge and sediment discharge, some implicit functional relations are developed from the observed data. This methodology can be used for any given field situation with fair degree of prediction of the breach characteristics due to overtopping flood. This algorithm can suitably be converted to a computer code on dam breach analysis.

### a. Methodology for Computation of Parameters Governing the Breach Process

- i. From the given predictor variables like capacity of the reservoir,  $\bar{Q}_{in}$ ,  $H_D$ ,  $L_{DB}$ ,  $A_D$ , and dam fill properties  $\gamma_b$ ,  $c$ ,  $\phi$ , and  $d_{50}$  the following non-dimensional parameters can be found out:  $CAP_N$ ,  $\tau_{*c}$ ,  $V_{SRN}$ .
- ii. Peak breach discharge ( $Q_{Wp}$ ) and breach duration( $t_{95}$ ) can be obtained from Equation (5.2), Figure 5.3.
- iii. Predicting  $Q_{Wp}$  the following nondimensional numbers:  $Q_{PN}$ ,  $Q_{APN}$ ,  $Q_{PSN}$  can be computed.
- iv. The  $\eta$  can be computed knowing  $V_{SRN}$  from Equation (4.20b), Figure 4.38(c).
- v. The reservoir level corresponding to  $h_{up}$ ,  $h_{wr*}$  can be computed knowing  $h_{wrm}$ , from Figure 4.38(d), Equation (4.20c).
- vi. Reservoir level at any time of breach, ( $h_{wr}$ ), can be obtained knowing  $t_{95}$ ,  $V_{SRN}$ ,  $Q_{PSN}$  and  $t_*$  corresponding to  $h_{wrm}$  from Equation 4.17b, Figure 4.34(b). Reservoir time scale,  $t_*$  can be obtained from Figure 4.34(d), Equation (4.17c).
- vii. Knowing  $h_{up}$ ,  $h_{wr}$ ,  $h_{wr*}$ , and  $h_{wrm}$ ,  $h_u$  at any instant of breach can be found out from Figure 4.40(b), Equation (4.20c)
- viii. Knowing  $h_u$  and  $h_{cm}(h_{wr} - h_u)$  at any time of breach,  $c_d$  can be obtained for  $h_u/h_{cm}$  from Figure 4.27(b).

ix. Knowing  $h_u$  and  $c_d$ ,  $q_w$  can be computed from Figure 4.27(a), Equation (4.13a)

x. Water level at crest can be obtained assuming critical state of flow there,

$$h_{wc} = \left( \frac{q_w^2}{g} \right)^{\frac{1}{3}}$$

xi. Knowing  $h_{wc}$  at any time, drop of water level at crest with respect to  $H_D$  can be calculated. So,  $B_{cr}$  can be obtained from Figure 4.29(a), Equation (4.15a)

xii. So,  $Q_w = q_w * B_{cr}$

xiii. Knowing  $h_{cm}$ ,  $\Delta H_m$ , and  $V_{SRN}$ ,  $\Delta H$  can be found out from Figure 4.36, Equation (4.19a).

xiv. Knowing  $Q_{APN}$ ,  $V_{SRN}$ , and  $t_{95}$ ,  $t_{**}$  can be found out from Figure 4.35(c), Equation (4.18b)

xv. Knowing  $\Delta H$ ,  $L_{DB}$ ,  $V_{SRN}$  and  $h_u$ ,  $dh_{cm}/dt$  can be obtained from Figure 4.37(c), Equation (4.19b).

xvi. From estimated  $t_{95}$ ,  $B_{cr}$ ,  $Q_{PN}$ ,  $B_7$  can be obtained from Figure 4.29(b), Equation (4.15b).  $B_7$  can fairly be taken as equal to  $B_8$ .

xvii. From estimated  $B_8$ ,  $h_{wr}$ ,  $\Delta H$ , and  $Q_w$ ,  $V_w''$  can be computed applying continuity equation. (as,  $h_{wr} - \Delta H = h_w''$ ).

xviii.  $E_2$  can be computed after the estimation of  $V_w''$  and  $h_w''$

xix. Knowing  $E_1 \approx h_{wr}$  and  $E_2$ ,  $\Delta H$ ,  $L_{DB}$  at any time  $(V_*)_{av}$  can be obtained from Figure 4.39, Equation (4.21)

xx. From estimated  $\bar{V}_*$ ,  $g_*^*$  can be computed from Equation (4.22), Figure 4.40,  $Q_s$  for given  $\gamma_b$  can be computed.

xxi. With estimated  $h_u$ ,  $\Delta H$ ,  $\bar{V}_*$  at any instant,  $C = \frac{Q_s}{Q_w}$  can be computed from Figure 4.41, Equation (4.23c). So  $Q_s$  can be obtained knowing the corresponding  $Q_w$ .

xxii. The average of above two values of  $Q_s$  obtained from previous two steps can be taken for further computation.



xxiii. With  $t_{95}, V_{SRN}, \tau_{*c}, Q_{PN}$ , time of occurrence of peak breach discharge ( $t_{wp}$ ) can be computed from Equation (5.3), Figure 5.4.

xxiv. Final top breach width ( $B_{cr})_f$  can be obtained from Figure 5.5, Equation (5.6) for known  $Q_{PN}, \tau_{*c}$

xxv. Final depth of erosion ( $D_{er}$ ) at crest can be calculated from Figure 5.6, Equation (5.8) after computing  $(B_{cr})_f$ .

xxvi. With estimated value of terminal top width erosion  $(B_{cr})_f$  and depth erosion  $(D_{er})$ , the side slope ( $z$ ) of final breach cross section can be obtained from Figure 5.7, Equation (5.9)

xxvi. Peak sediment discharge intensity ( $q_{sp}$ ) can be estimated using Equation (5.10c), Figure 5.8(a) for a known  $Q_{WP}$ .

xxvii. Time of occurrence of peak sediment discharge intensity ( $t_{sp}$ ) can be obtained from Figure 5.8 (b), Equation (5.11c), once  $t_{wp}$  is computed.

With the above procedure, it is possible to predict the following variables at any instant of breach.

- a.  $h_{wr}, h_{cm}$
- b.  $\Delta H, \Delta E$
- c.  $\bar{V}_*$
- d.  $Q_W$  and  $Q_S$

To supplement these results particularly on final breach morphological variables like  $B_{cr}, D_{er}, A_{er}$  and peak breach discharge another approach has been suggested, taking into consideration the average inflow discharge to the reservoir  $\bar{Q}_{in}$  and capacity of the reservoir as follows:

1. Final top breach width at the crest  $(B_{cr})_f$  can be obtained from Figure 5.9(a) for a given  $A_D$  and  $V_{SRN}$ . For its better estimation the average of present estimation and the estimated value in step xxv, can be taken.
2. For a given value of the capacity of the reservoir,  $\bar{Q}_{in}, H_D$ , and  $Q_{PSN}$ , the peak outflow can be obtained from Figure 5.9(d). The average of the value of  $Q_{WP}$  estimated in step ii and present computation can be taken for further use.

3. From Figure 5.9(b), Table 5.12,  $D_{er}$  can be computed for a given  $A_D$ ,  $(Q_{in})_{av}$ . The average of  $D_{er}$  from step xxvi and its present value can be taken.
4. The final area of erosion at crest can be obtained from Figure 5.9(c), Table 5.12 so  $z$  can be obtained for  $(\bar{B}_{cr})_f$  and  $\bar{D}_{er}$ .

**b. Method to Compute Breach Hydrograph and Breach Sediment Discharge graph**

In the section 5.6a, a detailed methodology to compute outflow discharge and sediment discharge with time in the breach knowing dam geometry, and soil properties of embankment fill is given. In addition to this, a method based on the shape of hydrograph given in Equation (5.12) is suggested in this section. This method is tested for two field data namely Teton dam breach and Huaccoto dam breach.

- i. For a given value of  $V_{SRN}$ ,  $\tau_{*c}$ ,  $m_{wf}$ ,  $m_{wr}$  can be computed from Figures 5.12(a) and (b) respectively. The Equations (5.12) can be referred.
- ii. Using the earlier estimation of  $Q_{WP}$  and  $t_{wp}$  in steps ii and xxiii respectively,  $m_{wf}$  and  $m_{wr}$ , the breach water discharge with time can be obtained.
- iii. The value of  $m_{sf}$  can be obtained from Figure 5.14(a), Equation (5.14). For given  $\tau_{*c}$ ,  $CAP_N$  and computed  $Q_{APN}$ . The value of  $m_{sr}$  can be assumed to lie within 2.5 to 3.0. With the earlier estimation of  $q_{sp}$  and  $t_{sp}$  in steps xxvii and xxviii, the sediment discharge at any time can be computed.

**c. Comparison of Overall Estimated Breach Parameters**

The final breach dimensions are depth of erosion  $D_{er}$ , width of erosion  $B_{cr}$  and side slope of the bank ( $z$ ) at the crest of the breach profile. The duration of the breach process is considered as the time taken from the start of erosion till 95 percent of sediment is eroded ( $t_{95}$ ). In the breach process the controlling flow parameters are the magnitude of peak water discharge ( $Q_{WP}$ ), sediment peak discharge intensity ( $q_{sp}$ ) and their corresponding time of occurrence namely  $t_{wp}$  and  $t_{sp}$  respectively. These parameters are computed for Teton dam and Huaccoto

dam data using the procedure suggested in sections 5.6a and 5.6b and are presented in Table 5.13.

**TABLE 5.13**  
**COMPARISON OF ESTIMATED RESULTS FOR**  
**TETON AND HUACCOTO DAM BREACH**

S.NO	Variables	Teton Dam				Huaccoto Dam			
		Estimated	Observed	BEED	% Error	Estimated	Observed	BEED	% Error
1	$Q_{wp}$ $m^3/sec$	67,028	65,000	68,581	+3.12				
2	$q_{sp} \times 10^6$ $cm^3/sec/cm$	93.8	-	103.95	9.75	31.9	-	-	-
3	$t_{95}$ (hr)	1.5	1.5	1.35	0			-	-
4	$t_{wp}$ (hr)	1.27	1.5	1.35	-15.3	22.8	17.8		30.2
5	$t_{sp}$ (hr)	1.32		1.35	+3.6	4.45			
6	$(B_{cr})_f$ (m)	212.5	200	295	+6.3	168	200~300	298.5	22
7	$D_{er}$ (m)	84.6	79	93	+7.1	91.1	107	85	-14.8
8	$z$	0.57	0.5	0.675	+10	0.52	1.0	1.67	-48

This result is presented in a form of bar charts for better overall comparison of estimated results with observed and BEED simulated values for Teton dam in Figures 5.17(a) and (b) and for Huaccoto dam in Figure 5.17(c).

#### **d. Flow Chart for Computation of Breach Process**

The procedure suggested in sections 5.6a and 5.6b for the estimation of variables controlling the breach process is presented in a logical sequence in a form of flow chart shown in Figure 5.18. This flow chart suggest a method of computation in a sequence given as reservoir level( $h_{wr}$ ), crest height of sediment bed level( $h_{cm}$ ), head of water acting over the crest ( $h_u$ ), breach width at the crest( $B_{cr}$ ), breach water discharge( $Q_w$ ), drop in water level ( $\Delta H$ ), energy loss ( $\Delta E$ ), average shear velocity( $\bar{V}_*$ ) and sediment discharge ( $Q_s$ ).

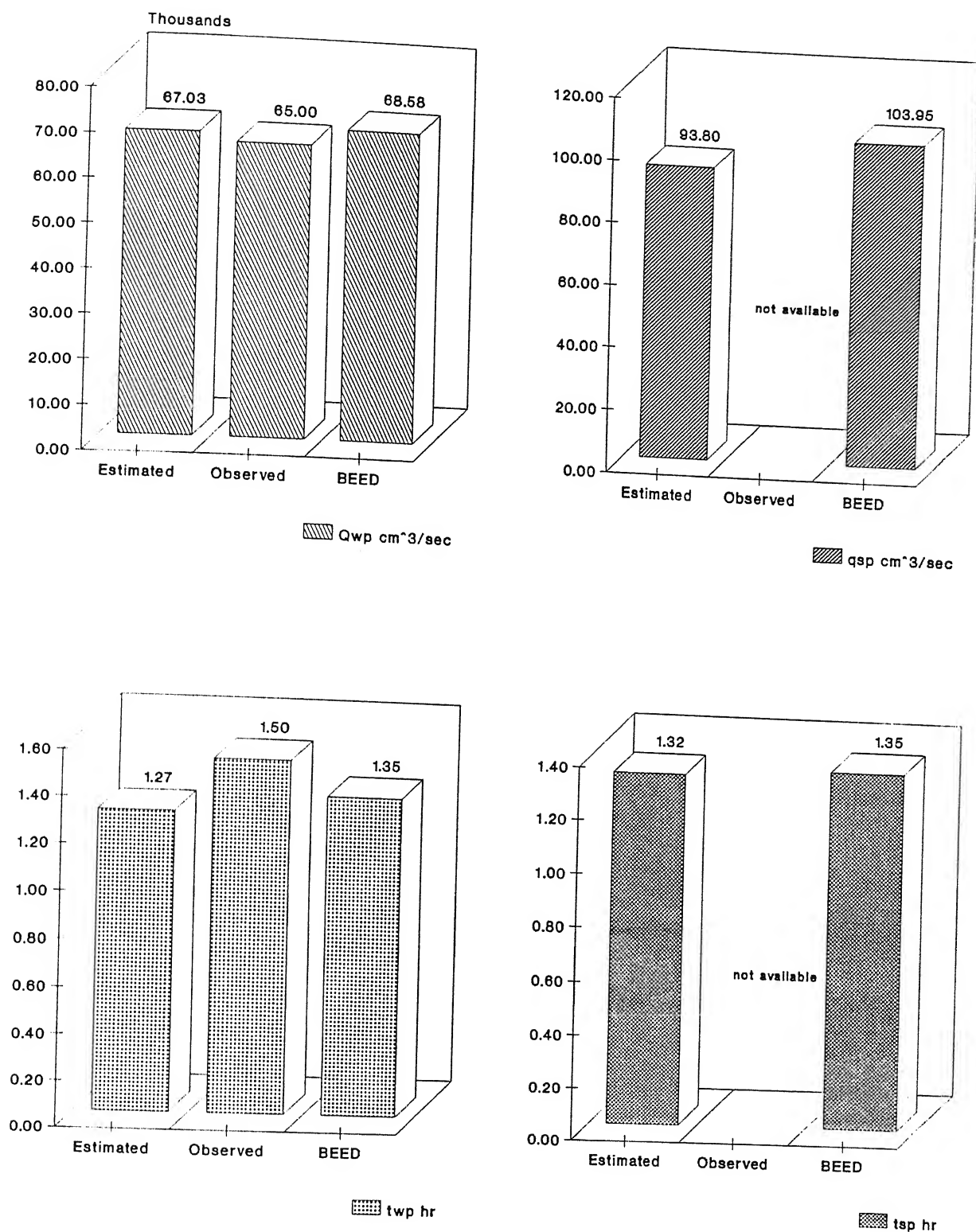


Fig. 5.17(a): Comparison of estimated flow parameters for Teton dam breach with observed and simulated values of BEED model

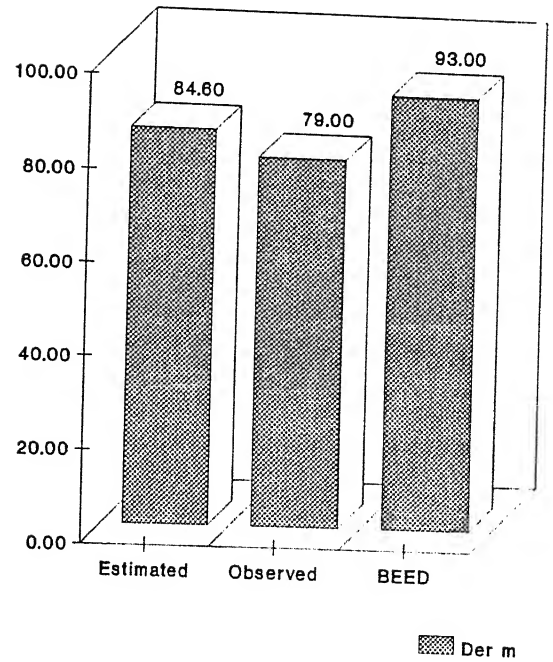
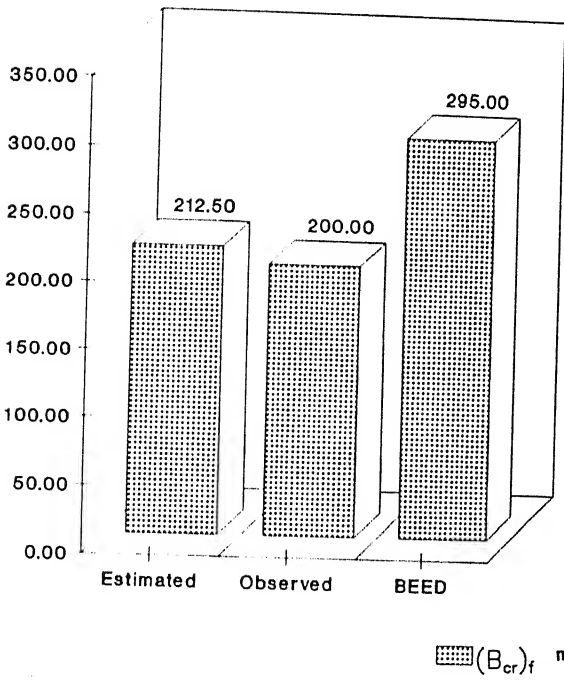
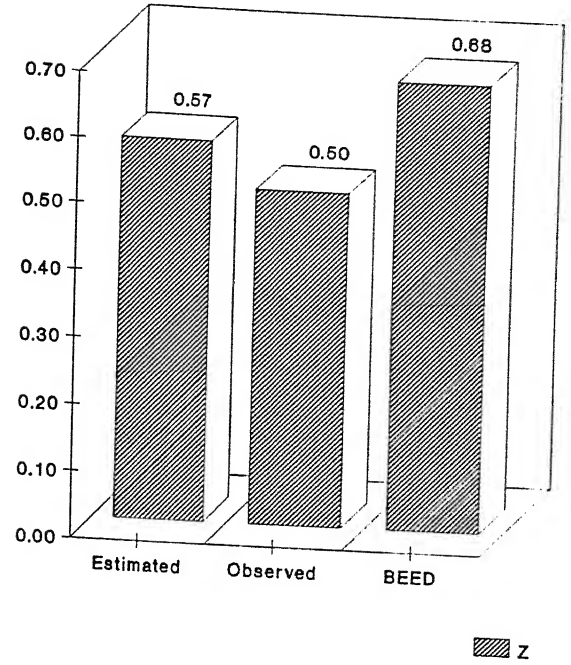
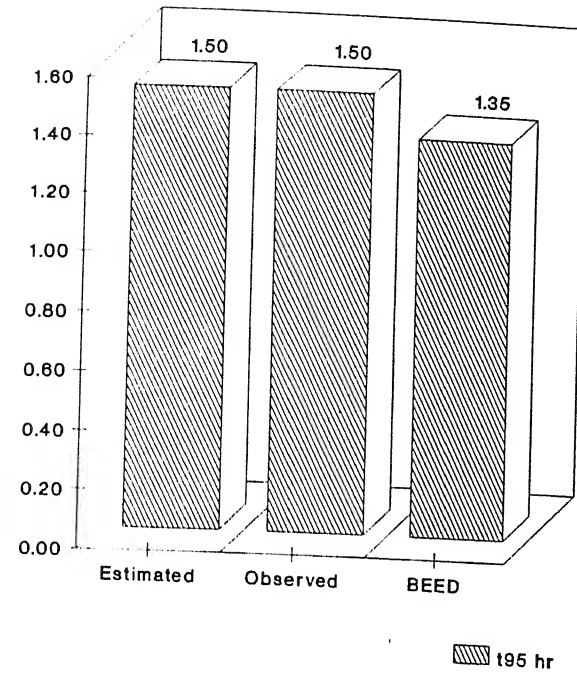


Fig. 5.17(b): Comparison of estimated final breach dimensions for Teton dam breach with observed and simulated value of BEED model

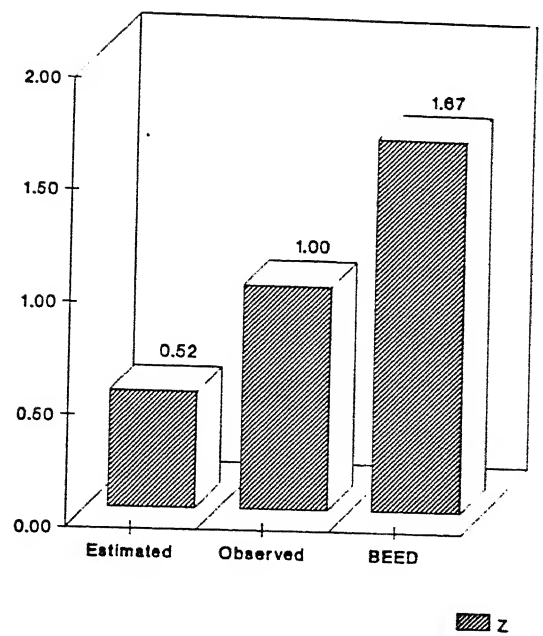
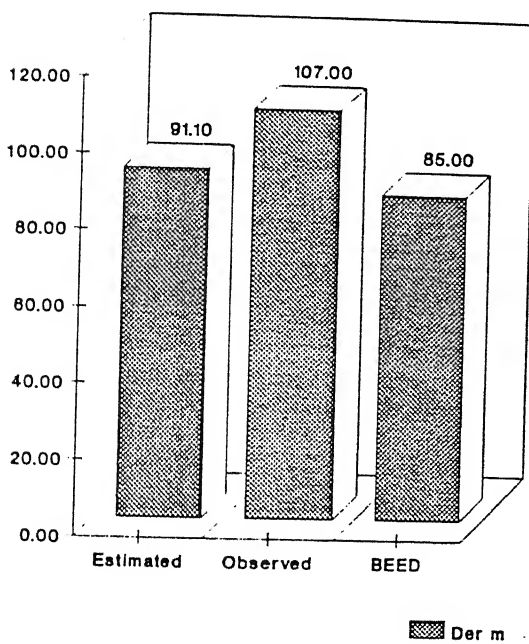
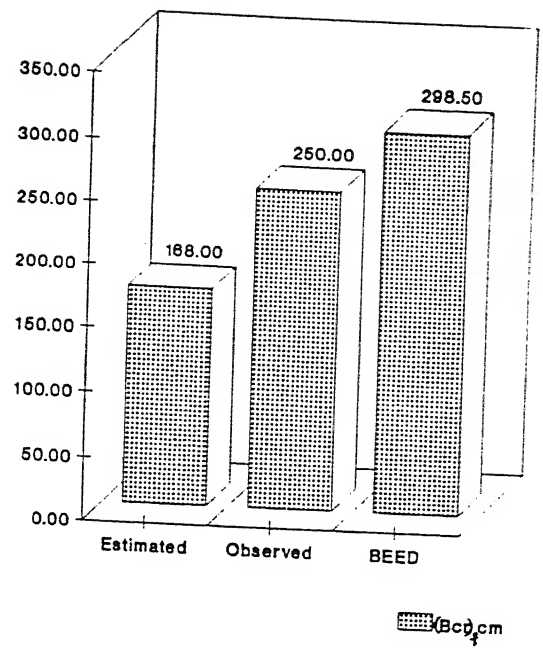
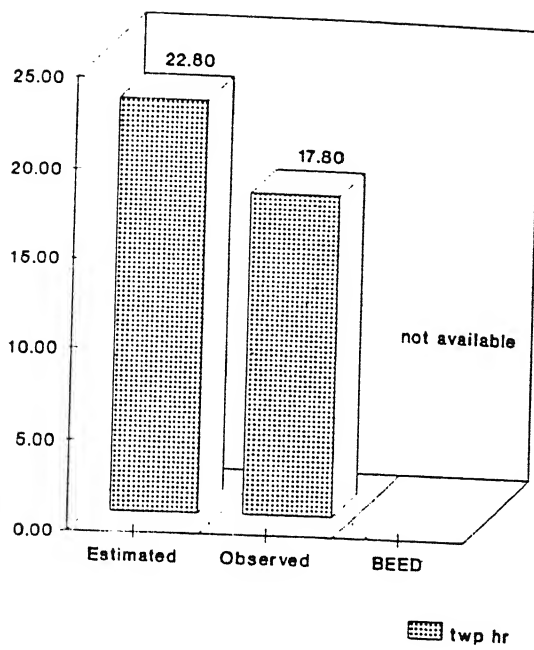


Fig. 5.17(c): Comparison of estimated final breach dimensions for Huaccoto dam breach with observed and simulated values of BEED model

COMPUTATION OF CRITERION VARIABLES  
DURING DAM BREACH PROCESS

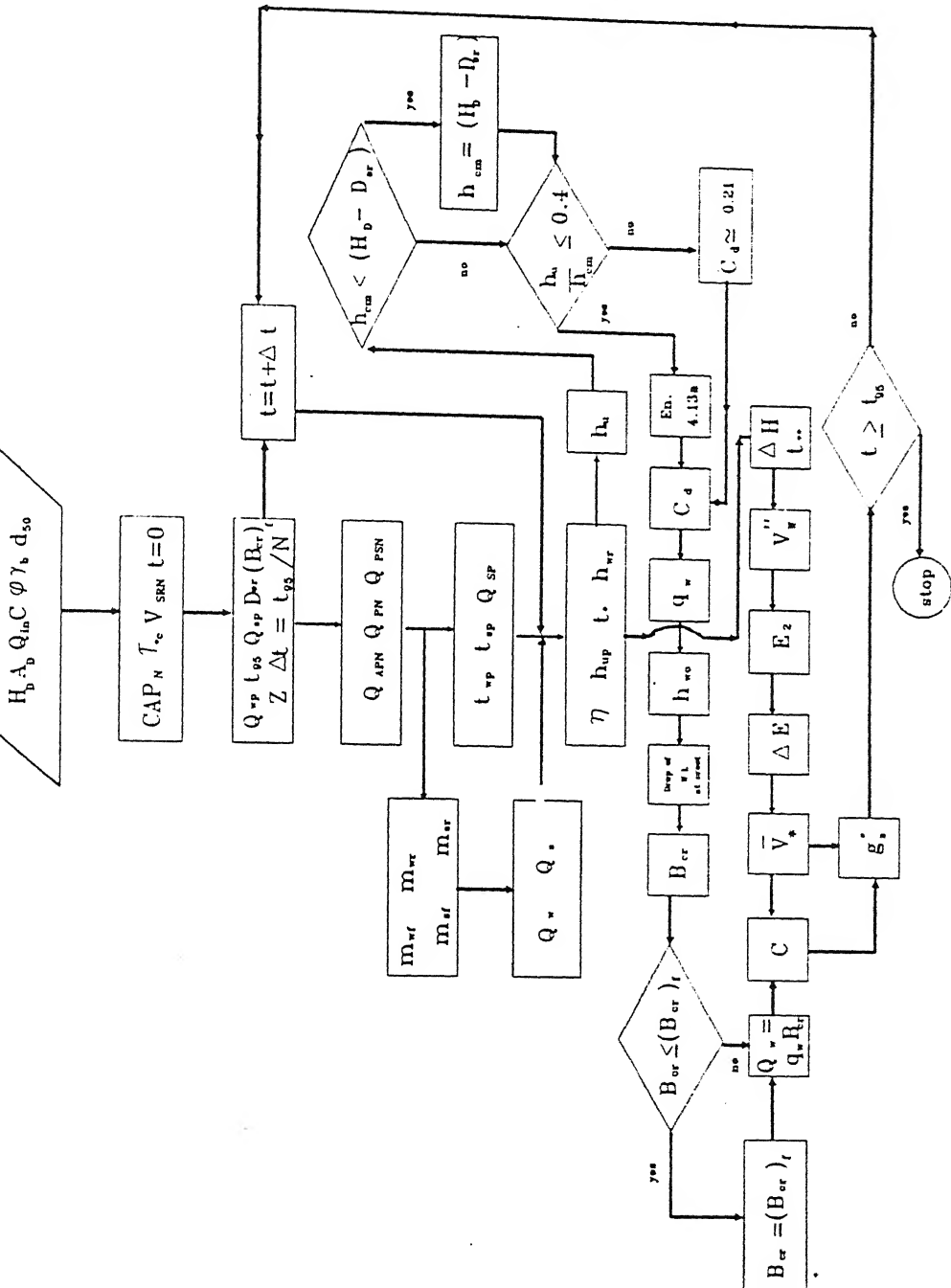


Fig. 5.18: Flow chart for computation of breach criterion variables during breach process

## 5.7 Discussion of Results and Method of Computation

### a. Discussion of Results

Functional relations established through the comparison with two field events can not be considered as final. Present analysis does not involve large number of laboratory tests on different types of soil and geometry of embankments. Only two field data are incorporated in recommending some relations. Still the present study predicts the available field data quite closely. It may be emphasized that this problem is governed by flow mechanism which is controlled by some major parameters like  $Q_{PN}$ ,  $Q_{PSN}$ ,  $Q_{APN}$ ,  $V_{SRN}$ ,  $CAP_N$  and  $\tau_{*c}$ . Though there may be slight variation in the relation for prediction of output variables, when different combinations of laboratory data and field data are used in regression analysis, the basic trends do not vary much.

It may be admitted here that these experiments are conducted for constant inflow into the reservoir ( $Q_{in}$ ), which may not be true in case of field. So the experiments with temporal variation of  $Q_{in}$  are necessary to strengthen these findings. Also the experiments are carried out with homogeneous fill embankment dam, which is not necessarily true for actual dams. Keeping these two limitations in view, one may consider the results obtained in the present study which can be treated as a fairly good step towards the prediction purpose.

### b. Comments on the Procedure to Compute Dam Breach Process

As soon as overtopping of flow occurs, erosion of sediment in the embankment sets in. Erosion of sediment leads to the formation of breach. The breach depth, breach width, side slope of breach banks and longitudinal bed slope vary as the breach processes continue. The variations of these breach dimensions depend upon the difference in water level upstream and downstream of the embankment. Breach dimensions, breach erosion of sediment and outflow in breach are related with this difference in water level  $\Delta H$  which is function of time. The magnitude of variation with time is related with functional parameters involving embankment dimensions, inflow to the reservoir and its capacity and erosion resisting properties of embankment soil. A methodology to compute this process is described in section 5.6a. All the dimensions, quantity of water flow and volume of sediment erosion in a breach can be predicted from the initiation of breach process till it ends.



Another approach to predict breach outflow discharge and sediment discharge is carried by nondimensionalising hydrograph and sediment discharge graph by their peak values and their time of occurrence in the section 5.6b. These peak values and their corresponding time of occurrence can be predicted using the procedure suggested in section 5.6a. The shape of nondimensionalised hydrograph and sediment discharge graph are represented in the form of Equation (5.12), the magnitude of the exponent ' $m$ ' is correlated with breach parameters. In this method the shapes of the hydrograph are the important controlling parameters i.e. the magnitude of  $m_{wr}$ ,  $m_{wf}$  and  $m_{sf}$  which indirectly are controlled by the breach mechanism. In other words, all the mechanism in the breach process is lumped in the values of  $m_{wr}$ ,  $m_{wf}$  and  $m_{sf}$ . One has to be very careful in predicting these parameters since the observed hydrograph is very much sensitive to these parameters. Though in the present study, prediction of the falling limb of water and sediment discharge graph with time are done fairly well, more numbers of field and experimental observation are required to strengthen the functional relationships of  $m_{wr}$ ,  $m_{wf}$ ,  $m_{sf}$  and  $m_{sr}$ .

### c. Limitations of the Present Approach

i. In the comparison of the result, it may be noticed that the functional relationships particularly for terminal breach morphological features are developed using the present lab data and the data of Teton dam and Huaccoto dam. The same functional relations are again verified on these two field events, which is not a correct approach. These functional relations should have been tested in some other field events. But due to the lack of required information about other dam breach cases, this has been done specially. However, it may be stressed upon that the functional relations only for lab data come very close to the mixed data of both lab and field in most of the cases. The developed functional relations among the variables of dam breach will be strengthened after testing in some more field events.

ii. Calculation of velocity at the downstream end of the dam ( $V_w$ ):

The width of the breach at downstream end is taken equal to the width of breach at a section slightly upstream of it. This needs verification.

iii. Computation of sediment concentration (C) or sediment load ( $g_s^*$ ):

As shown in Figure 4.41 and Figure 4.40 the correlation is not in good agreement with the breach parameters for C or  $g_s^*$  respectively.

iv. Average inflow discharge into the reservoir:

As the total inflow hydrograph for Teton dam was not available,  $\bar{Q}_{in}$  has been taken equal to half of the maximum inflow discharge. This seems to be arbitrary although this assumption predicted  $Q_w$  value fairly close to the observed one, it can be suggested to take:

$$\bar{Q}_{in} = \frac{\text{Total in flow volume of water}}{\text{Time base of hydrograph}}$$

The importance of this is felt, as it is required first to compute peak outflow discharge ( $Q_{WP}$ ) and subsequently other related breach parameters. In the present experimental study,  $Q_{in}$  was constant.

## 5.8 Concluding Remarks

From the study on the comparison of results, it is found that the present experimental observation of embankment dam breaching gives acceptable relations among the dam breach parameters, though it is tested for only two historical cases. This study helps in predicting the final values of the breach process of prototype dam failure close to their observed values. It is believed that present study will help in the development of numerical models more appropriately in simulating the breach process almost near to the field observation.

**PART II**  
**WASHOUT PROCESS OF FUSE PLUGS**

## **PART II**

### **WASHOUT PROCESS OF FUSE PLUGS**

Breach formation due to overtopping of flow is a process in which both lateral and vertical erosion dominate. In washout of a fuse plug, lateral erosion is restricted because of solid boundary walls and mostly vertical erosion process prevails all over its width. Experiments are carried out to measure the water level variation and sediment bed level variation during the washout process. Method to compute the breach outflow hydrograph, volume of sediment eroded and flow parameters associated with washout process are presented in Chapter VI.

Analysis of outflow discharge and sediment discharge over the washout sediment beds of fuse plug is presented in Chapter VII. Energy loss associated with sediment washout and transportation is analysed using data of mobile bed and its analogous rigid bed sediment profiles. A method to predict the washout process of fuse plug is also suggested.

## CHAPTER VI

### SCHEME OF EXPERIMENTS ON FUSE PLUG WASHOUT

Fuse plug can be treated similar to an emergency spillway. This comes into action when the reservoir level exceeds the assigned maximum water level. Fuse plugs are made up of soil embankments. The location of fuse plug depends on the topography along longitudinal axis of the dam for disposing safely the washed out soil and excess water downstream without endangering the dam body. The bottom level of the fuse plug is placed at full reservoir level (FRL) and its top level is at maximum reservoir level (MRL). Length of the fuse plug depends on the design criteria for releasing the excess water to be discharged downstream. Since the top level of the fuse plug is well below the embankment level, the excess water spreads completely across the length of the fuse plug. This cause the erosion of fuse plug material all over the lateral length of the fuse plug. Washout process in the fuse plug can be treated as two-dimensional erosion process in which erosion in vertical downward direction and in longitudinal direction takes place freely. The erosion in lateral direction is confined as it is not allowed to spread to the main dam body. Soil fill in the fuse plug is meant to be washed out when flow overtops. Hence, the erosion process in the fuse plug is called as 'washout process'.

The present study on the washout behaviour of fuse-plug due to overtopping is essentially a laboratory scaled model study. All the experiments were carried out in the Hydraulic laboratory of Indian Institute of Technology, Kanpur. The major objective of this

Experiments were carried out in two phases. In the first phase of experiments the mechanism involved in washout process of soil due to overflow on fuse-plug was planned to study. In the second phase of experiments sediment bed washout profiles are modeled as rigid bed profiles. On these analogous rigid bed profiles flow characteristics corresponding to discharge and energy loss are studied.

In the present chapter, details of flume, fuse-plug model, soil used for model preparation, basic data measurement and the procedure to compute basic variables involved in the problem are presented.

## 6.1 Details of Flume and Fuse Plug Model

The flume which is used for embankment breach study is also used for the washout study for fuse plug. Only the position of test section was varied. The test section for all experiments was maintained at 15m from the inlet.

### a. Fuse Plug Model Preparation

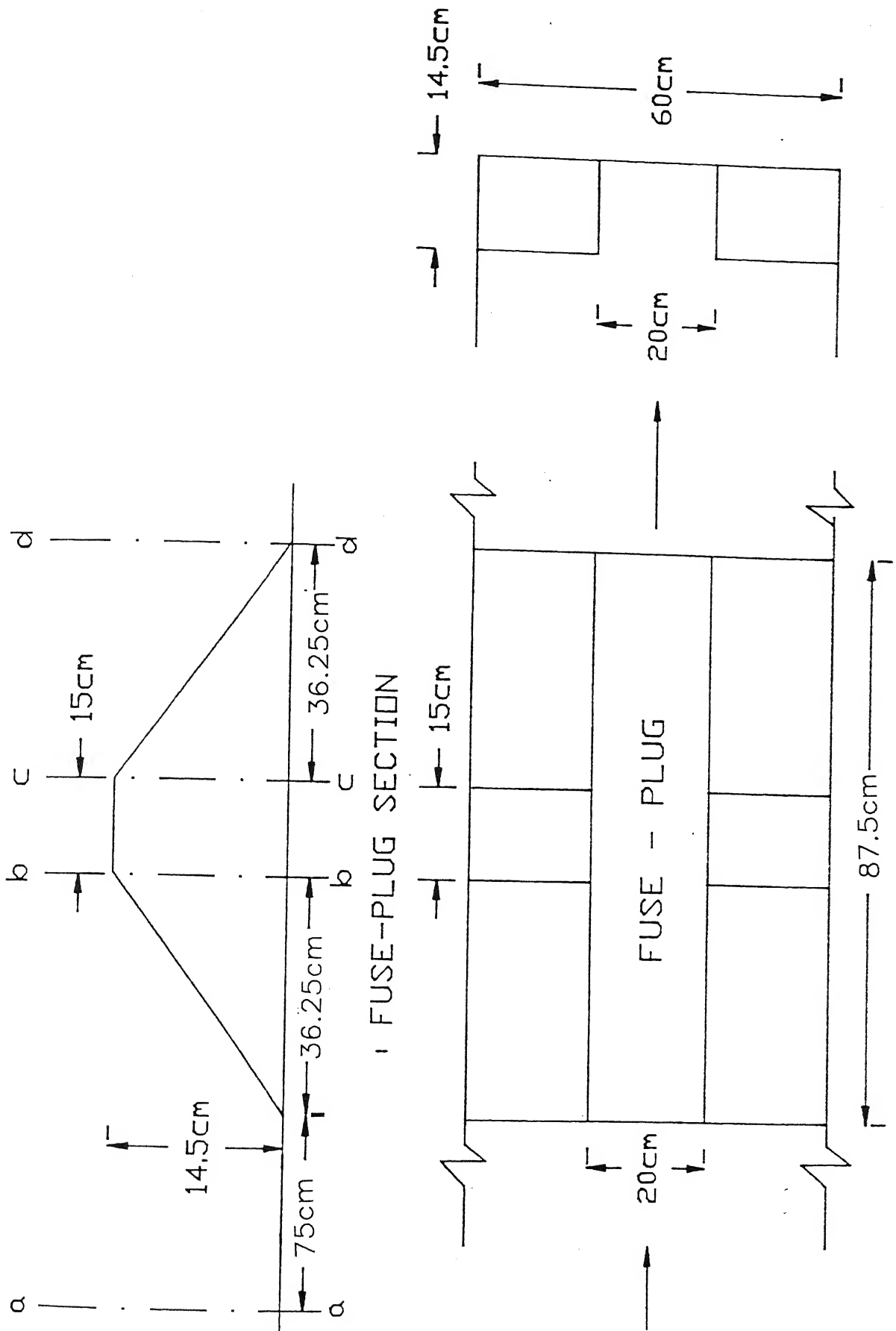
The model of earthen dam was made in wood with a rectangular breach section at the centre. This breach section was filled with compacted soil and is called as the fuse-plug on the dam body. The fuse plug section had the dimensions as crest width ( $B_f$ ) of 0.15m, bottom width ( $B_b$ ) of 0.875m and height ( $H_D$ ) of 0.145 m with upstream and downstream face slopes as 1 vertical to 2.5 horizontal. The central breach cut was a rectangular section of width 20cm in the centre. Figure 6.1(a) shows the detailed plan and sections of the fuse plug. Figure 6.1(b) shows the photographs of the fuse plug model used in the experiment.

In all the models of fuse-plug experiments the following geometry of the model were kept constant.

$$H_D = \text{Height of fuse plug} = 0.145\text{m}$$

$$B_f = \text{width of fuse-plug} = 0.20 \text{ m}$$

$$\text{Slopes of upstream and downstream faces of the fuse plug} = 1(V) : 2.5(H)$$



PLAN VIEW OF THE WOODEN MODEL SECTIONAL VIEW  
Fig. 6.1: FUSE PLUG MODEL IN PLAN AND SECTIONAL VIEW

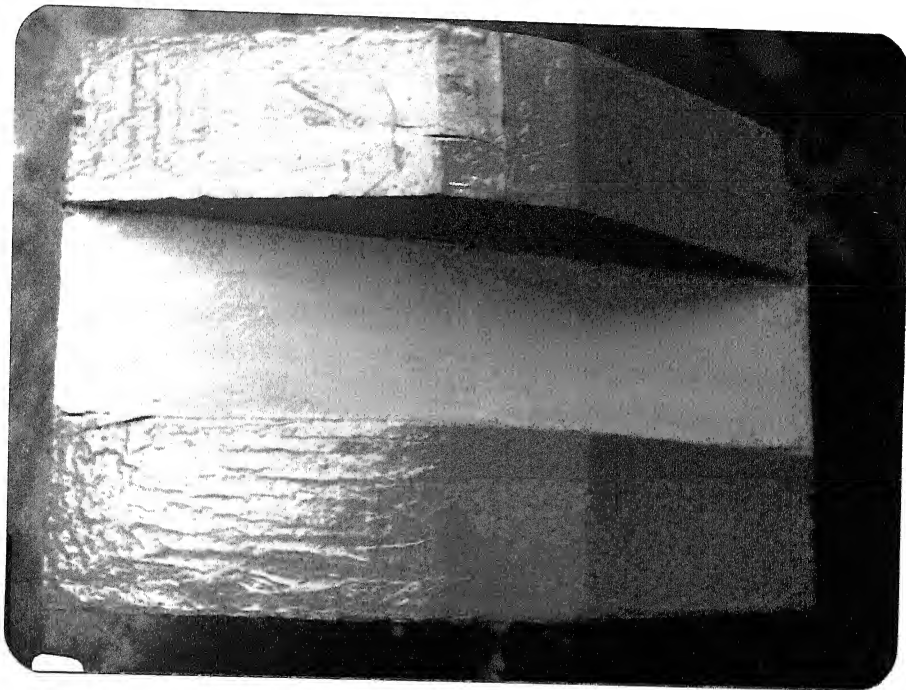


Fig. 6.1: Photograph of fuse plug model



### b. Source of Soil used for the Preparation of Fuse Plug

In the experiments of phase-A, cohesionless sand was used as fuse plug fill material. This sand was collected from the river Ganga near Kanpur. Details of the sand are already given in chapter III in connection with embankment breach study. Since experimental data based on the experiments conducted by Rajpal (1995) are used extensively in this study, it is proper to describe the soil used by him for his experiments. He conducted the experiments on three different soil fill in the breach section of fuse-plug model namely, i. fine cohesionless sand (type-A soil), ii. Cohesive soil (type-B soil), collected from I. I. T., Kanpur campus, and iii. mix of type-A and type-B soil in the proportion, 3:2. The particle size distribution curves for these soils are shown in Figure 6.2, and their other properties are presented in Table 6.1. In the second phase of experiments the fine sand from river Ganga at Kanpur and coarse sand from river Yamuna at Kalpi were used for model preparation. The location of Kalpi is 100 km south of Kanpur. The sand from this river is very coarse. The size distributions for these sands are shown in Figure 6.2. The particles are well graded, relatively coarse and very angular.

TABLE 6.1  
TYPES OF SOILS USED FOR THE FILL OF FUSE PLUG

Types of soil	$d_{50}$ (mm)	$\phi$ (degree)	C (KPA)	$\gamma_b$ 9810 * N/M <sup>3</sup>	w %	Remark
A	0.16	32.1	0.00	1.58	12	Cohesionless fine sand collected from River Ganga near Kanpur, India
B*	0.28	33.1	1.60	1.98	14	Cohesive soil collected from I.I.T, Kanpur campus
C*	0.18	29.2	0.85	2.03	15	Mix of Type-A and Type-B soil in the proportion 3:2
D	0.60	36.6	0.00	1.62	12	Coarse sand from River Yamuna at Kalpi 100km south of Kanpur
E	0.37	35.2	0.00	1.65	12	Mix of Type-A and Type-D soil in the proportion 1:1

\* Soil used by Rajpal (1995) for fuse plug fill

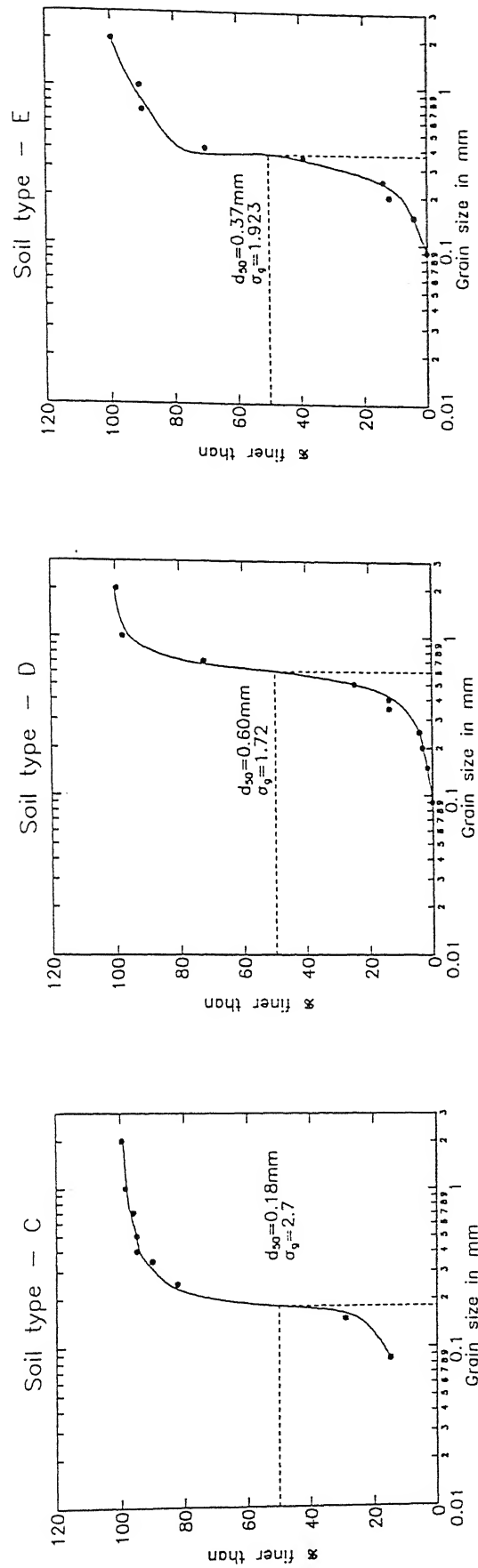


Figure 6.2 : Particle size distribution for soil types - C, D, and E

### c. Preparation of Fuse Plug Model

The wooden dam model block was fitted inside the flume at a distance of 15 meters from the inlet. Sufficient care was taken to prevent the flow of water beneath the dam model bottom and the flume bed by making it leak proof. The fuse plug portion of the dam model was open rectangular cut. This breach washout section was filled with wet soil with proper compaction, layer by layer. The wet soil was prepared by adding required quantity of water to dry soil for proper compaction. Each layer was of 5cm thickness. After compacting each layer, the top of it was scratched for next layer to adhere properly with the previous layer. The weight of dry soil and wet soil before filling the breach section and the left out excess wet soil after filling the breach section were measured for each experiment to find out bulk density and water content. Soil samples with same bulk density and water content were tested in the Geotech laboratory of the institute. Tests were aimed to determine the angle of friction and cohesion of the samples. This was carried out because the fuse plug dimensions were small and any sampling of soil in it would have weakened the compaction.

## 6.2 Experimental Procedure

### a. Aim of the Study

Experiments were planned to study the erodible characteristics of sediment in the fuse plug in the first phase. Erodible characteristics are crest variation, outflow hydrograph, eroded sediment discharge graph, erosion rate, relative energy loss and discharge relations. In the second phase of experiments, discharge relation developed on eroded crest was compared with discharge characteristics of simulated rigid bed profiles. In addition to this, energy loss occurring during the flow over the rigid bed profiles is computed. From these two studies, a relation on the magnitude of energy spent in eroding and transporting the sediment is postulated in terms of sediment concentration.

Experiments for the present study were carried out under two phases.

Phase-I: Erodible Fuse Plug Model

This phase of study refers to the experiments which were conducted to know the mechanism of washout of soil in the fuse plug. The major objective of this part of study was the following:

- i. From the basic information on variations of water levels in the reservoir, over the fuse plug model and the sediment bed variation with time, the involved mechanism in soil-water interaction under highly dynamic condition like washout process of fuse plug be analysed.

#### Phase-II: Analogous Rigid Bed Profile Study

The second phase of experiments was carried out with the aim of having following major objectives.

- i. To verify outflow discharge relation for a erodible bed profile of constant width.
- ii. Energy loss characteristics during washout of the fuse plug.

#### b. Basic Data Collected

The basic data collected are : water surface variations in reservoir and water surface level and sediment bed level variations along the fuse-plug.

##### i. Water Surface Variation

Water surface variation in the reservoir and at 3-sections along the centerline of the fuse plug were measured with respect to time. Different persons measured the water surface levels using point gauge referring a common digital clock. The typical water surface profiles recorded are shown in Figure 6.3. It may be observed that the water surface level gradually increases, attains peak and starts decreasing rapidly during the washout of the fuse-plug. Later on, the variation in water surface level reaches gradually to a constant value, depending on the inflow condition. Erosion of the top surface of the fuse plug starts well before the occurrence of maximum water level in the reservoir. The water level variation at other sections indicate sudden drop followed by mild rises and then decreasing as the wash out process continues. These observations were seen in all the water surface profiles recorded at sections a., b, c and d as indicated in Figure 6.3.

##### ii. Sediment Bed Profiles

Sediment bed profiles were marked on both the non-erodible sides of fuse-plug during the wash out at different intervals of time. This marking was carried out using coloured pencils. The average profile of these two was considered as the profile acting along the center line of

the fuse plug. This centerline profile is plotted with the cross-section of the embankment for run no. 1404 in Figure 6.4. It may be observed that the erosion starts on the downstream face almost parallel to the downstream face of fuse plug.

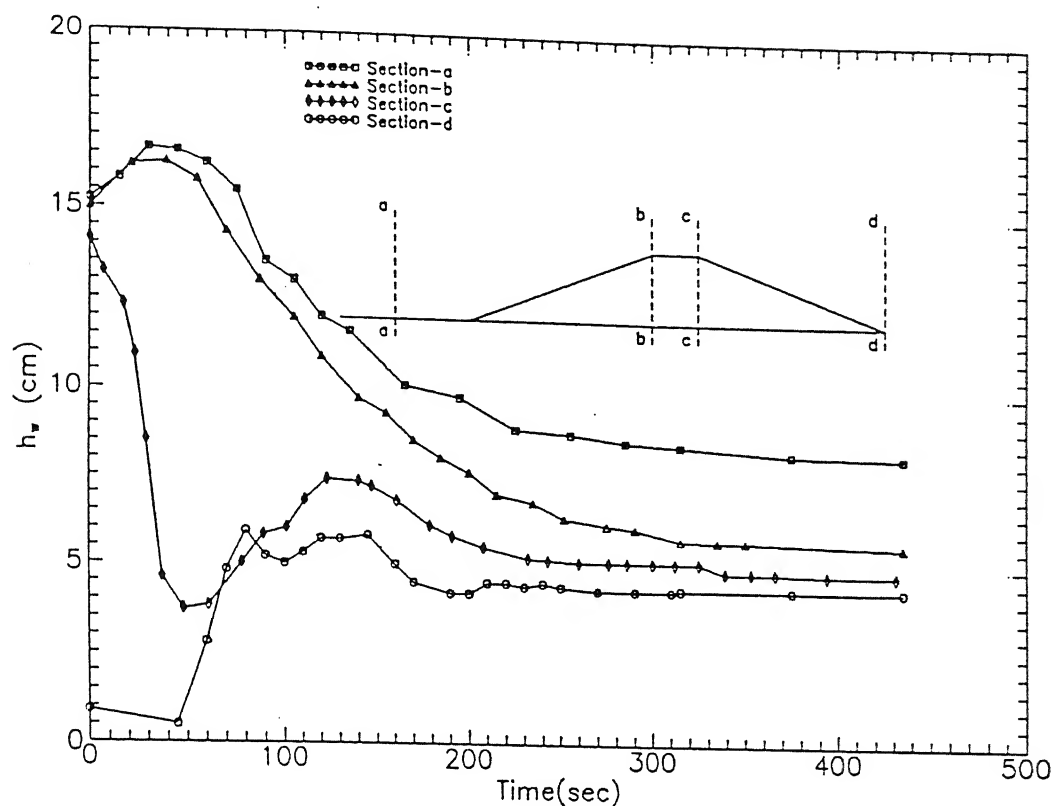


Fig. 6.3: Typical variations of water surface profiles at four different sections, a, b, c and d for run no 1404

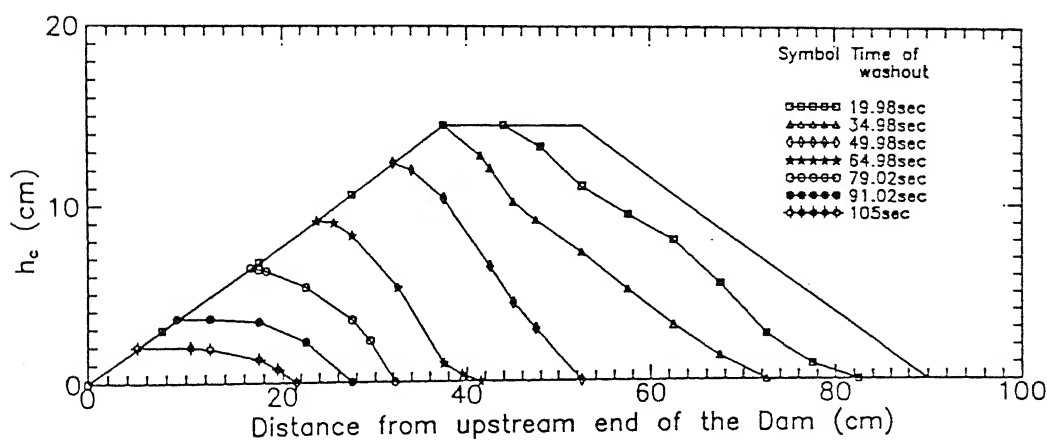


Fig. 6.4: Variation of sediment bed profile with time for run no. 1404

This continues for quite sometime till the erosion on the upstream edge of the fuse plug get flatten as the crest starts moving upstream, simultaneously decreasing its height. A typical variation of the crest is shown in Figure 6.5. It may be noted that the erosion of the fuse plug occurs althrough the width of the fuse-plug and level of erosion is almost uniform across fuse-plug.

### 6.3 Method of Computation of Basic Variables

Among the computed variables, the water discharge ( $Q_w$ ) and the sediment discharge ( $Q_s$ ) with time are the two most important variables which throw enough light on the wash out behaviour of a fuse plug. Due to their importance, detailed study was carried out.

#### a. Breach Water Discharge ( $Q_w$ )

The water discharge ( $Q_w$ ) flowing over fuse-plug is computed from the governing equation of continuity as follows:

$$Q_w - Q_{in} = A_s \frac{dh_{wr}}{dt} \quad (6.1)$$

Where  $Q_{in}$  = incoming discharge to the reservoir,  $A_s$  = Water surface area in the reservoir (constant in the present case as flume was prismatic),  $\frac{dh_{wr}}{dt}$  = rate of water level variation in the reservoir. In the above Equation (6.1),  $Q_{in}$ ,  $A_s$  are known quantities and the water level variation ( $dh_w / dt$ ) in the reservoir can be obtained from the measured water surface ( $h_{wr}$ ) which is a function of time. Thus the outflow discharge  $Q_w$  can be computed. A typical outflow discharge for a fuse plug is given in Figure 6.6.

#### b. Sediment Discharge ( $Q_s$ )

Volume of sediment eroded is computed by measuring the area between two consecutive sediment bed profiles. This area multiplied by the fuse-plug width gives the volume of sediment eroded during that time interval. Computation of sediment eroded at different intervals of time for consecutive sediment bed profiles is carried out and is plotted by adding in a cumulative way appropriately. Figure 6.7 represents a typical variation of cumulative

sediment volume with time. It may be observed that the increase in the cumulative volume  $\Sigma V_s$  is steep in the beginning and later on it remains constant.

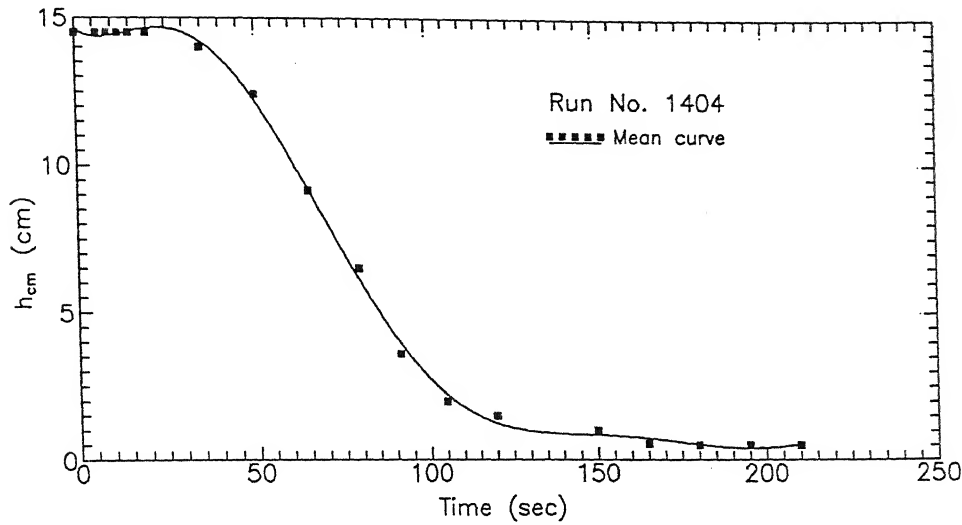


Fig. 6.5: A typical variation of crest of sediment bed profile  $h_{cm}$  (for run no 1404)

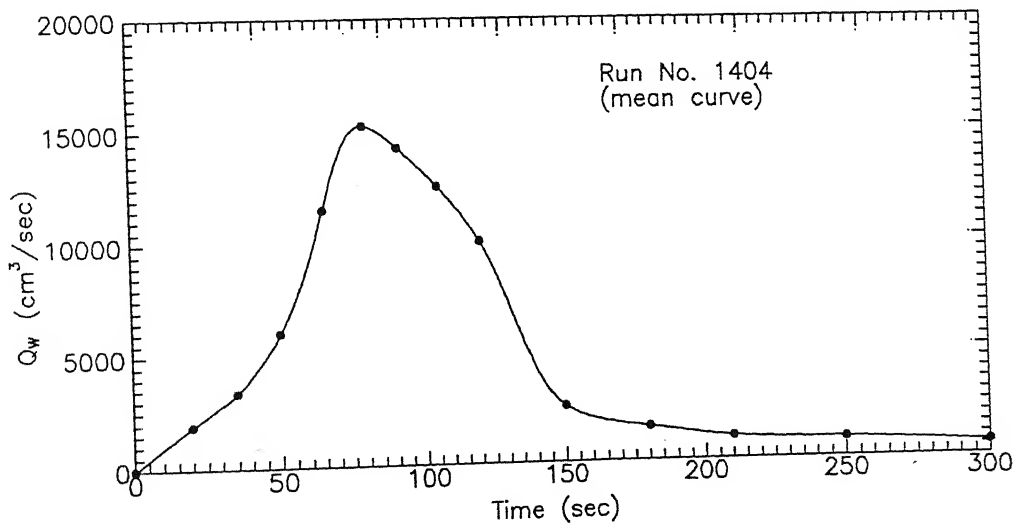


Fig. 6.6: A typical variation of outflow discharge with time for run no 1404 during wash out of fuseplug

By taking the derivatives of the  $\Sigma V_s$  with time, as  $\Delta \Sigma V_s / \Delta t = Q_s$ , the sediment discharge ( $Q_s$ ) is computed. The typical sediment discharge variation with time is plotted in Figure 6.8. The variation is asymmetric having a steep rising curve with gradual receding limb.

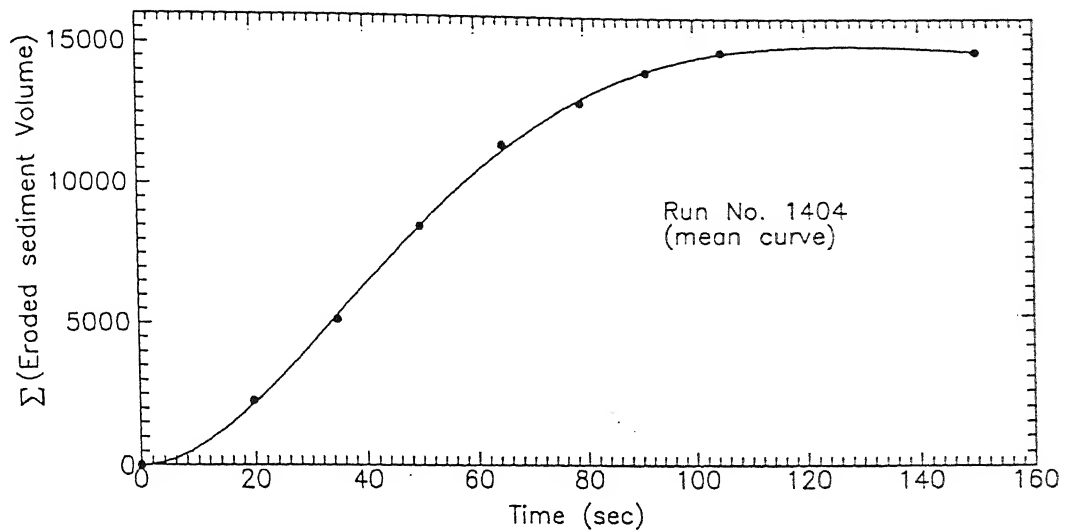


Fig. 6.7: A typical variation of cumulative volume of eroded sediment from fuse plug body with time for run no 1404

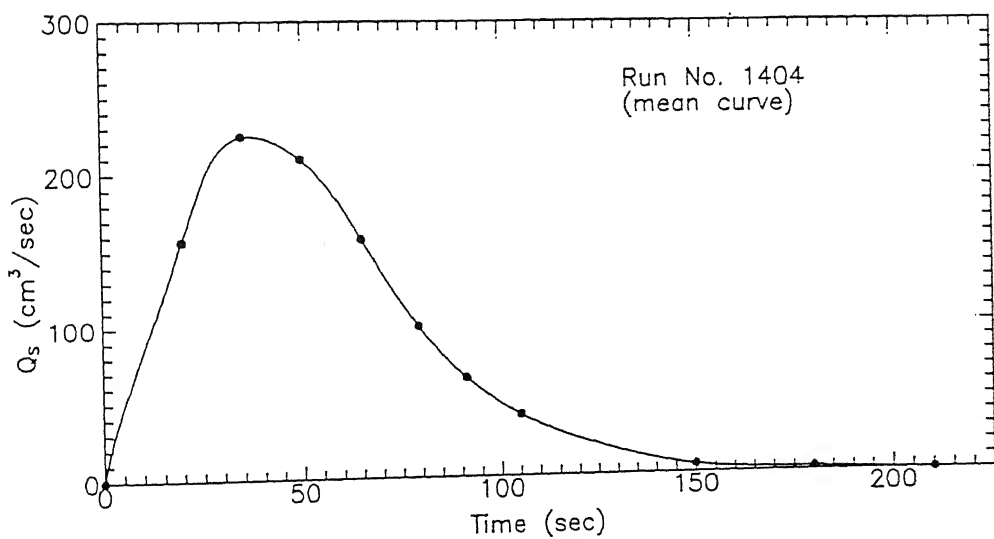


Fig. 6.8: Variation of sediment discharge with time



## 6.4 Details on the Number of Experiments Conducted

In Table 6.2 number of experiments in different phases of fuse plug are listed. Details of experiments on washout process of fuse plug study are given in Table 6.3(a). In Table 6.3(b) the experimental information of Rajpal (1995) is presented. Table 6.4 contains the details of the experiments conducted mainly with a purpose to evaluate energy loss relations. The details of experiments on rigid bed profiles analogous to sediment bed profiles are listed in Table 6.5.

**TABLE 6.2**  
**NUMBER OF EXPERIMENTS CONDUCTED ON FUSE PLUG WASHOUT STUDIES**  
**IN DIFFERENT PHASES**

Types of Soil Used	Phase A	Phase B	
	No of Experimental Data used in the Analysis	Mobile Sediment bed Profile	Analogous Rigid bed profile of Run No 1404
A	6 + 5*	2	6
B	5*	-	-
C	6*	-	-
D	-	2	-
E	-	2	-

Soil type-E (Ganga Sand : Yamuna Sand = 1:1)

\* Rajpal (1995)'s data

**TABLE 6.3a**  
**EXPERIMENTS CONDUCTED ON WASHOUT OF**  
**FUSE PLUG WITH TYPE - A SOIL FILL**

S No	Run No	$Q_{in}$ cm <sup>3</sup> /sec	Soil Type	Model Geometry	Purpose
1	1204	545.10	A	$H_D = 0.145$ m	To study washout process of fuse-plug
2	1404	5770.30	A	$B_f = 0.2$ m	
3	1804	6531.30	A	$B_{fb} = 0.875$ m	
4	1904	5210.00	A	$B_{fr} = 0.15$ m	
5	2104	5368.51	A	U/S and D/S slope= 1(V):2.5(H)	
6	2204	4210.95	A	-	

**TABLE 6.3b**  
**EXPERIMENTS CONDUCTED BY RAJPAL (1995) ON WASHOUT OF**  
**FUSE PLUG WITH THREE DIFFERENT SOIL FILLS: A, B AND C**

S No	Run No	$Q_{in}$ cm <sup>3</sup> /sec	Soil Type	Model Geometry	Purpose
1	S1-1	1373	A	Same	To Study the Washout process of Fuse Plug
2	S1-2	1035	A	as	
3	S1-3	1514	A	mentioned	
4	S1-4	2247	A	in	
5	S1-5	2320	A	Table 6.3a	
1	S2-1	2801	B	Same	To Study the Washout process of Fuse Plug
2	S2-2	5926	B	as	
3	S2-3	2962	B	mentioned	
4	S2-4	5732	B	in	
5	S2-5	4367	B	Table 6.3a	
1	S3-1	6060	C	Same	To Study the Washout process of Fuse Plug
2	S3-2	5820	C	as	
3	S3-3	3800	C	mentioned	
4	S3-4	7100	C	in	
5	S3-5	3850	C	Table 6.3a	
6	S3-6	5000	C		

**TABLE 6.4**  
**EXPERIMENTS CONDUCTED IN PHASE-B**

S No	Run No	$Q_{in}$ cm <sup>3</sup> /sec	Soil Type	Model Geometry	Purpose
1	1502	1267.80	A	Same as Phase I experiments	To study energy loss characteristics of washout of fuse-plug
2	1702	560.85	A		
3	1802	942.50	D		
4	0303	904.02	D		
5	0503	972.80	E		
6	0603	1139.54	E		

**TABLE 6.5**  
**DETAILS OF EXPERIMENT ON RIGID SEDIMENT BED PROFILES**  
**( IN PHASE-B) ANALOGOUS TO MOBILE BED PROFILES OF RUN NO. 1404**

Sl. No	Run No.	$h_u/h_{cm}$	$Q_{in}$ ( $cm^3/sec$ )	$h_{cm}$ ( $cm$ )	Soil Used
1	2501	0.387	874.74	4.6	Type - A
		0.523	1499.32		
		0.681	2395.29		
		0.935	3621.02		
		1.304	7468.19		
		2.064	14535.33		
2	3001	0.350	821.9	5.0	Type - A
		0.535	1860.1		
		0.600	1932.6		
		0.614	1972.8		
		1.083	5580.0		
		1.051	8644.2		
3	0402	0.195	573.63	7.5	Type - A
		0.326	1338.84		
		0.485	2530.16		
		0.676	4570.68		
		0.837	8129.83		
		1.110	10838.3		
4	0702	0.12	385.64	9.0	Type A
		0.20	765.25		
		0.23	1125.44		
		0.35	1866.62		
		0.40	2851.02		
		0.42	3048.53		
		0.48	4032.50		
		0.54	5007.03		
		0.57	5732.40		
5	0802	0.041	247.20	13.5	Type - A
		0.081	637.68		
		0.116	1049.94		
6	0902	0.047	331.13	14.1	Type - A
		0.085	484.88		
		0.090	528.13		

## **CHAPTER VII**

# **ANALYSIS AND RESULTS OF WASHOUT PROCESS OF FUSE PLUG**

The analysis of washout of fuse plug is carried out with the basic variables obtained from the experiments for different inflow scenario to the reservoir and variation in the fuse-plug fill properties. The analysis has been done under the following subheads:

- 7.1. Reservoir time scale and length scale
- 7.2. Outflow discharge relation
- 7.3. Sediment bed profile variation
- 7.4. Sediment discharge characteristics
- 7.5. Erosion velocity
- 7.6. Study on analogous rigid bed profile to instant erodible bed profile
- 7.7. Prediction of  $Q_W$  and  $Q_S$  with time

Finally a procedure is suggested for the prediction of the variables controlling the washout process of fuse plug.

### **7.1 Reservoir Time Scale and Length Scales**

In order to predict the washout characteristics of the fuse plug, the only observation that may be possible during the washout is the reservoir water level variation with time as shown in Figure 7.1(a) as a typical case. Considering this as the major information available to develop

scales for length and time, the gradient of water surface  $\Delta h_{wr}/dt$  is plotted against time as shown in Figure 7.1(b). It may be observed that the gradient has positive peak and negative peak crossing over the zero. The time taken between the zero value of the gradient to the maximum value of the negative gradient is considered as the time scale ( $T_*$ ). The magnitude of the difference in water levels, corresponding to these times is considered as the length scale ( $H_*$ ). The velocity scale is defined as the ratio of the length scale to the time scale. These scales are used for further analysis. In the analysis of fuse-plug characteristics flow and sediment movement variation, the length scale and time scale of the reservoir are used extensively. So it is necessary to relate these scales with incoming flow, geometry of the fuse-plug, and the soil fill properties. Based on these variables, inflow discharge intensity ( $q_{in}$ ) is nondimensionalised with  $V_{SR}$  and  $H_D$  as:  $q_{in}/(V_{SR}H_D)$ . This parameter called as  $Q_{in}$  number in short form, henceforth will be referred as ( $Q_{INN}$ ), used for analysis of nondimensionalised depth scale ( $H_*/H_D$ ) and nondimensionalised time scale  $H_*/T_*V_{SR}$  as shown in Figures 7.1(c) and (d) respectively. It may be observed that the depth scale increases with increase in  $Q_{INN}$ , reaches a peak and then decreases with further increase in its value. The functional relation among them can be written as:

$$\frac{H_*}{H_D} = 0.0937 - 0.043X + 0.142X^2 - 0.045X^3 + 0.005X^4 - 0.00019X^5 \quad (7.1a)$$

$$\text{Where } X = \left( \frac{\bar{q}_{in}}{V_{SR}H_D} \right)$$

The time scale in a nondimensional form with  $V_{SR}$  and  $H_D$  is found to be almost invariant with the  $Q_{INN}$  parameter and is of the order of 0.02. However very slight variation is observed and the relation from regression analysis as:

$$\left( \frac{H_*}{T_*V_{SR}} \right) = 0.000236 \left( \frac{\bar{q}_{in}}{V_{SR}H_D} \right) + 0.02 \quad (7.1b)$$

In Table 7.1 the time scale and length scales for different runs of experiments are shown along with other major variables in the washout process for the present study and for the experiments conducted by Rajpal(1995) on the same fuse plug model with three different fuse plug fills. These information are used in further analysis.

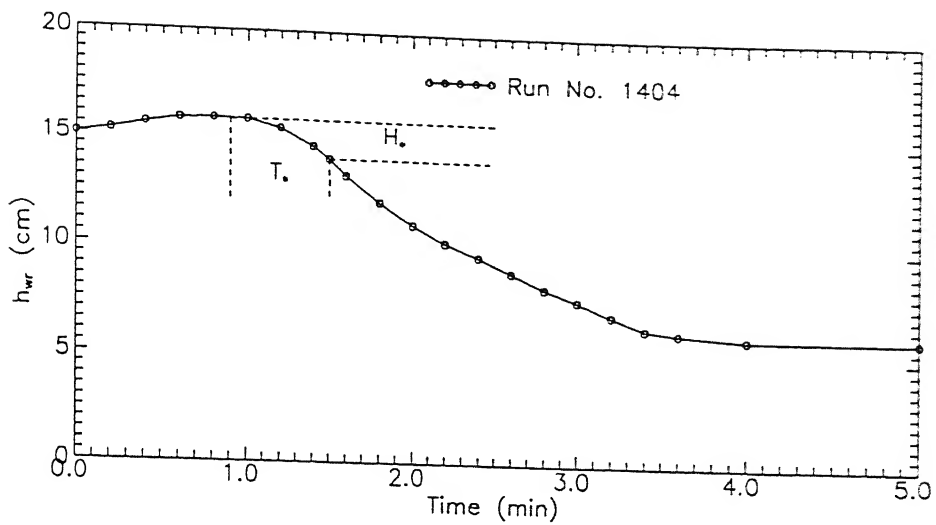


Fig. 7.1(a): A typical variation of reservoir water level indicating reservoir time scale( $T_*$ ) and reservoir depth scale( $H_*$ )

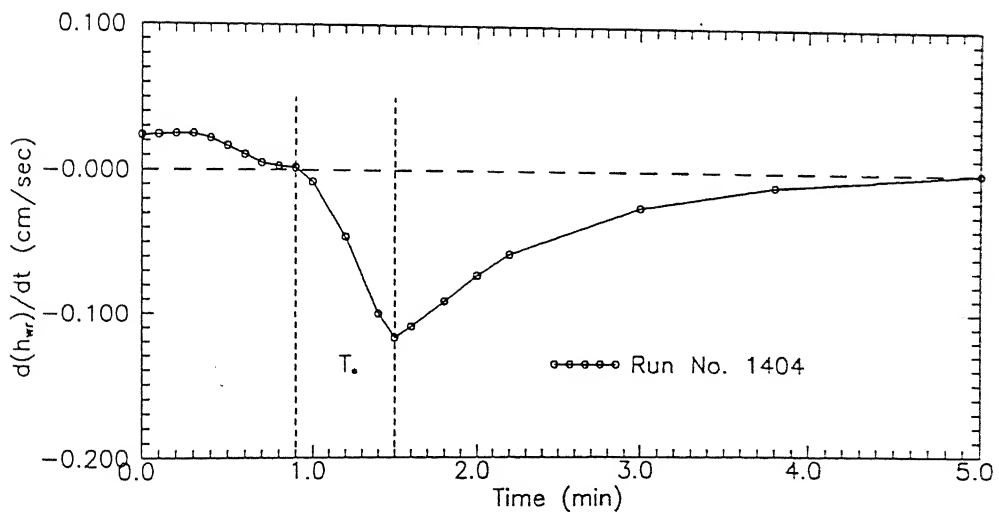


Fig. 7.1(b): Variation of rate of reservoir water level with time indicating time scale( $T_*$ )

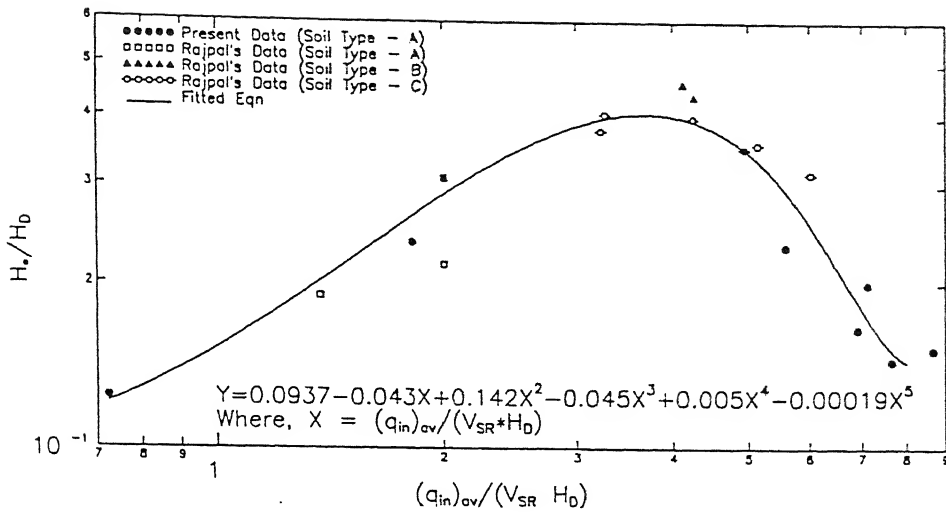


Fig. 7.1(c): Variation of nondimensional reservoir drop with average inflow discharge intensity, soil resisting velocity and height of the Dam

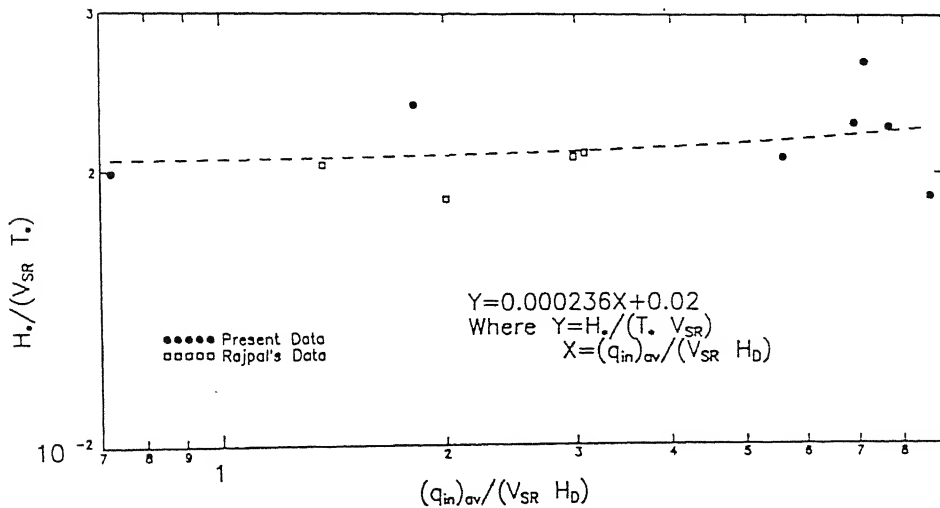


Fig. 7.1(d): Variation of nondimensional reservoir time scale with average inflow discharge intensity soil resisting velocity and height of the dam

TABLE 7.1

**VARIABLES USED IN FUSE PLUG ANALYSIS  
PRESENT STUDY (TYPE-A SOIL)**

Run No.	H <sub>D</sub>	Q <sub>in</sub>	Q <sub>wp</sub>	H <sub>*</sub>	T <sub>*</sub>	t <sub>50</sub>	V <sub>SR</sub>	(dh <sub>erod</sub> /dt) <sub>max</sub>	X <sub>22</sub>
present	(cm)	cm <sup>3</sup> /sec	cm <sup>3</sup> /sec	cm	sec	sec	cm/sec	cm/sec	
1204	14.5	545.10	12,393.4	1.8	34.8	45.0	3.00	0.310	7.03
1404	14.5	5770.30	15,528.0	2.1	36.0	40.0	3.40	0.232	8.33
1804	14.5	6531.30	16,637.0	2.2	45.0	32.5	4.15	0.318	9.09
1904	14.5	5210.00	14,758.0	2.4	40.8	32.5	4.25	0.360	8.01
2104	14.5	5368.51	13,313.0	2.9	42.0	31.0	2.98	0.260	7.27
2204	14.5	4210.95	13,132.0	3.4	63.0	44.0	4.45	0.224	7.31

**RAJPAL'S (TYPE-A SOIL)**

S1-1	14.5	1373	9,600	3.45	56.0	31.0	2.50	0.33	5.29
S1-2	14.5	1035	6,700	2.75	52.0	47.0	2.25	0.20	3.86
S1-3	14.5	1514	8,200	3.15	65.0	65.5	3.65	0.17	4.72
S1-4	14.5	2247	8,500	3.40	63.0	60.0	1.95	0.18	4.79
S1-5	14.5	2320	8,700	3.00	55.0	40.5	2.20	0.22	4.95

**RAJPAL'S (TYPE-B SOIL)**

S2-1	14.5	2801	3,672	4.50	1032	684	0.45	0.015	0.88
S2-2	14.5	5926	7145	6.35	882	771	0.48	0.020	1.58
S2-3	14.5	2962	5140	8.10	852	486	0.44	0.026	1.22
S2-4	14.5	5732	7822	6.70	648	498	0.60	0.017	1.76
S2-5	14.5	4367	5238	7.00	1980	1200	0.48	0.007	1.21

**RAJPAL'S (TYPE-C SOIL)**

S3-1	14.5	6060	8,150.0	5.2	450	261.0	1.37	0.0467	2.85
S3-2	14.5	5820	10,170.0	5.1	213	96.0	1.14	0.0760	3.63
S3-3	14.5	3800	6,936.3	5.5	264	184.8	0.76	0.0476	2.55
S3-4	14.5	7100	9,539.0	4.6	333	279.0	1.38	0.0400	3.24
S3-5	14.5	3850	8,554.0	5.9	306	171.0	1.38	0.0500	3.15
S3-6	14.5	5000	7,613.0	5.8	456	187.8	1.30	0.0600	2.73

where, H<sub>D</sub> = Height of Fuse Plug  
 Q<sub>in</sub> = Inflow to the Reservoir  
 Q<sub>wp</sub> = Maximum outflow  
 t<sub>50</sub> = time at which h<sub>c</sub> is eroded upto 50% of its height  
 V<sub>sv</sub> = Sediment erosion velocity = Q<sub>s</sub>/A

$$X_{22} = \frac{\left( \frac{q_{wp}}{H_*} \right)}{\sqrt{\frac{\Delta \rho}{\rho_w} g d_{50} + \frac{C}{\rho_w}}} = \frac{q_{wp}}{H_* V_{SR}}$$

V<sub>SR</sub> = sediment resisting velocity



## 7.2 Outflow Discharge Relation

The outflow discharge computed from continuity equation is plotted against the head acting on the crest ( $h_u$ ) as shown in the Figure 7.2(a). This contains the data of present work and Rajpal's (1995) work for fuse plug model with cohesionless type-A soil. It may be observed that  $Q_w$  varies almost linearly with  $h_u$  instead of  $\frac{3}{2}$  power law variation as in the case of weir flow. This may be due to rapid erosion of the crest during the wash out process. This analysis is further carried out by computing coefficient of discharge  $c_d$  as:

$$c_d = \frac{Q_w}{\left( \frac{2}{3} L \sqrt{2g} h_u^{\frac{3}{2}} \right)} \quad (7.2a)$$

The computed value of  $c_d$  is plotted against  $h_u/h_{cm}$  as shown in Figure 7.2(b), where  $h_{cm}$  is the height of the crest above the bed level. It may be observed that as  $h_u/h_{cm}$  increases,  $c_d$  decreases. The relation between them by regression analysis can be written as:

$$c_d = 0.63 \left( \frac{h_u}{h_{cm}} \right)^{-0.2} \quad (7.2b)$$

combining both the Equation (7.2a) and (7.2b), an equation for discharge  $Q_w$  can be written as:

$$Q_w = 0.42 L \sqrt{2g} h_u^{1.3} h_{cm}^{0.2} \quad (7.2c)$$

The outflow discharge depends on the crest height ( $h_{cm}$ ) of erodible sediment bed profile along with the head of water over the crest as shown in Equation (7.2c).

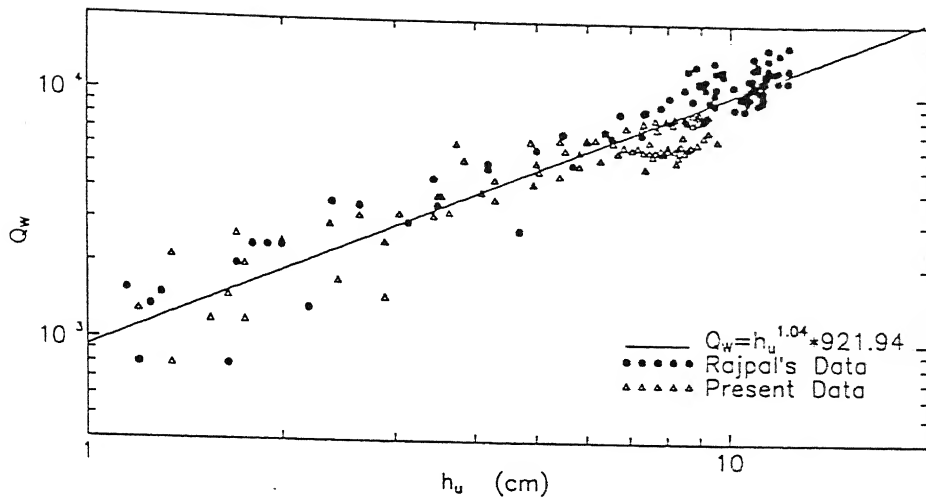


Fig. 7.2(a): Relation between head of water over erodible sediment crest ( $h_u$ ) with outflow discharge  $Q_w$

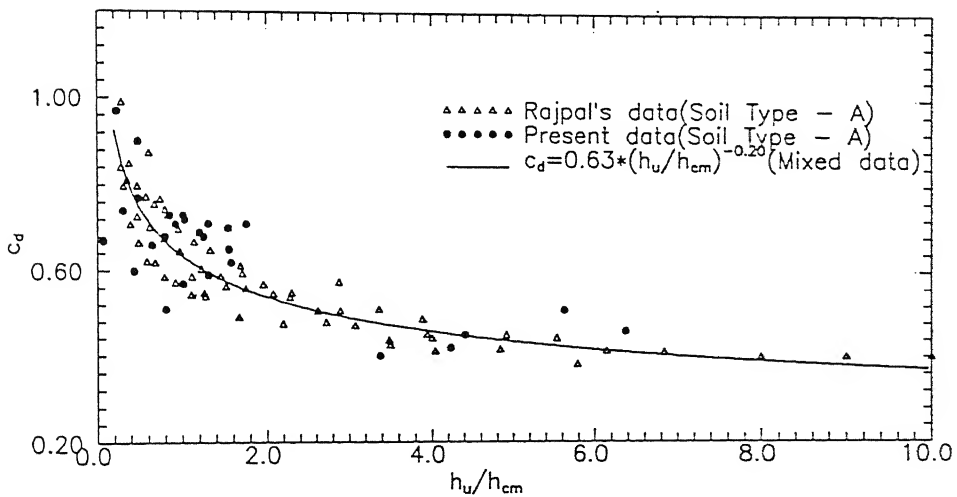


Fig. 7.2(b): Variation of coefficient of discharge ( $c_d$ ) with ratio of head of water over erodible sediment crest to the height of the erodible crest

### 7.3 Erosional Characteristics of Sediment Crest and Bed Profiles

The crest of the sediment bed, described in last paragraph is denoted as  $h_{cm}$ . It controls the flow passing through the breach. Its location and height vary with the washout of fuse plug. Hence, it is necessary to know the crest location and its variation with respect to time.

#### a. Crest Location

The position of the crest of the sediment bed profile recedes from downstream top edge towards the upstream as the flow occurs over the crest. This is due to the erosion of the downstream face. The position of the crest is measured at various water levels over the crest and plotted as receding length versus drop in water level over the crest as shown in Figure 7.3(a). The receding length,  $X_m$  is measured as the distance from the upstream end of the fuse plug to the crest horizontally. Receding length decreases as drop increases. The receding length is nondimensionalised with base length ( $L_{DB}$ ) and drop is nondimensionalised with  $H_D$  and is plotted as shown in Figure 7.3(b). The trend in variation is same as in dimensional case. the relation between them is written from regression analysis as:

$$\frac{X_m}{L_{DB}} = 0.97 - 2.25X + 3.28X^2 - 1.92X^3 \quad (7.3a)$$

$$\text{where } X = (\text{Drop in water level at crest} / H_D)$$

#### b. Sediment Bed Profile Downstream of Crest

From the eroded sediment profile, it was observed that the upstream surface before the crest, varies very gradually or almost remains horizontal from the upstream slope to the crest. But the downstream surface varies steeply. The nondimensional downstream sediment surface profile in the form  $h_c / h_{cm}$  is plotted against  $((x - x_m) / (x_{50} - x_m))$  as shown in Figure 7.3(c), where  $h_c$  = height of the sediment bed at any location  $x$ , measured from upstream end of the dam,  $h_{cm}$  = height of the crest,  $x_m$  = the position at which  $h_{cm}$  occurs and  $x_{50}$  = the distance at which  $h_c = 0.5h_{cm}$ . Position of  $h_{cm}$ ,  $X_m$ ,  $X_{50}$ , and  $L_{DB}$  are shown in definition sketch,

Figure 7.3(d). It was observed that  $h_c / h_{cm}$  decreases as  $X$  increases. The relation between

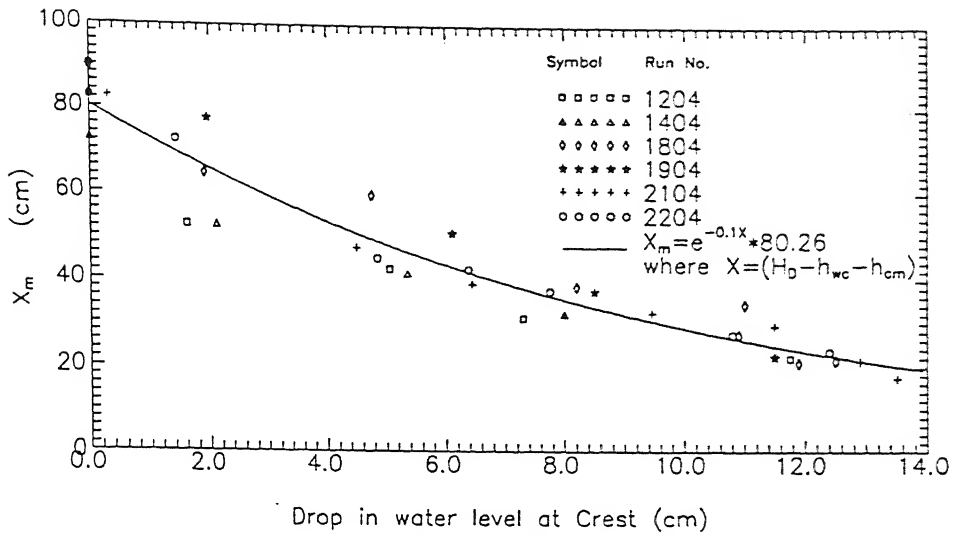


Fig. 7.3(a): Variation of receding length of the erodible sediment crest( $X_m$ ) with the Drop in water level

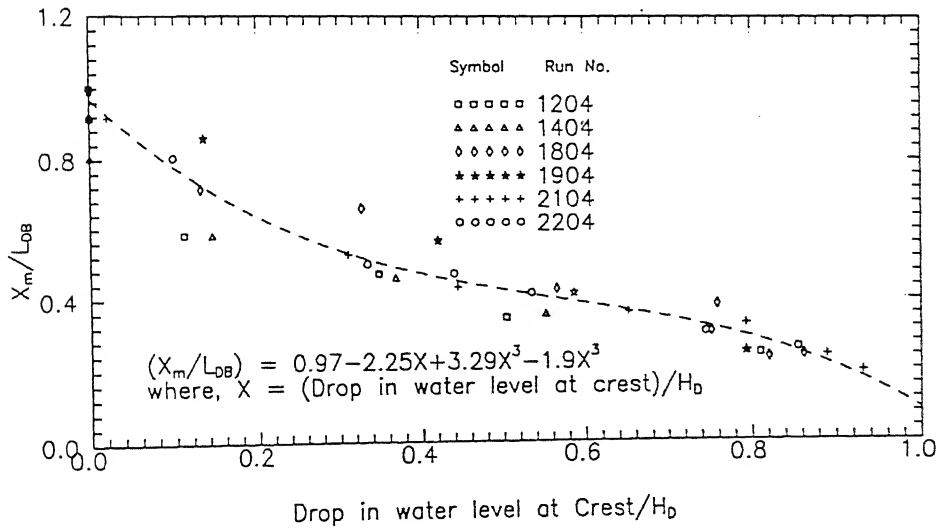


Fig. 7.3(b): Variation of nondimensional receding length of sediment crest with nondimensional drop of water level at the crest

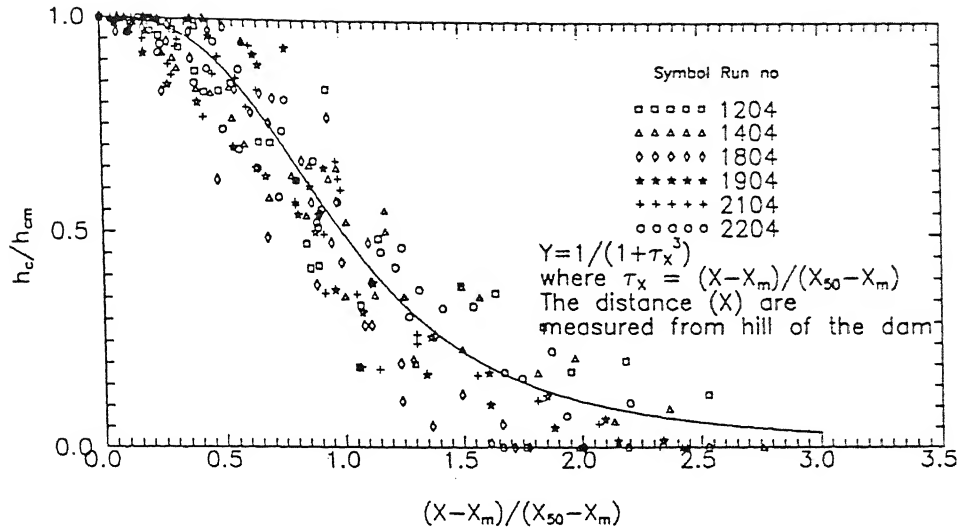


Fig. 7.3(c): Variation of nondimensional erodible sediment bed profile

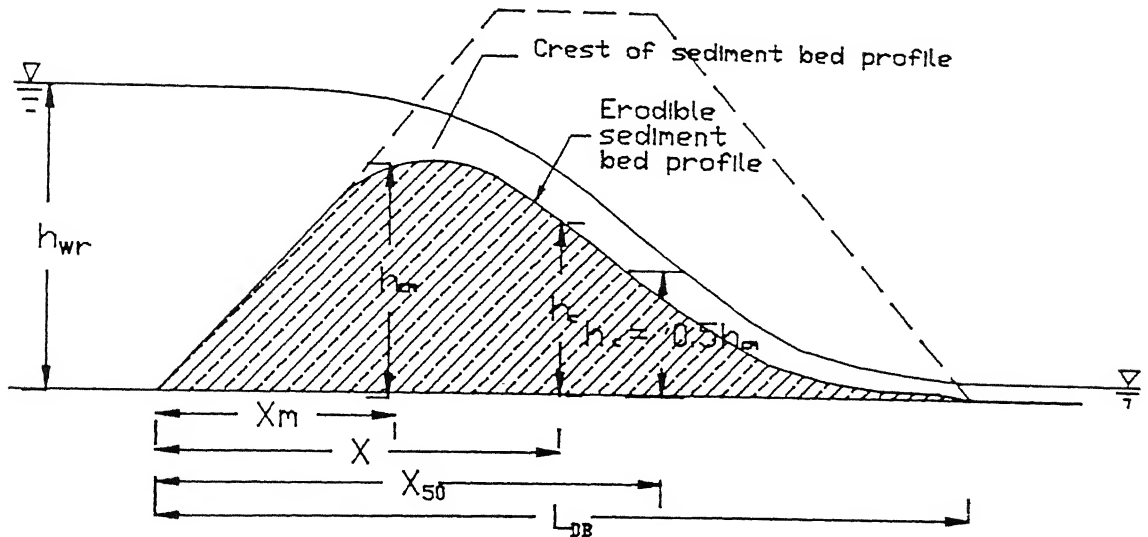


Fig. 7.3(d): Definition sketch for the scales  $X_m$ ,  $X_{50}$ ,  $L_{DB}$  and  $h_{cm}$

them is given by analysis as:

$$\frac{h_c}{h_{cm}} = \frac{1}{1 + \left( \frac{X - X_m}{X_{50} - X_m} \right)^{3.0}} \quad (7.3b)$$

Length scale  $x_{50}$  of erosion surface profile is nondimensionalised with  $L_{DB}$  and is plotted against  $t / T_*$ . It can be observed that  $(x_{50} / L_{DB})$  decreases with increase in  $t / T_*$  as shown in Figure 7.3(e). The relationship between them can be written as:

$$\frac{X_{50}}{L_{DB}} = 0.85 e^{-0.56(t/T_*)} \quad (7.3c)$$

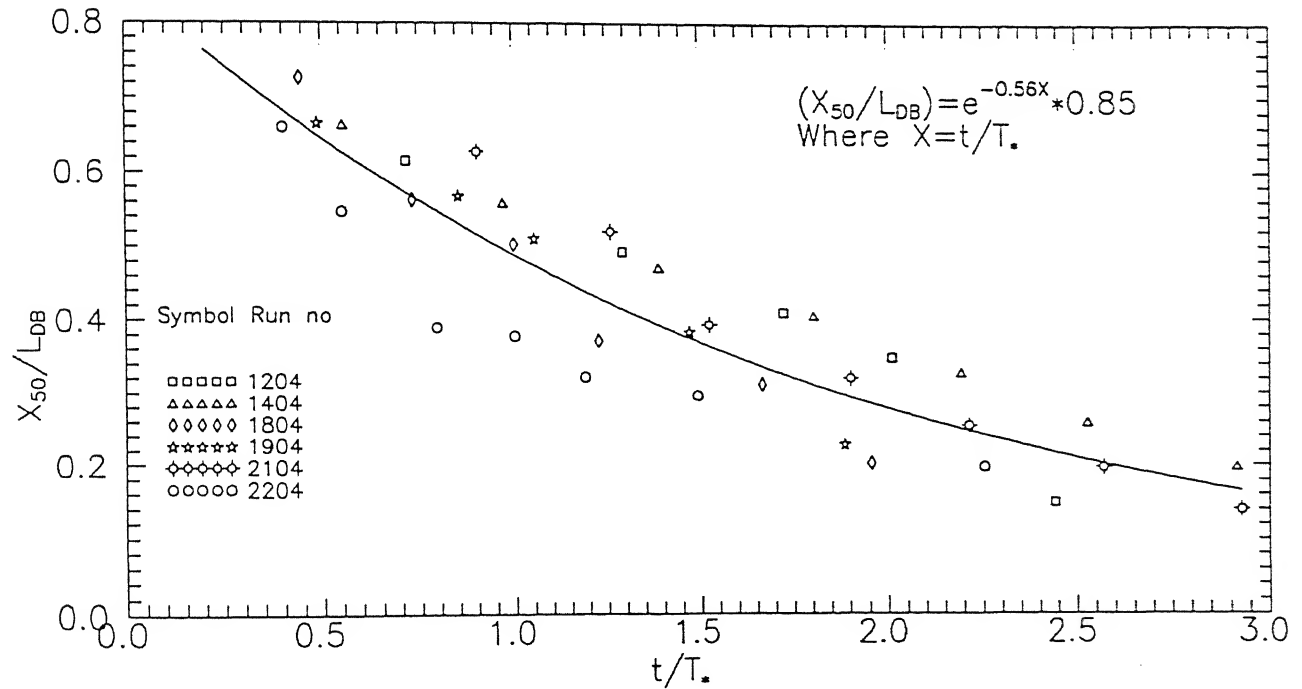


Fig. 7.3(e): Variation of nondimensional profile length scale ( $X_{50}$ ) with nondimensional time ( $t$ )

### c. Crest Level Variation with Time

In last paragraph, variation of position of receding length is described. This is found to be a function of time. Figure 7.3(f) shows the variation of nondimensional crest height  $h_{cm}/H_D$  with nondimensional time  $t/t_{50}$ . Here  $t_{50}$  is the time at which 50 percent of maximum crest height occurs. The data plotted in Figure 7.3(f) includes the data of the present study along with Rajpal's (1995) experiments. The relation between them may be written as:

$$\frac{h_{cm}}{H_D} = \left[ \frac{1}{1 + \left( \frac{t}{t_{50}} \right)^{2.5}} \right] \quad (7.3d)$$

The variation of time scale  $t_{50}$  is shown in Figure 7.3(g). Time scale is nondimensionalised with  $T_*$  and is plotted against  $H_D/H_*$ . The relation between them as obtained from regression analysis may be written as:

$$\frac{t_{50}}{T_*} = 0.296 \left( \frac{H_D}{H_*} \right)^{0.633} \quad (7.3e)$$

Here both scales  $T_*$  and  $H_*$  are the scales obtained from reservoir water level variation.

### d. Rate of Crest Erosion

Rate of crest erosion ( $dh_{cm}/dt$ ), is mainly controlled by the incoming flow velocity ( $V_u = \sqrt{2gh_u}$ ) and the properties of fill material of the fuse plug. The rate of crest erosion is plotted against incoming flow velocity over the crest. It may be observed in the Figure 7.3(h), that the rate of crest variation initially increases, attains peak and then decreases very steeply. This variation is observed in all the flow runs. Multiple values of rate of crest erosion for same value of incoming flow velocity exist near the peak region as can be observed from Figure 7.3(h).

Rate of crest erosion is non-dimensionalised with velocity of flow  $\sqrt{2gh_u}$  and is plotted against  $t/t_{50}$  as shown in Figure 7.3(i). It may be observed that the non-dimensional rate of erosion is increasing in the beginning of washout process till it reaches maximum value.

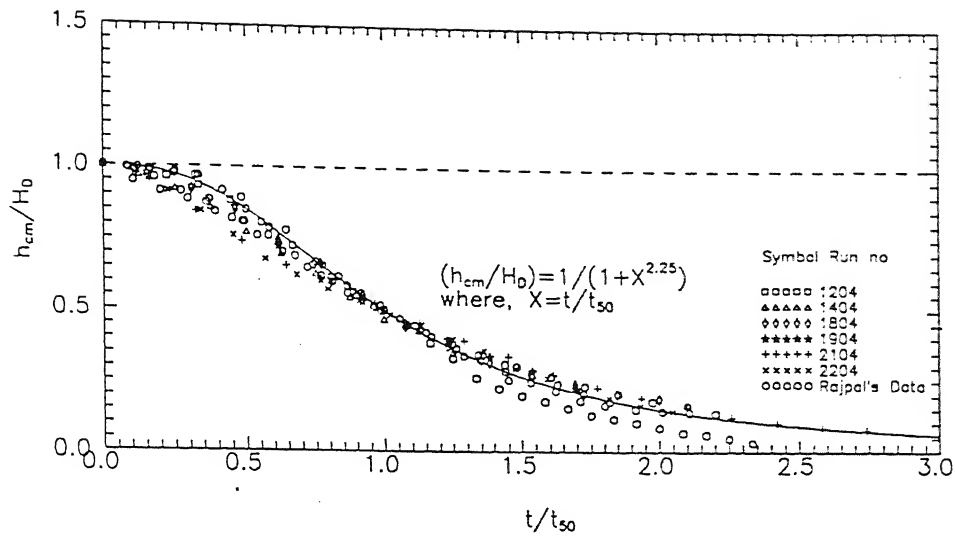


Fig. 7.3(f): Variation of nondimensional crest height ( $h_{cm}/H_0$ ) with nondimensional time ( $t/t_{50}$ ).

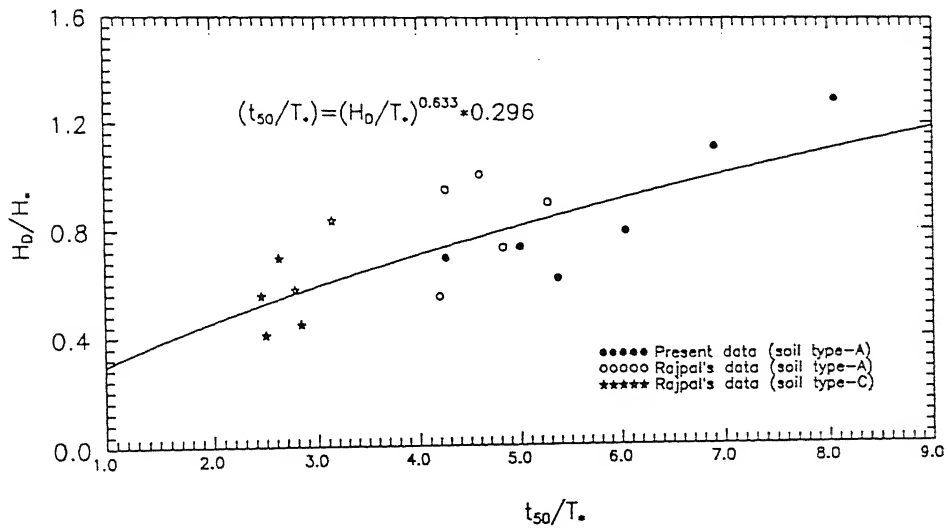


Fig. 7.3(g): Variation of nondimensional time scale of erodible sediment bed profile, ( $t_{50}/T_*$ ) with reservoir length scale ( $H_*$ ) and height of fuse plug ( $H_0$ )



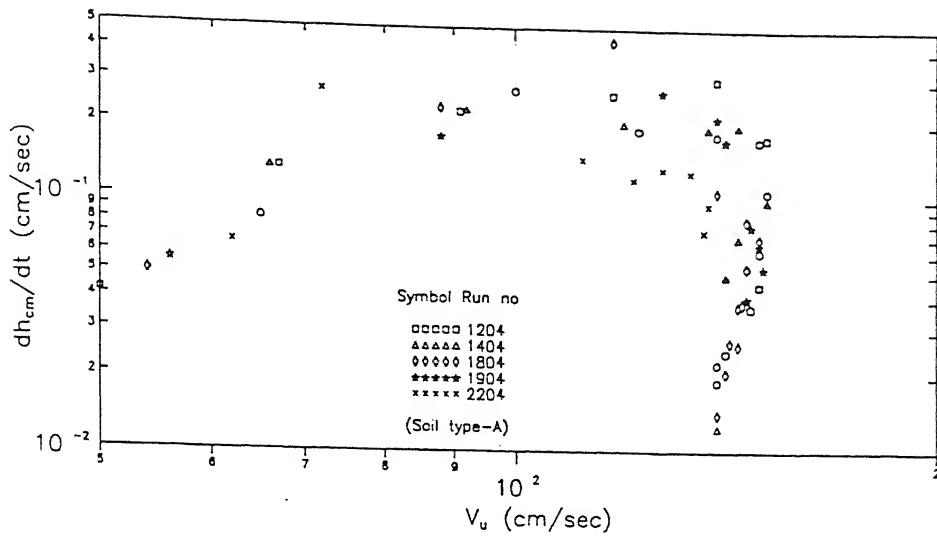


Fig. 7.3(h): Rate of erosion of crest height of erodible sediment bed with incoming flow velocity( $V_u$ )

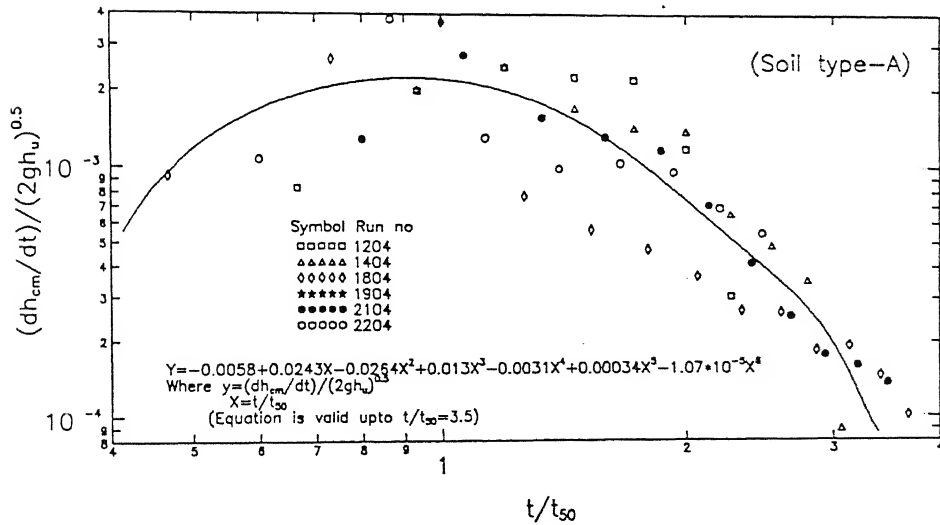


Fig. 7.3(i): Variation of nondimensional rate of erodible sediment crest with its nondimensional time

It decreases with further increase in  $t/t_{50}$ . The magnitude of maximum erosion coefficient is of the order of  $2 \times 10^{-3}$ . The functional relation among them can be written as:

$$Y = -0.0058 + 0.0243X - 0.0264X^2 + 0.013X^3 - 0.0031X^4 + 0.00034X^5 - 1.07 \times 10^{-5}X^6 \quad (7.3f)$$

$$\text{where } Y = (dh_{cm}/dt) / \sqrt{2gh_u} \text{ and } X = t/t_{50}$$

This equation is valid upto  $t/t_{50} = 3.5$ .

The relation shown in Figure 7.3(i) does not contain sediment properties of the soil used in the fuse plug. To consider this aspect in the analysis of rate of crest erosion, the soil resisting velocity ( $V_{SR}$ ) is incorporated in the nondimensional parameter  $X_{22}$ , which involves soil and flow properties. The maximum value of  $dh_{cm}/dt$  is nondimensionalised with  $V_{SR}$  and is plotted against  $X_{22}$  as shown in Figure 7.3(j). The relation between them is obtained by regression analysis as:

$$\frac{(dh_{cm}/dt)_{max}}{V_{SR}} = (X_{22})^{3.27} \times 1.9 \quad (7.3g)$$

$$\text{where } X_{22} = \frac{(q_{wp}/H_s)}{\sqrt{\frac{\Delta\rho}{\rho_w}gd_{50} + \frac{c}{\rho_w}}}$$

It may be noted that the maximum rate of crest erosion varies as  $q_{wp}^{3.27}$ ,  $V_{SR}^{-2.27}$  and  $H_s^{3.27}$

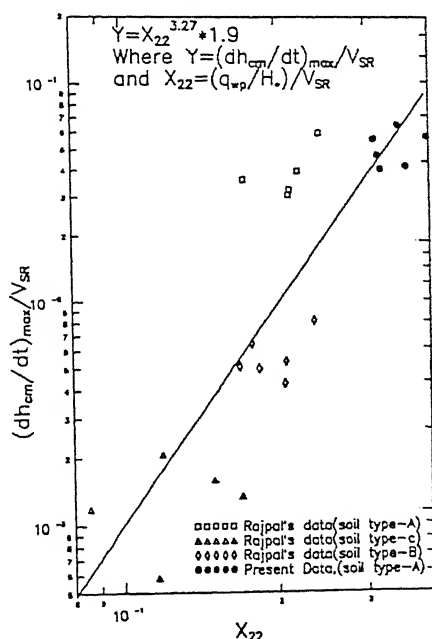


Fig. 7.3(j): Variation of maximum rate of erodible sediment crest in a nondimensional form with its nondimensional maximum outflow discharge intensity ( $q_{wp}$ ), reservoir length scale and soil resisting velocity

As the sediment resisting velocity increases magnitude of  $dh_{cm}/dt$  decreases and discharge intensity of peak flow  $q_{wp}$  increases as the magnitude of  $dh_{cm}/dt$  increases. These observations sounds physically meaningful.

## 7.4 Erosion Velocity

Erosion Velocity is a measure of erosive characteristic of soil of fuse plug fill. Erosion velocity ( $V_{sv}$ ) is computed as:

$$V_{sv} = \frac{(\text{Volume of sediment eroded between two successive sediment profiles})}{\Delta t B_{fp} (\Delta \bar{h}_c)}$$

where  $(\Delta \bar{h}_c) = \text{average height of erosion between successive sediment profiles,}$

$\Delta t$  = duration of time in seconds between two successive sediment profiles and  $B_{fp}$  = width of the fuse-plug. Erosion velocity  $V_{sv}$  is plotted against velocity of flow at the crest  $V_u = \sqrt{2gh_u}$  as shown in Figure 7.4(a). It may be observed that  $V_{sv}$  is maximum almost immediately at the starting of the erosion and then decreases as  $V_u$  increases. There is a sudden decrease in  $V_{sv}$  when  $V_u$  is of the order of 150 cm/sec. This is observed in almost all the runs in present data.

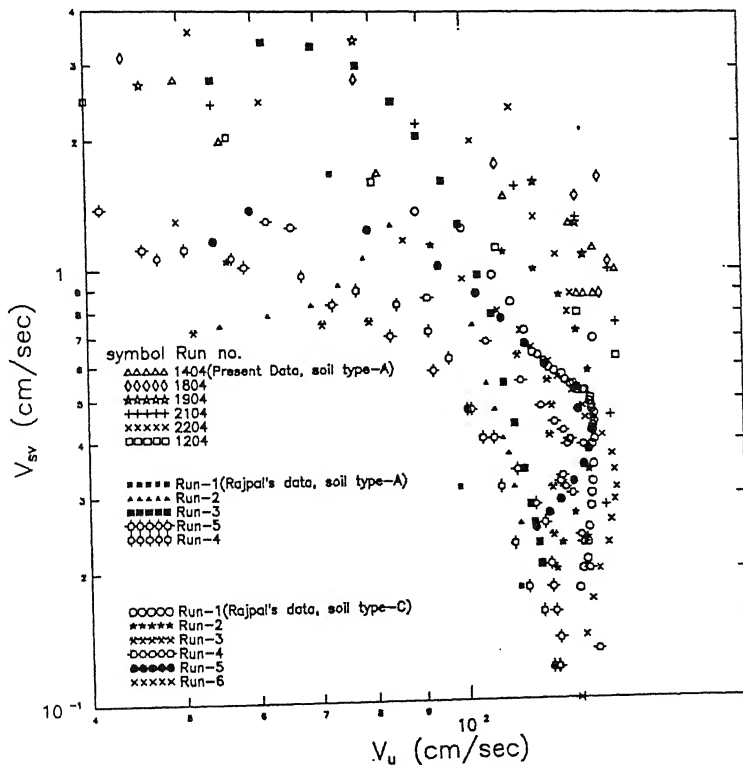
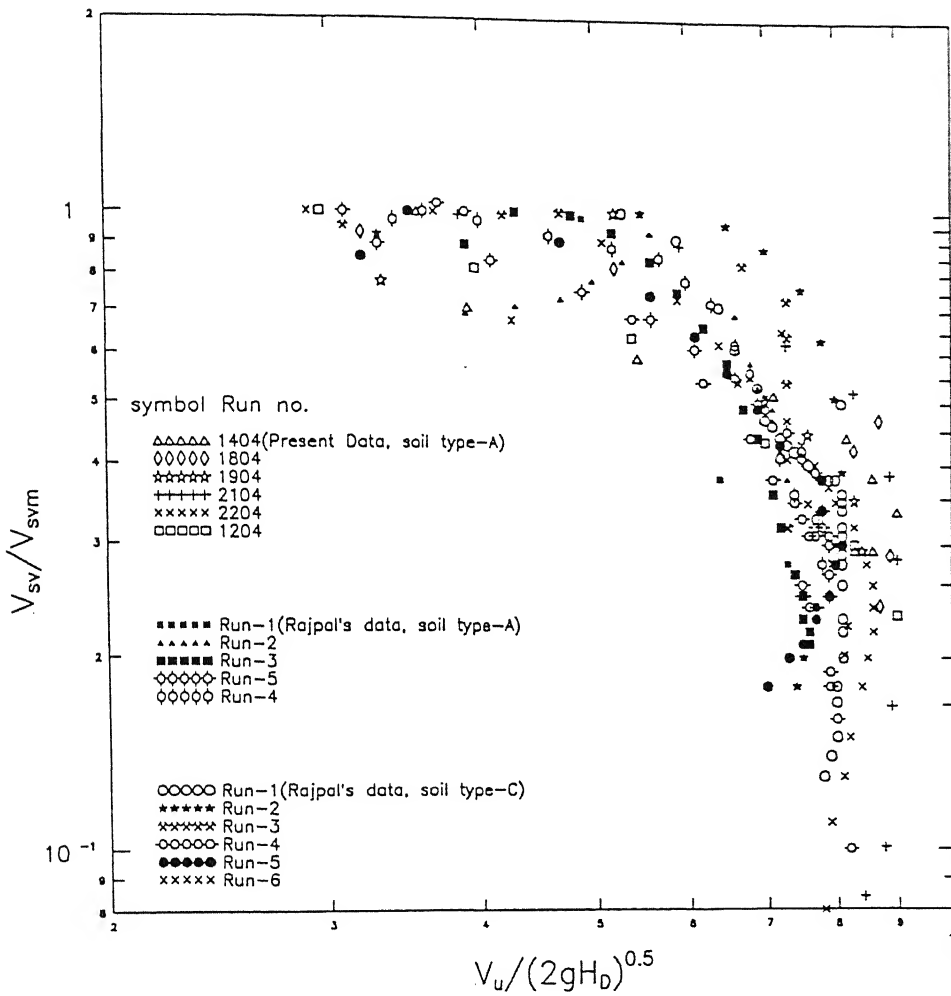


Fig. 7.4(a): Variation of average sediment erosion velocity ( $V_{sv}$ ) at any time of washout of fuse plug with incoming flow velocity ( $V_u$ )

Erosion velocity  $V_{SV}$  is nondimensionalised by its maximum value  $V_{SVM}$  and plotted against nondimensional incoming flow velocity ( $V_u$ ) with respect to  $\sqrt{2gH_D}$  where  $H_D$  is height of fuse plug.



**Fig. 7.4(b):** Variation of nondimensional average sediment erosion velocity ( $V_{SV}$ ) at any time of washout of fuse plug with nondimensional incoming flow velocity ( $V_u$ )

It may be observed that  $V_{SV}/V_{SVM}$  remains almost constant for major part of the erosion process. During the final stage of the erosion it decreases very sharply which can be seen from Figure 7.4(b).

Magnitude of erosion velocity scale  $V_{SVM}$  is nondimensionalised with sediment resisting velocity  $V_{SR}$  and plotted against parameter  $X_{22}$  as shown in Figure 7.4(c). The parameter  $X_{22}$  is given as:

$$X_{22} = \frac{(q_{wp} / H_*)}{\sqrt{\frac{\Delta\rho}{\rho} g d_{50} + \frac{c}{\rho}}} \quad (7.4)$$

Magnitude of  $V_{SVM}/V_{SR}$  increases with increase in parameter  $X_{22}$ . The relation among them is developed including Rajpal's data for three different types of fuse plug fills along with present data. The magnitude of  $V_{SVM}/V_{SR}$  is of the order of 0.8 and 0.03 for cohesionless soil (type-A soil) and cohesive soil (type-C soil) respectively.

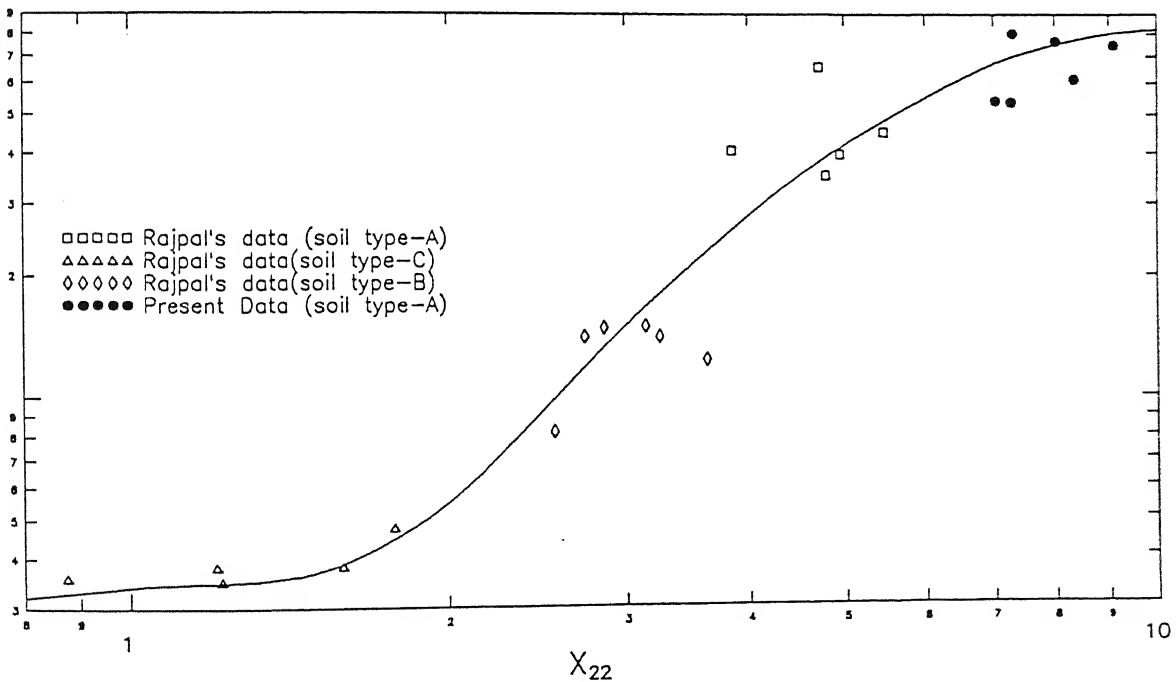


Fig. 7.4(c): Variation of nondimensional scale of sediment erosion velocity ( $V_{SVM}$ ) with maximum outflow discharge intensity, reservoir length scale ( $H_*$ ) and  $V_{SR}$

## 7.5 Sediment Discharge Characteristics

The rate of cumulative volume of sediment eroded is considered as the sediment discharge ( $Q_s$ ). A typical variation of  $Q_s$  with time is shown in Figure 7.5(a). It may be observed that the  $Q_s$  has steep rising limb attaining a peak and decreases later on. Taking the magnitude of the peak value of sediment discharge  $Q_{SP}$ , its corresponding time  $t_{SP}$ , the time at which 50% of  $Q_{SP}$  occur on the receding limb noted as  $t_{SP/2}$ , the nondimensional plot of  $(Q_s/Q_{SP})$  against  $[(t-t_{SP})/(t_{SP/2}-t_{SP})]$  is as shown in Figure 7.5(b). The data on the rising limb are very few. There is a clear variation of the receding limb as can be seen from Figure 7.5(b). Receding limb data is analysed further. The relation between them as shown in Figure 7.5(c) is obtained from analysis as:

$$\frac{Q_s}{Q_{SP}} = \frac{1}{\left[1 + \left(\frac{t - t_{SP}}{t_{SP/2} - t_{SP}}\right)^{2.0}\right]} \quad (7.5a)$$

### a. Sediment Concentration (C)

Sediment concentration is obtained by dividing  $q_s$  by  $q_w$ , where  $q_w$  is the water discharge intensity and  $q_s$  is the sediment discharge intensity. They are plotted against  $(h_u/h_{cm})$  as shown in Figure 7.5(d). It may be observed  $(h_u/h_{cm})$  increases, sediment concentration decreases. This decreasing rate is related by regression analysis as:

$$\frac{q_s}{q_w} = 0.088 - 0.1134 \frac{h_u}{h_{cm}} + 0.06 \left(\frac{h_u}{h_{cm}}\right)^{2.0} - 0.015 \left(\frac{h_u}{h_{cm}}\right)^{3.0} + 0.001 \left(\frac{h_u}{h_{cm}}\right)^{4.0} \quad (7.5b)$$

It may be noted here that the sediment concentration as high as 10%, is attained in the beginning of the washout period. Later on as washout continues,  $(h_u/h_{cm})$  increases and sediment concentration decreases.

The variation of  $(h_u/h_{cm})$  is studied in Figure 7.5(e) with respect to drop in water level in the upstream and downstream of the fuse plug ( $\Delta H$ ), which is nondimensionalised with  $H_D$  and  $Q_{PN2}$ . where  $Q_{PN2}$  is written as:

$$Q_{PN2} = \frac{q_{WP}}{\sqrt{gH_D^{3.0}}} \quad (7.5c)$$

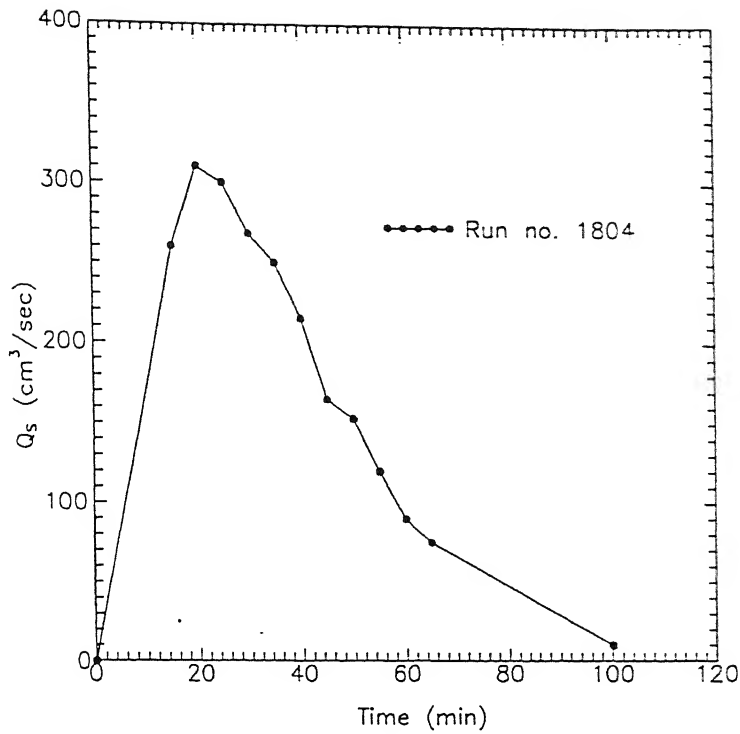


Fig. 7.5(a): A typical variation of sediment discharge ( $Q_s$ ) with time

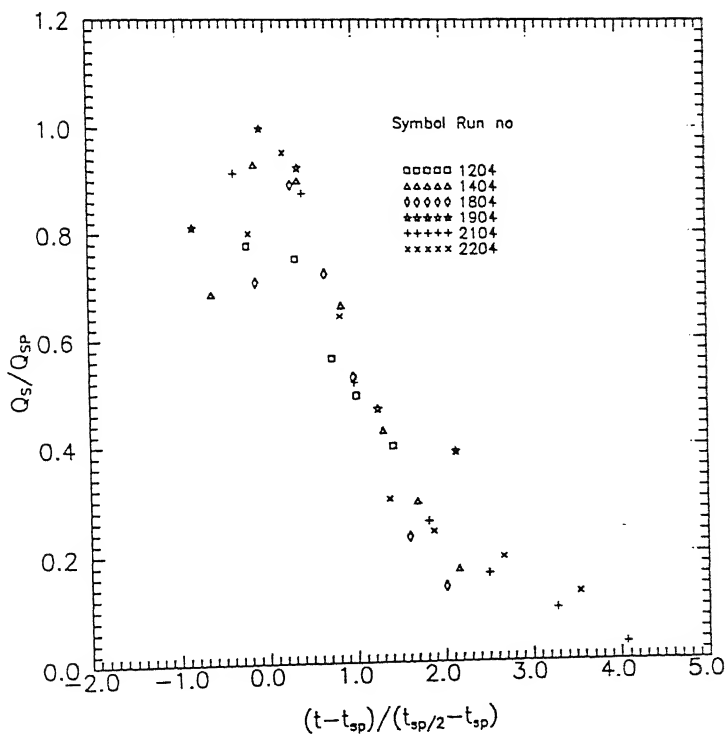


Fig. 7.5(b): Nondimensional sediment discharge graph

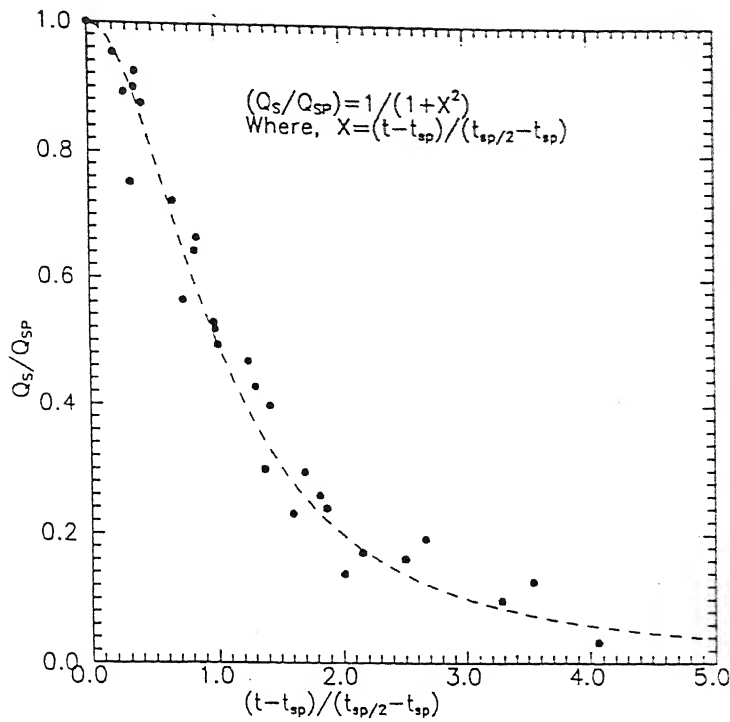


Fig. 7.5(c): Receding limb of nondimensional sediment discharge graph

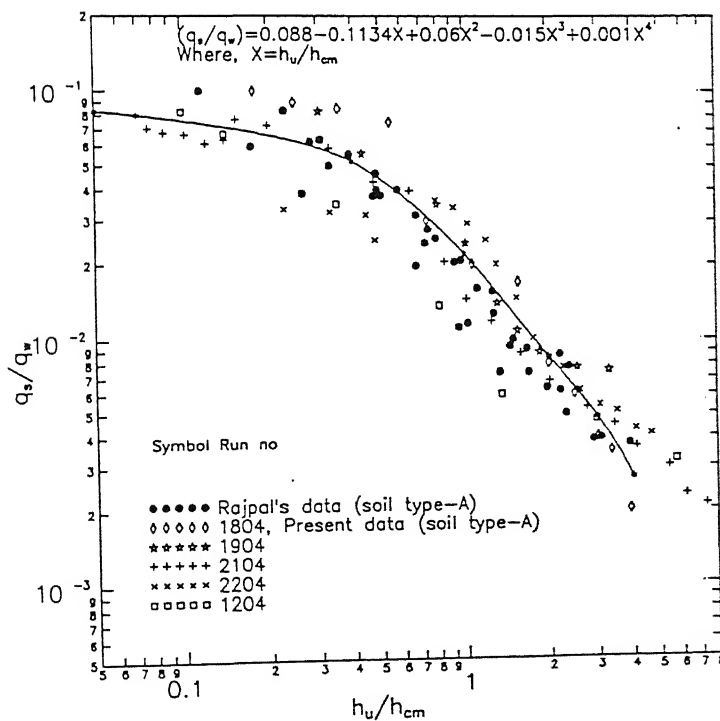


Fig. 7.5(d): Variation of sediment concentration with the ratio of head of water over crest of erodible bed to the crest height ( $h_{cm}$ )



The relation is given using regression analysis as:

$$\frac{h_u}{h_{cm}} = 9.91 - 7.34 \times \left[ \frac{\Delta H / H_D}{Q_{P.V.2}^{0.308}} \right] \quad (7.5d)$$

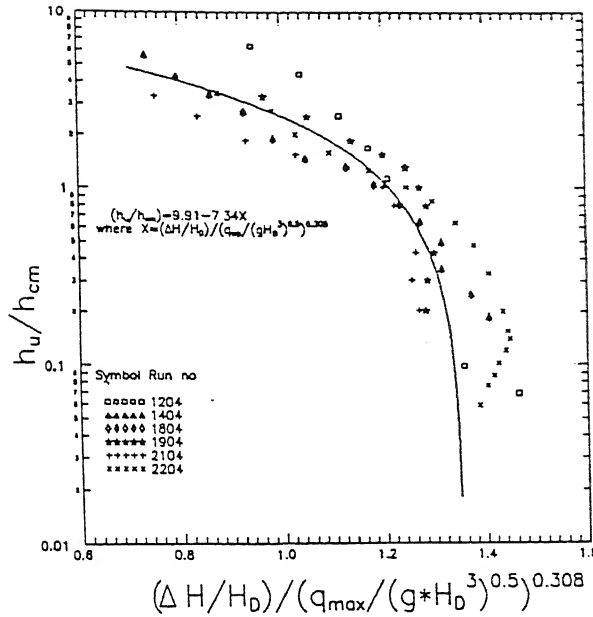


Fig. 7.5e : Variation of the ratio of head of water on the crest ( $h_u$ ) over the sediment bed to its height ( $h_{cm}$ ) with nondimensional drop of water  $\Delta H$ .

It is observed that sediment concentration  $q_s/q_w$  is the function of bed shear stress. With this in view, concentration ( $C$ ) is plotted against  $V_*^2/V_{SR}^2$  as indicated in Figure 7.5f. Concentration ( $C$ ), varies very steeply in the beginning of the erosion process indicating the difficulty in predicting  $C$  for given values of  $V_*^2/V_{SR}^2$ . This lead to correlate further with other parameters. Drop in the water level between downstream and upstream of the fuse plug, ( $\Delta H$ ) seems to be a important variable during the overtopping of the fuse-plug. Using regression analysis the following functional relation among them as shown in Figure 7.5(g) has been established:

$$\frac{q_s}{q_w} = \left[ \left( \frac{\Delta H}{H_D} \right)^{0.53} \times \left( \frac{V_*^{2.0}}{V_{SR}^{2.0}} \right)^{-1.77} \right] * 86.4 \quad (7.5e)$$

and the correlation coefficient  $R$  is 0.86. This indicates clearly, that the erosion process of the fuse-plug is a function of drop in the water surface level.

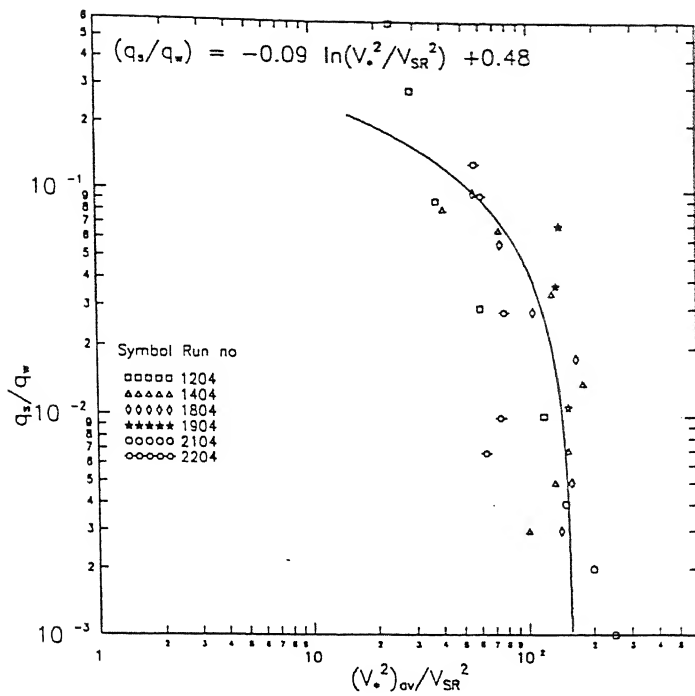


Fig. 7.5(f): Variation of sediment concentration(C) with average shear velocity( $V_*$ ) and soil resisting velocity( $V_{SR}$ )

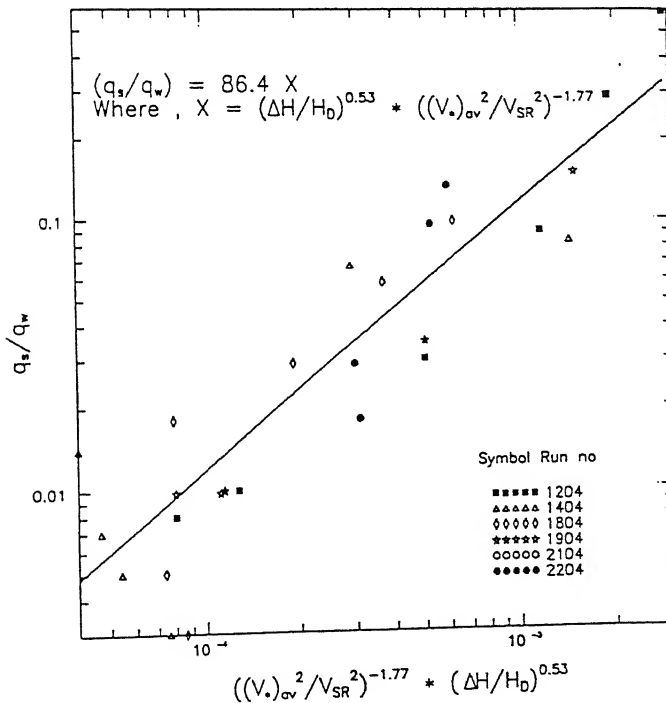


Fig. 7.5(g): Variation of sediment concentration(C) with average shear velocity( $V_*$ ) and soil resisting velocity( $V_{SR}$ ) and  $\Delta H$ .

## 7.6 Analogous Rigid Bed Profile Study

### a. Discharge Characteristics

The discharge and the flow depth relation obtained for the crest of erodible fuse plug sediment profile was found not to follow the weir type or spillway type relation. The value of exponent of the head acting over the erodible crest was of the order of unity instead of 3/2. This observation necessitated to verify on the rigid crest having the same sediment profile during the erosion. With this as aim, seven models of sediment profiles for the run no 1404, were built, one at a time, using cement and alluvial sand collected from river Ganga. This was done purposefully to maintain the same roughness characteristics of the mobile bed at a particular instant. For each rigid built-in sediment profile, experiments were carried out maintaining different ( $h_u/h_{cm}$ ) conditions. The discharge and head relations are plotted as shown in Figure 7.6(a). It may be noted that the discharge relationship follows weir relation as:

$$\frac{Q_w}{L} = h_u^{1.497} \times 20.7 \quad (7.6a)$$

where width of the fuse plug  $L = 20\text{cm}$ . From the Equation (7.6a), the coefficient of discharge works out as 0.707. Considering the contraction on either side of the rigid portion of the embankment into the analysis, the effective width is computed as:

$$L_{eff} = (L - 0.2h_u) \quad (7.6b)$$

This length is used in analysis and the discharge relationship is written as,

$$\frac{Q_w}{L_{eff}} = h_u^{1.53} \times 21.0 \quad (7.6c)$$

and  $c_d$  is found to be 0.71. From this analysis it may be noted that the flow characteristics over rigid bed crest follows exactly the weir relation. This leads to a question as to why the exponent of  $h_u$  in case of mobile bed is not equal to 1.5. It may be postulated that the crest level goes on changing rapidly with time due to erosion, probably this may be the case for the deviation from weir formula.

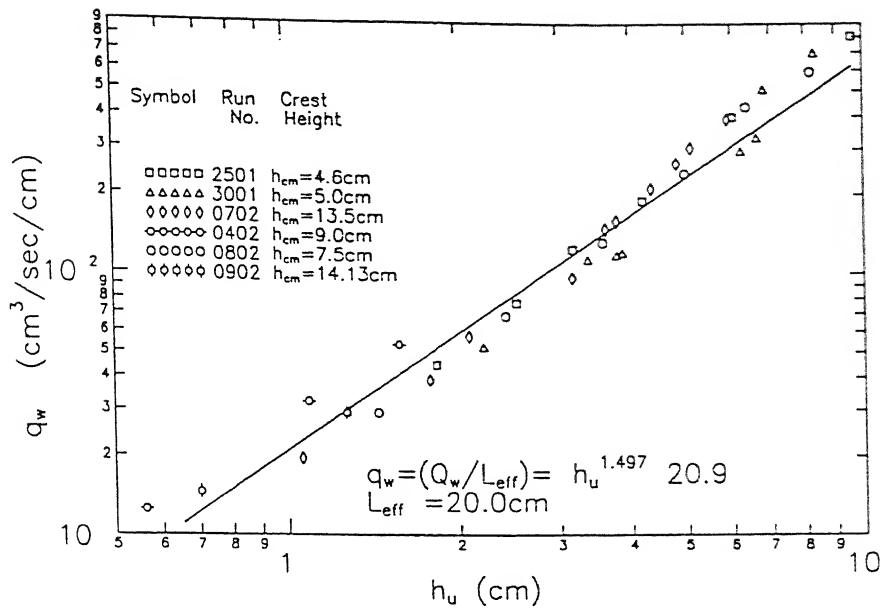


Fig. 7.6(a): The relation of head of water over analogous rigid sediment bed crest with its corresponding outflow discharge intensity( $q_w$ ) without considering contraction length of weir

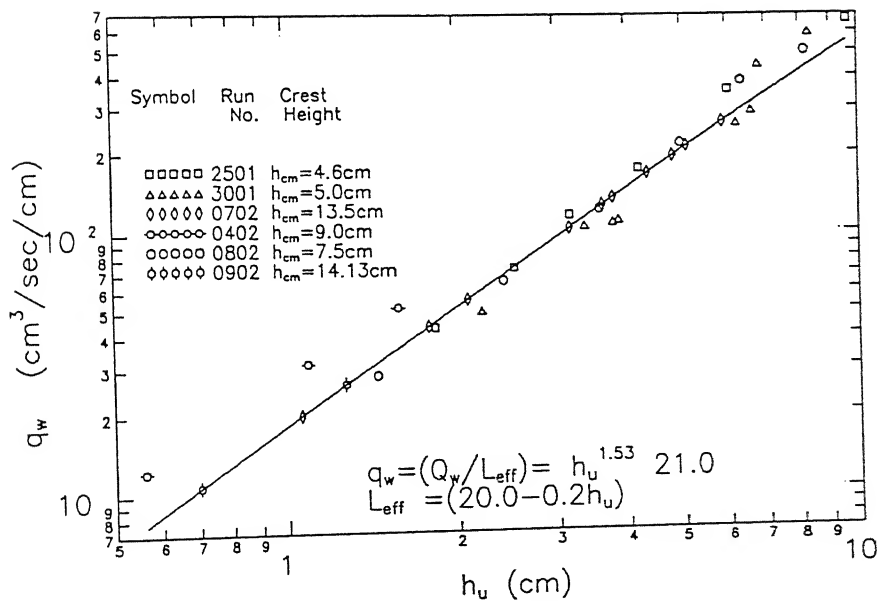


Fig. 7.6(b): The relation of head of water over analogous rigid sediment bed crest with its corresponding outflow discharge intensity( $q_w$ ) by considering the contraction length of weir.

## b. Energy Loss Characteristics

The energy levels at the upstream and the downstream of the rigid model are computed as  $E_1$  and  $E_2$ . This energy ratio  $E_2/E_1$  is plotted against  $h_u/h_{cm}$  as shown in Figure 7.6(c). As  $h_u/h_{cm}$  increases the ratio  $E_2/E_1$  increases. For higher value of  $h_u/h_{cm}$  this ratio reaches almost 0.8. The relations among them for rigid profiles of cohesionless sand from river Ganga and its corresponding mobile bed and coarse sand from river Yamuna are shown in Figure 7.6(d), and these relations between them may be written in Equations (7.6d), (7.6e), and (7.6f) respectively.

$$\frac{E_2}{E_1} = 0.14 + 0.86 \left( \frac{h_u}{h_{cm}} \right) - 0.31 \left( \frac{h_u}{h_{cm}} \right)^2 \quad (\text{Type-A soil, Rigid Profile}) \quad (7.6d)$$

$$\frac{E_2}{E_1} = 0.061 + 0.87 \left( \frac{h_u}{h_{cm}} \right) - 0.283 \left( \frac{h_u}{h_{cm}} \right)^2 \quad (\text{Type-A soil, Mobile Profile}) \quad (7.6e)$$

$$\frac{E_2}{E_1} = -0.038 + 0.79 \left( \frac{h_u}{h_{cm}} \right) - 0.234 \left( \frac{h_u}{h_{cm}} \right)^2 \quad (\text{Type-D and E soil, Mobile Profile}) \quad (7.6f)$$

Figure 7.6(d) reveals their inter-relationship. This curve relates the energy level at downstream due to flow over a rigid bed not involving any erosion or transport of sediment over the fuse-plug surface. It is of interest to know how much extra energy loss due to the same bed profile occurs if it is made mobile. For this condition energy level at upstream and downstream are plotted against  $h_u/h_{cm}$  for two different soils namely: type-A soil, fine sand collected from river Ganga and type-D soil, coarse sand collected from river Yamuna. It may be observed that the energy relation curve lies below the rigid bed and for Yamuna sand lies below the Ganga sand. This is due to the size variation of the sediment collected from those rivers. Median sediment size is 0.16mm for river Ganga sand and for river Yamuna sand it is 0.6mm. This relation clearly shows the amount of energy spent in eroding and transporting it, depending on the size of the sediment as well as  $h_u/h_{cm}$ .

For type-A soil, it was of interest to relate the magnitude of energy loss that occurred exclusively for sediment erosion and transportation. This is achieved by computing the difference of energy loss between the rigid and corresponding mobile bed of sediment profile for the same value of  $E_1$  from Figure 7.6(d). This value is plotted to its corresponding value of  $Q_s/Q_w$ .

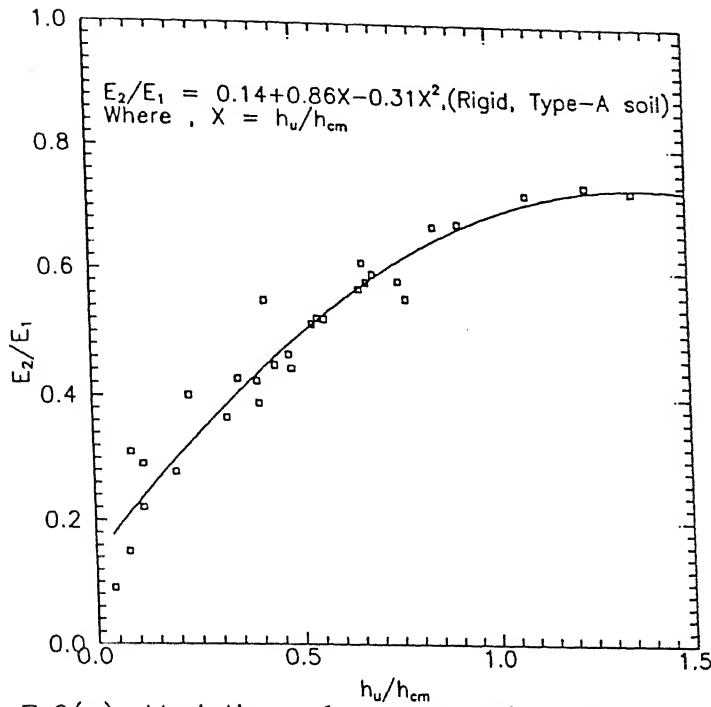


Fig. 7.6(c): Variation of energy ratio, between downstream and upstream of fuse plug to the ratio of head of water over the rigid crest of analogous erodible sediment bed to its crest height

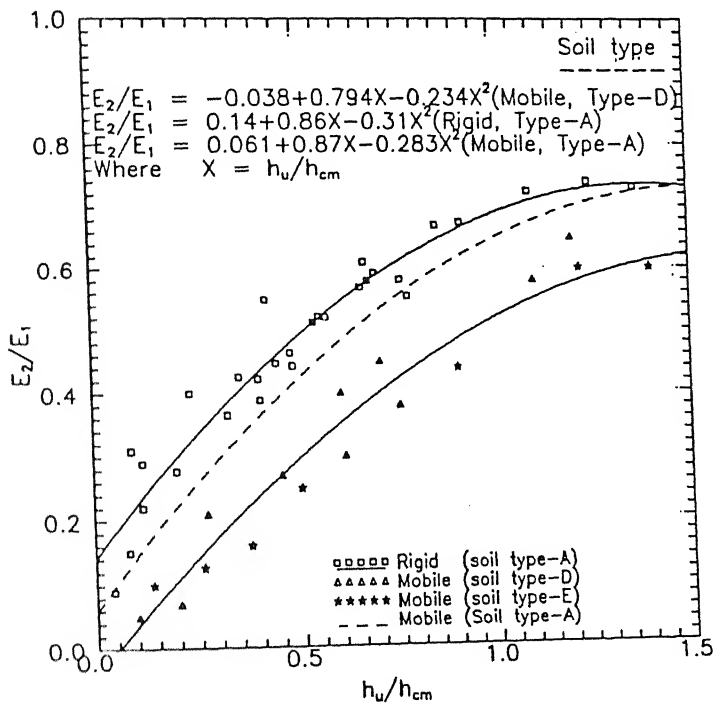


Fig. 7.6(d): Energy loss characteristics in mobile and analogous rigid sediment bed profile models with different  $h_u/h_{cm}$

The  $h_u/h_{cm}$  is the link to get these values corresponding to each other as the experiments conducted in two different phases. The relation between them is plotted in Figure 7.6(e). It can be observed from Figure 7.6(e) that the energy loss  $(dE)_{RM} / E_1$  increases very steeply, the concentration increases from 0.01 to 0.05. Later on energy loss gradually increases with further increase in concentration. Here  $(dE)_{RM}$  is defined as follows,

$$(dE)_{RM} = [(E_2)_{rigid} - (E_2)_{mobile}] \quad (7.6g)$$

It may be noted that 10% of the upstream energy ( $E_1$ ) is spent when the sediment concentration is 0.14. This is the stage of hyperconcentration flow. This type of analysis could not be carried out for coarse sediment of river Yamuna sand because of nonavailability of concentration information for a given  $h_u/h_{cm}$ .

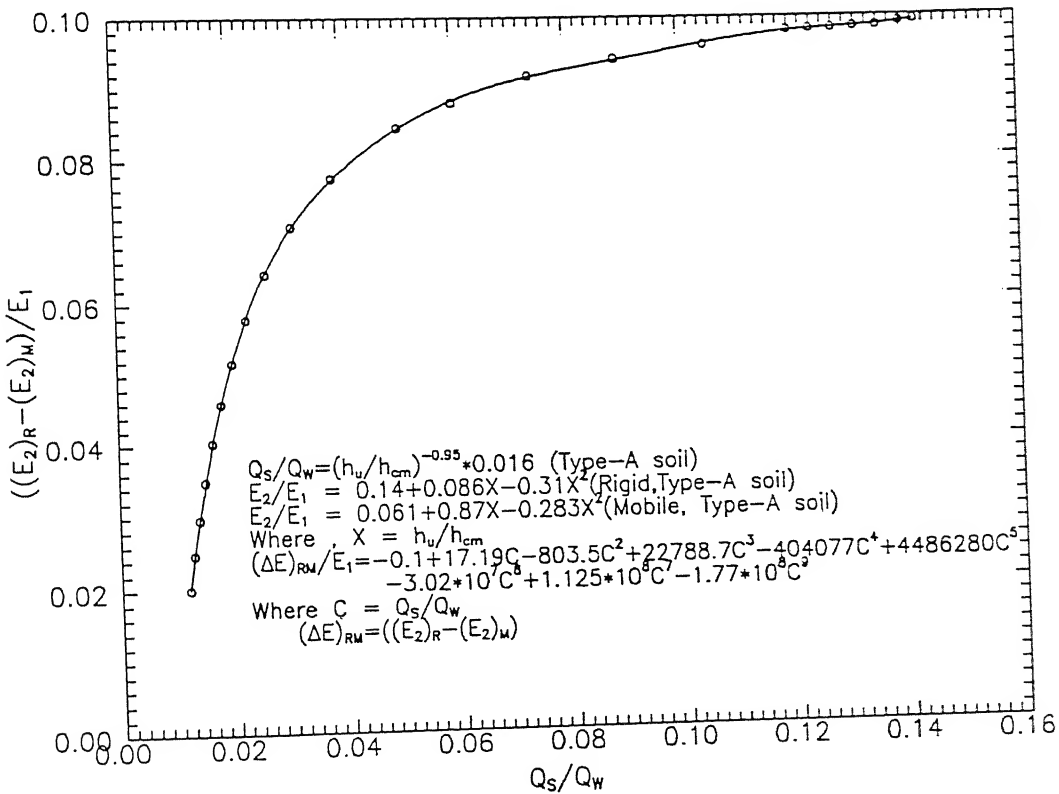


Fig. 7.6(e): Variation of nondimensional magnitude of the difference in energy loss between mobile and its analogous rigid sediment bed profile with concentration of sediment

## 7.7 Hydrograph and Sediment Discharge Graphs

In fuse-plug washout study, in addition to the information regarding crest movement, crest variation and rate of crest variation, one will be interested to know the outflow discharge and sediment discharge at any instant of time. The determination of these quantities for any given flow situation for a given fuse plug with certain properties of fill materials will enable one to understand the mechanism involved in the fuse-plug washout process. Keeping this aspect in view both water discharge and sediment discharge at any time are analysed in the following paragraphs.

### a. Variation of Water Discharge Intensity with Time

The discharge intensity ( $q_w$ ) over the fuse-plug is plotted against time as a sample case in Figure 7.7(a). It may be observed that  $q_w$  increases, reaches a peak and then decreases gradually, reaches a state of equilibrium discharge intensity as the time increases. This relationship is observed in almost all the experimental runs.

Using the peak value of  $q_w$  and its corresponding time  $t_{wp}$  as scales,  $q_w/q_{wp}$  is plotted against  $t/t_{wp}$  as shown in Figures 7.7(b), (c), and (d) for soil types *A*, *B* and *C* respectively. For soil type *B* and *C* the peak value  $q_{wp}$  occurs almost at the end of sediment washout in fuse-plug. Hence, Figures 7.7(c) and (d) contain only rising limb of the variation of water discharge with time. The relation between  $q_w/q_{wp}$  and  $t/t_{wp}$  is written in the form:

$$\frac{q_w}{q_{wp}} = \left( \frac{t}{t_{wp}} \right)^n \exp \left\{ 1 - \left( \frac{t}{t_{wp}} \right)^n \right\} \quad (7.7a)$$

The value of 'n' is obtained by trial and error method of fitting curve. The values of exponent 'n' are given below.

Type of Soil	Exponent (n) in eqn 7.7a
A	2.50
B	0.50
C	0.45



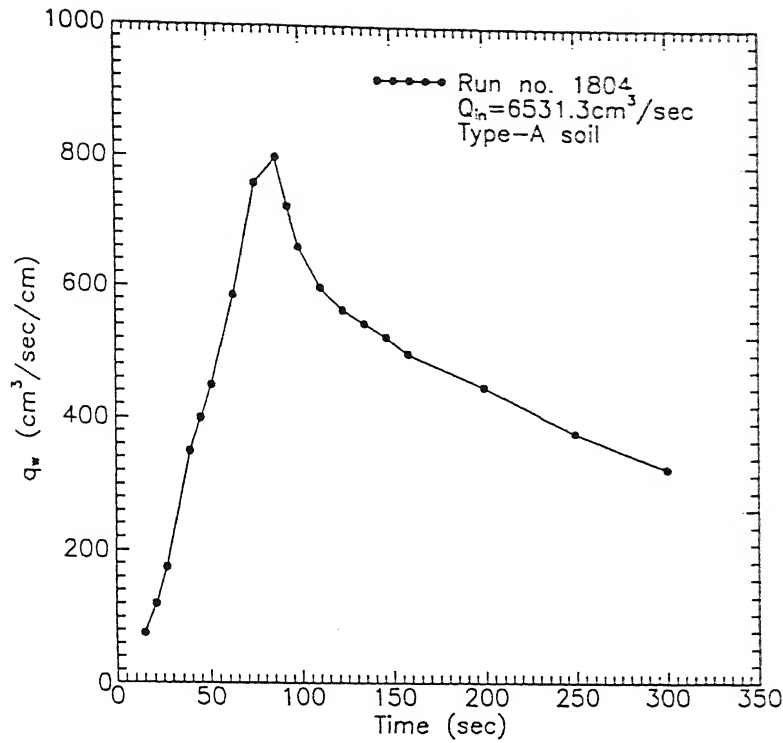


Fig. 7.7(a): A typical variation of water discharge intensity ( $q_w$ ) with time for run no. 1804

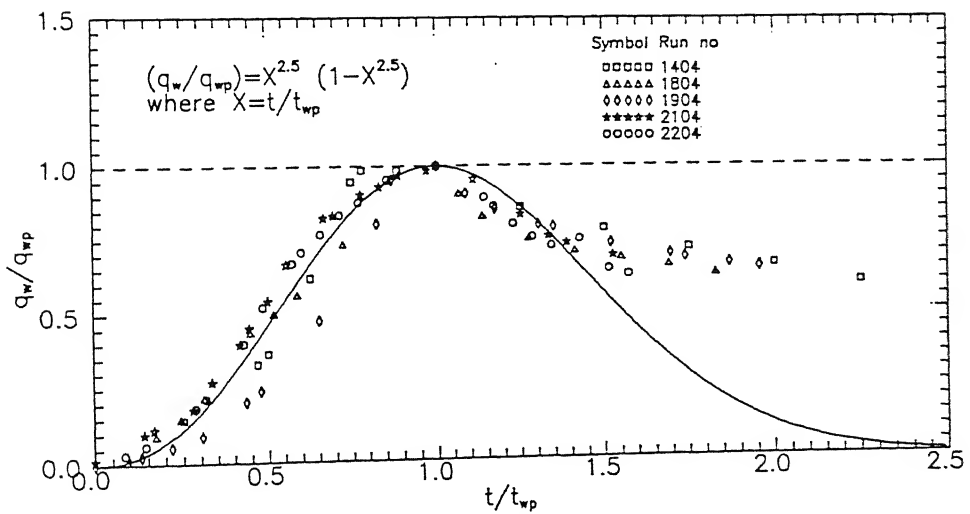


Fig. 7.7(b): Nondimensional hydrograph for washout of fuseplug with type-A soil fill

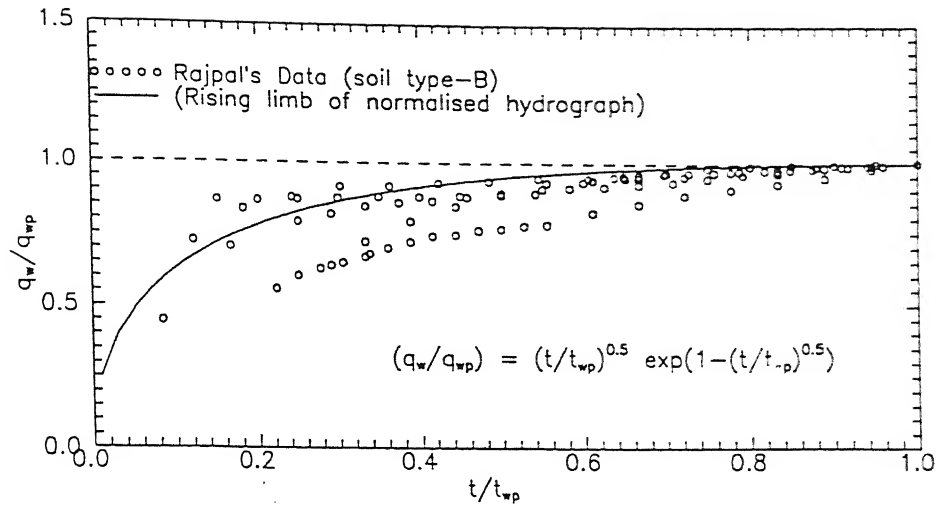


Fig. 7.7(c): Variation of normalised outflow discharge intensity( $q_w$ ) with normalised time( $t/t_{wp}$ ) for fuseplug with type-B soil fill

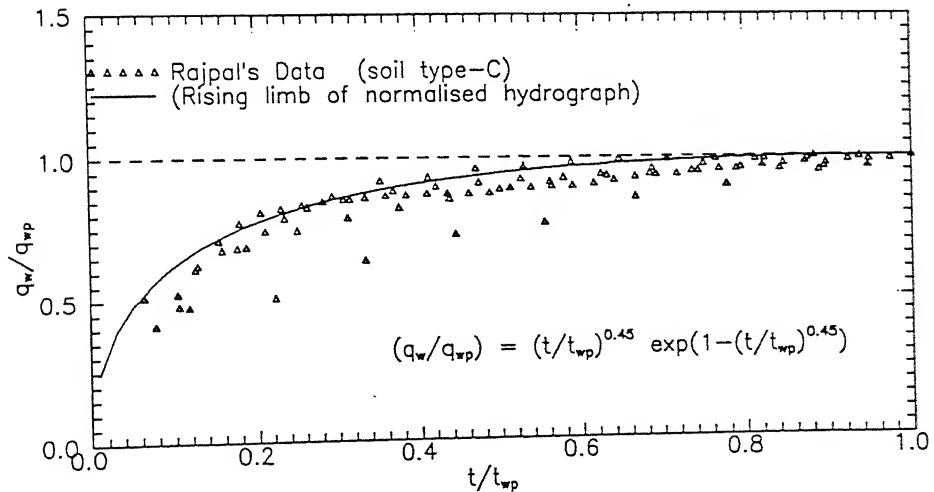


Fig. 7.7(d): Variation of normalised outflow discharge intensity( $q_w$ ) with normalised time( $t/t_{wp}$ ) for fuseplug with type-C soil fill

It may be noted that the value of exponent 'n' for cohesionless soil (type-A) is very high (2.5) whereas for cohesive soil or for its mix is of the order of 0.5. This may be due to presence of cohesion, which offers more resistance to the erosion and delay the washout process.

The scale  $q_{wp}$  is plotted against inflow discharge in a dimensionless form for all the three types of soils used in the present fuse-plug model as shown in Figure 7.7(e). It may be observed that  $q_{wp}$  is related to  $q_{in}$  as obtained from regression analysis:

$$\frac{q_{wp}}{\sqrt{gH_D^3}} = \left( \frac{gq_{in}}{V_{SR}^3} \right)^{0.45} \times 0.0057 \quad (7.7b)$$

To compute the outflow discharge at any time 't', it is essential to know the time scale parameter  $t_{wp}$ . This time of occurrence of peak discharge is nondimensionalised with  $q_{in}$  and capacity of the reservoir, plotted against nondimensional  $q_{wp}$  of the form  $\left( \frac{q_{wp}}{V_{SR} H_D} \right)$  as shown in Figure 7.7(f). The relation between them may be written as:

$$\frac{\bar{q}_{in} t_{wp}}{\text{Capacity}} = 0.384 - 0.0907X + 0.007X^2 - 0.00015X^3 \quad (7.7c)$$

$$\text{where, } X = \left( \frac{q_{wp}}{V_{SR} H_D} \right)$$

An interesting observation may be marked in Figure 7.7(f). The time to peak discharge closely is related to the peak discharge and sediment resisting velocity for a given capacity of the reservoir, inflow intensity and height of dam. This value initially decreases, reaches a minimum of the order of 0.06 then gradually increases and as the tail variation trend shows it may remain constant. This study shows there is a mutual inter-relationship among  $q_{in}$ , capacity,  $q_{wp}$ ,  $t_{wp}$ ,  $H_D$  and  $V_{SR}$ .

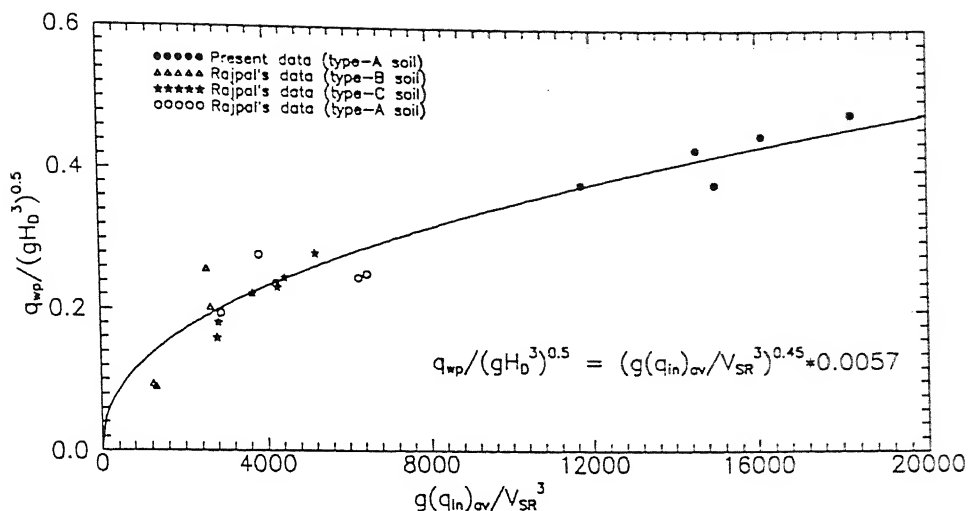


Fig. 7.7(e): Variation of nondimensional outflow discharge scale( $q_{wp}$ ) with average inflow discharge intensity and soil resisting velocity,  $V_{SR}$

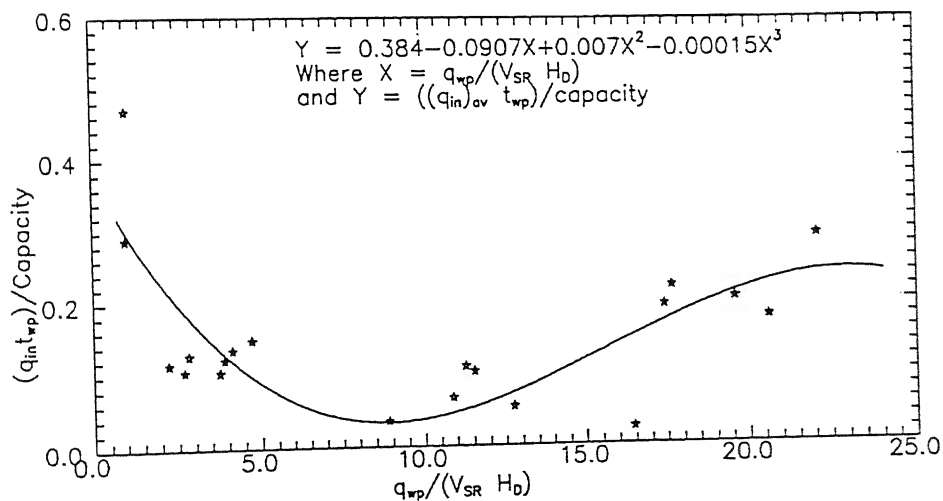


Fig. 7.7(f): Variation of nondimensionalised time with nondimensionalised maximum outflow discharge intensity

### b. Sediment Discharge Intensity with Time

The sediment discharge per unit width ( $q_s$ ) is plotted against time as can be seen in Figure 7.7(g). The variation of  $q_s$  with time follows similar trend of  $q_{wp}$ , increases initially reaches peak and gradually decreases with increasing time. Using the maximum value of sediment discharge intensity, ( $q_{sp}$ ), and its corresponding occurrence of time ( $t_{sp}$ ), as scales,  $q_s/q_{sp}$  is plotted against  $t/t_{sp}$ . All the data in type-A soil model of the present investigation and data of Rajpal is incorporated in the Figure 7.7(h). An empirical relation among them may be written as :

$$\frac{q_s}{q_{sp}} = \left( \frac{t}{t_{sp}} \right)^2 e^{\left[ 1 - \left( \frac{t}{t_{sp}} \right)^{2.0} \right]} \quad (7.7d)$$

The agreement between them may be considered fair.

The sediment discharge scales ( $q_{sp}$ ) is plotted with inflow discharge intensity ( $q_{in}$ ) in a nondimensional form using height of the fuse plug ( $H_D$ ) and sediment resisting velocity ( $V_{SR}$ ) as indicated in Figure 7.7(i). The relationship between them is obtained from regression analysis only for type-A soil.

$$\frac{q_{sp}}{\sqrt{g} H_D^3} = \left( \frac{g q_{wp}}{V_{SR}^3} \right)^{0.23} \times 0.01 \quad (7.7e)$$

In the computation of  $Q_S$  at any time, the time scale parameter  $t_{sp}$  is essential to be estimated. From the regression study it is found that  $t_{sp}$  highly depends on  $t_{wp}$  and  $q_{wp}$ . The ratio of time of occurrence of peak sediment discharge,  $t_{sp}$  to the time of occurrence of peak water discharge,  $t_{wp}$  taken as  $t_{sp}/t_{wp}$  is plotted against nondimensionalised peak water discharge  $q_{wp}$  as  $q_{wp}/(V_{SR} H_D)$  in Figure 7.7(j). It may be observed that the time scale ratio  $t_{sp}/t_{wp}$  decreases with increase in intensity of peak water discharge or decrease in soil resistivity velocity. The relation between them is obtained as:

$$\frac{t_{sp}}{t_{wp}} = \frac{1.67}{\left( \frac{q_{wp}}{V_{SR} H_D} \right)^{\frac{1}{2}}} \quad (7.7f)$$

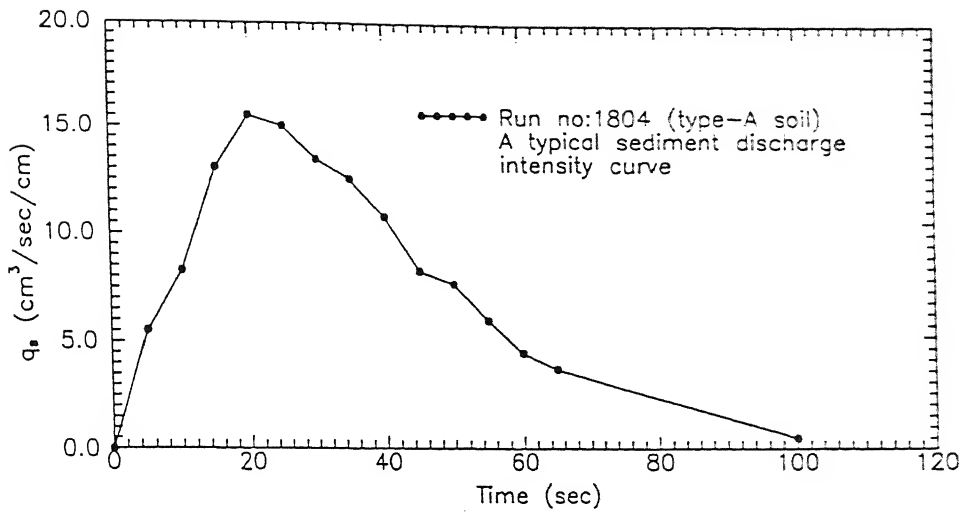


Fig. 7.7(g): A typical variation of the sediment discharge intensity for run no 1804 with time

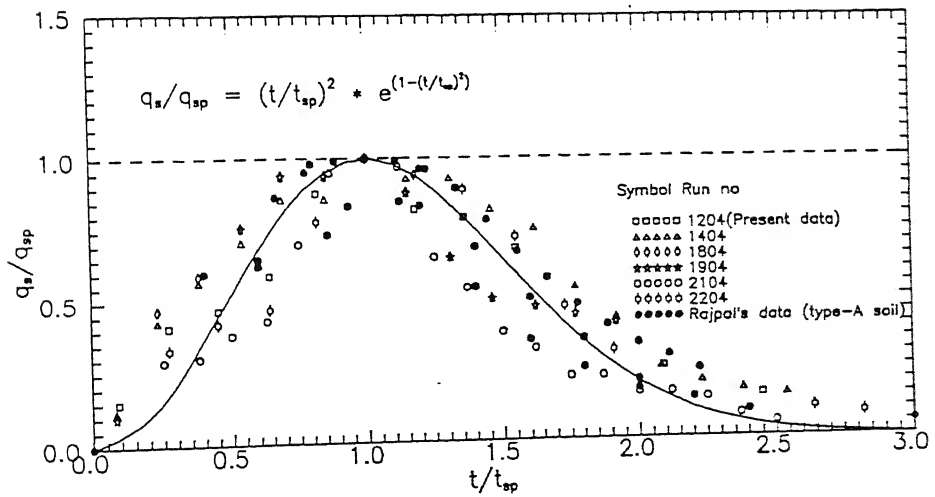


Fig. 7.7(h): Variation of nondimensional sediment discharge intensity with its normalised time ( $t/t_{sp}$ )

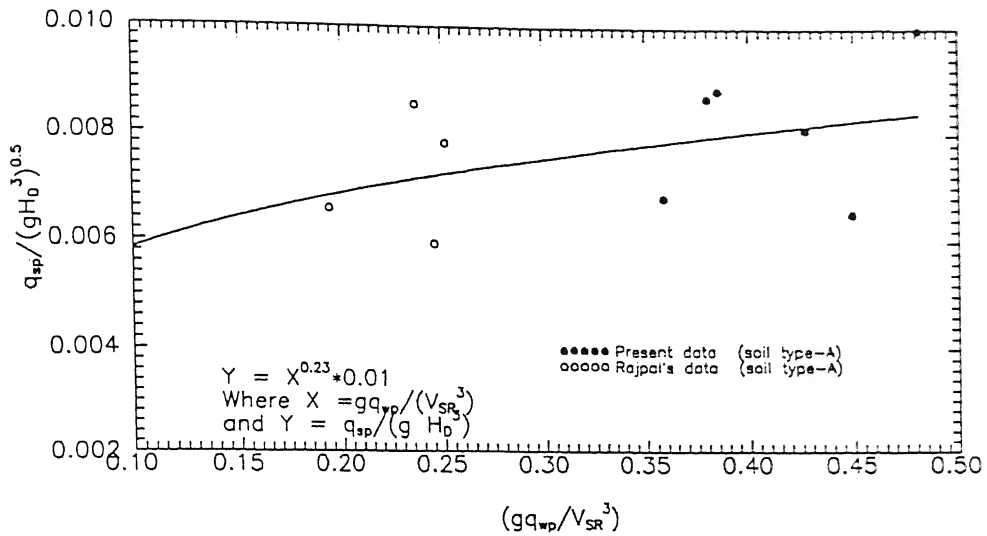


Fig. 7.7(i): Variation of sediment discharge intensity scale( $q_{sp}$ ) for type-A soil with peak outflow discharge( $q_{wp}$ ) and  $V_{SR}$

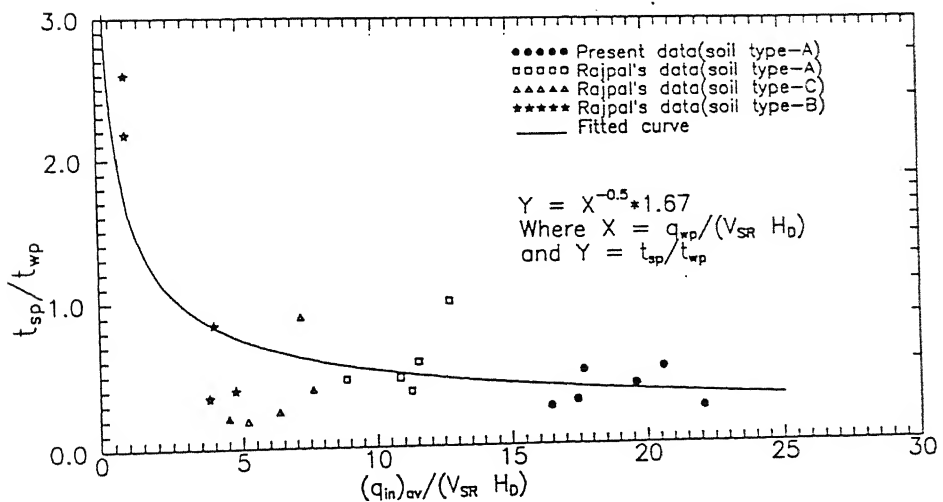


Fig. 7.7(j): Lag in the time of occurrence of peak sediment discharge with respect peak to outflow discharge.

### c. Time of Erosion ( $t_{95}$ )

Sediment erosion in the final stage of the washout process of fuse-plug becomes almost zero and only the water will be flowing out. Time corresponding to 95% of the erosion of sediment in the fuse-plug is used as erosion time and is denoted as  $t_{95}$ . In order to find  $t_{95}$  for any given situation, it is nondimensionalised with reservoir time scale ( $T_*$ ) and is plotted against  $q_{in}$  along with  $V_{SR}$  and  $H_D$  as indicated in Figure 7.7(k). The functional relation among them may be written as:

$$\frac{t_{95}}{T_*} = 2.55 - 0.72X + 0.1X^2 - 0.0013X^3 \quad (7.7g)$$

$$\text{where, } X = \frac{\bar{Q}_{IN}}{V_{SR} H_D} = Q_{INN} (Q_{IN} - \text{Number}).$$

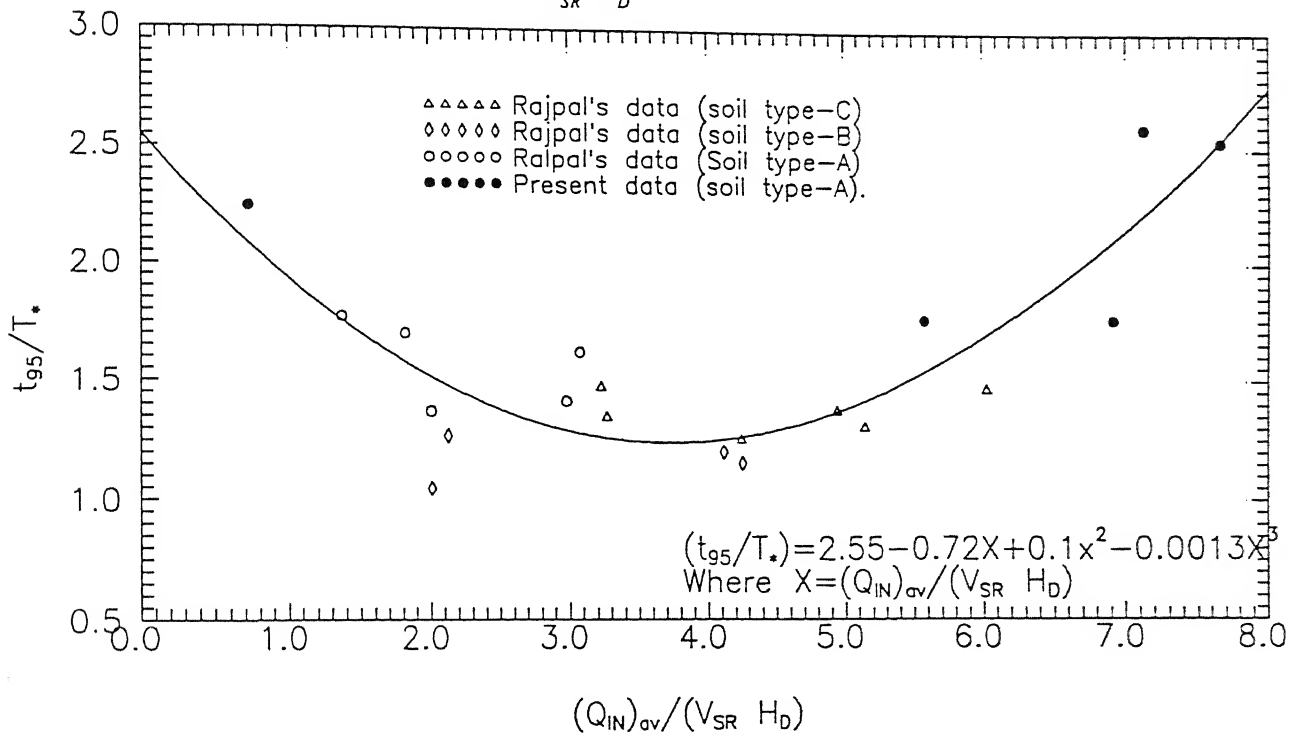


Fig. 7.7(k): Variation of nondimensional duration of washout process with average inflow discharge intensity  $V_{SR}$  and height of the fuse plug

It is observed that the ratio  $t_{95}/T_*$  decreases and reaches minimum of the order of 1.25 and increases further with increase in  $q_{in}$ . It may be mentioned here that increase in  $t_{95}$  may occur due to increase in  $q_{in}$  or due to decrease in  $V_{SR}$  for a given height of the dam. This observation can be seen very clearly in the Figure 7.7(k).



## 7.8 Methodology to Predict Washout Process of Fuse Plug

### a. Procedure to predict Washout Variables

- i. From the known value of average inflow discharge intensity ( $\bar{q}_{in}$ ), soil resisting velocity ( $V_{SR}$ ), height of fuse-plug ( $H_D$ ), the reservoir time scale ( $T_*$ ) and drop scale ( $H_*$ ) can be computed from Figures 7.1(c) and 7.1(d), Equations (7.1a) and (7.1b).
- ii. Knowing  $T_*$  and  $H_*$  and fuse-plug geometry,  $t_{50}$ ,  $X_{50}$  can be computed from Figures 7.3(e) and 7.3(g), Equations (7.3c) and (7.3e) respectively.
- iii. The duration of washout ( $t_{95}$ ) can be obtained from Figure 7.7(k), Equation (7.7g).
- iv. The crest height of erodible sediment bed ( $h_{cm}$ ) during washout can be computed by knowing  $t_{50}$  from Figure 7.3(f), Equation (7.3d) and hence  $dh_{cm}/dt$  can be obtained.
- v. The sediment bed height ( $h_c$ ) at any location ( $X$ ) from the crest position can be obtained from Figure 7.3(c), Equation (7.3b).
- vi. From Figure 7.5(e), Equation (7.5d) head of water over the crest ( $h_u$ ) at any time of washout process can be computed knowing  $t_{50}$ .
- vii. From the known values of  $h_u$  and  $h_{cm}$ , discharge coefficient  $C_d$  can be obtained from Figure 7.2(b), Equation (7.2b) and  $Q_w$  from Equation (7.2c), Figure 7.2(a).
- viii. Assuming flow to be critical at the crest the water level at crest ( $h_{wc}$ ) can be estimated for known outflow intensity and subsequently drop of water level at the crest can be computed.
- ix. The receding length ( $X_m$ ) of the crest of sediment bed from upstream face of the fuse plug can be obtained knowing drop of water level at crest from Figure 7.3(b), Equation (7.3a).
- x. The maximum value of sediment eroding velocity ( $V_{SYM}$ ) can be obtained from the mean curve of Figure 7.4(c) once  $q_{wp}$  and  $V_{SR}$  are known.
- xi. The maximum value of outflow intensity  $q_{wp}$  can be obtained from known values of ( $\bar{q}_{in}$ ),  $V_{SR}$  and  $H_D$  from Figure 7.7(e), Equation (7.7b).
- xii. The average velocity of eroded sediment can be obtained from Figure 7.4(b) for known  $V_u(\sqrt{2gh_u})$  at any time of washout process.
- xiii. The average eroded height of bed profile ( $\bar{\Delta}h_c$ ) at any time  $\Delta t$  can be obtained from the predicted bed profile,  $h_c = f(x)$ , Figure 7.3(c), Equation (7.3 b).

- xiv. Assuming uniform erosion along the width of fuse-plug, eroded sediment volume  $\forall_s$  at any instant of washout process can be obtained knowing  $(\bar{\Delta}h_c)$ ,  $B_{fp}$ .
- xv. So the sediment discharge,  $Q_s = d(\sum \forall_s)/dt$  can be estimated.
- xvi. From known value of  $h_u/h_{cm}$ ,  $C = q_s/q_w$  can be obtained from Figure 7.5(d), Equation (7.5b). Using the predicted value of  $q_w$  in step vii,  $q_s$  can be estimated. The average value of estimated of  $q_s$  and its computed value in step xv can be used.
- xvii. The energy loss  $(\Delta E)_{RM}$  can be related to  $h_u/h_{cm}$ , using the Figure 7.7(c).
- xviii. The drop of water level  $\Delta H$  can be obtained for a given value of  $h_u/h_{cm}$ , during the washout process from Figure 7.5(e), Equation (7.5d).
- xix. From the computed values of  $\Delta H$ ,  $q_s/q_w$  and known values of  $V_{SR}$  and  $H_D$ , average bed shear stress  $\bar{V}_*$  can be computed from Figure 7.5(g), Equation 7.5(e).
- xx. Time of occurrence of peak water discharge ( $t_{wp}$ ) can be obtained from Figure 7.7(f), Equation (7.7c).
- xxi. Time of occurrence of sediment peak discharge ( $t_{sp}$ ) can be obtained from Figure 7.7(j) Equation (7.7f).

### b. Prediction of Water and Sediment Discharge During Washout Process

Knowing  $q_{wp}$ ,  $t_{wp}$ ,  $q_{sp}$  and  $t_{sp}$  the normalised hydrograph and sediment discharge graph can also be obtained by estimating the exponent 'm' in Equation (7.7a) properly.

In the present method, no functional relation has been suggested to get these exponents for a given situation. For normalised hydrograph of type-A soil fill,  $m=2.5$  whereas for type - B soil fill  $m \cong 0.5$ , as shown in Figures 7.7(b), (c) and (d).

For normalised sediment discharge graph for type-A soil fill  $m = 2.0$  as shown in Figure. 7.12 (h), Equation (7.7d).

### c. Flow Chart

The steps mentioned in the previous section are represented in a more compact form in a flow chart. For given geometry of the fuse plug, the properties of its fill material, the reservoir capacity and inflow discharge characteristics, the suggested flow chart can be transformed to a computer code to know the various washout variables involved in the fuse plug at different time of washout. The time step can be chosen for the computation once the duration of washout is estimated with the established functional relation in the present study.

# COMPUTATION OF CRITERION VARIABLES DURING WASHOUT PROCESS OF FUSE PLUG

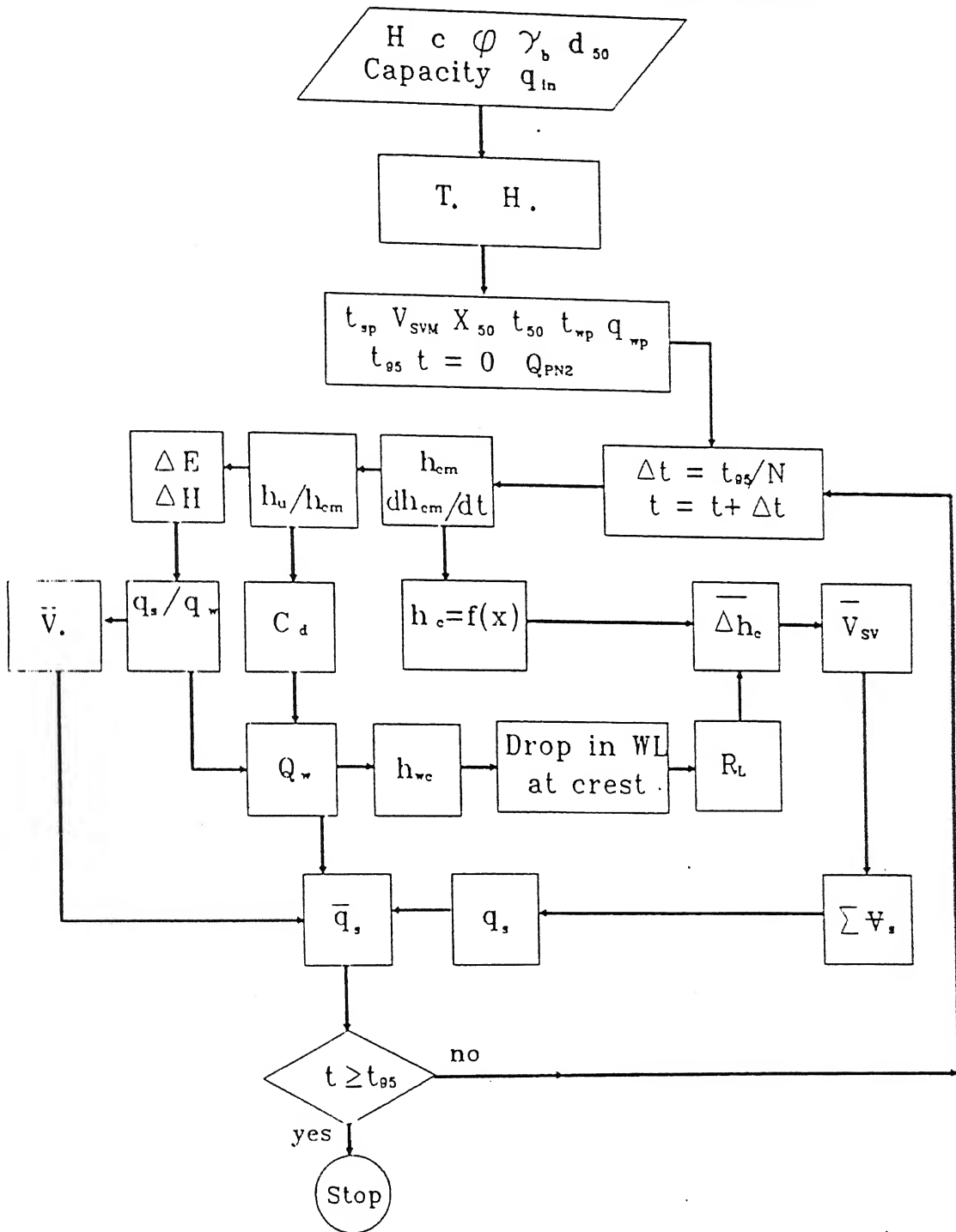


Fig. 7.7(1): Flow chart to compute the variables controlling fuse plug washout process

## 7.9 Conclusions and Limitations

Fuse-plug washout and dam breach process by their inherent character look same outwardly. But in case of fuse-plug there is restriction on its possible lateral erosion. This causes the flow characteristics to change. Contrary to dam breach, in fuse-plug study the importance is laid on how quickly it gets washed out by releasing reservoir water without endangering the main structures like spillway and dam body. From the analysis of experimental data obtained from washout process of fuse-plug model studies with three different soil fills, *type-A* (cohesionless) soil, *type-B* (cohesive) soil, and *type-C* (mixture of cohesionless and cohesive soil in 60:40 ratio) the following conclusion may be drawn.

### a. Conclusions

- i. Introduction of time scale and length scale of the reservoir may be very significant parameters to study the washout behaviour of the fuse-plug as it relates implicitly both the flow characteristics and properties of the fill material.
- ii. Crest height ( $h_{cm}$ ) of the sediment bed profile during the washout and its rate of variation can be predicted during the washout of fuse plug which will help to predict the sediment bed profile,  $h_c(X)$ .
- iii. Prediction of water discharge passing through the fuse-plug during washout is attempted only in the rising part of washout hydrograph. From the study of the relation between  $t_{wp}$  and  $t_{95}$ , it may be observed that the washout process is almost in the final stages of erosion when water discharge attains its peak value.
- iv. Prediction of some of the key controlling parameters like, peak water discharge intensity ( $q_{wp}$ ), time of occurrence of  $q_{wp}$  and peak sediment discharge ( $q_{sp}$ ) and its time of occurrence  $t_{sp}$  is possible by the present approach. But the prediction of  $q_{sp}$  demonstrated only for cohesionless (type-A soil) of a particular value of average grain size ( $d_{50} = 0.16mm$ ), which can not be generalised.

### b. Limitations

The present study has its limitations also as described below.

- i. In the present analysis, geometry of the fuse-plug is maintained constant. Experiments with different geometry of the fuse-plug are needed for generalisation of the analysis.

- ii. The prototype information available in literature could not be used in the present analysis because of the limitations on the available information. Hence the validity of present procedure needs to be tested with field data.

Lastly it can be said that being handicapped with these two limitations, the analysis has not lost the rationality, rather it has a newness in its own form.

## **CHAPTER VIII**

# **CONCLUSIONS AND RECOMMENDATIONS**

### **8.1 General**

Breach formation in a dam and washout process of a fuse plug due to overtopping flow have been considered and analysed in the preceding chapters.

Erosion of sediment, channelisation, crest movement, crest widening, sediment transport and energy dissipation are the processes associated with breach formation. These processes have been experimentally studied with two types of soil embankment models, cohesionless and cohesive soils. Water surface levels, sediment bed levels, and width of breach at different sections along the breach in the direction of flow, have been continuously measured from the instant of start of breach till the stabilisation of the breach. Twelve and five runs have been carried out with cohesionless and cohesive soil embankment models, respectively.

Analysis of data involves development of relations for flow over the breach, widening and deepening of the breach, sediment discharge and energy loss associated with the breach formation. Analysis of field data along with the experimental data from the present study leads to prediction of final breach dimensions and peak discharges associated with them. A method to predict the breach process has also been developed and verified with limited available field data.

A weak granular embankment, which may or may not have a clay cover, is built along the axis of the dam body to act as automatic excess flood releasing device. The embankment is

designed to be washed out during high floods. Such an auxiliary outlet which augments the service spillway by passing large flood flows is called a fuse plug. Experiments are conducted on the fuse plug models built of different types of soils. Water surface levels are measured continuously at different locations. Eroded Sediment beds are marked on the fuse plug side walls. Analysis of flow over the fuse plug, erosion of sediment and energy loss have been carried out. Discharge characteristics of non-erodible fuse plug profiles are measured and compared with erodible fuse plug profiles.

Based on the analysis of experimental data, major conclusions for embankment dam breach and fuse plug have been presented under separate headings.

## 8.2 Dam Breach Process

Experimental data is analysed in terms of criterion variables and predictor variables. Predictor variables are dam geometry, capacity of reservoir and inflow discharge. The criterion variables are variations of breach geometry, outflow discharge, erosion rate of bed and width, sediment discharge and energy loss. Some of these functional relations have been modified suitably using available field data, so that the prototype breach process can be predicted with more confidence. Analysis of the results is presented under the headings namely, breach morphology, breach hydraulics, and breach erosion.

### a. Morphological Characteristics

- i. Photographs taken during breach process for cohesionless soil embankment show the different states of erosion, channelisation, collapsing of bank, crest formation, and channel widening.
- ii. Planform of the breach channel in cohesionless embankment and cohesive embankment has converging section, throat and diverging section. The position of the throat moves upstream as the process continues. This is evident from the photographs taken during the breach process.
- iii. The cross-sections of breach during erosion of cohesionless soil embankment is almost rectangular in shape, having steep banks, accompanied by bank collapsing. The cross sectional shape in cohesive soil embankment appears more like trapezoidal at the contraction section (upstream) and more like rectangular at the throat section.

- iv. Formation of flow cascade and water falls were observed in cohesive soil embankment breach. In cohesionless soil embankment breach, these flow patterns were not present.

#### b. Discharge Characteristics of Flow

- i. Flow in a cohesionless embankment breach behaves similar to flow over an erodible crest spillway. The alignment of spillway is straight in the beginning of the breach but as the breach progresses, it becomes curved with concaving in the direction of flow. This is clearly observed in photos of breach process.

Flow in the case of a cohesive soil embankment breach is analogous to that over a broad crested weir, with a cascade type of flow on the downstream face in the beginning and later it is more like a water fall.

- ii. The discharge coefficient,  $c_d$  is found to be varying during the breach process. It decreases with increase in the ratio of head over crest ( $h_u$ ) to the height of the crest ( $h_{cm}$ ). This variation continues till  $h_u/h_{cm}$  is equal to 0.4. For higher values of  $h_u/h_{cm}$ , the magnitude of  $c_d$  remains fairly constant. Rate of crest erosion is higher during  $h_u/h_{cm} < 0.4$  and gradually decrease as  $h_u/h_{cm}$  increases. This indicates that the coefficient of discharge  $c_d$  decreases during crest erosion.
- iii. Variation of reservoir level ( $h_{wr}$ ), head acting over the crest of weir ( $h_u$ ), drop in water level between reservoir and down stream of the dam ( $\Delta H$ ) and height of crest ( $h_{cm}$ ) with time from the start of the breach process are analysed combinedly for both types of soil embankments. The scales used for normalising these variables are functionally related with breach parametric numbers based on peak breach discharge ( $Q_{WP}$ ), height of the dam ( $H_D$ ), cross-sectional area of the dam ( $A_D$ ) and soil resisting velocity ( $V_{SR}$ ). The breach parametric numbers are  $Q_{PSN}$ ,  $Q_{APN}$  and  $V_{SRN}$ .

#### c. Erosional Characteristics of Breach

- i. Variations of crest height  $h_{cm}$ , crest width  $B_{cr}$  and crest cross-sectional area  $A_{cr}$  are functionally related to either time variable or drop in water level at the crest, separately for cohesionless and cohesive soil embankments. Variations of crest height  $h_{cm}$  with drop in water level is carried out for combined data of cohesive and cohesionless soil embankment breach.



For cohesionless soil embankment, crest height measured from the top of the dam varies with  $\frac{2}{3}$  power law while the width of erosion at the crest is found to vary with a power of 0.57 of the drop in water level at the crest.

For cohesive soil embankment, width of erosion at the crest attains maximum value at the beginning of breach erosion and thereafter remains fairly constant at a value equal to 1.2 times the height of dam ( $H_D$ ).

- ii. Rate of erosion of crest height ( $h_{cm}$ ), crest width ( $B_{cr}$ ) and crest cross-sectional area ( $A_{cr}$ ) are related to drop of water level, time and velocity of flow at crest.

For cohesionless soil embankments, rate of crest height erosion is related to drop in water level at the crest. Rate of width erosion at crest is related to flow velocity at crest and time.

For cohesive soil embankments, rates of crest height and crest width erosion varies with drop of water level between upstream and downstream of dam ( $\Delta H$ ).

For combined data of cohesionless soil embankment and cohesive soil embankment, the rate of crest height erosion is related to drop in the water level between reservoir level and downstream water level ( $\Delta H$ ).

Rate of erosion of crest height, crest width or cross-sectional area varies very steeply during initial state of erosion process. As the erosion process proceeds, the magnitude of these rates decreases. Contrary to the assertions as in numerical models of dam breach, the rates of erosion of the crest dimensions related with any of the flow parameters at the crest are found to vary with breach process.

#### d. Flow Characteristics

Mean velocity of the flow,  $\bar{V}_w$  computed from breach flow discharge ( $Q_w$ ) and the average wetted flow cross-sectional area ( $\bar{A}_f$ ) is averaged over the breach length at any instant of breach process for further computation of other breach variables. This average velocity, average hydraulic radius ( $\bar{R}_h$ ), energy gradient ( $\bar{S}_f$ ) and the average velocity of the flow at the down stream top edge of the dam is related to, water surface slope, bed shear velocity and critical depth of flow for cohesionless embankment breach flow.

- i. It is observed from the analysis, that the mean flow velocity varies  $\bar{R}_h^{-0.069}$  and  $\bar{S}_f^{0.279}$  individually. The applicability of Manning's equation is tried for breach flow and it is found from regression analysis that relation exists considering both  $\bar{R}_h$  and  $\bar{S}_f$  together as:  $V_w \propto \bar{R}_h^{-0.28} \bar{S}_f^{0.34}$ . However, when  $V_w$  is plotted against Manning's relation  $\bar{R}_h^{2/3} \bar{S}_f^{1/3}$ , it is found to agree closely with regression relation stated above.
- ii. Flow velocity at the downstream top edge of the embankment when nondimensionalised with bed shear velocity ( $V_*'$ ) and also with critical velocity at this section  $\sqrt{gy_c'}$ , are found to vary with water surface gradient  $\bar{S}_w$  as  $\bar{S}_w^{0.5}$  and  $\bar{S}_w^{0.41}$  respectively. From these relations it may be observed that  $\frac{V_*'}{\sqrt{gy_c'}}$  variation with  $\bar{S}_w$  is comparatively better correlated.

### e. Sediment Transport Characteristics

The sediment discharge intensity ( $q_s$ ) is related with flow discharge intensity ( $q_w$ ), bed shear velocity ( $V_*$ ), drop in water surface levels ( $\Delta H$ ) along with sediment resisting velocity ( $V_{SR}$ ).

- i. For cohesionless sediment embankment breach  $q_s$  varies as  $q_w^{1.43}$
- ii. The ratio of cumulative volume of sediment eroded to the cumulative volume of water flowed is found to vary inversely with increase in the time of breach process.
- iii. The sediment discharge intensity ( $q_s$ ) is found to vary as square of the bed shear stress ( $\tau_o$ )
- iv. Sediment concentration defined as  $\frac{q_s}{q_w}$  is found to be of very high order, 8 to 10 percent in the beginning of breach process, later on its magnitude decreases with increase in breach time or decrease in drop level ( $\Delta H$ ). It may be noted that when sediment concentration exceeds 8 percent, the flow can be treated as hyper concentrated flow.
- v. Sediment load  $g_s^*$  is found to increase with increase in square of the bed shear stress for combined data of cohesionless and cohesive soil embankment breach.
- vi. The relation between the sediment load ( $g_s^*$ ) with ratio of bed shear velocity to sediment resisting velocity as  $(\frac{V_*}{V_{SR}})^2$  is found to vary with a quadratic polynomial relation obtained

from regression analysis. This relation has a good agreement for higher values of  $\frac{V}{V_{SR}}$

However for lower values of  $\frac{V}{V_{SR}}$  large scatter is found to exist.

- vii. Sediment concentration for combined data is analysed, first carrying out regression analysis with sediment and embankment geometry parameters and then their relation is graphically represented. Regression relation of the data shows large scatter indicating a poor relationship.

#### f. Energy Loss Characteristics

Energy loss is defined as the difference in energy upstream of the embankment to the downstream of the embankment. It is related with water surface slope ( $S_w$ ) computed as  $\frac{\Delta H}{L_{DB}}$

in the breach section. Relative energy loss  $\frac{\Delta E}{E_1}$  varies as  $\left(\frac{\Delta H}{L_{DB}}\right)^{2/3}$  in the cohesionless soil embankment breach. For combined data, the quadratic polynomial relation found to agree closely in comparison to other relations.

#### g. Final Breach Dimensions Based on Laboratory and Field Data

Final depth and width of breach erosion, duration of the breach and peak flow discharge during breach are considered here as terminal breach parameters. These quantities are analysed using present laboratory data along with field data available in literature. Analysis is carried out like reservoir capacity, height of dam as known parameters. Since, the sediment properties and inflow discharge relations are not available for field data, they are excluded in the analysis.

- i. Peak flow discharge is found to control the breach process and breach geometry. It is related to capacity of the reservoir ( $CAP$ ) and height of the dam ( $H_D$ ). From the analysis, it is found that the peak flow discharge increases with  $2/3$  power of the reservoir capacity and square root of the height of the dam.
- ii. Breach width ( $B_{cr}$ ) is found to vary with peak flow discharge ( $Q_{WP}$ ) with a power 0.57 along with reservoir capacity and height of the dam.
- iii. Breach depth of erosion ( $D_{er}$ ) is found to be 0.74 times the height of the dam

- iv. Duration of the breach  $t_{95}$ , nondimensionalised with depth of erosion ( $D_{er}$ ) is related to capacity of the reservoir, width of erosion ( $B_{cr}$ ), peak flow discharge ( $Q_{WP}$ ) and height of the dam  $H_D$ . The analysis indicates a poor relationship between these parameters. This is, possibly due to lack of inclusion of embankment material properties.

#### h. Major Criterion Variables Controlling the Breach Process

The prediction of breach criterion variables like terminal breach geometry i.e., ( $B_{cr}$ ),  $D_{er}$ ,  $Z$  and the peak outflow water discharge ( $Q_{WP}$ ), sediment discharge ( $Q_{SP}$ ) and their time of occurrence,  $t_{wp}$  and  $t_{sp}$  are very much essential to study the breach erosion process. To arrive at a functional relationship for these breach variables in the analysis, two field data, Teton dam data and Huaccoto dam data are included along with the present experimental data.

- i. The duration of breach ( $t_{95}$ ) varies with soil resisting velocity number as  $V_{SRN}^{1.67}$ .
- ii. The breach peak discharge ( $Q_{WP}$ ) varies with Shields entrainment number as  $\tau_{*c}^{2.47}$  and  $CAP_N^{0.2}$ . It may be noted that  $Q_{WP}$  is very much sensitive to  $d_{50}$  as  $\tau_{*c}$  is a function of  $d_{50}$ .
- iii. Time of occurrence of peak breach discharge ( $t_{wp}$ ) varies as  $V_{SRN}^{2.0}$ ,  $Q_{PN}^{1.2}$ , and  $\tau_{*c}^{-0.43}$ .
- iv. The terminal breach width at top of the crest ( $B_{cr}$ ) varies as  $\tau_{*c}^{0.5}$ ,  $Q_{APN}^{0.35}$ .
- v. The ratio of terminal depth of breach ( $D_{er}$ ) to width of breach is related with  $Q_{PSN}$  and  $V_{SRN}$  numbers and is found to vary as  $Q_{PSN}^{0.053}$ ,  $V_{SRN}^{0.176}$ . This indicates that the geometry of the breach depends more on the soil properties than the breach peak flow.
- vi. The side slope of the breach cross section is found to be dependent on the final depth of erosion, width of erosion at crest, and height of the dam.

The analysis of peak sediment discharge intensity ( $q_{sp}$ ) and its time of occurrence ( $t_{sp}$ ) includes the simulated result of BEED model.

- vii. The breach sediment discharge intensity ( $q_{sp}$ ) is found to vary inversely with  $V_{SRN}$  as  $V_{SRN}^{-2.2}$ . This relation is obtained by non dimensionalising  $q_{sp}$  by  $Q_{WP}/H_D$ . The peak sediment discharge occurs earlier to the breach peak water discharge in almost all the experimental observations.
- viii. The ratio of  $t_{sp}$  to  $t_{wp}$  varies in a increasing trend with  $Q_{PSN}$ . The time to peak sediment discharge is related to time of occurrence of peak flow discharge ( $t_{wp}$ ).

- ix. In the conclusions stated above from 1 to 8, the peak flow discharge is considered to be an important variable in most of the cases. However,  $Q_{WP}$  itself is a result of breach process. Hence, instead of  $Q_{WP}$  another discharge parameter was essential to replace  $Q_{WP}$ . For this reason, the average inflow into the reservoir is considered to be an appropriate variable in further analysis.
- x. The final breach width  $(B_{cr})_f$ , depth of erosion  $(D_{er})$  and eroded cross-sectional area  $(A_{er})$  at crest in a nondimensional form with  $A_D$  and  $\bar{Q}_{in}$  varies with soil resisting velocity as  $V_{SRN}^{-2.54}$ ,  $V_{SRN}^{-2.81}$ , and  $V_{SRN}^{-2.64}$  respectively.

### i. Methodology to Predict Breach Process

Breach process involves the variations of breach geometry along with water and sediment discharges with time. Prediction of these information is carried out systematically based on the analysis of experimental results and also with two field observations. Procedure for prediction is presented in an algorithm and in a flow chart form.

1. An algorithm to predict reservoir water level, crest height and crest width during the breach process is presented. From these predicted values, computation of water discharge and sediment discharge graph during breach process are carried out. The distribution of normalised hydrograph and sediment discharge graph in the form of a equation  $Y = X^m e^{(1-X^m)}$  where  $Y$  represents normalised water and sediment discharges and  $X$  represents normalised time. The exponent ' $m$ ' in the above relation is found to have different magnitudes for rising limb and falling limb. Magnitudes of these exponents are related to parameters derived from dam geometry, soil properties and peak discharges, using present laboratory data and one field data of Teton dam. The scales like peak discharges and their corresponding time of occurrence are computed from the relations developed. The variations of discharge of water and sediment for different time during the breach process are compared with observed laboratory data, observed field data for the Teton dam and Huaccoto dam and also with predicted BEED model result for these two dam breach failure cases.
2. The breach dimensions like, final width of erosion, depth of erosion, side slope of the breach cross section and breach peak flow parameters like peak water discharge and peak sediment discharge and their corresponding time of occurrences and also duration of

breach are estimated using suggested methodology. These predicted results are compared with observed field data for Teton dam Huaccoto dam as shown in Table 8.1. Also these predicted results are compared with one numerical model namely BEED model. The agreement of the predicted results with observed data is shown in the percentage of error. It may be observed that the magnitude of percentage error for Teton dam is far less in comparison to Huaccoto dam. Here it should be noted that the inaccuracy in prediction of the breach variables for Huaccoto dam probably be due to the reported conflicting peak discharge values ranging from 10,000 to 18,000 m<sup>3</sup>/sec.

**TABLE 8.1**  
**COMPARISON OF ESTIMATED RESULTS FOR TETON AND HUACCOTO DAMS**

S.No.	Variables	Teton Dam				Huaccoto Dam			
		Estimated	Observed	BEED	% Error	Estimated	Observed	BEED	% Error
1	$Q_{wp}$ m <sup>3</sup> /sec	67,028	65,000	68,581	+3.12				
2	$q_{sp} \times 10^6$ cm <sup>3</sup> /sec/cm	93.8	-	103.95	9.75	31.9	-	-	-
3	$t_{gs}$ (hr)	1.5	1.5	1.35	0	-	-	-	-
4	$t_{wp}$ (hr)	1.27	1.5	1.35	-15.3	22.8	17.8		30.2
5	$t_{sp}$ (hr)	1.32		1.35	+3.6	4.45			
6	$(B_{cr})_f$ (m)	212.5	200	295	+6.3	168	200~300	298.5	22
7	$D_{cr}$ (m)	84.6	79	93	+7.1	91.1	107	85	-14.8
8	$z$	0.57	0.5	0.675	+10	0.52	1.0	1.67	-48

### 8.3 Washout Process in Fuse Plug

The results derived from the analysis of water level and sediment bed level during washout of sediment fill in fuse plug, are summarised under the headings namely outflow discharge relation, washout profile characteristics, sediment transport characteristics, energy loss characteristics, computation of outflow of water and sediment discharges. The experiments carried out using three types of soil as fill material in fuse plug. Five to six different inflow discharges were allowed into the reservoir for each type of soil fill. Experiments on simulated rigid washout profiles were carried out to verify the discharge relation.

### a. Outflow Discharge Relation

- i. The discharge intensity ( $q_w$ ) over the crest of the washout sediment profile is found to vary linearly with head acting over crest ( $h_u$ ). The discharge coefficient  $c_d$  computed based on weir relation is found to decrease with ( $h_u / h_{cm}$ ) having a power of 0.2, where  $h_{cm}$  is height of sediment crest at any time of washout process. Discharge relation, considering the variation of  $c_d$  is found to be related as:

$$Q_w = 0.42 L \sqrt{2g} h_u^{1.3} h_{cm}^{0.2}$$

- ii. Discharge characteristics over simulated rigid bed washout profiles were measured. They are found to follow weir type of relation having  $h_u^{3/2}$  and are independent of  $h_{cm}$ . This leads to conclude that the variation in co-efficient of discharge ( $c_d$ ) is mainly due to sediment bed profile erosion during washout process.
- iii. Co-efficient of discharge  $c_d$  for erodible fuse plug flows found to be function of the ratio  $h_u / h_{cm}$ . The magnitude of  $h_u / h_{cm}$  is related to drop in the water level between upstream and downstream of the fuse plug. The magnitude increases steeply during the initial stages of erosion from 0.08 to 1.0, later on there is gradual increase from 1 to 6.

### b. Washout Profile Characteristics

Characteristics of washout profiles includes the variation of crest, sediment profile, rate of crest erosion. These are related with time and depth scales derived from the rate of reservoir depletion during washout.

- i. Reservoir time scale ( $T_*$ ) and depth scale ( $H_*$ ) are measured from rate of depletion of reservoir having zero to negative maximum.
- ii. Nondimensionalised maximum crest height ( $h_{cm}/H_D$ ) is found to decrease with time as  $(h_{cm} / H_D) = 1 / (1 + (t / t_{50})^{2.5})$
- iii. Nondimensionalised sediment bed profile ( $h_c / h_{cm}$ ) is found to decrease with distance ( $X$ ) measured from the crest position as  $(h_c / h_{cm}) = 1 / (1 + (X/X_{50})^3)$
- iv. Scales  $X_{50}$  and  $t_{50}$  are related with reservoir depletion scales  $T_*$  and  $H_*$ .
- v. Rate of crest erosion  $(dh_{cm}/dt) / \sqrt{2gh_u}$  is found to increase initially with time, reaches a peak value of  $2 \times 10^{-3}$  and then starts decreasing with further increase in time. This

nondimensionalised erosion rate can be treated as erosion coefficient for fuse plug. The magnitude of this erosion coefficient is found to vary with time.

- vi. The maximum possible crest erosion rate ( $dh_{cm}/dt$ ) nondimensionalised with sediment resisting velocity  $V_{SR}$  is related to peak discharge  $q_{wp}$  in the form  $(q_{wp}/H \cdot V_{SR}) = X_{22}$  with power 3.27. This is carried out mainly to indicate the magnitude of rate of erosion for different types of soils.
- vii. Sediment erosion velocity  $V_{SV}$  nondimensionalised with its maximum value  $V_{SVM}$  is related to nondimensionalised flow velocity ( $V_u$ ) as  $V_u/\sqrt{2gH_D}$ . The magnitude of  $V_{SV}$  remains fairly constant as 0.9 when  $V_u/\sqrt{2gH_D} \approx 0.6$ . With further increase in  $V_u/\sqrt{2gH_D}$ , the sediment erosion velocity  $V_{SV}$  decreases very steeply. This variation is seen for all the three types of soils used in the fuse plug.
- viii. The sediment erosion velocity scale  $V_{SVM}$  nondimensionalised with soil resisting velocity  $V_{SR}$  is found to be a function of number  $X_{22}$ . As the magnitude of  $X_{22}$  increases from 1 to 10 the magnitude of  $V_{SVM}/V_{SR}$  increases from 0.03 to 0.8. The magnitude of  $V_{SVM}$  is higher for cohesionless soil and is of the order of 0.8 times  $V_{SR}$ .

### c. Sediment Transportation Characteristics

- i. The magnitude of sediment transported at any time  $Q_S$  nondimensionalised with its maximum value  $Q_{SM}$  is found to increase steeply in initial stages of erosion, reaches peak and then decreases gradually with increase in time. More data are available in later stages of erosion process. The receding limb of the sediment discharge ( $Q_S$ ) is analysed with time scale and found to follow a good relation as  $(Q_S/Q_{SM}) = 1/(1+X^2)$ , where  $X = (t - t_{sp})/(t_{sp/2} - t_{sp})$ .
- ii. Sediment concentration  $q_s/q_w$  is related to  $h_u/h_{cm}$ . It is found that  $q_s/q_w$  decreases with increase in  $h_u/h_{cm}$ . The relation between them is given by polynomial equation obtained from regression analysis.
- iii. Sediment concentration was found to be almost independent of bed shear velocity. However it is found to be a function of drop in the water level ( $\Delta H$ ).



#### d. Energy Loss Characteristics

- i. The ratio of energy at downstream end to the upstream of the fuse plug,  $E_2/E_1$  is related to  $h_u/h_{cm}$  for simulated rigid bed washout profiles. It is found that as  $h_u/h_{cm}$  increases  $E_2/E_1$  also increases.
- ii. Effect of erosion of the fuse plug material on the energy ratio  $E_2/E_1$  is related to  $h_u/h_{cm}$  along with rigid bed profile data. It was found that considerable energy loss occurs due to erosion of sediment at given state of flow.
- iii. The energy loss due to erosion and transportation of sediment is found from the relation  $[(E_2)_{\text{Rigid}} - (E_2)_{\text{Mobile}}]/E_1$  against sediment concentration  $Q_s/Q_w$ . It is found that the energy loss increases very steeply to a value of 0.9 with increase in sediment concentration to a magnitude upto 8 percent. With further increase in energy loss it is found to be nominal. Flow with sediment concentration higher than 8 percent is considered as hyperconcentrated flow.

#### e. Hydrograph and Sediment Discharge

- i. The normalised sediment discharge intensity  $q_s$  with its peak value  $q_{sp}$  is found to follow closely with time ratio  $t/t_{sp}$  as  $(q_s / q_{sp}) = X^2 \exp(1 - X^2)$ , where  $X = t/t_{sp}$ .
- ii. The peak sediment discharge  $q_{sp}$  is found to be a function of  $q_{wp}^{0.23}$
- iii. The time scale  $t_{sp}$  nondimensionalised with  $t_{wp}$ , the time at which maximum water discharge occurs is found to decrease with peak water discharge intensity as  $q_{wp}^{-0.5}$
- iv. Duration of washout process of fuse plug designated as  $t_{95}$  is found to be a function of reservoir time scale  $T_*$ , inflow discharge, soil resisting velocity  $V_{SR}$  and height of the fuse plug. The magnitude of  $t_{95}$  varies from 1 to 2.5 time  $T_*$ .

#### f. Outflow Hydrograph Characteristics

- i. The value of  $q_w/q_{wp}$  plotted against  $t/t_{wp}$  is found to increase initially, reaches peak and then decreases slowly to a value of incoming discharge ratio. The occurrence of peak discharge depends on the type of soil eroded. For cohesionless soil, the peak occurs almost in initial stage of washout process, whereas for cohesive soil fill it occurs at the later part of washout process. Because of this nature of variation, analysis of rising limb

of hydrograph is carried out in detail. All the rising limbs follow a relation  $(q_w / q_{wp}) = X^m \exp(1 - X^m)$ , where  $X = t/t_{wp}$ . The magnitude of exponent 'm' for cohesionless soil is 2.5 and it is 0.5 for cohesive soil.

- ii. The magnitude of peak water discharge  $q_{wp}$  is found to increase with increase in magnitude of inflow discharge  $q_{in}$  with a power of 0.45.
- iii. Time scale  $t_{wp}$  is the time at which peak water discharge occurs. This scale is found to decrease reaching a minimum value and then increases with increase in peak discharge  $q_{wp}$ .

#### 8.4 Suggestion for Further Work

- a. Experiments should be conducted for dam breach study as well as for fuse plug with temporal variation of the inflow discharge to the reservoir, taking its average  $\bar{Q}_{in}$ , more variation of dam geometry and its fill properties. The present developed functional relationships can be verified with the breach parameters obtained from these variations.
- b. The automation of data acquisition in terms of time and space should be planned for better accuracy of the data.

# REFERENCES

1. Annandale, G.W. (1995): 'Erodibility', *Journal of Hydraulic Research*, 33(4), 471-493.
2. Argon, Juan Antonio Garcia (1996): 'A Hydraulic Shear Stress Model for Rapid, Highly Concentrated Flow', *Journal of Hydraulic Research*, 34(5), 589-596.
3. Babb, A.O. and Mermel, T. W. (1968): Catalog of Dam Disasters, Failures and Accidents, PB179243; Washington, DC (Bureau of Reclamation).
4. Baccher, G.B., Pate, M.E., and Neufville, R.D. (1980): 'Risk of Dam Failure in Benefit Cost Analysis', *Water Resources Res.*, 16(3), 449-456.
5. Berga, L. (1992): New Trends in Design of Flood Assessment, ICOLD Symposium on Dams and Extreme Floods, Granada, Spain, September 1992.
6. Binnie, G. M. (1978): 'The Collapse of Dale Dyke Dam In Retrospect', *Quarterly J. Engg. Geol.*, 11, 305-325
7. Brown, R. J. And Rogers, D. C. (1997): 'A Simulation of the Hydraulics Events During and Following the Teton Dam Failure', in: *Proc Dam-Break Flood Routing Workshop*, 131-163; Washington DC (Water Resources Council)
8. Brown, R. J. and Rogers, D. C. (1981): BRDAM Users Mannual, 67, Denver, Co. (Water and Power Resources Services, U. S. Department of the Interior)
9. Brown C.O. and Graham, W. J. (1988): 'Assessing the Threat to Life From Dam Failure', *Water Resources Bull.*, 24, 1303-1304.
10. Central Water Commission (1989): Report on Dam Safety Activities in India, CWC Publication No. 47/89, 185 p., New Delhi, India.
11. Chatterjee, S. and Biswas, A.K. (1972): 'The Human Dimensions of Dam safety', *Water Power*, 24(1), 17-21.
12. Fread, D. L. (1984a): DAMBRK: The NWS Dam Break Flood Forecasting Model, National Weather Service(NWS) Report, NOAA, Silver Spring, MA.

13. Chee, S. P. (1988): 'Models and Scale Effects Related to Erosion of Granular Dams', *Modelling Soil-Water-Structure Interaction*; Balkema, 93-98.
14. Cochrane, H. (1989): 'The Economics of Dam Failure: Another Look at Catastrophic Losses', *Water Resources Res.*, **25**(9), 1931-1935.
15. Cristofano, E.A. (1965): Method of Computing Erosion Rate for Failure of Earthfill Dams, Denver, CO (U.S. Bureau of Reclamation).
16. Fread, D.L. (1984b): A Breach Erosion Model for Earthen Dams, National Weather Service (NWS) Report, NOAA, Silver Spring, MA.
17. Fread, D.L. and Harbaugh, T.E. (1973): 'Transient Hydraulic Simulation of Breached Earth Dams', *J.Hydraulics Division*, ASCE, 99, No. HY1, 139-154.
18. Graf, W. H and Song, T.(1995): 'Bed-Shear Stress in non-uniform and unsteady Open-Channel flows', *Journal of Hydraulic Research* **33**(5), 699-704.
19. Gruner, E. (1967a): 'The Mechanism of Dam Failure'; in: *9th Congress of the International Commission on Large Dams*, Istanbul, Turkey, Question No. 34, R. 12, 197-206.
20. Gruner, E. (1967b): 'The Safety of Reservoirs'; in: *World Dams Today*, 104-109; Tokyo (Japan Dam Association).
21. Gruner, E. (1969): 'Vigilance over Reservoirs', *Water and Water Engg.*, Sept.1969, 369-373.
22. Gruner, E.(1963a): 'Dam Disasters': in: *Proc. Institution of Civil Engineers*, London, Vol. 24, Paper No. 6648, 47-60.
23. Hagerty, D.J.(1991a): 'Piping/Sapping Erosion. I: Basic considerations', *J.Hydraulic Engg.*, **117**(8), 991-1008.
24. Hagerty, D.J.(1991b): 'Piping/Sapping Erosion. II: Identification-Diagnosis', *J.Hydraulic Engg.*, **117**(8), 1009-1025.
25. Han, K.Y., Lee, J.T. and Lee, W.H.(1986): 'Characteristics of Outflow Hydrograph Due to Earth Dam Breaching'; in: *Proc. 5th APD-IAHR Congress*, Seoul, South Korea, 145-159.
26. Haris, G. W. And Wagner, D. A. (1967): Outflow From Breached Earth Dams, Unpublished B. Sc. Thesis, Department of Civil Engineering, University of Utah, Salt Lake City, UT.
27. Houston, M.(1985): 'Discussion of Breaching Characteristics of Dam Failures by T.C. MacDonald and J.Langridge-Monopolis', *J.Hydraulic Engg.*, **85**, No. HY7; 1125-1129.
28. Jansen, R.B.(1980): *Dams and Public Safety, A Water Resources Technical Publication*; Denver, CO (Water and Power Resources Service, U.S. Department of the Interior).

29. Jansen, R.B., editor(1988): *Advanced Dam Engineering*; New York (Van Nostrand Reinhold).
30. Johnson, F.A. and Illes, P.(1976): 'A Classification of Dam Failures', *Water Power and Dam Construction*, 28(12), 43-45.
31. Laginha Serafim, J. and Coutinho-Rodrigues, J.M. (1989): 'Statistics of Dam Failure: A preliminary Report', *Water power and Dam Construction*, 41(4), 30-34.
32. Laginha Serafim, J.(1981): 'Safety of Dams Judged From Failures', *Water power and Dam Construction*, Dec. 1981, 32-35.
33. Lai, Jhin-Sung. and Shen, Hsieh W.(1996): 'Flushing Sediment Through Reservoirs', *Journal of Hydraulic Research*, 34(2), 237-255.
34. Lane, E.W.(1955): 'Design of Stable Channels', *Trans. Am. Soc. Civil Engg.*, 120, 1234-1260.
35. Lou, W.C. (1981): Mathematical Modelling of Earth Dam Breaches, Unpublished Ph.D Dissertation Colorado State University, Fort Collins, CO.
36. Loukola, E., Reiter, P., Shen, C., and Pan, S. (1993): 'Embankment Dams and Their Foundations: Evaluation of Erosion'; in: *Proc. Int. Workshop on Dam Safety Evaluation*, Grindewald, Switzerland, Vol. 4, 17-48.
37. Macchione, F. (1989): Discussion of 'Dimensionless Analytical Solutions for Dam-Breach Erosion by V.P.Singh and C.A. Quiroga', *J. Hydraulic Res.*, 27(3), 447-452.
38. MacDonald, T.C. and Langridge-Monopolis, J. (1984): 'Breaching Characteristics of Dam Failures', *J. Hydraulic Engg.*, 110, 567-586.
39. McCuen, Richard. H. And Snyder, Willard M.(1986): *Hydrographic Modelling Statistical Methods and Application*; Prentice Hall, New Jersey.
40. Middlebrooks, T.A. (1953): 'Earth-Dam Practice in the United States', *Trans. Amer. Soc. Civil Engg.* 118, 697-722.
41. Nogueira, V. D. Q. (1984): A mathematical model of Progressive Earth dam Failure, Unpublished Ph. D. Dissertation, Colorado State University, Fort Collins, CO.
42. Penman, A.D.M. (1986): 'On the Embankment Dam', *Geotechnique*, 36(3), 303-348.
43. Ponce, V. M.. (1982): 'Documented Cases of Earth Dam Breaches', SDSV Civil Eng. Services, No. 82140, 43, Sandiego State University, Sandiego, CA.
44. Ponce, V.M. and Tsivoglou, A.J. (1981): 'Modelling Gradual Dam Breaches', *J.Hydraulics Division* (Proc. Am. Soc. Civil Engg.), Vol 107, No. HY7, 829-838.

45. Powledge, G.R., Ralston, D.C., Miller, P., Chen, Y.H., Clopper, P.E. and Temple, D.M. (1989a): 'Mechanics of Overflow Erosion on Embankments. I: Research Activities', *J. Hydraulic Engg.* **115**(8), 1040-1055.
46. Powledge, G.R., Ralston, D.C., Miller, P., Chen, Y.H., Clopper, P.E. and Temple, D.M. (1989b): 'Mechanics of Overflow Erosion on Embankments II: Hydraulic and Design Consideration', *J. Hydraulic Engg.*, **115**(8), 1056-1075.
47. Quiroga, C.A. and Sing V.P.(1987): 'A Dam Breach Erosion Model: II. Application', *Water Resources Management*, **1**, 199-221.
48. Raudkivi, A. J.(1990) : 'Loose Boundary Hydraulics'; Chapter-10, 318 (Pergamon Press)
49. Seemanpalli, S.V. and Singh, V.P. (1992): 'Variational Method for Earth Dam Breach Analysis'; in: R.N. Chowdhury (ed.), *Geomechanics and Water Engineering in Environmental Management*, chapter 3; Rotterdam (Balkema).
50. Singh, K. P. And Snorrason, A. (1982): Sensitivity of Outflow Peaks and Flood Stages to the Selection of Dam Breach Parameters and Simulation Models, SWS contract Report **289**, 179, Surface Water Section, State Water Survey Division, Illinois Department of Energy and Natural Resources, Champaign, IL.
51. Singh, V.P. (1990): 'Dam Breach Modelling'; in: N.P. Cheremisinoff (ed.), *Encyclopedia of Fluid Mechanics, Vol. 10, Surface, Subsurface and Groundwater Flow Phenomena*, Chapter 13; New Jersey (Gulf Publishing).
52. Singh, V.P. and Quiroga, C. A. (1987a): 'A Dam-Breach Erosion Model: I.Formulation', *WaterResources Management*, **1**, 177-197.
53. Singh, V.P. and Quiroga, C.A. (1987b): Breach Erosion of Earthfill Dams (BEED) Model: Further Extensions, Military Hydrology Report, Environmental Laboratory, U.S. Army Engineer Waterways Experiment Station, Vicksburg, MS.
54. Singh, V.P. and Quiroga, C.A. (1988): 'Dimensionless Analytical Solutions for Dam Breach Erosion', *J. Hydraulic Res.*, **26**(2), 179-197.
55. Singh, V.P. and Regl, R. R. (1983): 'Analytical Solutions of Kinematic Equations for Erosion on a Plane, I. Rainfall of Indefinite Duration', *Adv. Water Resources*, **6**, 2-10.
56. Singh, V.P. and Scarlatos, P.D. (1987a): 'Modelling of Gradual Earthfill Dam Erosion'; in: A.S. Balasubramaniam, S. Chandra, D. T. Bergado, and P. Nutalaya (eds), *Environmental Geotechnics and Problematic Soils and Rocks*, 129-138; Rotterdam (Balkema).
57. Singh, V.P. and Scarlatos, P.D. (1988): 'Analysis of Gradual Earth Dam Failure', *J. Hydraulic Engg. ASCE*, **114**(1), 21-42.
58. Singh, V.P. and Scarlatos, P.D. (1989): Breach Erosion of Earthfill Dams and Flood Routing: BEED Model, Miscellaneous Paper EL- 79-6, Military Hydrology Report 17,

Environmental Laboratory, U.S. Army Engineer Waterways Experiment Station, Vicksburg, MS.

59. Singh, V. P., Scarlatos, P. D., Collins, J. G., and Jourden, M. R.. (1986a): 'Hydrodynamics of Earth Fill Dam Breach Erosion', in: ASCE Water Forum'86, Long Beach, CA, 1, 1-9.
60. Singh, V. P., Scarlatos, P. D., Collins, J. G., Collins, J. G. and Jourden, M. R.. (1988a): 'Breach Erosion of Earthfill Dams (BEED) Model', in: Natural Hazards, 1, 161-180.
61. Singh, V.P. and Woodhiser, D.A. (1976): 'A Nonlinear Kinematic Wave Model for Watershed Surface Runoff', *J. Hydrol.*, **13**, 221-243.
62. Singh, V.P. (1996): *Dam Breach Modelling Technology*; Kluwer Academic Publisher.
63. Stream Line (1995): HR Wallingford, Oxfordshire, OX10 8BA, UK, Dec., 1-4.
64. Surya Rao, S and Shukla, M. K. (1971): 'Characteristics of Flow over Weirs of Finite Crest width', *J. Of Hyd. Div., Proc. ASCE*, Nov., 1807-1816
65. Tang, W.H. and Yen, B.C. (1991): 'Dam Safety Inspection Scheduling', *J. Hydraulic Engg.*, **117**(2), 214-229.
66. Tinney, E.R. and Hsu, H.Y. (1962): 'Mechanics of Washout of an Erodible Fuse Plug', *Trans. Amer. Soc. Civil Engg.*, **127**, 31-59.
67. Vanoni, Vito A.(1977 ): *Sedimentation Engineering*(ed.), ASCE-Manuals and Reports on Engineering Practice -No. 54
68. Verma, Rajpal S. (1995): *Homogeneous Earthen Dam Breach Analysis*, Unpublished M. Tech. Dissertation, I. I. T. Kanpur, India.
69. Wan, Zhaohui. And Wang, Zhaoyin(1994): 'Hyperconcentrated Flow'; Chapter-7; Rotterdam (Balkema).
70. Wetmore, J. N. And Fread, D. L. (1984): 'The NWS simplified Dam Break Flood Forecasting Model for Desk-Top and Hand-Held Microcomputers', National weather Service Report, NOAA, Silver Spring, MA.

## APPENDIX

### Sample Calculation for $\tau_{*c}$

Fine cohesionless Soil (Type-A soil) :

$$d_{50} = 0.16 \text{ mm}$$

$$\frac{V_{*c}}{\sqrt{\frac{\Delta\rho}{\rho} g d_{50}}} = 0.27$$

Where  $V_{*c}$  = Critical Shear Velocity

$$\frac{(\tau_{oc})_{cohesion} + (\tau_{oc})_{friction}}{\Delta\rho g d_{50}} = (0.27)^{2.0} = 0.0729 = \tau_{*c}$$

[For type-A soil,  $(\tau_{oc})_{cohesion} = 0.0$ ]



### Calculation for $\tau_{*c}$ for soil fill of Teton Dam:

$$d_{50} = 3 \text{ mm}, \quad \phi = 40^\circ, \quad c = 49 \text{ kPa}$$

$$\left[ \frac{V_{*c}}{\sqrt{\frac{\Delta\rho}{\rho} g d_{50}}} \right]_{d=3\text{mm}} = 0.20976$$

$$\frac{\tau_{oc}}{\Delta\rho g d_{50}} = (0.20976)^2 = 0.044$$

$$\begin{aligned} (\tau_{oc})_{cohesionless} &= (0.044) \times (1.65 \times 10^3 \times 9.81 \times 3/10^3) \\ &= (0.044) \times 48.56 = 2.1366 \text{ kgf/m}^2 \end{aligned}$$

$$\begin{aligned} (\tau_{oc})_{cohesive} &= 1.15 \times 49 = 56.35 \text{ kPa} \\ &= 5.74 \text{ kgf/m}^2 \end{aligned}$$

$$\text{Combined Shear stress} = 2.1366 + 5.74 = 7.88 \text{ kgf/m}^2$$

$$\frac{(\tau_{oc})_{Combined}}{(\Delta\rho g d_{50})} = \frac{7.88}{48.56} = 0.162$$

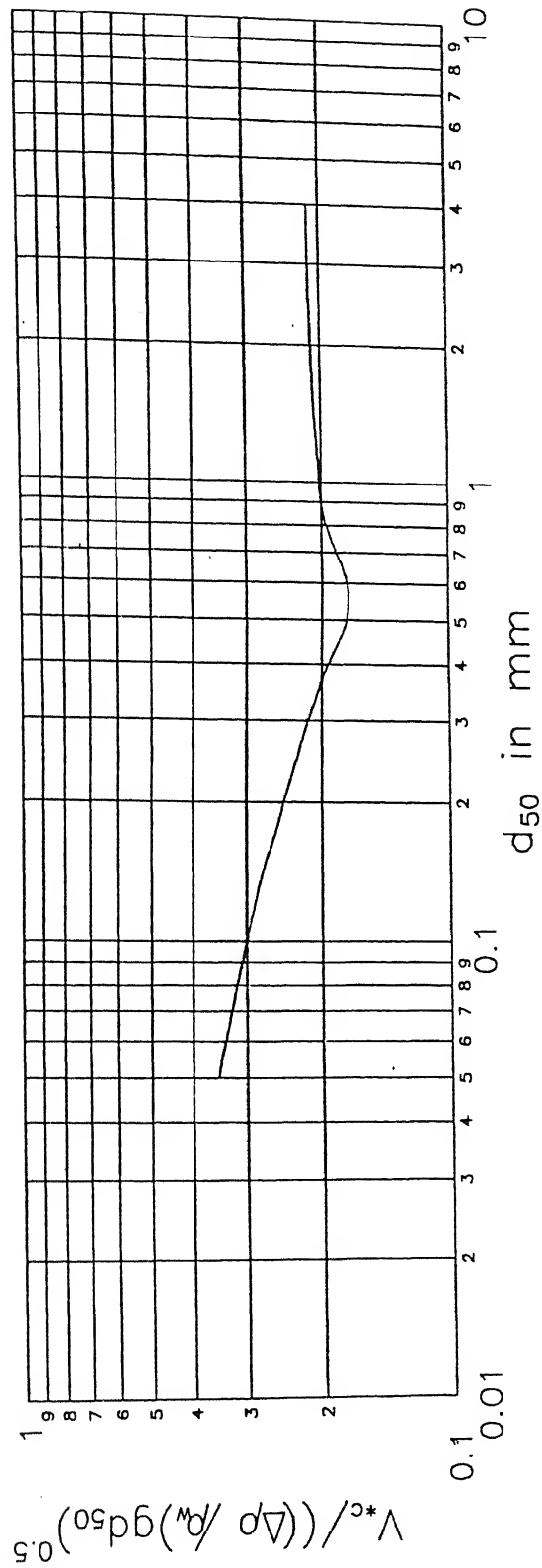


Fig. A1 : Variation of nondimensional bed shear stress with particle size of soil(mm) obtained from Shield's curve



128596

Date Slip

Ship

**128596**

This book is to be returned on the date last stamped.

[illegible]

Δ 1 5 0 2 Α